uOttawa

L'Université canadienne
Canada's university

FACULTÉ DES ÉTUDES SUPÉRIEURES ET POSTOCTORALES

uOttawa

L'Université canadienne
Canada's university

FACULTY OF GRADUATE AND POSDOCTORAL STUDIES

Marius Gabriel Ivan

AUTEUR DE LA THÈSE / AUTHOR OF THESIS

Ph.D. (Chemistry)

GRADE / DEGREE

Department of Chemistry

FACULTÉ, ÉCOLE, DÉPARTEMENT / FACULTY, SCHOOL, DEPARTMENT

Photochemistry Applied in Optical Lithography. Use of Spectroscopic and Imaging Techniques for the Characterization of Chemical Processes in Thin Polymer Films

TITRE DE LA THÈSE / TITLE OF THESIS

J.C. Scaiano

DIRECTEUR (DIRECTRICE) DE LA THÈSE / THESIS SUPERVISOR

CO-DIRECTEUR (CO-DIRECTRICE) DE LA THÈSE / THESIS CO-SUPERVISOR

EXAMINATEURS (EXAMINATRICES) DE LA THÈSE / THESIS EXAMINERS

Christian Detellier

Pudupadi Sundararajan

Javier Giorgi

Mitchell Winnik

Gary W. Slater

Le Doyen de la Faculté des études supérieures et postdoctorales / Dean of the Faculty of Graduate and Postdoctoral Studies

Photochemistry Applied in Optical Lithography. Use of Spectroscopic and Imaging Techniques for the Characterization of Chemical Processes in Thin Polymer Films

Marius Gabriel Ivan

Thesis submitted to the

Faculty of Graduate and Postdoctoral Studies

in partial fulfillment of the requirements for the degree of

Doctor of Philosophy

in the Ottawa-Carleton Chemistry Institute

Department of Chemistry, University of Ottawa, Canada

Université d'Ottawa · University of Ottawa

Candidate

Marius Gabriel Ivan

Supervisor

Professor J.C. Scaiano

Your file Votre référence
ISBN: 978-0-494-49362-5
Our file Notre référence
ISBN: 978-0-494-49362-5

To my parents, for everything.

Pãrintilor mei, pentru tot ce au fãcut pentru mine.

Abstract

Most of the research presented in this thesis deals with photochemistry applied to optical lithography, a technology used to manufacture computer chips, memories, and integrated circuits in the micro- and nano-regime.

Photochemical reactions induced in thin polymer films by laser radiation at 248, 193 and 157 nm were studied extensively, employing spectroscopy and microscopy techniques. Fluorescent dyes that would change their properties upon interaction with a chemical species were used to gain insights about the photoproducts formed during irradiation. Photolysis of photoacid generators (PAGs) leads to formation of acid, which will then catalyze deprotection of polymer pendant groups. The amount of acid formed as a function of incident dose was determined for different PAGs at various wavelengths and in different resist formulations using Coumarin 6, a fluorescent dye that changes its spectroscopic properties upon interaction with the proton. New and more transparent PAGs, obtained in the group, were characterized at different wavelengths.

The amount of acid determined by in polymer titration was used in calculation of the catalytic chain length (CCL). This is a novel method which employs two fluorescent sensors embedded in a polymer film.

Hydrofluoric acid (HF) was detected in films of fluorinated polymers exposed to laser radiation at 157 nm, using a fluorescent sensor especially designed and synthesized in the group.

The influence of laser radiation on the polymer film was studied using pyrene as fluorescent probes sensitive to the environment changes. Formation of excimers was observed in exposed areas; a very interesting finding is that the molecules forming the excimers do not separate after they emit light, remaining in

close proximity for days. The influence of temperature on the excimers in thin polymer films was studied, using polymers with different Tg.

Acknowledgements

I have many persons I want to thank to for their help and support offered during my PhD years. First of all I thank my supervisor, Prof. J. C. Scaiano, Tito for his family, friends and students, for the extraordinary chance he gave me, that of having him as a professor and as a mentor. I learned from Tito not just Chemistry, I learned what it takes to succeed in life, how to detect, approach problems and find solutions, how to be a successful scientist and manager at the same time. I also learned that Chemistry and good food, in particular Argentinean barbeques, go hand in hand during the many dinners that Tito and his wife Elda offered to his students at their place. They welcome all of us in their home, making us feel part of their big family. I also owe Tito my first lesson of skiing, which I will surely never forget.

My parents deserve all my gratitude, they did everything they could to help and support me. I thank them for their hard work and the sacrifices they made, for their trust in me. I thank Andreea, my wife, for her support and understanding, for being there whenever I needed something.

Gonzalo Cosa and Michelle Chretien were the first two people who welcome me in Canada, and who guided me during my first days here. Their advices were very precious and I thank both of them for that. The relationship with Gonzalo has developed during the years, and it turned into friendship. He helped me in many aspects, he kindly answered my numerous questions and I thank him for that. He was there for an advice when I needed it.

During my first PhD years in the group I met many people who helped me or with whom I collaborated. Luca Maretti, Dr. Carolina Aliaga, and Dr. Alexis Aspée helped me with my first projects with their explanations, advices and ideas which were very much appreciated.

Irina Denisova and Bojana Rakic are my friends from the Department of Chemistry here at the University of Ottawa, with whom I spent most of my time during the first two years of my PhD. I thank them for all the nice moments, for the long bike rides in Gatineau Park and in Ottawa during which I discovered the beauty of these places.

Dr. Carlos Sanrame is one of the people who were always there when I had a question, and most importantly, he had an answer for everything. I learned many things from Carlos, and in particular that besides knowledge, a chemist has to be patient, perseverant and calm when something just does not seem to work fine, and he will surely find the right solution. The parties that Carlos and his wife Eugenia organized at their home were great, with true Argentinean food and wine, making me to hardly wait for the moment they would announce the next one. I thank Carlos and Eugenia for being true friends.

I thank Larisa Mikelsons for the patience and understanding she showed when my books, papers and notebooks were spread all over our little desk. With Marie Laferriere I collaborated, and we shared experience, hopes that we would get excellent results, and that we would overcome the many challenges that the project we started posed to us.

I thank Gino Cuglieta, our technician, for his help, understanding and collaboration during the times some of the equipment I used was not working properly. I also thank Dr. Claudio Cara, Dr. Vincent Maurel, and Dr. Atsushi Goto for their help and suggestions, and for the nice time and discussions we had in our office. With Mathieu Frenette I collaborated for some projects, and I thank him for all the good ideas he gave me, for the useful advices and discussions. I thank Kathy Focsaneanu for being a nice and kind person, for all the cards and small treats that she put in our mail boxes for every Christmas, Easter, or Valentine's Day. I thank Betty Yakimenko for her help during these years, for the

cakes and cookies she baked for us, and for her attempts to make us millionaires by playing at lottery.

Dorothy and Roy Wallace welcome me into their home during my first winter holyday here in Ottawa. I thank them for their trust, kindness and friendship, and for the nice moments we have spent since then.

With Dr. Sergiu Coseri, a post doc at National Research Council in Ottawa, I spent lots of time talking about home, about Romania and friends from far away. I thank him for all the time we spent together, for the nice traditional dinners we cooked, and the fun we had. I thank Madalina Popa for all her support and encouragements, for everything she did for me. I thank Prof. Eveline Popovici from "Al. I. Cuza" University in Iasi, Romania, for her help.

I guess I was very fortunate to meet nice people and have so many wonderful friends. The Scaiano Groups has always been great, with smart, fun and interesting people with whom it was a pleasure to work. I will surely miss them, the atmosphere from the group, the university, and Ottawa.

List of abbreviations

2PE	2-pyperidin-1-yl-ethanol
AFM	atomic force microscopy
BTP	2-Benzothiazol-2-yl-phenol
BTTIPS	2-Benzothiazol-2-yl-phenol
C4	7-Hydroxy-4-methyl-chromen-2-one (Coumarin 4)
C4TIPS	4-Methyl-7-(triisopropylsilanyloxy)-coumarin
C4*t*-BOC	7-*tert*-butoxycarbonyloxy-4-methylcoumarin
C6	Coumarin 6
$C6H^+$	monoprotonated Coumarin 6
CA	chemical amplification
CCL	catalytic chain length
CMOS	complementary metal-oxide systems
CNC	7-hydroxy-4methyl-2-oxo-*2H*-chromene-3-carbonitrile
CNCTIPS	7-triisopropylsilanyloxy-4methyl-2-oxo-2H-chromene-3-carbonitrile
DRAM	dynamic random access memory
DMF	dimethylformamide
DTBPI-OCS	*di*-(4-*tert*-butyl-phenyl) iodonium orthocamphor sulfonate
DTBPI-PFOS	*di*-(4-*tert*-butyl-phenyl) iodonium perfluorooctane sulfonate
DUV	deep ultraviolet
EC	ethyl cellulose
EUV	extreme ultraviolet
EUVL	extreme ultraviolet lithography
FP	fluorinated polymer
GPC	gel permeation chromatography
HOMO	highest occupied molecular orbital

IC	internal conversion
IBL	ion beam lithography
ISC	intersystem crossing
LER	line edge roughness
LUMO	lowest unoccupied molecular orbital
LFP	laser flash photolysis
LIPS	laser induced periodic structures
MST	microsystem technology
NA	numerical aperture
NIL	nanoimprint lithography
NMR	nuclear magnetic resonance
PAB	post application baking
PAC	photoactive compound
PAG	photoacid generator
PAG1	1-methyl-4-oxo-thiochromanium triflate
PAG2	1-methyl-thiochromanium triflate
PBOCTS	poly(4-*tert*-butoxycarbonyloxystyrene)
PEB	post exposure baking
PGMEA	propylene glycol methyl ether acetate
PHOST	poly(4-hydroxystyrene)
PMMA	poly(methyl methacrylate)
PMSSQ	polymethylsilsesquioxane
POMMMIE	poly[[octahydro-5-(methoxycarbonyl)-5-methyl-4,7 methano-*1H*-indeno-1,3—diyl]-1,2-ethanediyl]
RT	room temperature
RPM	rotations (revolutions) per minute
t-Boc	*tert*-butoxycarbonyloxy

TFA thin film analyser

TIPS triisopropylsilyl

TBPPMS-Otf *tert*-buthyl-phenyl pentamethylsulfonium triflate

TBPPMS-PFBS *tert*-buthyl-phenyl pentamethylsulfonium perfluorobuthane sulfonate

TPS-OTf triphenylsulfonium triflate

VUV vacuum ultraviolet

XP 1215aA commercial name of a photoresist designed by Shipley for photolithography at 157 nm

XP 0921 commercial name of a fluorinated polymer designed and synthesized by DuPont (same as PFP or FP)

XRL X-ray lithography

mM milimolar

μM micromolar

ns nanosecond

cm centimeter

mm milimeter

eV electron volt

Table of Contents

List of Figures

List of Schemes

List of Charts

List of Tables

Introduction

1 Introduction

1.1 Where light and matter meet

Light is one of the key ingredients that has triggered the formation and evolution of life under all its forms on Terra. Photochemical processes have been around since the first photons were emitted in the universe. While photochemical processes are as old as the universe, their systematic study started towards the end of the 19th century. Modern photochemistry is a multidisciplinary science, laying at the border between different fields such as biology, materials science, medicine, physics, computational, organic and inorganic chemistry. The object of study in photochemistry is the interaction between light and matter, the transients and the photoproducts of the light triggered reactions.

Photochemistry makes use of photons from a relatively short interval of the electromagnetic spectrum, figure 1-1. Photochemical processes are induced most often by photons from the near UV (250 – 400 nm), the visible region (400 – 750 nm), and IR (> 750 nm). The development of light sources (lasers, lamps, photoreactors) has led to novel applications of photochemical and photophysical processes in areas such as microelectronics, photodynamic therapy (PDT), photonics, communications, nanotechnologies, medicine, entertainment, automotive, photo-recording and photo-reading, photocatalysis, photosynthesis, photovoltaics. [1]

Upon absorption of a photon, a molecule is promoted from the ground state (S_0) to the excited state (S_1). In terms of the Molecular Orbital Theory, and depending on the chromophore, the most encountered transitions are π–π^* and n-

π^*, corresponding to promotion of an electron from the HOMO to the LUMO. [2, 3] If the photons absorbed possess a high energy, σ–σ^* transitions may occur as well. Once in excited state, the molecule may either go back to its ground state by releasing the excess energy as heat (internal conversion – IC) or as light (fluorescence), or intersystem cross (ISC) to the triplet state (T_1). Although ISC is a spin-forbidden transition, it still occurs due to a process called spin-orbit coupling. From the triplet state the molecule can emit light at a longer wavelength than in the case of fluorescence (phosphorescence), or it may undergo bond breaking, leading to formation of reaction intermediates, figure 1-2. These reaction intermediates (radicals, ions, or carbenes) can recombine while they are still surrounded by the solvent cage or may escape the solvent cage and lead to formation of photoproducts.

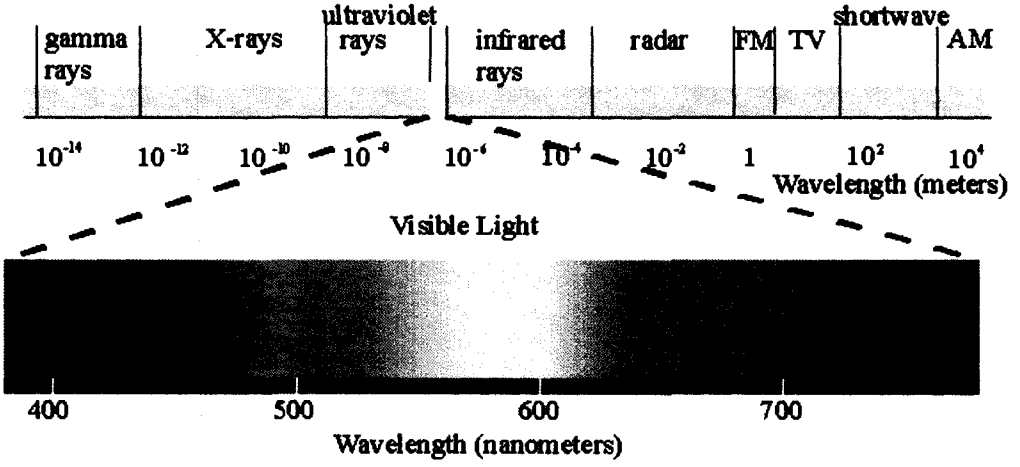

Figure 1-1. The electromagnetic spectrum with the visible region expanded between 400 and 750 nm.[a]

The time scale of the photophysical and photochemical processes varies depending on the chromophore, solvent, temperature, presence or absence of the quenchers. An excited singlet state is very short lived, at room temperature (RT)

[a] http://www.yorku.ca/eye/spectru.htm

being usually in the order of 10^{-15} – 10^{-6} s, while the triplet may last between 10^{-6} to 30 s. [2-4] A molecule in the excited state is very reactive, having many opportunities to release its excess energy. The study of excited states, reaction intermediates involved in photochemical reactions, and their kinetics is done using different techniques, among which are time-resolved fluorescence, phosphorescence and laser flash photolysis (LFP). [5, 6] These techniques monitor the emission or absorption spectra of the short lived intermediates using fast pulsed lasers (10^{-15} – 10^{-9} s per pulse). [5, 6] While for unimolecular reactions picosecond and femtosecond pulsed lasers are the obvious choice, for reactions limited by diffusion control (for example free radicals combination) and even slower, the measurements may be done using nanosecond pulsed lasers.

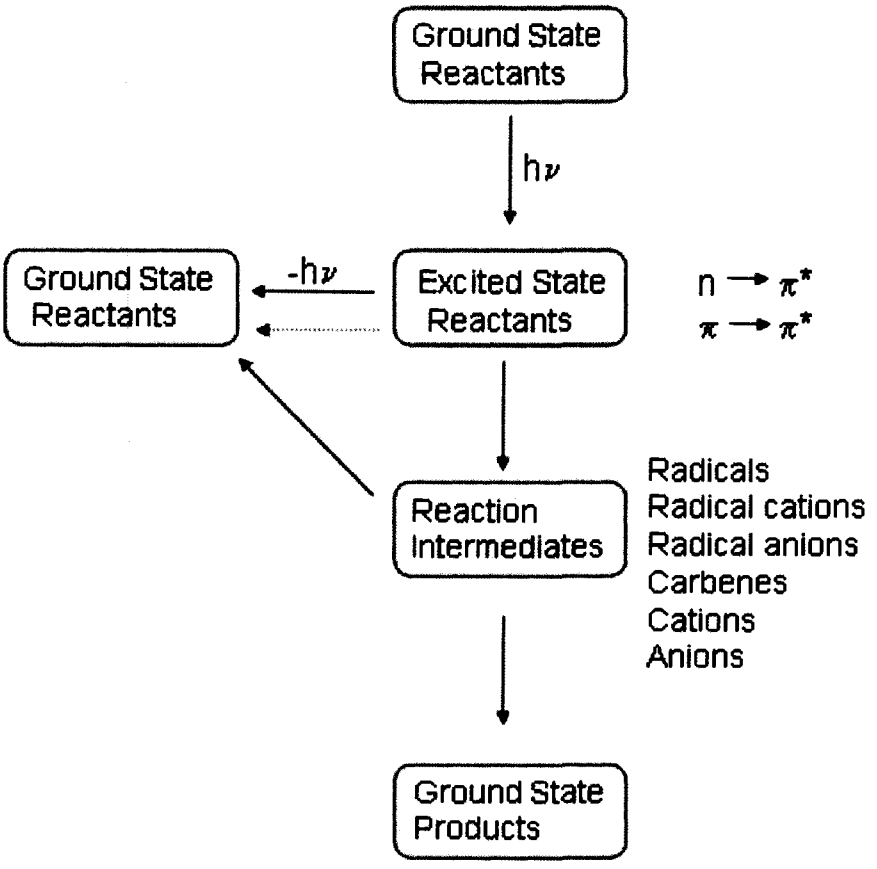

Figure 1-2. Possible reaction paths for a molecule upon absorption of a photon

The advancement of optical instrumentation has allowed scientists to develop new methods and techniques that allow an easy monitoring of (photo) chemical reactions. Fluorescence microscopy is a powerful technique used to characterize surfaces, thin films, and cell tissues and cultures. [7]

Nanotechnologies are the newest trend in science and research. Nanoparticles possess intriguing properties, different from the bulk material, some of them still hard to explain, such as the blinking of the quantum dots. [8] Many of the traditional fluorescent sensors may be replaced by functionalized nanoparticles. [8-10] Photochemistry may be employed in the process of synthesis of these nanoparticles. Their optical properties may be exploited and modified using various molecules to functionalize them. [11] Nanoparticles and nanostructures have already been studied for possible use in various fields, such as photodynamic therapy (PDT), photonics, solar cells, and computer chips. [8-10, 12] Considering its potential, the field of nanotechnologies is at an incipient stage, and the possibilities of growing seem unlimited at the moment.

1.2 Nano- and micro-lithography

Nanolithography is a well established field among nanotechnologies. It is the continuation of microlithography at the nanometer regime. Microlithography is a technique used to print integrated circuits on different substrates. [13-15] Photolithography is a special technique that makes use of light to transfer the pattern of a mask onto a resist and further to the substrate (usually a semiconductor, most often silicon). Depending on the source of radiation, lithography techniques may be divided into: photolithography or optical lithography (OL), electron beam lithography (EBL), extreme ultraviolet lithography (EUVL), ion beam lithography (IBL), and X-ray lithography (XRL). [13] Nanoimprint lithography

(NIL) is a technique that uses stamps containing features in the nanometer regime to transfer the image to the substrate. One of the steps in NIL consists of exposure of the imprinted resist film to radiation of a certain wavelength.

Most of the computer chips are obtained using photolithography. Other techniques have been developed as alternative to optical lithography, namely soft lithography. [16]

Most of the research done for this thesis is about photochemistry applied in photolithography, a technique used to manufacture computer chips, DRAM memory modules, or integrated circuits with very small dimensions (micrometer and nanometer sizes). [13, 14] The steps involved in the lithographic process are presented in figure 1-3. A photoresist is spin-coated on top of a silicon wafer (substrate), resulting a film with a thickness of a few hundreds of nanometers. The photoresist contains a special polymer, casting solvent, a photochemically active molecule, and other additives whose role is to give the photoresist the desired properties. Current state-of-the-art photoresists make use of a concept called chemical amplification (CA), developed at the beginning of 1980's by Ito, Wilson and Fréchet, presented in the next section of this chapter. [17-19] The wafer and the film are baked on a hot plate at a temperature that will cause the casting solvent to evaporate, for a total time varying between 60-90 s. Following the post application baking (PAB) treatment, the film is exposed, through a complicated optical system, to light passing through a mask. The pattern of the mask is transferred to the film, inducing changes in polarity between the exposed and unexposed areas. These changes in polarity, caused by chemical reactions, allow a selective developing of the film when the proper solvent is used. Positive photoresists have the exposed regions removed during the developing step, while the negative resists have their unexposed regions removed. After exposure to light originating from a light source, usually a laser (193 nm is the wavelength currently used by industry), the film is baked again, allowing the chemical reactions to occur in the exposed regions, a process called post-exposure baking (PEB). Following developing, the next step is etching the bare

parts of the wafer using hydrofluoric acid (wet etching) or plasma (dry etching), leading to formation of three-dimensional features. The photoresist layer left on selective areas after developing will protect the wafer underneath it during etching, thus transferring the image of the mask to the wafer. Stripping is the last step, when the photoresist left on the surface of the wafer is removed.

The size of the features (lithographic resolution – R) depends on the wavelength of the radiation (λ), and is inversely proportional to the numerical aperture (NA) of the optical parts according to Reyleigh's equation:

$$R = k_1 \lambda / NA \qquad \text{eq. 1.1}$$

where k_1 is a constant characteristic to the instrument in the range 0.4 - 1.

From eq. 1.1 it appears that there are two possible choices to reduce the lithographic resolution: decreasing λ or increasing the NA. During the past two decades both approaches were applied. The exposure wavelength has continuously decreased from visible to deep-UV, the wavelengths used being G-line (436 nm) and I – line (365 nm) from mercury discharge lamps, followed by the use of lasers emitting in the deep UV: 248 nm (KrF) and 193 nm (ArF). Initially the industry estimated that by 2005 the manufacturing of computer chips would be done using lasers at 157 nm (F_2), but the major challenges regarding the high absorbance of the materials and the birefringence of CaF_2 optics have led to an extension of 193 nm. [20-22] The computer chips and DRAM memories are currently manufactured using dry lithography at 193 nm. For the next few years the wavelength used will still be 193 nm, but the technology will be immersion lithography. In immersion lithography the space between the wafer and the last lens of the optical projection system is filled with a liquid. Water is the first option since is cheap, is transparent at 193 nm, and is easily recycled. Research is

focused now towards development of liquids with a high refractive index, since this will lead to an increase in NA, and consequently a decrease in R. At the same time the refractive index of the resist will have to be adjusted close to the value of the liquid on top. Leaching of resist components into the liquid may damage the lens, a solution to this problem being the use of a transparent top coating that would stop these components from leaving the resist film.

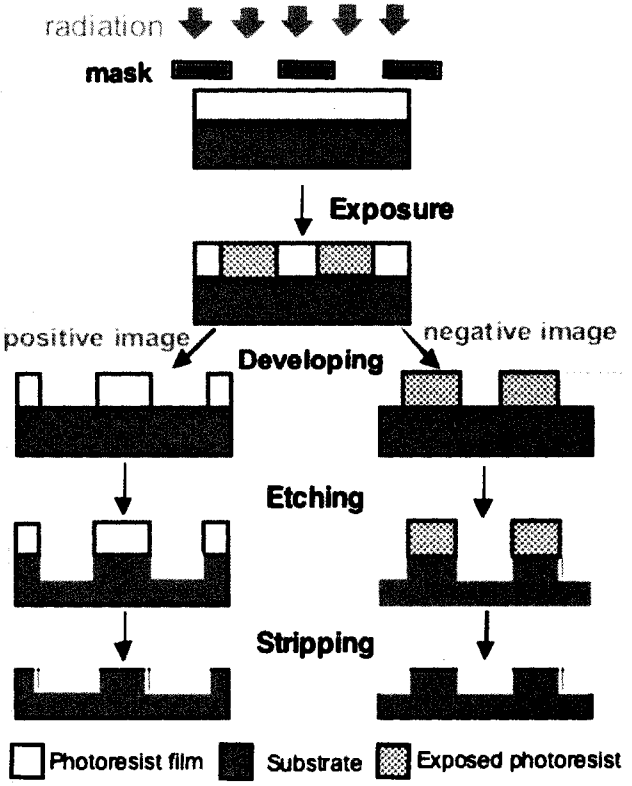

Figure 1-3. Photolithographic steps

1.3 Photoresists

In 1965 Gordon Moore, a physical-chemist and one of Intel's co-founders, mentioned that the microelectronics industry should attempt to double the number of the transistors embedded in a chip every year and a half in order to be

competitive.[23] The industry has closely followed the trend mentioned by Moore, which is now known as Moore's law. The current state-of-the-art processors have feature sizes of 65 nm, with the industrial scale production of 45 nm half pitch about to start soon.

As the industry moved to shorter wavelengths, the photoresists had to be changed, in order to meet the desired properties, such as : good adhesion to the substrate, formation of defect-free films, high thermal stability, high contrast and resolution, high sensitivity, solubility in the developing solvent, proper absorption at the exposure wavelength, etch resistance, ease of synthesis, and low price. Some of the commonly used solvents in resists are propylene glycol methyl ether acetate (PGMEA), ethyl lactate, 2-heptanone, etc. The casting solvent is the largest component of a resist, it influences the formation of the film and in the end the image obtained. The solvent must be easily removed during PAB.

The two most important parameters of a resist are the sensitivity and the absorbance at the exposure wavelength, especially in DUV and VUV where the number of photons is smaller compared to longer wavelengths, and the absorbance of the materials higher. For positive photoresists the sensitivity is defined as the incident dose (mJ/ cm^2) needed to completely remove the exposed area of the film during the developing step. For the negative photoresists the sensitivity is the dose at which 50 % of the film's thickness in the exposed areas was retained.

The most important component of the resist, and second in terms of mass, is the polymer. After the evaporation of the solvent during spin coating and PAB, the polymer remains the largest component of the resist film. Polymers used in photoresists have evolved at the same time with the exposure wavelength.

Besides the imaging tones (positive and negative), the resists may be classified depending on the nature of the polymer and the active ingredient:

- one component

- two or multi-component resists

In the one-component resists the polymer must be radiation sensitive, and undergo chemical changes induced by light (or electrons, depending on the source of radiation). Currently employed photoresists consist of two components: the polymer (insensitive to the incident radiation) and a light sensitive ingredient. The light-sensitive molecule will either be photolysed, and one of the photoproducts will react with the polymer, or it will sensitize the polymer, inducing a change in the solubility of the polymer in the exposed areas compared to the unexposed ones.

Photoresists may also be divided in two big categories as a function of the mechanism they are based on, which also coincides with their evolution in time:

- non-amplified (the first photoresists to be developed)
- chemically amplified (CA) photoresists (introduced at the beginning of 1990's).

The non amplified resists were used in lithography in the visible-near UV (436 and 365 nm), while the CA photoresists have been used in the DUV at 248 and 193 nm. [14] The two-component non-amplified photoresists consisted of the radiation inert polymer – a novolac resin, and the photoactive component (PAC) – diazonaphtoquinone, scheme 1-1. Novolac (obtained by acid-catalyzed copolymerization of cresol and formaldehyde) is soluble in aqueous base solutions, but it becomes insoluble when diazonaphthoquinone is added to the polymer film. However, upon absorption of a photon, diazonaphtoquinone releases nitrogen, forming a carbene, which undergoes a Wolff rearrangement to form a ketene. The ketene further reacts with water traces present in the film, producing indenecarboxylic acid, scheme 1-1. The carboxylic acid is soluble in aqueous base solutions, thus inducing solubility in the exposed areas of the photoresist.

According to Reyleigh's equation, the feature size may be downsized if the exposure wavelength is decreased. The decrease of the exposure wavelength posed many challenges due to the low sensitivity of the novolac/

diazonaphthoquinone resist, the low quantum yield in the range 0.2 – 0.3, and its high absorbance. It was clear that there was a need for a breakthrough in the way the resists were designed.

The breakthrough came when Ito, Wilson, and Fréchet proposed the concept of *chemical amplification* (CA) in 1982. [14, 18, 24-26] In CA one absorbed photon leads in the end to hundreds of chemical events, with an exponential increase in resist sensitivity. The photon is absorbed by a photochemically active molecule, a photoacid generator (PAG) which upon photolysis produces acid and other photoproducts. [13, 14, 26-28] The acid will then catalyze a chemical reaction involving pendant groups of the polymer, causing a change in the polymer's solubility. The acid is the catalyst since it is recovered after every reaction cycle, scheme 1-2. The catalytic chain length (CCL) is the number of chemical events catalyzed by one proton, and it has been reported to be in the range of 800 – 1000, depending on the photoresist and the working conditions. [29]

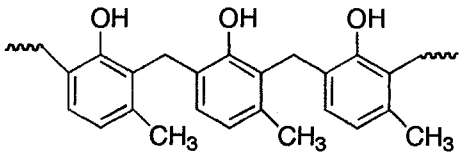

Novolac

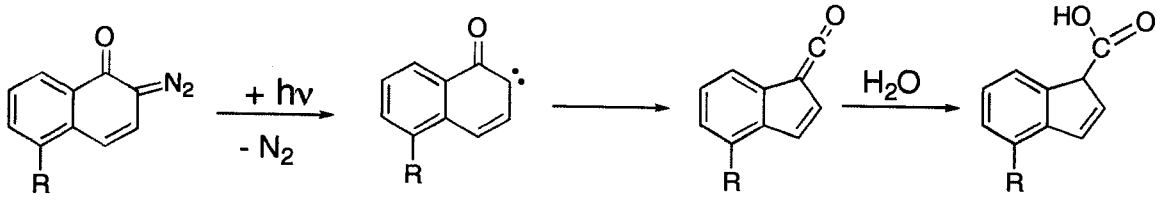

Diazonaphtoquinone

Scheme 1-1. Novolac resist and the photochemical transformation of diazonaphtoquinone derivative.

The chemical change caused by the acid induces a difference in solubility in the exposed *vs.* unexposed regions of the film. This difference may be caused in many ways, but the most common is the deprotection of an esteric pendant group and formation of either carboxylic acid or phenol, scheme 1-2. The examples from scheme 1-2 are typical for photoresists used at 248 nm – poly(4-*tert*-butoxycarbonyloxystyrene) - PBOCST (a), and at 193 nm - poly(*tert*-butylacrylate) (b). The phenolic resists used at 248 nm are too opaque at 193 nm. The acrylic-based resists worked best at 193 nm. Most polymers used in photoresists are *co*- or *ter*-polymers, with each monomer bringing certain properties to the polymer matrix. [14] For example, the monomer protected with *tert*(butoxycarbonyloxy) group, *t*-Boc, plays the role of the solubility switch. [24-26]

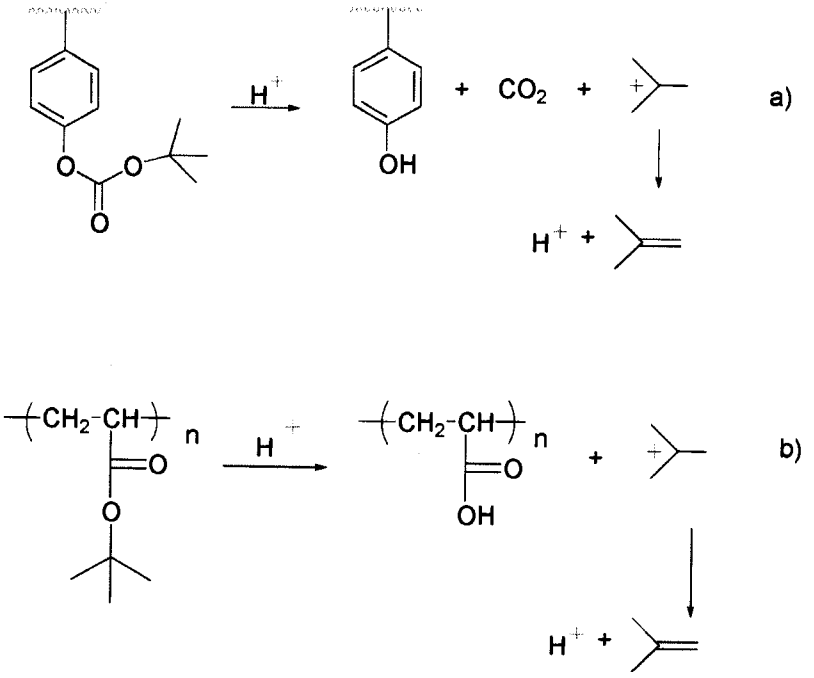

Scheme 1-2. Acid catalyzed deprotection reactions of a typical 248 nm PBOCST-based resist (a) and of a 193 nm poly(*tert*-butylacrylate) – based resist (b). The acid, which catalyzes the deprotection, is produced by photolysis of the PAG, and is recovered in the last step from the tertiary carbocation.

Typical PAGs are aryl sulfonium and iodonium salts, extensively presented in chapter 3. [24-26] One of the most difficult problems for the microelectronics industry was the airborne contamination of the resists with bases. [30] Organic volatile bases used in various chemical processes or incorporated in different materials are a problem for CA resists because they react with the acid formed on the top of the resist film, inducing defect in the developed image. [14] One solution to this problem was the filtration of the air. The exposures are done in the so-called clean rooms, where the air is filtered to remove chemical contaminants and microparticles as well. Another solution is the use of resists that have low activation energy of deprotection and that do not require baking for the deprotection to occur. Thus the acid can catalyze the deprotection immediately after formation, at room temperature, avoiding the delay until PEB is done and not being consumed by the contaminant. [14]

1.4 Rationale and research objectives

1.4.1 Rationale

At the moment this thesis project was started, 157 nm was seen as the next wavelength to be used in optical lithography after the 193 nm era. It is known that at 157 nm most of the organic compounds absorb, this being a big challenge for resist developers. [31, 32] One of the goals of this project was to study the photochemistry of the PAGs previously used at 193 and 248 nm, and to check for their acid formation abilities at 157 nm. In microelectronics industry the competition is tough, and the chip manufacturers like to keep the research costs as low as possible by utilizing at the next exposure wavelength as much as possible from the experience, knowledge and materials employed at the previous wavelength. Each exposure wavelength employed by industry had its own set of challenges, and in general polymers used at the previous exposure wavelength were too opaque at the next one, so new polymers had to be designed and synthesized. The PAG, which represents only a small fraction of the resist, makes only a minor contribution to the overall absorbance at the exposure wavelength at 193 and 248 nm (the PAG loading is most often ~ 2-6 % from the dry polymer weight). Thus PAGs used at 248 nm were found in resists designed for exposure at 193, and even at 157 nm. But 157 nm is a very energetic radiation which may lead to different photochemistry due to excitation of the molecules to S_2 or even higher states. Some of the best PAGs at 248 and 193 nm contain two or three phenyl rings in their structures (see chapter 3), making them too absorbent at 157 nm. So there was a need for a systematic study of photoacid generation at 157 nm, and for the design and synthesis of new PAGs.

Most of the reports published on optical lithography at 157 nm were concerned with technical aspects (optics, masks, lasers, costs). There had been a few reports about the interaction between laser radiation at 157 nm and different

polymers, but not in the photolithographic context. [33-35] In this light, we decided to study PAGs, previously employed in optical lithography at 248 and 193 nm, in resist formulations designed for 157 nm. Most of these PAGs contained two or three phenyl rings in their structures, so we decided to test new and more transparent PAGs as well, with only one phenyl ring. Some of them were synthesized in our group and were completely new structures, some were supplied by Rohm and Haas Electronics (former Shipley) from Marlborough, MA. Different polymers were used as well, since the polymer matrix influences the diffusion of the acid and the performance of the photoresist. [24, 26, 36-38]

The tools employed to characterize and quantify the formation of acid in thin polymer films were absorption in UV-vis, fluorescence and excitation spectroscopy, and fluorescence microscopy. Although the films were very thin (thickness less than 1 μm), by adding very sensitive fluorescent acid sensors, it was possible to detect extremely small amounts of acid. Fluorescence is a very sensitive technique which allowed recording of signals characteristic to the fluorescent acid sensor.

Fluorescence imaging was extensively used since it offers the possibility of observing the exposed and unexposed areas of a film in the same image. The contrast between the exposed and unexposed areas was very clearly evidenced by using the right set of excitation wavelengths and optical filters in the fluorescence microscope. The latent image, that is the image obtained in the photoresist during exposure, will later be transferred to the substrate.

In order to observe the differences between PAG's behavior at different wavelengths, experiments were done in which films obtained using the same stock solutions were exposed at 248, 193 and 157 nm.

The catalytic chain length (CCL) is a parameter which gives the number of *t*-Boc groups deprotected by one proton. It was calculated to be anywhere between 100 – 1000, depending on the resist and processing conditions. The method employed by McKean *et al.* was to monitor, using FTIR, the signal of the carbonyl group disappearing from the exposed films as a function of the incident dose (so as

a function of the amount of acid produced) and the post-exposure baking (PEB) time. [29] We decided to develop a new method that would allow calculation of CCL based on fluorescent sensors. [39]

Since at 157 nm the polymer absorbs as well, we studied the physical and chemical transformations that the polymer undergoes during exposure. [40] At this wavelength the polymer is not photochemically inert as in optical lithography in CA resists used at 193 and 248 nm. It is thus important to study the chemical and physical changes induces by the absorbed photons.

1.4.2 Research Objectives

The research done over the past four years as part of the PhD requirements has been concerned with the photochemistry of PAGs and polymers at 157, 193 and 248 nm, and with spectroscopic and imaging methods used to characterize the chemical and physical changes of the photoresist film.

Different PAGs, some of them provided by Rohm & Haas Electronics from Marlborough, MA, some of them synthesized in the lab, were analyzed and their acid formation abilities at different exposure wavelengths were studied. Most of the analytical methods employed fluorescent sensors for the detection of acid formed in thin polymer films.

Chapter 2 makes a brief presentation and introduction of the fluorescent molecules employed throughout the thesis.

Coumarin 6, a fluorescent sensor sensitive to the pH of the environment was extensively used to monitor and quantify acid formation in polymer films as a function of the incident dose. These results are presented in Chapters 3 and 4. PAGs with a high quantum yield at longer exposure wavelengths may be too absorbent at shorter wavelengths. It is necessary to develop more transparent

PAGs that will absorb less photons but still produce enough acid to allow deprotection of *t*-Boc groups in the exposed areas.

Although CCL has been previously determined, attempts to design and develop a protocol that would allow determination of CCL using fluorescent probes were made, and the result presented in Chapter 4.

In photolithography at 157 nm the absorbance of the materials employed for various resist formulations is the main problem. Even fluorinated terpolymers especially designed for photolithography in the VUV are not completely transparent. The high energy of the photons, combined with the high absorbance of the polymer lead to unavoidable photochemical reactions that involve the polymer. Thus the polymer matrix is not photochemically inert, undergoing chemical and physical changes. Fluorescence spectroscopy and microscopy, absorbance, atomic force microscopy and laser flash photolysis were the methods employed to monitor the transformations of the polymer. One of the interesting findings was that the polymer produced hydrofluoric acid, a corrosive photoproduct that may damage the optical parts. The results are presented in Chapter 5.

Pyrene and its derivatives are excellent fluorescent probes and some of the most studied by photochemists. Pyrene was employed as fluorescent probe in thin films obtained by spin casting solutions of polymers having different Tg. The goal of the project, taking advantage of pyrene's ability to form excimers, was to study the photophysical processes that occur during exposure at different wavelengths and the influence of the polymer's Tg on the behavior of the film. Spectroscopic techniques, as well as fluorescence microscopy were used to characterize the exposed films containing pyrene, and the results are presented in Chapter 6. Some of the results show interesting behavior of the pyrene-containing exposed polymer films after baking. It is possible to "erase" some of the images by thermal treatment, while others withstand long periods of baking without any change, depending on their polymer's Tg.

1.5 Future directions in lithography and computer chip manufacturing

The technology for manufacturing computer chips and DRAM memories will have to dramatically change in the future. CA photoresist work very well at 193 nm for resolution at 65 and 45 nm, using immersion 193 nm with water and high refractive index liquids. [41] However, as the size of the circuits shrinks, the problems and the costs rise dramatically. Acid diffusion from the exposed into unexposed areas is becoming a critical issue. Line edge roughness (LER), determined by the size of the polymer molecule, also starts to alter the developed image. [42] One solution would be to use polymers with lower molecular weight, namely oligomers. Double exposure at 193 nm is a possibility explored by some manufacturers and laboratories around the world.

Photolithography at 157 nm was seen as the next logical step after 193 nm. The high absorbance of the materials, the birefringence of CaF_2 optics, the high costs and just a minimal gain in resolution compared to 193 nm, determined the industry to announce in 2003 that they decided to skip 157 nm from the roadmap for microelectronics, focusing on different ways to improve dry and immersion 193 nm.

Since the size of the features depends on the wavelength of the incident light, it is clear that the next step will be the use of radiation at even shorter wavelength, the best candidate being extreme ultraviolet (EUV) light with a wavelength of 13.4 nm. [43, 44] The challenges in EUV lithography are also big. Everything absorbs at this wavelength, and the optics will have to be reflective. EUV is seen as the wavelength used to obtain features as small as 23 nm. For this to happen, completely new photoresists have to be developed. Polymers and CA are not an option, due to problems related to absorbance, acid diffusion in the unexposed areas and LER. New materials have already been tested, especially molecular glasses. [45-47] Molecular glasses consist of molecules having a high molecular weight (~ 1000 dalton), which do not crystallize.

CMOS (complementary metal-oxide structures) are obtained after filling the spaces from the silicon wafer obtained during the lithographic process with a metal, usually copper. CMOS are the basis of the microelectronics industry and are present in our everyday life in computers, TV sets, radios, MP3 players, DVD players, cars, cell phones, etc. Technologies that will be used to manufacture microelectronic devices in the so called post-CMOS era are only in exploratory stage.

Photolithography is employed not only for fabrication of computer chips, but for 3D integrated microcircuits as well. Microsystems technology (MST), and in particular MEMS (microelectromechanical systems) are now integrated with CMOS-based devices. For the manufacturing of MEMS diazonaphtoquinone/ novolac resists are currently used, but it is expected that in the near future CA amplified resists will be employed, in a tendency to decrease their feature size to below 1.0 micrometer. MEMS have found a wide area of applications such as sensors, micro-chromatographs, etc. Lab-on-a-chip is a concept introduced by analytical chemists and makes use of microchannels.

Nanomaterials open a new age of possibilities for microelectronics. The bottom-up approach is seen as a possible candidate to replace photolithography. Building structures following a given path is desirable, but there are many obstacles to be overcome.

Block-copolymers possess intriguing properties, form ordered structures and are also studied for a potential use in microelectronics. Carbon nanotubes are also interesting materials whose properties make them suitable for applications in microelectronics industry. [48]

1.6 References

(1) Anpo, M.; Yamashita, H., *Surface Photochemistry.* Wiley Series in Photoscience and Photoengineering, ed. Anpo, M. 1996, Chichester, New York, Brisbane, Toronto, Singapore: John WIley & Sons.

(2) Turro, N. J., *Modern Molecular Photochemistry.* 1991, Sausalito, Clifornia: University Science Books.

(3) Gilbert, A.; Baggot, J.; Wagner, P. J., *Essentials of Molecular Photochemistry.* 1991, Boca Raton, Ann Arbor, Boston, London.

(4) Valeur, B., *Molecular Fluorescence - Principles and Applications.* 2002, Weinheim, New York, Chichester, Singapore, Toronto: Wiley - VCH Verlag GmbH.

(5) Scaiano, J. C., *Nanosecond laser flash photolysis: a tool for physical organic chemistry*, in *Reactive intermediate chemistry*, Moss, R. A., Platz, M., and Jones, M., Editors. 2004, Wiley-Interscience: Hoboken, N.J. p. 847-871.

(6) Cosa, G.; Scaiano, J. C., "Laser Techniques in the study of drug photochemistry", *Photochem. Photobiol.* **2004**, *80,* 159-174.

(7) Lichtman, J. W.; Conchello, J.-A., "Fluorescence microscopy", *Nature Methods* **2005**, *2,* 910-919.

(8) Alivisatos, A. P., "Perspectives on the Physical Chemistry of Semiconductor Nanocrystals", *J. Phys. Chem.* **1996**, *100,* 13226-13239.

(9) Parak, W. J.; Gerion, D.; Pellegrino, T.; Zanchet, D.; Micheel, C.; Williams, S. C.; Boudreau, R.; Le Gros, M.; Larabell, C. A.; Alivisatos, P. A., "Biological applications of colloidal nanocrystals", *Nanotechnol.* **2003**, *14,* R15-R27.

(10) Alivisatos, P., "The use of nanocrystals in biological detection", *Nature Biotechnology* **2004**, *22,* 47-52.

(11) Maurel, V.; Laferriere, M.; Billone, P.; Godin, R.; Scaiano, J. C., "Free Radical Sensor Based on CdSe Quantum Dots with Added 4-Amino-2,2,6,6-Tetramethylpiperidine Oxide Functionality", *J. Phys. Chem. B* **2006**, *110,* 16353-16358.

(12) Galian, R. E.; Laferriere, M.; Scaiano, J. C., "Doping of photonic crystal fibers with fluorescent probes: possible functional materials for optrode sensors", *J. Mater. Chem.* **2006**, *16,* 1697-1701.

(13) *Introduction to Microlithography*, ed. Thompson, L., Willson, C. G., and Bowden, M. J. 1994, Washington, DC: American Chemical Society.

(14) Ito, H., *Chemical Amplification Resists for Microlithography*, in *Microlithography Molecular Imprinting*, Springer-Verlag, Editor. 2005: Berlin, Heidelberg. p. 37-425.

(15) Wallraf, G. M.; Hinsberg, W. D., "Lithographic Imaging Techniques for the Formation of Nanoscopic Features", *Chem. Rev.* **1999**, *99,* 1801.

(16) Michel, B.; Bernard, A.; Bietsch, A.; Delamarche, E.; Geissler, M.; Juncker, D.; Kind, H.; Renaulst, J.-P.; Rothuizen, H.; Schmid, H.; Schmidt-Winkel, P.; Stutz, R.; Wolf, H., "Printings meets lithography: Soft approaches to high-resolution patterning", *IBM J. Res. & Dev.* **2001**, *45,* 697-719.

(17) Ito, H., "Chemical amplification resists: History and development within IBM", *IBM J. Res. & Dev.* **2000**, *44,* 119-130.

(18) Ito, H.; Wilson, C. G.; Fréchet, J. M. J., *Symp. VLSI Technol.* **1982**, *260,* 262.

(19) Ito, H.; Wilson, C. G., "Chemical Amplification in the Design of Dry Developing Resist Materials", *Pol. Eng. Sci.* **1983**, *23,* 1012-1018.

(20) Feiring, A. E.; Crawford, M. K.; Farnham, W. B.; Feldman, J.; French, R. H.; Leffew, K. W.; Petrov, V. A.; Schadt, F. L.; Wheland, R. C.; Zumsteg, F. C., "Design of very transparent fluoropolymer resists for semiconductor manufacture at 157 nm", *J. Fluor. Chem.* **2003**, *122,* 11-16.

(21) Cho, S.; Jacobs-Klauck, A.; Yamada, S.; Xu, C. B.; Leonard, J.; Zampini, A., "Investigation of a fluorinated ESCAP based resist for 157 nm lithography", *Proc. SPIE* **2002**, *4690,* 522-532.

(22) Burnett, J. H.; Levine, Z. H.; Shirley, E. L., "Intrinsic birefringence in calcium and barium fluoride", *Phys. Rev. B* **2001**, *64,* 241102-241101 - 241102-241104.

(23) Moore, G. E., "Cramming more components onto integrated circuits", *Electronics* **1965**, *38*

(24) McKean, D. R.; Allen, R. D.; Kasai, P. H.; Schaedeli, U. P.; MacDonald, S. A., "Acid Generation and Acid Diffusion in Photoresist Films", *SPIE* **1992**, *1672,* 94-103.

(25) Reichmanis, E.; Houlihan, F. M.; Nalamasu, O.; Neenan, T. X., "Chemical Amplification Mechanism for Microlithography", *Chem. Mater.* **1991**, *3,* 394-407.

(26) MacDonald, S. A.; Willson, C. G.; Frechet, J. M. J., "Chemical Amplification in High-Resolution Imaging Systems", *Acc. Chem. Res.* **1994**, *27,* 151-158.

(27) Dektar, J. L.; Hacker, N. P., "Photochemistry of Diaryliodonium Salts", *J. Org. Chem.* **1990**, *55,* 639-647.

(28) Dektar, J. L.; Hacker, N. P., "Photochemistry of Triarylsulfonium Salts", *J. Am. Chem. Soc.* **1990**, *112,* 6004-6015.

(29) Mc Kean, U. S. D.; MacDonald, S. A., "Acid Photogeneration from Sulfonium Salts in Solid Polymer Matrices", *J. Polym. Sci. A: Polym. Chem.* **1989**, *27,* 3927.

(30) MacDonald, S. A.; Hinsberg, W. D.; Wendt, H. R.; Clecak, N. J.; Willson, C. G., "Airborne Contamination of Chemically Amplified Resist. 1. Indentification of Problem", *Chem. Mater.* **1993**, *5,* 348-356.

(31) Toriumi, M.; Satou, I.; Itani, T., "Vacuum ultraviolet spectra of fluorocompounds for 157 nm lithography", *J. Vac. Sci. Technol. B* **2000**, *18,* 3328-3331.

(32) Kunz, R. R.; Bloomstein, T. M.; Hardy, D. E.; Goodman, R. B.; Downs, D. K.; Curtin, J. E., "Outlook for 157 nm resist design", *J. Vac. Sci. Technol. B* **1999**, *17,* 3267-3272.

(33) Costela, A.; Garcia-Moreno, I.; Florido, F.; Figuera, J. M.; Sastre, R.; Hooker, S. M.; Cashmore, J. S.; Webb, C. E., "Laser ablation of polymeric materials at 157 nm", *J. Appl. Phys.* **1995**, *77,* 2343-2350.

(34) Brannon, J. H.; Lankard, J. R.; Baise, A. I.; Burns, F.; Kaufman, J., "Excimer laser etching of polyimide", *J. Appl. Phys.* **1985**, *58,* 2036-2042.

(35) Srinivasan, R.; Braren, B.; Dreyfus, R. W., "Ultraviolet laser ablation of polyimide films", *J. Appl. Phys.* **1987**, *61,* 372-376.

(36) Houlihan, F. A.; Hinsberg, W. D.; Morrison, M.; Sanchez, M. I.; Wallraff, G.; Larson, C.; Hoffnagle, J., "Determination of coupled acid catalysis-diffusion processes in a positive-tone chemically amplified phototresist", *J. Vac. Sci. Technol. B* **2000**, *18,* 1874-1885.

(37) Hinsberg, W.; Houle, F.; Sanchez, M.; Morrison, M.; Wallraf, G.; Larson, C.; Hoffnagle, J.; Brock, P.; Breyta, G., "Effect of Resist Components on Image Spreading During Postexposure Bake of Chemically Amplified Resists", *Proc. of SPIE* **2000**, *3999,* 148-154.

(38) Pohlers, G.; Barclay, G.; Razvi, A.; Stafford, C.; Barbieri, T.; Cameron, J. F., "Why do weak acids not work in 193-nm photoresists? Matrix effects on acid catalyzed deprotection", *Proc. SPIE* **2004**, *5376,* 79-93.

(39) Frenette, M.; Ivan, M. G.; Scaiano, J. C., "Use of fluorescent probes to determine catalytic chain length in chamically amplified resists", *Can. J. Chem.* **2005**, *83,* 869-874.

(40) Ivan, M. G.; Laferriere, M.; Sanrame, C. N.; Scaiano, J. C., "On the Question of Acid Generation upon 157-nm Laser Exposure of Fluorinated Polymers", *Chem. Mater.* **2006**, *18,* 2635-2641.

(41) Kusumoto, S.; Shima, M.; Wang, Y.; Shimokawa, T.; Sato, H.; Hieda, K., "Advanced materials for 193 nm immersion lithography", *Polym. Adv. Technol.* **2006**, *17,* 122-130.

(42) Pawloski, A. R.; Acheta, A.; Levinson, H. J.; Michaelson, T. B.; Jamieson, A.; Nishimura, Y.; Willson, C. G., "Line edge roughness and intrinsic bias for two methacrylate polymer resist systems", *J. Microlith. Microfab. Microsyst.* **2006**, *5,* 023001- 023001 - 023001- 023016.

(43) Bratton, D.; Yang, D.; Dai, J.; Ober, C. K., "Recent Progress in high resolution lithography", *Polym. Adv. Technol.* **2006**, *17,* 94-103.

(44) Silverman, P. J., "Extreme ultraviolet lithography: overview and development status", *J. Microlith. Microfab. Microsyst.* **2005**, *4,* 011006-1011006-1011005.

(45) Yang, D.; Chang, S. W.; Ober, C. K., "Molecular Glass photoresists for advanced lithography", *J. Mat. Chem.* **2006**, *16,* 1693-1696.

(46) Bratton, D.; Ayothi, R.; Felix, N.; Cao, H.; Deng, H.; Ober, C. K., "Molecular Glass Resists for Next Generation Lithography", *Proc. of SPIE* **2006**, *6153,* 61531D-61531 - 61531D-61539.

(47) Chang, S. W.; Ayothi, R.; Bratton, D.; Yang, D.; Felix, N.; Cao, H. B.; Deng, H.; Ober, C. K., "Sub-50 nm feature sizes using positive tone molecular glass resists for EUV lithography", *J. Mater. Chem.* **2006**, *16,* 1470-1474.

(48) Hoenlein, W., "New Prospects for Microelectronics: Carbon Nanotubes", *Jpn. J. Appl. Phys.* **2002**, *41(no1),* 4370-4374.

Fluorescent and Prefluorescent Sensors Used in Various Media

2. Fluorescent and Prefluorescent Sensors Used in Various Media

2.1 Introduction

In photolithography all the reactions occur within a thin polymer film of a few hundreds of nanometers, making it difficult for researchers to investigate the intermediates or the photoproducts using classic analytical or monitoring techniques. The amount of material confined in the very small volume of a thin resist film may be insufficient for techniques such as nuclear magnetic resonance (NMR), mass spectrometry or gel permeation chromatography (GPC). Thus, it is desirable to develop a technique that would allow detection of chemical or physical changes of the polymer matrix or the photoacid generators (PAGs) without having to strip many films and collect large amounts of the exposed materials, a task that would prove challenging.

A very sensitive and elegant technique has been previously reported; it makes use of fluorescent and prefluorescent probes added to the resist formulations. [1, 2, 3, 4] These probes will have their emission or absorption properties altered upon interaction with a certain species present or generated in the film. Embedding a fluorescent molecule that will sense the presence of another molecule or a change in the morphology of the polymer matrix is a fast and sensitive method. The emission signal of the sensor is immediately affected and it can be recorded using a spectrophotometer. If one looks at the formation of acid in the exposed areas, it is possible to record, besides the emission spectrum, a latent image using fluorescence microscopy.

Fluorescent sensors are used in a variety of media, being continuously developed and improved.[5, 6] A basic condition for a molecule to show fluorescence is to absorb light at the desired wavelength, so it has to contain a chromophore in its

structure. A chromophore is not necessarily a fluorophore. Once in excited state, a molecule has plenty of possibilities to use the excess energy it gained through absorption of a photon. [6, 7] The *Jablonski* diagram from figure 2-1 shows some of the paths that a molecule may undergo upon absorption of light.

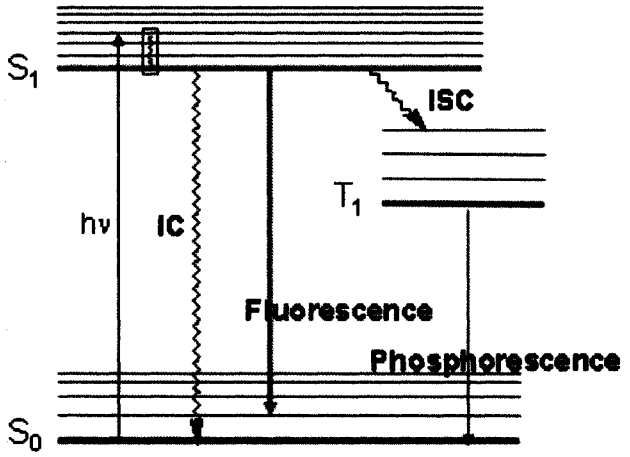

Figure 2-1. Jablonski diagram showing possible pathways for a molecule upon absorption of a photon; IC- internal conversion, ISC- intersystem crossing, S_0 – singlet ground state, S_1 – singlet excited state, T_1 – triplet state.

As shown in figure 2-1, absorption of a photon provides an excess energy that will cause the molecule to reach the first excited singlet state, S_1. From an upper vibrational level corresponding to S_1, the molecule will decay very fast to the S_1 level through a process called vibrational relaxation. From S_1 there could take place an internal conversion (IC) when the energy is released to the environment as heat, or the molecule may emit a photon of less energy than the one absorbed, a process called fluorescence. Although a spin-forbidden transition, depending on the molecular structure, the presence of other compounds, and the surroundings, the molecule may undergo intersystem crossing (ISC) from S_1 to T_1, the lowest excited triplet state. From T_1 the molecule may go back to its ground state by emitting a

photon of an even longer wavelength than in the case of fluorescence, a process called phosphorescence.

There are many de-excitation pathways that compete with fluorescence: internal conversion, energy transfer, electron transfer, proton transfer, conformational change, intra- or intermolecular charge transfer, excimer or exciplex formation, intersystem crossing, or photolysis.[5, 6, 8] Fluorescence is influenced by many factors such as pH, temperature, viscosity, polarity, pressure, oxygen and other quenchers. [6] Due to the high sensitivity of the fluorescent molecules towards the surrounding environment, they have found wide use in biological and medicinal applications, materials science, and analytical chemistry. Other properties of fluorescent molecules are exploited in gathering information about free volume, diffusion, microviscosity of polymers or kinetics of polymerization. [6, 9] Solid surfaces or three-dimensional materials such as clays, zeolites or porous glasses were also characterized using fluorescent sensors. [6, 10-12]

When monitoring different properties of an environment (acidity, polarity, temperature, etc), the fluorescent probe can be physically mixed with the surroundings or may be covalently attached to a surface, polymer or peptide. [6] For analytical purposes, the fluorescent probes may react with the analyte and form a complex with different emission properties compared to the initial probe: shift in emission wavelength, have their fluorescence quenched or enhanced following formation of the complex. For example, biologically compatible fluorescent molecules are used to detect the presence of reactive oxygen species in cells. [13] The presence of reactive oxygen species in excess such as singlet oxygen, superoxide, hydroxyl, hydroperoxyl, alkoxyl or peroxyl radicals may lead to oxidative stress, DNA damage, mutagenesis and in the end to cell death. Thus, it is important to monitor and quantify presence of these species inside cells, and many fluorescent sensors with high sensitivity and selectivity have been developed. [13]

Due to the advancement in optical instrumentation, it is possible to monitor fluorescence of a single molecule through a technique called single molecule fluorescence.

One important parameter used to characterize a fluorescent molecule is the *fluorescence lifetime*, (τ).[6, 7] The fluorescence lifetime is given by the following equation:

$$\tau = \frac{1}{k_f^S + k_{IC}^S + k_{ISC}} \qquad 2.1$$

where τ - fluorescence lifetime, k_f^S – rate constant for radiative deactivation from S_1 to S_0 by emission of a photon ($S_1 \rightarrow S_0$), k_{IC}^S – rate constant for deactivation of the S_1 excited state through internal conversion, k_{ISC} – rate constant for deactivation from S_1 state to T_1 state through intersystem crossing, $S_1 \rightarrow T_1$.

It is possible to monitor the decay of the fluorescence and calculate the fluorescence lifetime of a molecule by using laser flash photolysis in the picoseconds regime. [14-16] A fluorescent probe may have different fluorescence lifetimes depending of the environment. Thus, besides spectroscopic parameters such as emission wavelength and intensity of emission, one may use the fluorescence lifetime of the probe to gather information about the monitored property or analyte. Newer optical instrumentation allows imaging of fluorescence lifetimes of molecules in thin films or on surfaces even for single molecules. [17]

One of the most widely used techniques in biology, medicine, materials science and microelectronics is fluorescence microscopy. [18, 19] Instead of recording the emission spectra with a fluorimeter, one records an image using an optical microscope having a lamp as excitation source, and different sets of excitation and emission filters. Fluorescence imaging offers numerous advantages over

spectroscopy, especially in cases where the confinement of the fluorophore in a certain area or volume is crucial. Penetration of a fluorophore through the cell membrane may be monitored with an optical microscope, and changes in fluorescence recorded with a digital camera. [18, 19] The same technique is used, for example, to record latent images of photoresist films exposed to laser radiation through a mask, when acid diffusion from the exposed areas towards the unexposed ones, an unwanted process, may be monitored using fluorescence imaging. [1-4, 20]

The work presented in this thesis makes use on a large scale of fluorescent and prefluorescent molecules employed as sensors for different chemical species or properties of the environment.

2.2 Results and Discussion

Various fluorescent sensors were used in different projects throughout this thesis. The fluorescent molecules were used either for analytical purposes, as detectors of different species, or as sensors capable of showing modifications of the environment. Experiments involving some of the fluorescent probes are presented in detail in the next chapters.

2.2.1 Use of Coumarin 6 as acid sensor in thin polymer films

Chemically amplified photoresists are currently used in computer chip manufacturing, and have been the choice for microelectronic industry for the past two decades. [21] These resists contain a photochemically active ingredient called photoacid generator (PAG), which upon absorption of a photon may photolyse, leading to formation of a Brönsted acid and other photoproducts. During a thermal treatment of a suitably designed film, the acid will catalyze deprotection of some pendant acid labile groups from the polymer chain, causing a change in solubility in the exposed regions, as opposed to the unexposed ones. This change will be exploited during the developing step, when either the exposed regions will be removed (positive tone photoresist) or the unexposed regions will be developed, leaving the exposed regions of the film on top of the substrate (negative tone resists). The acid catalyzes the deprotection, then is recovered and catalyzes another reaction, to a total of up to 800 – 1000 deprotection reactions per proton, scheme 2-1. [22] The number of pendant groups deprotected by one proton gives the catalytic chain length (CCL), an important parameter in CA resists. It is important to quantify the amount of acid formed in polymer films as a function of the exposure dose. Various techniques have been developed throughout the past two decades. [21] The technique used in the present study makes use of a fluorescent molecule,

Coumarin 6, capable of changing its absorption and emission spectra upon protonation, figure 2-2.

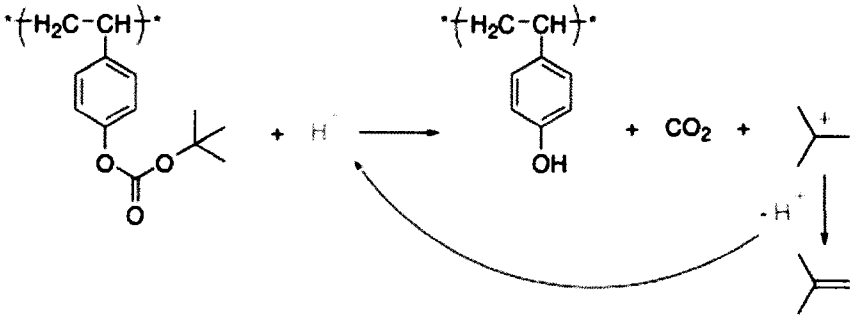

Scheme 2-1. Chemical amplification mechanism showing deprotection of a *t*-Boc protected polymer - poly(*p*-*t*-butyloxycarbonyloxystyrene) (PBOCST), formation of poly(*p*-hydroxystyrene) (PHOST), carbon dioxide, and isobutene with recovery of the proton.

Corrent *et al.* used ^{1}H NMR to detect the first protonation site in Coumarin 6, proving that the N atom from the heterocyclic ring protonates first. [23] In the presence of an excess of acid, Coumarin 6 may be double protonated, with the proton attached to the second N atom from the molecule, scheme 2-2.

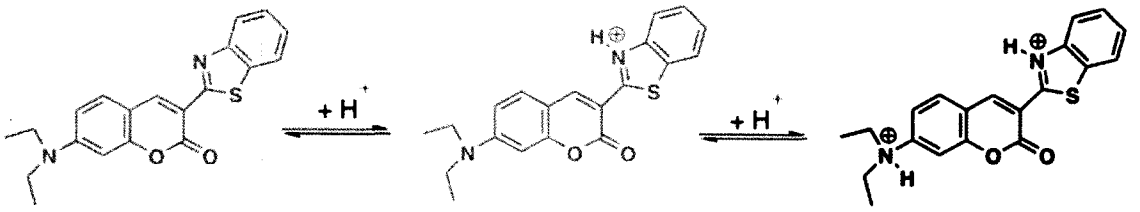

Scheme 2-2. Reaction between Coumarin 6 (C6) and the proton, leading to formation of monoprotonated Coumarin 6 ($C6H^{+}$) or double protonated Coumarin 6.

In the presence of excess of acid, Coumarin 6 exhibits a peak in absorption centered at ~ 380 nm, characteristic to the double protonated form of the dye. The absorbance and fluorescence spectra of neutral and monoprotonated forms of C6 are shown in figure 2-2.

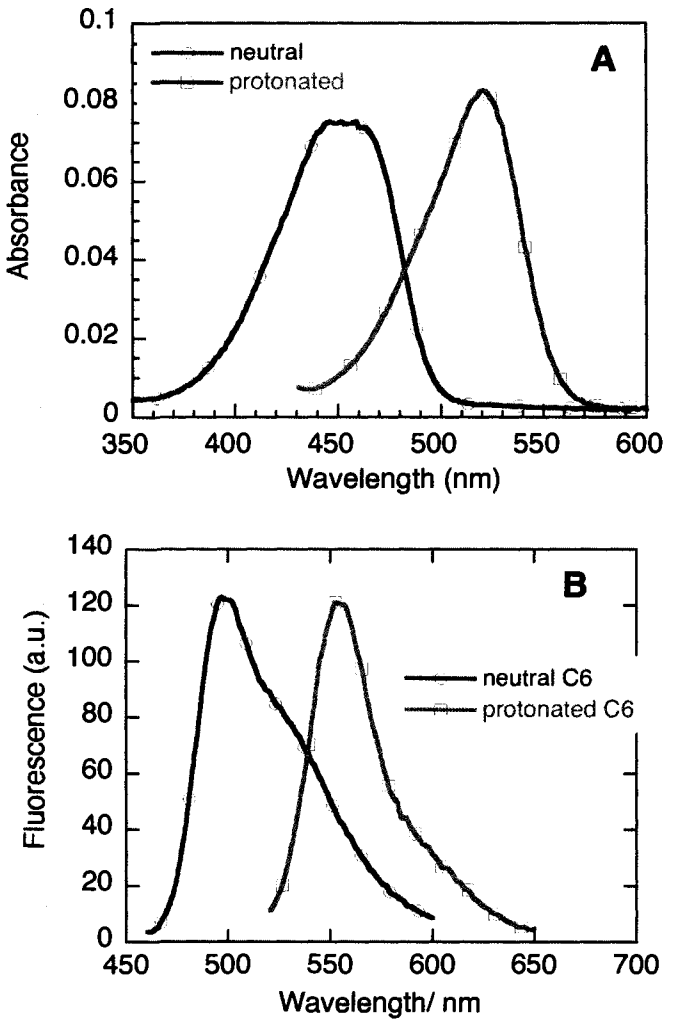

Figure 2-2. Absorption (A) and fluorescence spectra (B) of neutral (green) and monoprotonated (red) Coumarin 6 embedded in thin films (thickness ~ 800 nm) of poly(methyl methacrylate) (PMMA) containing triphenylsulfonium triflate (TPS-OTf) as photoacid generator. The spectra of neutral Coumarin 6 were recorded prior to exposure, while the absorption and emission of the protonated Coumarin 6 were recorded after exposure to UV radiation (mostly 254 nm) from a mercury lamp in a HTG exposure unit. The excitation wavelengths were 450 nm for the neutral form and 510 nm for the monoprotonated form of Coumarin 6. The composition of the spin coated solution, expressed as mass %, was 14.92 % PMMA, 84.58 % 2-heptanone, 0.44 % TPS-OTf, and 0.07 % Coumarin 6.

The absorbance and fluorescence spectra were obtained using thin films of poly(methyl methacrylate) (PMMA) exposed to radiation at 254 nm from a mercury lamp in an exposure unit. The films were obtained by spin coating, on top of an 1 inch (2.54 cm) quartz discs, a few drops from a solution containing 0.3000 g PMMA (14.92 %), 1.7000 g 2-heptanone (84.58 %), 0.0090 g TPS-OTf (0.44 %), and 0.0015 g Coumarin 6 (0.07 %). The semiconductor industry usually expresses the amount of PAG and other additives as % weight relative to the polymer loading. This way of expressing the composition of the photoresists solution will be employed throughout this thesis. To a solution containing 15.0 wt % PMMA and 85.0 wt % 2-heptanone were added 9.0 mg TPS-OTf and 1.5 mg Coumarin 6, representing 3.0 % and 0.5 % based on polymer weight. After spin coating at 3000 rotations per minute (rpm) for 20 s, the films were baked inside an oven at 90 °C for 60 s, allowing the solvent to evaporate. This step is called post application baking (PAB). After PAB the films were rapidly cooled to room temperature (RT) by placing them on a metallic surface, and then exposed to light at 254 nm. The next step was baking inside the oven at 90 °C for 60 s in order to help the acid diffuse through the PMMA film and protonate Coumarin 6, a step called post exposure baking (PEB). The same film was used to record absorbance and fluorescence of the neutral Coumarin 6, then following exposure it was used to record fluorescence and absorbance of the protonated Coumarin 6. For the fluorescence spectra the excitation wavelengths were 450 nm for the neutral C6 and 510 nm for the monoprotonated Coumarin 6, $C6H^+$.

The large shift (~ 60 nm) towards the red in absorption and emission spectra of Coumarin 6 upon protonation makes it an ideal sensor for acid in different media. [2, 23, 24] The fluorescence mechanism involves charge-transfer from the electron rich diethylamino moiety to the heterocyclic benzothiazole. [23] The same observation was made by Hora Machado *et al.*, who noticed that a compound similar to Coumarin 6, 3-(benzoxazol-2-yl)-7-(N, N, -diethylamino)chromen-2-one (S is replaced by O in the benzothiazole ring) shows a dependence of the emission

wavelength on the polarity and/ or hydrogen bonding ability of the solvent used, with a bathochromic shift in more polar solvents. [25] Their calculations showed that in excited state the C – C bond between the benzoxazole ring and the chromen ring is 1.391 Å, compared to 1.457 Å in ground state. This means that in excited state the conjugation extends over the coumarin ring. The C – N bond between the N from the diethylamino group and the coumarin is 1.358 Å in S_1 state compared to 1.376 Å in S_0 state. This proves that the non-bonding electrons from the N atom are involved in electron coupling in excited state, bringing a $^1(n, \pi^*)$ component into the excited singlet state S_1, which has a predominantly $^1(\pi,\pi^*)$ character, lowering the S_0-S_1 energy gap. Double protonation at the two N atoms perturbs the charge transfer mechanism and increases the energy gap between S_0 and S_1. The absorbance is shifted into the blue region, at ~ 380 nm. Corrent *et al.* reported that the pKa = 1.6 for the neutral Coumarin 6 to monoprotonated Coumarin 6 equilibrium in 50/ 50 water/ methanol solution. [23] Coumarin 6 interacts not only with Brønsted acids, but with Lewis acids as well. $AlCl_3$ added into a solution of Coumarin 6 in trichlorobenzene caused a change in the absorption spectrum, with a shift of the maximum from ~ 450 to ~ 520 nm. [23] As it will be shown in future chapters, Coumarin 6 was used also in experiments involving fluorescence microscopy, with the goal of capturing latent images showing acid formation in the exposed regions of thin polymer films containing a PAG and the dye.

2.2.2 Use of a Coumarin 4 derivative as fluorescence sensor for deprotection

One of the most important parameters of a chemically amplified resist is the catalytic chain length (CCL). CCL is given by the number of *t*-Boc deprotected groups per proton, and it has previously been reported to be in the range of 100 – 1000. [22] The usual method consist in quantification of *t*-Boc deprotected groups by following the disappearance of the IR peak characteristic to the carbonyl group at ~ 1750 cm^{-1}.

Using fluorescence sensors we attempted to develop a protocol that would allow detection of the CCL using fluorescence spectroscopy. Coumarin 6 was employed in acid-base titration in PMMA films in order to quantify the amount of acid generated during exposure. 7-hydroxy-4-methylcoumarin (Coumarin 4, C4) has been previously reported as a fluorescent dye that shows differences in emission spectra depending on the environment or the solvent. [26] For the current project C4 was protected at the hydroxyl group with a *tert*-butoxycarbonyloxy (*t*-Boc) group, mimicking the *t*-Boc protected polymers used in the CA photoresists. The 7-*tert*-butoxycarbonyloxy-4-methylcoumarin (C4TBOC) probe was synthesized by Mathieu Frenette, and reported to work as an excellent prefluorescent probe for spectroscopic measurements, with absorbance centered at ~ 320 nm, and fluorescence maximum at ~ 380 nm. [1, 27] More results and discussion involving C4TBOC are presented in chapter 4.

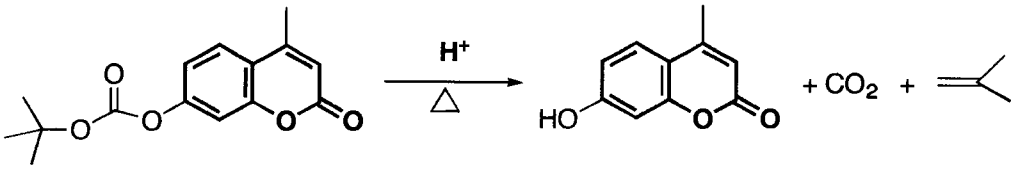

C4TBOC
Non- fluorescent

C4
Fluorescent

Scheme 2-3. Deprotection of 7-(tert-butoxycarbonyl-oxy)-4-methylcoumarin (C4-TBOC) catalyzed by acid, with formation of fluorescent 7-hydroxy-4-methylcoumarin (C4).

2.2.3 Detection of Fluoride Using Fluorescent Sensors

The high energy that the photons at 157 nm possess (7.9 eV) may cause formation of HF in fluorinated polymers that were proposed to be used in photolithography at 157 nm. [28, 29] Formation of hydrofluoric acid is an unwanted side reaction, since HF is highly corrosive and can damage the expensive optical parts. Thus detection of HF is an important task. Since fluorescence is a very sensitive technique, we decided to use fluorescent sensors that would change their emission properties upon interaction with a fluoride anion. Previous reports in literature showed that it was possible to detect different anions using fluorescent sensors, [30-32] and in particular fluoride. [33-36]

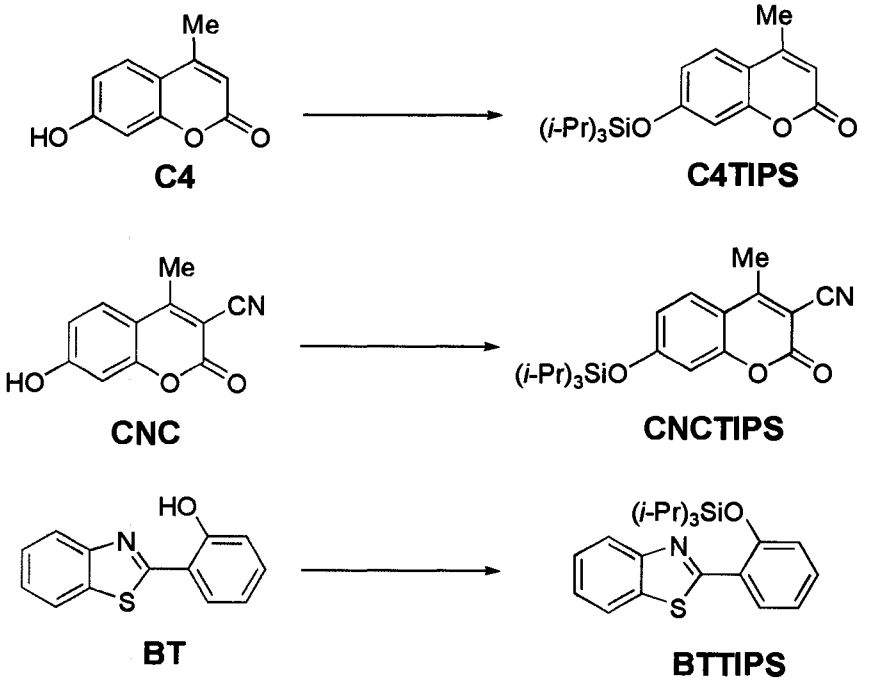

Scheme2-4. Reaction schemes for obtaining the fluoride probes

The fluorescent sensors presented in scheme 2-4 were synthesized by Dr. Carlos Sanrame. A detailed experimental procedure employed for the synthesis of

these molecules will be presented in a publication that is presently in preparation The fluorescent probes 7-Hydroxy-4-methyl-2-oxo-2*H*-chromene-3-carbonitrile (CNC), 2-Benzothiazol-2-yl-phenol (BTP), and 7-Hydroxy-4-methyl-chromen-2-one (C4) were functionalized with *tri*-isopropylsilyl-chloride (i-Pr)$_3$SiCl, in the presence of imidazole and using dimethylformamide (DMF) as solvent at 85 °C. Upon functionalization with (i-Pr)$_3$SiCl, the new molecules, CNCTIPS, BTTIPS and C4TIPS respectively, either show fluorescence in a different region (CNCTIPS and BTTIPS), or their fluorescence is quenched (C4TIPS). Their initial fluorescence is restored upon reaction with fluoride, when the initial fluorescent molecule is formed, scheme 2-5. Fluoride has a well-known affinity for the Si-O bond, thus even small amounts of fluoride may be detected using these sensors. Fluorescence microscopy and spectroscopy were employed to study films of a fluorinated polymer containing C4TIPS, exposed to laser radiation at 157 nm, and the detailed results are presented in chapter 5. [2]

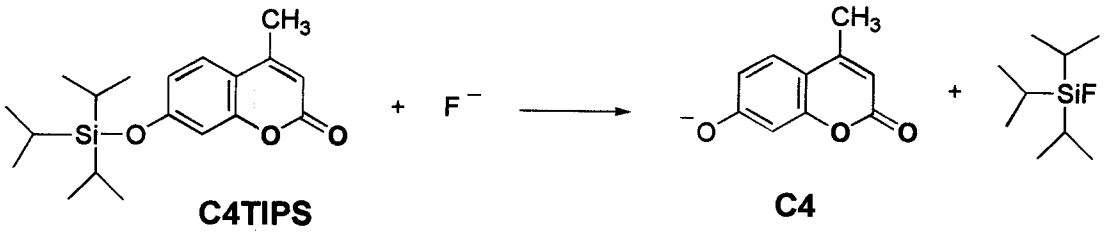

C4TIPS **C4**

Scheme 2-5. Reaction between non-fluorescent C4TIPS and fluoride anion, with formation of fluorescent Coumarin 4 (C4) and triisopropylsilyl fluoride.

Initial screening of these fluoride sensors showed that C4TIPS gave very good results in thin films and solution, while CNCTIPS and BTTIPS performed better especially in solution. Experimental results and discussion involving C4TIPS as prefluorescent probe are shown in chapter 5.

Absorbance and fluorescence spectra in solution were recorded for CNCTIPS, 5.0 x 10^{-6} M in tetrahydrofuran (THF), figure 2-3. The source of fluoride anions was tetrabutylammonium fluoride (TBAF) dissolved in THF. A stock solution of TBAF, 1.0 M in THF, from Aldrich, was diluted with THF (inhibitor free, from Aldrich), obtaining 5.0 mL TBAF 1.5 x 10^{-4} M in THF. From this solution, aliquots of 10.0 or 20.0 μL (microliter) were added to a quartz cuvette (1.0 cm light path) containing 3.0 mL (milliliter) CNCTIPS 5.0 x 10^{-6} M in THF, then absorbance was recorded after the solution was left in the sample compartment for 2 minutes, with occasional stirring. This procedure was repeated each time aliquots of TBAF were added. The absorption spectra are shown in figure 2-3 A.

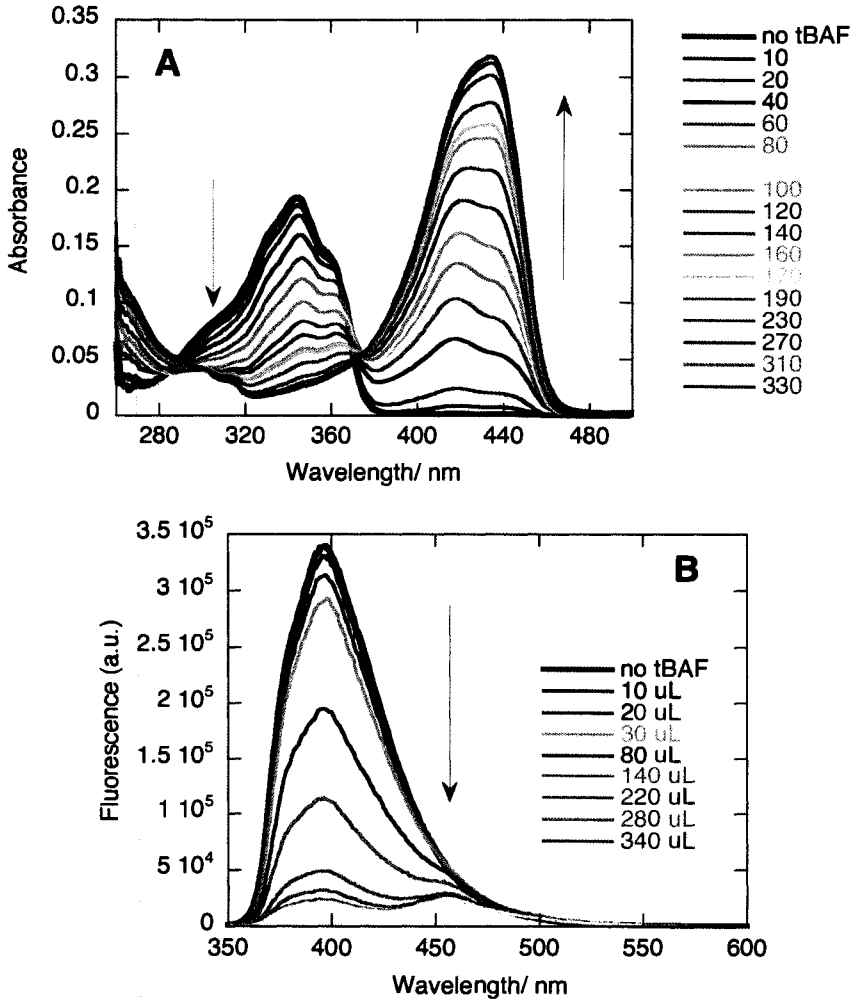

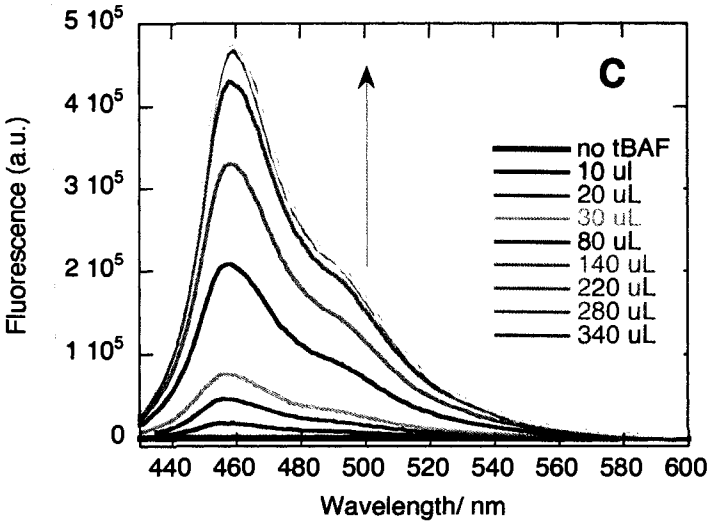

Figure 2-3. Absorbance (A) and fluorescence (B, C) spectra of CNCTIPS 5.0 x 10^{-6} M in THF to which aliquots of 10 or 20 μL of TBAF 1.5 x 10^{-4} M in THF were added. The values in the legend represent the total volume of TBAF in THF added until that point. For the fluorescence spectra the excitation wavelengths were 345 nm (B) and 425 nm (C). The same rectangular quartz cuvette, 1.0 cm x 1.0 cm was used for both absorbance and fluorescence experiments.

From the absorption spectra, figure 2-3 A, it is clear that as TBAF is added, there is a transformation of one species into another, supported by the isosbestic point at 372 nm. This reaction is the deprotection of CNCTIPS and formation of CNC, which has an absorption maximum at ~ 430 nm. The spectrum of the new species shows two peaks centered at ~ 420 and 440 nm. While at small volumes of TBAF added the intensity is higher at 420 nm, after 160 μL were added, the intensities of these two peaks are similar. At volumes of TBAF higher than 160 μL, the absorbance at 440 nm is higher compared to the peak at 420 nm. This behavior may be caused by the changes in the polarity and the ionic strength of the solvent as TBAF is added. Previous reports showed a dependence of the emission spectra of C4 on the polarity of the solvent. [26] The fact that the absorbance of CNC is higher than the starting CNCTIPS may be due to a higher extinction coefficient of CNC compared to CNCTIPS, since the number of moles is the same for both species.

The two graphs from figure 2-3 B and C show fluorescence spectra corresponding to the disappearance of CNCTIPS (fig 2-3 B) and formation of CNC (figure 2-3 C). Both CNC and CNCTIPS are fluorescent, with CNC showing a higher intensity in the emission after 280 μL TBAF in THF were added. Adding more TBAF does not lead to an increase in fluorescence, nor a decrease, showing that all CNCTIPS was deprotected. The way to discriminate between these two species is to use different excitation wavelengths, preferably monitoring the appearance of a signal rather than a disappearance, such as formation of CNC using excitation at 425 nm. In terms of absorbance, CNC absorbs ~ 1.5 times more compared to CNCTIPS. In terms of emission intensity, CNC (λ_{ex} = 425 nm) shows a fluorescence intensity that is ~ 1.35 times higher than the starting value of CNCTIPS (λ_{ex} = 345 nm).

The ratio between the number of moles of TBAF in a volume of 10 μL of TBAF 1.5 x 10^{-4} M in THF relative to the number of moles of CNCTIPS in 3.0 mL solution 5.0 x 10^{-6} M is 1 : 10. Thus, after addition of 100 μL TBAF in THF the molar ratio is TBAF : CNCTIPS = 1 : 1. Since the reaction is equimolar, one would expect that addition of more TBAF should not lead to an increase in fluorescence, since all CNCTIPS should be deprotected. As seen from figure 2-3 this is not the case, since the absorbance of CNC doubles upon addition of TBAF in THF up to ~ 270 μL, then it remains constant. This means that there is a need for ~ 2.7 moles of TBAF to deprotect 1.0 moles of CNCTIPS. This may be caused by the fact that TBAF is in equilibrium between the dissociated ions and the non-dissociated form in THF.

Another probe synthesized in the lab and tested in THF against TBAF is BTTIPS, whose structure is shown in chart 2-1. The absorbance spectra in figure 2-4 A were recorded after addition of 10 or 20 μL aliquots of 1.5 x 10^{-4} M TBAF in THF to 3.0 mL BTTIPS 5.0 x 10^{-6} M in THF. The solution was in a 1.0 cm x 1.0 cm quartz cuvette, inside the spectrophotometer. After each addition it was allowed two

minutes for the reaction to complete, occasionally stirring. The excitation wavelength used for the fluorescence measurements was 320 nm. The same sample was used to record the absorption and fluorescence spectra, even though in figure 2-4 B there are fewer traces than in the case of absorbance. This was done in order to have a less crowded graph, and to easily notice the small decrease in fluorescence between the trace obtained with 230 and 320 μL.

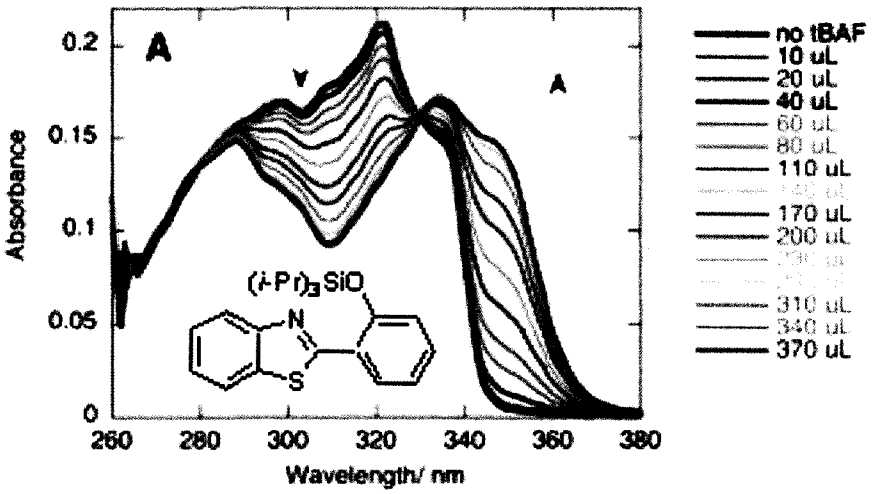

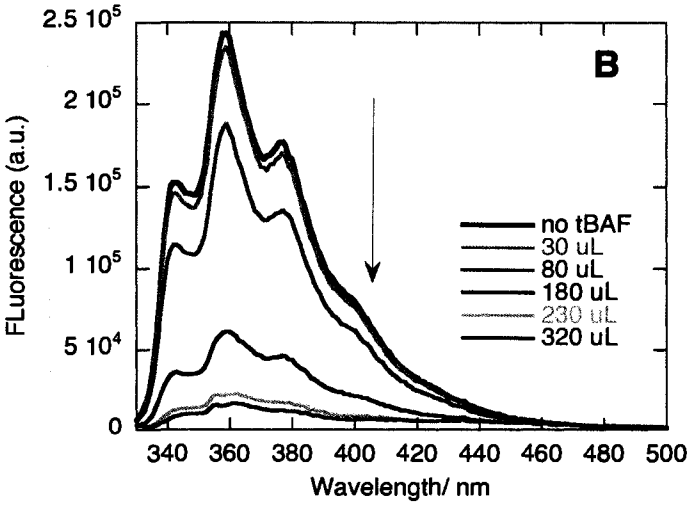

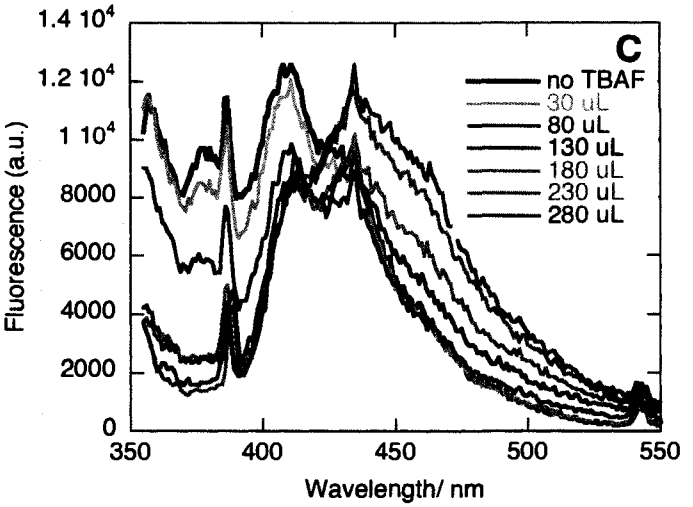

Figure 2-4. Absorbance (A) and fluorescence (B, C) of 3.0 mL BTTIPS 5.0 x 10^{-6} M in THF to which 10 or 20 μL aliquots of 1.5 x 10^{-4} M TBAF in THF were added. The excitation wavelengths for fluorescence were 320 nm (B) and 348 nm (C). The solutions were in rectangular quartz cuvettes, 1.0 cm optical path.

The absorbance spectra show a neat transformation from one species (BTTIPS) into another one (BTP), as indicated by the isosbestic point at 330 nm. The peak at 320 nm decreases, while a new one appears at 348 nm. The fluorescence spectra show a decrease in fluorescence as TBAF is added in increasing amounts. Excitation at 347 nm did not lead to any clear trend as it was the case in figure 2-4 B. After an initial decrease in fluorescence, the intensity increased and a new peak at 435 nm appeared.

The clear change in absorbance and the decrease in fluorescence as a function of the amount of TBAF show that BTTIPS works well as a fluoride sensor. The change in absorbance is directly proportional to the amount of TBAF added until ~ 280 μL, a value similar to that obtained in the case of CNCTIPS. Above this value the intensity of the peak at 348 nm is constant. This may prove that it is indeed a matter of how much TBAF is in its dissociated form in THF, this being the limiting factor for the presence of F^- in solution; 1 out of 2.8 moles of TBAF is dissociated.

2.2.4 Pyrene as a Fluorescent Sensor in Polymer Films

Pyrene is a polyaromatic hydrocarbon that possesses unique photochemical and photophysical properties. [7, 8] These properties have made pyrene and its derivatives a group of extensively studied molecule by photochemists. An interesting property of pyrene is its ability to form excimers. An excimer is an entity consisting of two pyrene molecules in a sandwiched-like arrangement. The name is derived from the words "excited" and "dimer". The excimer is formed when a molecule in excited state encounters another pyrene molecule in ground state, chart 2-1. If the distance between the two molecules is of ~ 3.5 Å, then some of the energy from the excited molecule is transferred to the one in ground state, forming an excimer with the energy intermediate between the ground state and the excited state.

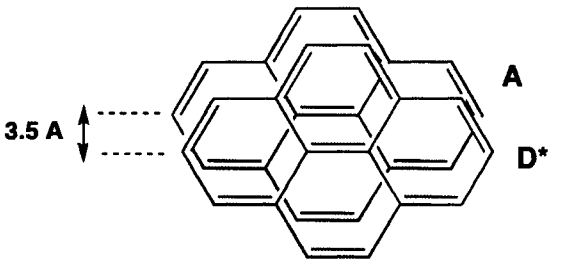

Chart 2-1. Representation of a pyrene excimer formed between a molecule in excited state (D*) and a molecule in ground state (A).

The fluorescence and absorption of pyrene, shown in figure 2-5, are influenced by the environment. The ability of pyrene to form excimers, as well as its fluorescence sensitivity towards different properties of the surroundings (polarity, viscosity, temperature) make it a suitable fluorescent probe in thin polymer films, Langmuir-Blodget films, clays, zeolites, and micelles. [37-40]

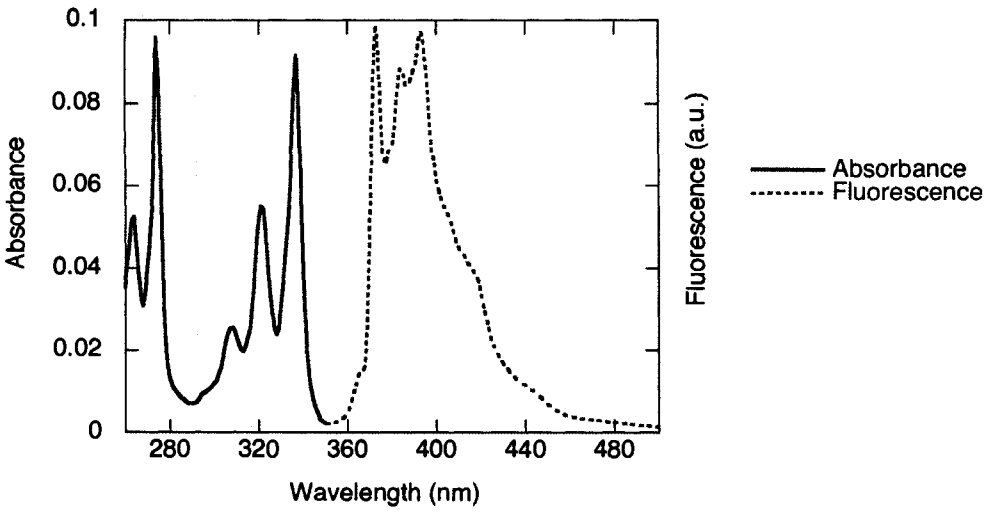

Figure 2-5. Absorbance (continuous line) and fluorescence (dashed line) of pyrene in a thin PMMA film. The spectra were recorded using a thin PMMA film obtained by spin coating at 2000 rpm for 20 s a solution containing 85 wt % 2-heptanone (solvent), 15 wt % PMMA and Pyrene 0.33 % relative to the dry polymer weight. The excitation wavelength for the fluorescence spectrum was 330 nm.

Use of pyrene in polymer films serves two purposes and the results and discussion are presented in chapter 6. Pyrene has been used as dopant in poly(methyl methacrylate) in photolithography at 308 nm. [41] Its role was to help induce depolymerization in the exposed areas, thus creating a difference in solubility between the exposed and the unexposed regions. Another reason why we studied pyrene in thin films was related to the sensitivity of its fluorescence towards the environment. Photochemical and photophysical properties of polymer films exposed to laser radiation at 157, 193, and 248 nm would influence the emission properties of pyrene, and this would be easily detectable using fluorescence spectroscopy and microscopy.

2.3 Conclusions

Fluorescence is a sensitive and powerful technique, allowing detection of different species even at concentrations in the micromolar regime. Fluorescent probes presented in this chapter work in different reaction media like thin polymer films or solution, detecting different species such as ions or radicals. Fluorescence techniques span a large area, with applications in kinetics, analytical chemistry, polymer study, and microelectronic industry.

The properties and applications of the fluorescent probes briefly introduced in this chapter will be largely discussed in the next chapters.

2.4 References

(1) Frenette, M.; Coenjarts, C.; Scaiano, J. C., "Mapping Acid-Catalyzed Deprotection in Thin Polymer Films: Fluorescence Imaging Using Prefluorescent 7-Hydroxycoumarin Probes", *Macromol. Rapid. Comm.* **2004**, *25,* 1628-1631.

(2) Ivan, M. G.; Laferriere, M.; Sanrame, C. N.; Scaiano, J. C., "On the Question of Acid Generation upon 157-nm Laser Exposure of Fluorinated Polymers", *Chem. Mater.* **2006**, *18,* 2635-2641.

(3) Mason, M. D.; Ray, K.; Pohlers, G.; Cameron, J. F.; Grober, R. D., "Probing the Local pH of Polymer Photoresist Films Using a Two-Color Single Molecule Nanoprobe", *J. Phys. Chem. B* **2003**, *107,* 14219-14224.

(4) Scaiano, J. C.; Laferriere, M.; Ivan, M. G.; Taylor, G. N., "A Protocol for the Verification of Acid Generation in 157 nm Lithography", *Macromolecules* **2003**, *36,* 6692-6694.

(5) Lakowicz, J. R., *Principles of Fluorescence Spectroscopy.* 1999, New York: Kluwer Academic/ Plenum.

(6) Valeur, B., *Molecular Fluorescence - Principles and Applications.* 2002, Weinheim, New York, Chichester, Brisbane, Singapore, Toronto: Wiley-VCH Verlag GmbH.

(7) Gilbert, A.; Baggot, J.; Wagner, P. J., *Essentials of Molecular Photochemistry.* 1991, Boca Raton, Ann Arbor, Boston, London: Blackwell Scientific Publications.

(8) Turro, N. J., *Modern Molecular Photochemistry.* 1991, Sausalito, California: University Science Books.

(9) Ballesteros, O. G.; Maretti, L.; Sastre, R.; Scaiano, J. C., "Kinetics of Cap Separation in Nitroxide-Regulated "Living" Free Radical Polymerization: Application of a Novel Methodology Involving a Prefluorescent Nitroxide Switch", *Macromolecules* **2001**, *34,* 6184-6187.

(10) Anpo, M.; Yamashita, H., *Surface Photochemistry*. Wiley Series in Photoscience and Photoengineering, ed. Anpo, M. Vol. 1. 1996, Chichester, New York, Brisbane, Toronto, Singapore: John Wiley & Sons.

(11) Ramamurthy, V., *Surface Photochemistry*. Wiley Series in Photoscience and Photoengineering, ed. Anpo, M. Vol. 1. 1996, Chichester, New York, Brisbane, Toronto, Singapore: John Wiley & Sons.

(12) Scaiano, J. C.; Garcia, H., "Intrazeolite Photochemistry: Toward Supramolecular Control of Molecular Photochemistry", *Acc. Chem. Res.* **1999**, *32,* 783-793.

(13) Gomes, A.; Fernandes, E.; Lima, J. L. F. C., "Fluorescence probes used for detection of reactive oxygen species", *J. Biochem. Biophys. Meth.* **2005**, *65,* 45-80.

(14) Alonso, E. O.; Johnston, L. J.; Scaiano, J. C.; Toscano, V. G., "Laser Flash Photolysis Studies of Carbocations Generated from (Naphthylmethyl)phosphonium Chlorides", *J. Am. Chem. Soc.* **1990**, *112,* 1270-1271.

(15) Cosa, G.; Vinette, A.; McLean, J. R. N.; Scaiano, J. C., "DNA Damage Detection Technique Applyiing Time-Resolved Fluorescence Measurements", *Anal. Chem.* **2002**, *74,* 6163-6169.

(16) Cosa, G.; Scaiano, J. C., "Laser Techniques in the Study of Drug Photochemistry", *Photochem. Photobiol.* **2004**, *80,* 159-174.

(17) Szmancinski, H.; Lakowicz, J., "Fluorescence lifetime-based sensing and imaging", *Sensors and Actuators B* **1995**, *29,* 16-24.

(18) Pepperkok, R.; Ellenbrg, J., "High-troughput fluorescence microscopy for systems biology", *Nature Reviews* **2006**, *7,* 690-696.

(19) Lichtman, J. W.; Conchello, J.-A., "Fluorescence Microscopy", *Nature Methods* **2005**, *2,* 910-919.

(20) Ray, K.; Mason, M. D.; Grober, R. D., "Quantum Yield of Photoacid Generation in 193-nm Chemically Amplified Resists by Fluorescence Imaging Spectroscopy", *Chem. Mater.* **2004**, *16,* 5726-5730.

(21) Ito, H., *Chemical Amplification Resists for Microlithography.* Adv. Polym. Sci., ed. Springer-Verlag. Vol. 172. 2005, Berlin Heidelberg. 37-245.

(22) McKean, U. S. D.; MacDonald, S. A., "Acid Photogeneration from Sulfonium Salts in Solid Polymer Matrices", *J. Pol. Sci. Part A: Polym. Chem.* **1989**, *27,* 3927.

(23) Corrent, S.; Hahn, P.; Pohlers, G.; Connoly, T. J.; Scaiano, J. C.; Fornes, V.; Garcia, H., "Intrazeolite Photochemistry. 22. Acid-Base Properties of Coumarin 6. Characterization in Solution, the Solid STate, and Incorporated into Supramolecular Systems", *J. Phys. Chem. B* **1998**, *102,* 5852-5858.

(24) Feke, G. D.; Grober, R. D.; Pohlers, G.; Moore, K.; Cameron, J. F., "On-wafer spectrofluorometric method for determination of relative quantum yields of photoacid generation in chemically amplified resists", *Anal. Chem.* **2001**, *73,* 3472-3480.

(25) Hora Machado, E.; Severino, D.; Ribeiro, J.; De Paula, R.; Gehlen, M. H.; de Oliveira, H. P. M.; Santos Matos, M. d.; de Mirand, J. A., "Solvent effects on the photophysics of 3-(benzoxazol-2-yl)-7-(N, N, -diethylamino)chromen-2-one", *Photochem. Photobiol. Sci.* **2004**, *3,* 79-84.

(26) Abdel-Mottaleb, M. S. A.; El-Sayed, B. A.; El-Kady, M. Y.; Abo-Aly, M. M., "Fluorescence Properties and Excited State Interactions of 7-hydroxy-4-methylcoumarin Laser Dye", *J. Photochem. Photobiol. A: Chem.* **1989**, *46,* 379-390.

(27) Frenette, M.; Ivan, M. G.; Scaiano, J. C., "Use of fluorescent probes to determine catalytic chain length in chemically amplified resists", *Can. J. Chem.* **2005**, *83,* 869-874.

(28) Lee, K.; Jockusch, S.; Turro, N. J.; French, R. H.; Wheland, R. C.; Lemon, M. F.; Braun, A. M.; Widerschpan, T.; Dixon, D. A.; Li, J.; Ivan, M.; Zimmerman, P., "157 nm Pellicles (Thin Films) for Photolithography: Mechanistic Investigations on the VUV and UV-C Photolysis of Fluorocarbons", *J. Am. Chem. Soc.* **2006**, *127,* 8320.

(29) Shirai, M.; Shinozuka, T.; Takashiba, S.; Horiguchi, Y.; Irie, S.; Itani, T., "Evaluation of 157-nm Resist Structure - Outgassing Relationship Using In-Situ QCM Technique", *Proc. SPIE* **2004**, *5376,* 541548.

(30) Mehata, M. S.; Tripathi, H. B., "Fluorescence quenching of 6-methoxyquinoline: an indicator for sensing chloride ion in aqueous media", *J. Luminescence* **2002**, *99,* 47-52.

(31) Mei, M.; Wu, S., "Fluorescent sensors for a, w-dicarboxylate anions", *New J. Chem.* **2001**, *25,* 471-475.

(32) Jayaraman, S.; Verkman, A. S., "Quenching mechanism of quinilinium-type chloride-sensitive fluorescnt indicators", *Biophys. Chem.* **2000**, *85,* 49-57.

(33) Lee, D. H.; Im, J. H.; Lee, J.-H.; Hong, J.-I., "A new fluorescent fluoride chemosensor based on conformational restriction of a biaryl fluorophore", *Tetrahedron Lett.* **2002**, *43,* 9637-9640.

(34) Lee, S. H.; Kim, H. J.; Lee, Y. O.; Vicens, J.; Kim, J. S., "Fluoride sensing with a PCT-based calix[4]arene", *Tetrahedron Lett.* **2006**, *47,* 4373-4376.

(35) Ward, C. J.; Patel, P.; James, T. D., "A molecular colour sensor for fluoride", *Chem. Lett.* **2001**, 406-407.

(36) Zhou, L.; Zhang, X.; Wu, S., "Fluoride-selective colorimetric sensors based on hydrazone functionality", *Chem. Lett.* **2004**, *33,* 850-851.

(37) Kalyanasundaram, K.; Thomas, J. K., "Environmental Effects on Vibronic Band Intensities in Pyrene Monomer Fluorescence and Their Application in Studies of Micellar Systems", *J. Am. Chem. Soc.* **1977**, *99,* 2039-2044.

(38) Labbe, P.; Reverdy, G., "Adsorption Characteristics of Polycyclic Aromatic Compounds on Clay: Pyrene as a Photophysical Probe on Laponite", *Langmuir* **1988**, *4,* 419-425.

(39) Ellison, C. J.; Torkelson, J. M., "Sensing the Glass Transition Temperature in Thin and Ultrathin Polymer Films via Fluorescence Probes and Labels", *J. Pol. Sci. Part B: Polym. Phys.* **2002**, *40,* 2745-2758.

(40) Matsui, J.; Mitsuishi, M.; Miyashita, t., "A Study on Fluorescence Behavior at the Interface of Polymer Langmuir-Blodgett Films", *J. Phys. Chem. B* **2002**, *106,* 2468-2473.

(41) Webb, R. L.; Langford, S. C.; Dickinson, J. T.; Lippert, T. K., "Sensitization of PMMA to laser ablation at 308 nm", *Appl. Surf. Sci.* **1998**, *127-129,* 815-820.

Imaging and Quantification of Acid Formation in Thin Polymer Films

3. Imaging and Quantification of Acid Formation in Thin Polymer Films

3.1 Introduction

Advancement towards smaller circuit size can be achieved by decreasing the exposure wavelength or by increasing the numerical aperture.[1, 2] Microeletronics industry has been able until now to follow Moore's law, in fact a prediction made in 1965, dictated by economical reasons, which stated that the number of circuits in a silicon chip should double every one and a half year. [3] Advancing from exposure using I-line (365 nm) to Xe-Hg lamps working at 254 nm or KrF lasers at 248 nm required a change in the diazonaphtoquinone/ novolac positive resist (see Scheme 1-1 Chapter 1 for structures) used in microlithography in the 1970s and early 1980s. The quantum yield for diazonaphtoquinone in the range 0.2 – 0.3, and the high absorption of novolac below 250 nm were two major problems that had to be overcome. The sensitivity of the resists was too small to be suitable for light sources in the deep UV region, where the 254 nm Hg discharge lamp has a small output. Even an increase in the quantum yield to 1 would not have been enough to make the process suitable for industrial scale. Research was focused at the beginning of 1980s on finding a way to increase sensitivity of the photoresists by a few orders of magnitude.

The breakthrough came when Ito, Willson, and Fréchet proposed the concept of chemical amplification (CA) in 1982.[4] The idea behind this concept was to have an absorbed photon generate a chain of reactions. Ito et al. proposed a mechanism in which a photoacid generator (PAG) would be decomposed upon absorption of a photon, giving a Brönsted acid and other photoproducts. The acid then catalyzed a chemical reaction involving pendant groups (deprotection) which results in change

of solubility/ polarity in the polymer, allowing selective dissolution of the exposed and unexposed regions. [1] The catalytic chain length (CCL) varied between 800 – 1100 events/ proton. [5,6]

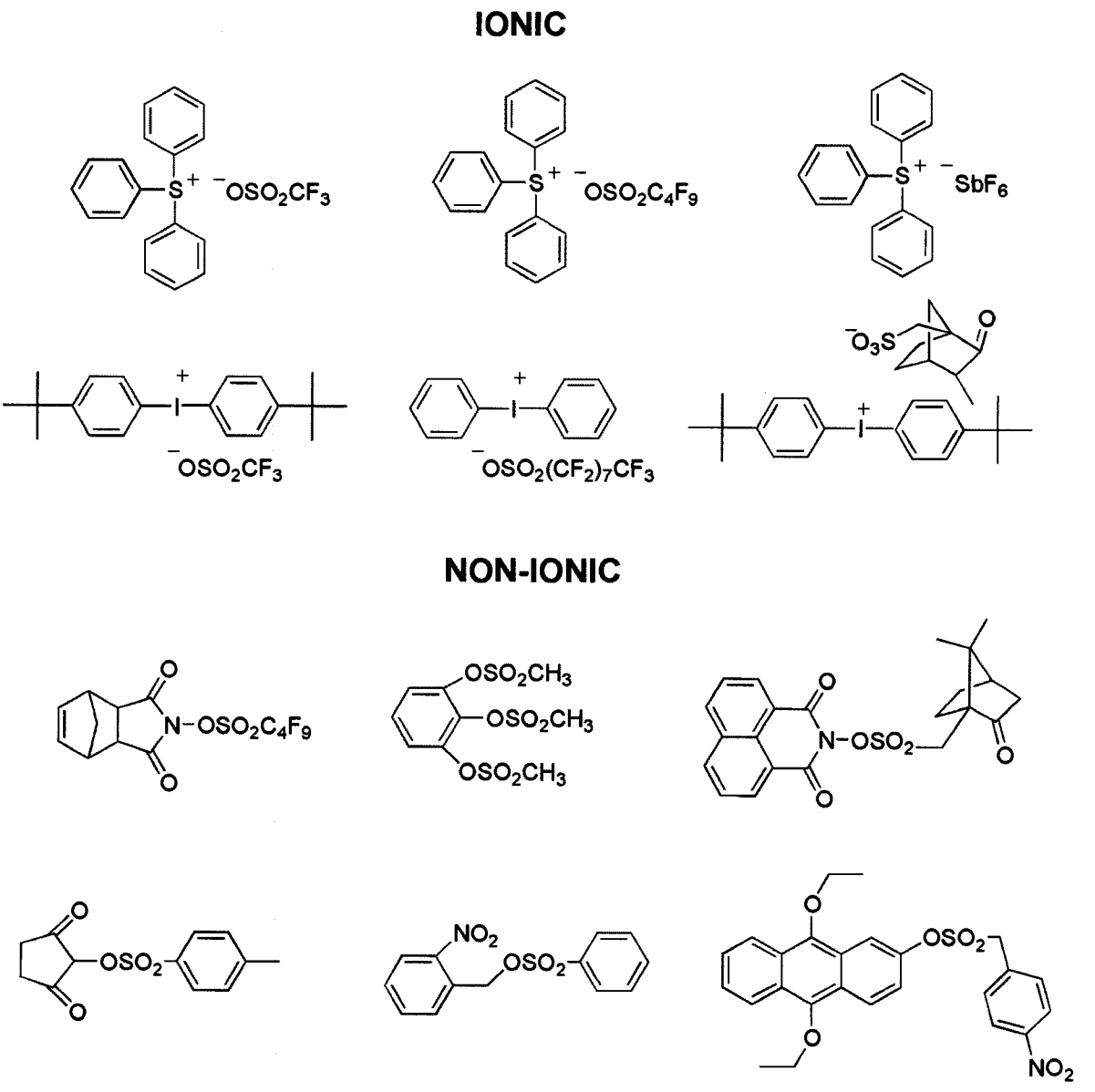

Chart 3-1. Structures of common photoacid generators: ionic onium salts (triphenyl sulfonium and diaryl iodonium) in the first two rows, non-ionic PAGs in the last two rows of the chart.

Photoacid generators were first used as photoinitiators in cationic polymerization by Crivello,[7, 8] who laid down the foundation of a new field, namely use of photosensitive organic salts as photoinitiators in cationic polymerization. The so called "onium salts" were further developed, with diaryliodonium and triphenyl sulfonium salts being the most studied. [1, 7, 9, 10]

Photoacid generators may be divided into two big categories: ionic and non-ionic. Examples of typical PAGs are shown in chart 1, with the first two rows showing structures of ionic PAGs, and the last two rows showing non-ionic structures.

The ionic "onium" salts may have an organic or inorganic counteranion. The non-ionic PAGs could be also classified in different classes: organohalide, sulfonate ester, sulfone, etc. [1] The choice of the PAG is influenced by its absorbance at the irradiation wavelength, thermal stability, toxicity, strength of the generated acid, diffusion in the polymer matrix, etc. Examples of most encountered anions are hexafluoroantimonate (SbF_6^-), trifluoromethanesulfonate (triflate $CF_3SO_3^-$), perfluorooctane sulfonate ($CF_3(CF_2)_7SO_3^-$), and perfluorobutane sulfonate ($CF_3(CF_2)_3SO_3^-$).

The photochemistry of PAGs has been intensively studied, with emphasis on triphenylsulfonium triflate (TPS-OTf) and diaryl iodonium salts. [7, 11-14] By far, the most extensively used PAG in CA photolithography has been triphenylsulfonium trifluoromethanesulfonate (triflate), which generates the strongest acid. [1, 12, 15] The photolysis mechanism of TPS-OTf is shown in scheme 3-1. The products may be formed through direct photolysis or through triplet energy transfer, or electron transfer from a sensitizer. For triplet energy transfer the sensitizer is usually a ketone (acetone, xanthone), while for electron transfer anthracene is employed.[11, 12]

Non-ionic photoacid generators have been used especially in chemically amplified photoresists. [16] Another type of PAGs are polymeric photoacid generators. [17]

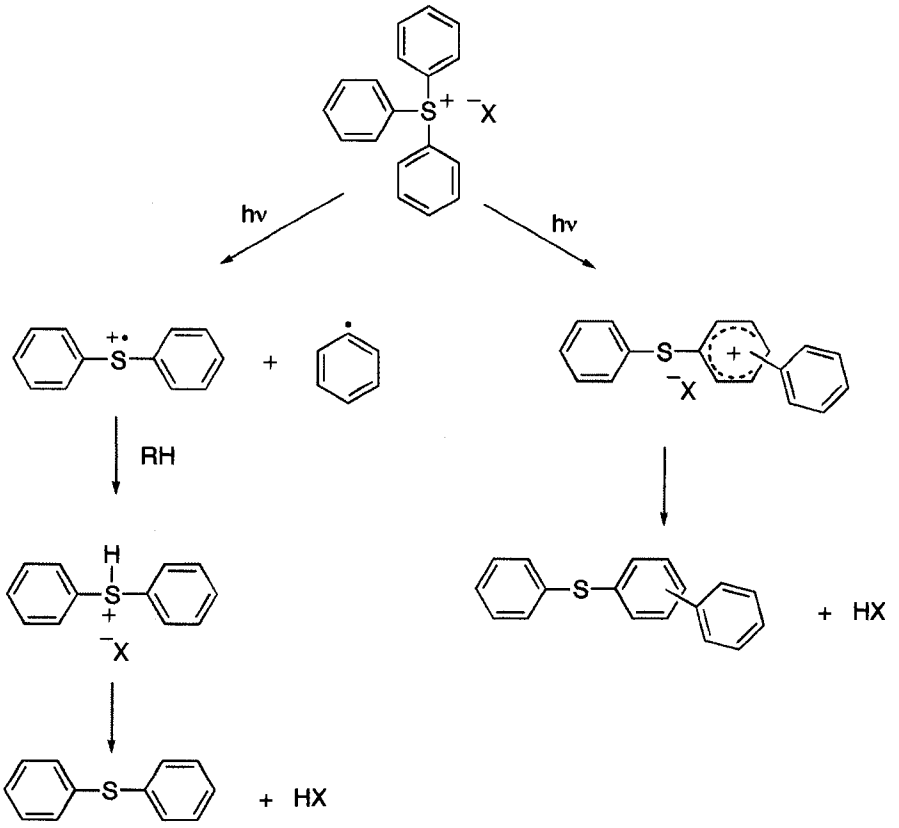

Scheme 3-1. The homolytic (left) and heterolytic (right) pathways of the photolysis of triphenylsulfonium photoacid generator; X may be one of the following anions: SbF_6^-, $CF_3SO_3^-$, $CF_3(CF_2)_7SO_3^-$, $CF_3(CF_2)_3SO_3^-$. The homolytic cleavage leads to formation of diphenylsulfinyl radical cation and phenyl radical in the solvent cage, which may either recombine to form the starting material, or escape the solvent cage and give in the end diphenyl sulfide and acid as main photoproducts. The heterolytic cleavage initially leads to the formation of diphenyl sulfide and phenyl cation. The phenyl cation may attack the diphenyl sulfide and form the starting material, or it electrophilically attacks one of the rings from the diphenyl sulfide, leading to the formation of 2-, 3-, or 4-(phenylthio)biphenyl and acid. These two mechanisms of photolysis (hemolytic and heterolytic) are inferred from the study of the multitude of primary photoproducts from triphenylsulfonium salts bearing different substituents.[12]

3.2 Results and Discussion

The goal of this project was to develop a methodology that allows an easy assessment of the ability of PAGs to form acid when exposed to radiation at different wavelengths. The techniques used to monitor acid formation were based on spectroscopic measurements of the signal characteristic to an acid sensor, Coumarin 6. Optical absorbance, fluorescence and excitation spectra, and fluorescence latent images were recorded and analyzed in order to obtain qualitative and quantitative data. Quantitative information may be obtained by doing *in-film* titrations, where known amounts of base are added to the solution prior to spin coating. Previous reports showed that Coumarin 6 works as an excellent acid sensor in thin films. [18-21] The discussion blends with the results and the data obtained, rather than being a separate section by itself. Due to the high volume of data, it was considered easier for the reader to follow the discussion immediately after the experimental results for each subsection.

3.2.1 Verification of acid generation at 157 nm

The advancement towards shorter wavelengths has fueled research in the field of photosensitive materials that show higher transparence at the exposure wavelength. A compromise between transparency and efficiency started to be evident at 193 nm, when phenolic resists, that would also act as sensitizers, were too opaque. However, at 157 nm all organic materials absorb, thus the task of finding materials that are transparent enough but at the same time photosensitive, is more challenging. [19] The CA photoresists are still used in deep-UV (DUV) and vacuum-UV (VUV) photolithography. However, the resist components for 157 nm have to show a higher transparency, allowing photons to evenly penetrate throughout the film. [20, 22] At the moment this project was started, 157 nm was seen as the next exposure wavelength to be used in CA photolithography. [23] While new polymers had been synthesized with low absorbance at 157 nm, the PAGs received

less attention and the goal of this project was to show that PAGs previously used at longer exposure wavelengths were capable of forming acid upon absorption of a photon at 157 nm. Although it was expected that the photochemistry would not be wavelength dependent, at 157 nm the incident energy is very high, 182 kcal/ mol (7.88 eV) of photons, enough to break bonds that were not involved at longer wavelengths, and to produce "hot" intermediates. [24-26] The energy absorbed by the molecules could lead to excitation in higher excited states, called Rydberg states. [26-28]

While many previous reports described the interaction between radiation at 157 nm and different polymers,[29-32] photoacid generation at this wavelength in chemically amplified resists had not been reported. The goal was to develop a protocol that would prove that acid was formed upon exposure, and that would allow testing of new PAGs at this wavelength. Commercial and home-made resists were tested during this project (a collaboration with Marie Laferriére, a graduate student from the group) from a qualitative point of view, followed by other projects involving quantification of acid.

3.2.1.1 Detection of acid formation in a commercial photoresist exposed to laser radiation at 157 nm, using absorbance and fluorescence spectroscopy

The qualitative analysis was done *in-situ*, adding a fluorescent acid sensor, Coumarin 6, to the commercial resist XP1215Aa prior to spin coating on a CaF_2 mirror. Part of this project was a collaboration with the graduate student Marie Laferriére. XP1215Aa was a resist especially designed for photolithography at 157 nm. Coumarin 6 had been previously shown to act as an acid sensor by changing its absorption and emission properties upon protonation. [33, 34] The resist contains an onium salt as the PAG, and a fluorinated polymer from DuPont, previously described. [35, 36] The thickness of the spin coated film was 144 nm, as measured

with a Luzchem TFA-11 thin film analyzer. After spin coating, the films were baked inside an oven at 90 °C for 60 s. The absorption and fluorescence spectra of resist films unexposed and exposed at 254 nm for 2 minutes in a HTG exposure unit are shown in figure 1. The exposure time was long enough to allow formation of acid in a quantity sufficient to protonate C6. The spectra obtained in films were similar to those previously reported by others and recorded in thin resist films. [23, 33, 34] Absorption spectra were recorded with a Cary-1 spectrometer, while fluorescence spectra were recorded using an LS-50 luminescence spectrometer from Perkin Elmer. The excitation wavelengths were 450 nm for the neutral form of Coumarin 6, while the protonated form was excited at 500 nm.

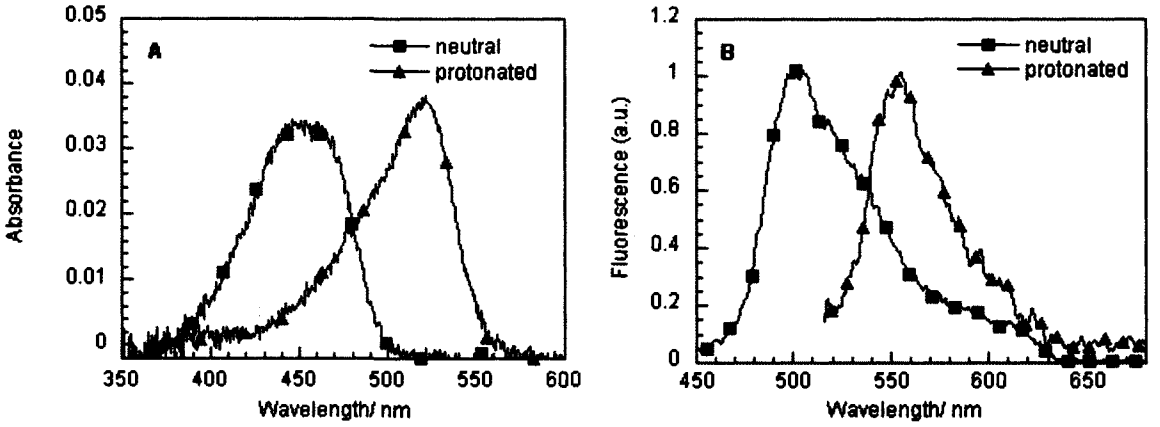

Figure 3.1. Absorbance (A) and fluorescence (B) of exposed (▲) and unexposed (■) films of XP1215Aa films containing Coumarin 6, exposed to continuous wave radiation at 254 nm. The excitation wavelengths for the fluorescence spectra were 450 nm for the neutral form (unexposed), and 500 nm for the protonated (exposed) Coumarin 6.

3.2.1.2 Imaging of films exposed to 157 nm

Following exposure at 254 nm, which proved that the PAG formed acid upon exposure and that C6 worked as a suitable acid sensor in the resist film, the next step was exposure at 157 nm. Films obtained by spin coating the same resist containing C6 were exposed to 157 nm. In order to discriminate between the exposed and unexposed regions, copper masks having hexagonal holes with 60 μm center-to-center, similar to those used in X-ray applications, were placed on top of the film. Exposure of the films leaves a latent image, recorded using a camera and a fluorescence microscope, figure 2. Exposure was done under a nitrogen atmosphere using an MSX-250 excimer laser from MPB Technologies, connected to the sample compartment through a sealed pipe. The incident dose was ~ 2.3 mJ/ cm^2/ shot, 35 shots, and the repetition rate was 1-3 Hz. The fluorescence images were recorded with a Zeiss Universal microscope, having a 50-watt mercury arc lamp as a light source. For more details on the microscope and filters used, see the experimental section.

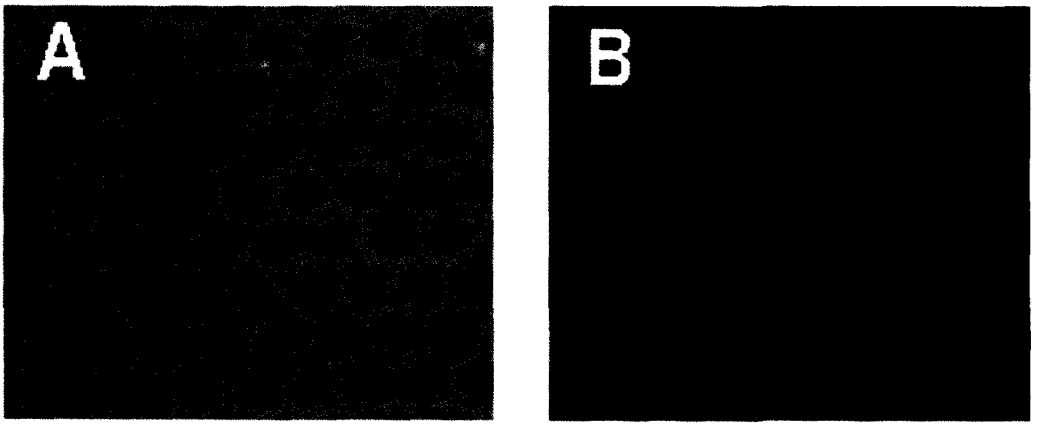

Figure 3-2. Fluorescent images of Coumarin 6 containing resists (XP1215Aa), exposed to 35 shots (2.3 mJ/ cm^2/ shot) or ~ 81.0 mJ/ cm^2 at 157 nm. The optical filters used to record fluorescent images allowed excitation at 485 (± 12) nm for the "negative" image (A), and 546 (± 12) nm for the "positive" image (B).

It is important to record both the "negative" and the "positive" images of resist films containing C6. The image from figure 2 A shows in the unexposed areas fluorescence of C6, the neutral form, while the exposed areas (dark areas) do not exhibit emission in the green. The absence of emission from the exposed areas could also be due to the presence of a different species which absorbs at a wavelength different from that specific to C6 or may be caused by the absence of C6, destroyed during exposure. Figure 2B shows emission in red in the exposed regions, characteristic to protonated C6, $C6H^+$, when excited at a wavelength where $C6H^+$ absorbs. This proves that acid was generated in the areas exposed to laser radiation at 157 nm. The resist XP1215Aa from Shipley (currently Rohm and Haas Electronics Materials) contained a small amount of base which neutralized the acid formed when only one shot was delivered. No image or signal characteristic to $C6H^+$ was detected. Increasing the dose, the acid formed was in a bigger amount compared to the base, and the excess acid protonated C6. However, in home-made films containing PAG and C6, after exposure to only one shot at 157 nm, the signal in emission characteristic to $C6H^+$ was detected.

3.3 Acid formation abilities of two heterocyclic sulfonium salts exposed to 248, 193, and 157 nm

As the exposure wavelength employed in optical lithography becomes shorter, the challenges of finding suitable polymers and PAGs grow bigger. [1] At 157 nm the most important obstacle to overcome is the high absorbance of the resists used for photolithography at 193 nm. Acrylates-based resists used at 193 nm are too absorbant at 157 nm. Fluorinated polymers are a viable choice and show reasonable transparency. However, PAGs especially designed for this wavelength, with higher transparency, are not widely available.

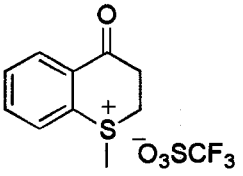

PAG1

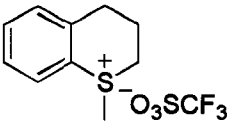

PAG2

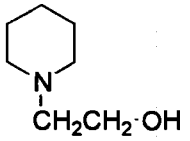

2PE

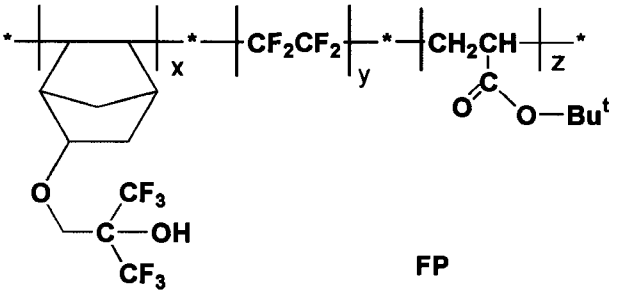

FP

Chart 3-2. Structures of heterocyclic photoacid generators (PAG1, PAG2) characterized during this study, the base used for *in-film* titrations, 2-piperidin-1-*yl*-ethanol (2-PE), and of the fluorinated polymer used to obtain the films (FP).

There is a trade off between transparency and absorbance for PAGs and polymers used at 193 nm, and especially at 157 nm. [19] While new polymers, with

lower absorbance, were designed and synthesized, the PAGs used were the same employed in photolithography at 248 and 193 nm.[1] Two new heterocyclic sulfonium PAGs were synthesized in our group by Dr. Carlos Sanrame. 1-Methyl-4-oxo-thiochromanium triflate (PAG1) and 1-Methyl-thiochromanium triflate (PAG2), whose structures are shown in chart 3-2, contain only one phenyl ring in their structure, as opposed to two or three rings in previously reported structures of sulfonium PAGs.

The experiments were done in thin films obtained by spin coating a solution containing a fluorinated polymer (FP) whose structure is shown in chart 3-2. The polymer was especially designed and synthesized by DuPont for photolithography at 157 nm, and it was supplied by Rohm and Haas Electronic Materials. The absorption spectra of PAG1 (MW = 328) and PAG2 (MW = 314) in thin FP films were recorded using a Cary LS 50 spectrophotometer, figure 3.3. The films were obtained by spin coating a solution that contained 80 wt % 2-heptanone as solvent (99 % purity by volume, boiling point 150 °C), 20 wt % FP, and 2 wt % PAG based on the dry polymer weight. It is very important to remember that throughout this thesis the amount of PAG is expressed as % of the dry polymer weight and not as % mass from the entire solution. It is a common practice in lithography to express the amount of PAGs or other additives as wt % based on the dry polymer's weight. In terms of molar concentrations, the two PAGs in the stock solution are 1.11×10^{-2} M (PAG1), and 1.16×10^{-2} M (PAG2) respectively.

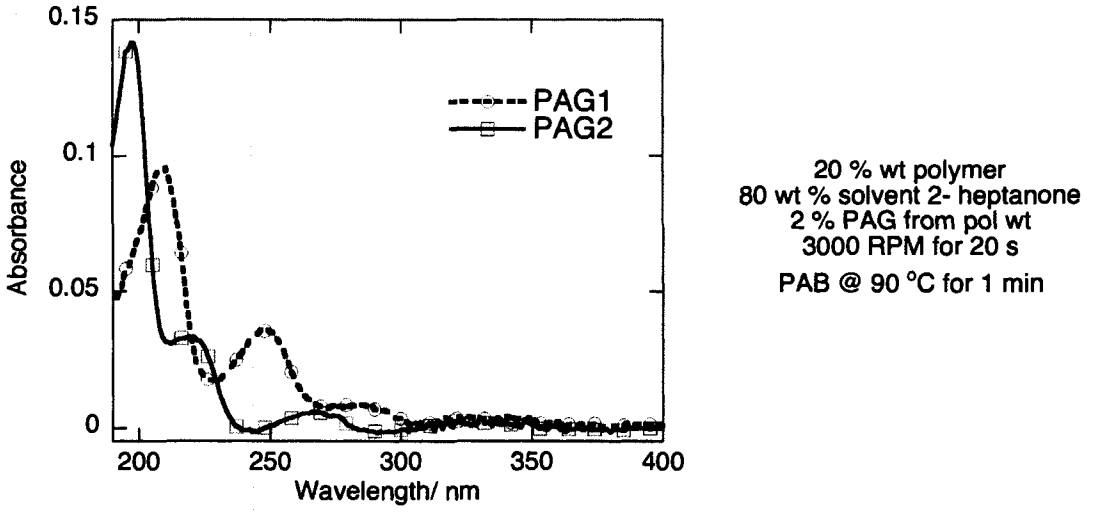

Figure 3-3 Absorbance of PAG1 and PAG2 in FP films obtained by spin coating on top of a quartz disc, at 3000 rpm for 20 s, a solution containing 80 wt % 2-heptanone, 20 wt % polymer, and 2 wt % PAG based on the polymer weight. The concentrations of the PAGs in the spin coated solutions were: 1.11×10^{-2} M (PAG1), and 1.16×10^{-2} M (PAG2).

The solutions were spin coated on top of 1 inch (2.54 cm) quartz discs at 3000 rpm for 20 s, followed by baking inside an oven at 90 °C for 60 s in order to remove the solvent.

The absorbance spectra of the two PAGs reflect their molecular structure. The recorded baseline was the polymer film without PAGs, so the value of the absorbance in the plots from figure 3.3 represents entirely the contribution of the PAGs. PAG1 contains a carbonyl group which induces a peak in absorption at 250 nm, whereas PAG2 is virtually transparent at 248 nm. However, at 193 nm PAG2 has an absorbance of 0.12, while the absorbance of PAG1 is 0.05. There is a fine trade off between the absorbance of a photoacid generator and the need to have resists which are transparent enough so that the incident light penetrates evenly throughout the film. The fact that PAG2 has a higher absorbance below 200 nm does not automatically mean that it will produce more acid than PAG1 at 193 nm. A comparison of their abilities to produce acid at 157 and 248 nm will be presented in the next section of chapter 3.

3.3.1 Comparison of acid formation abilities of PAG1 and PAG2 at 248, 193, and 157 nm

In order to mimic the conditions from industry, the experiments were done in thin polymer films (~ 400 nm). To the solutions used to obtain the films for the absorbance experiment, with the composition described in the previous section, we added Coumarin 6 in an amount representing 0.5 wt % based on the polymer weight (2.6×10^{-3} M in the solution to be spin coated). The molar ratios of photoacid generators relative to C6 were: PAG1 : C6 = 4.3 : 1 and PAG2 : C6 = 4.5 : 1. The solutions were spin coated on quartz discs, and the formation of acid upon exposure was monitored by recording the absorbance spectra of C6 and $C6H^+$, figure 3-4. The fluorescent acid sensor Coumarin 6 works excellent for detection of acid using absorbance and fluorescence.

From the plots shown in figure 3-4, one can notice an overall better performance of the two PAGs at 157 nm. After ~ 40.0 mJ/ cm^2 all the C6 is protonated (absorption maximum at ~ 520 nm). We were not able to record the absorbance spectra below 190 nm so we can only speculate about the absorbance of these PAGs at 157 nm. It is expected that both PAGs will show high absorbance at 157 nm, with more absorbance for PAG1 due to the carbonyl chromophore. The ratio of absorbance of $C6H^+$ *vs* neutral C6 (A_{520}/ A_{445}) from figure 3-4 shows that PAG1 and PAG2 have different acid formation ability when exposed to radiation at 157 nm. This may be the result of the higher absorbance of PAG1 due to the carbonyl or its photoproducts. The higher the absorbance of the film, the less photons are available for the PAGs' molecules to absorb, and this is a critical aspect especially at 157 nm, radiation easily absorbed by organic compounds. Photodarkening is a process that affects polymer films exposed to 157 nm at high incident doses. [27]

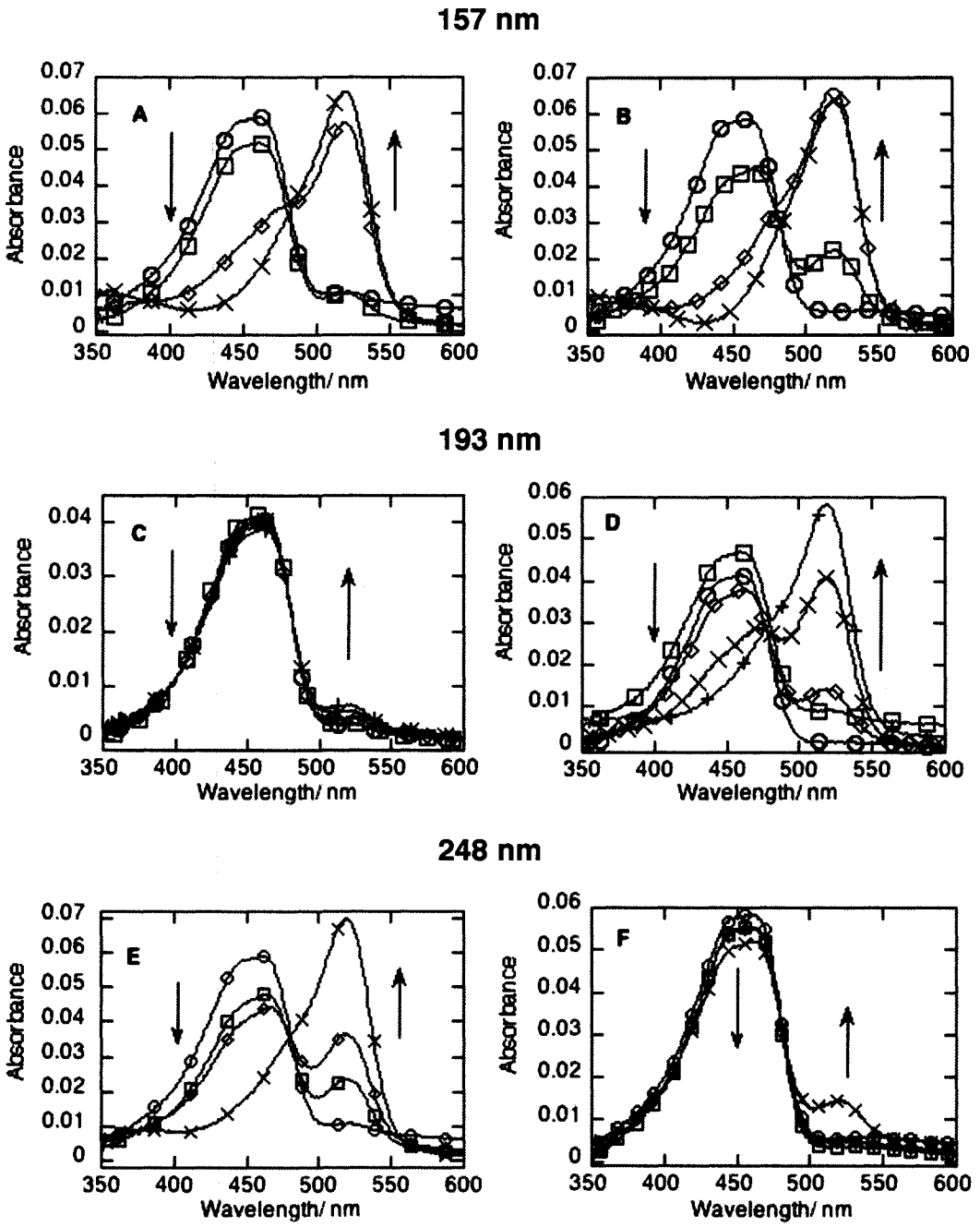

Figure 3-4. Absorbance of C6 and $C6H^+$ in FP films containing PAG1 (A, C, E) – left side of the figure, and PAG2 (B, D, F)- right side of the figure, exposed to laser radiation at 157 nm (A, B), 193 nm (C, D), and 248 nm (E, F). The incident dose were the following: 0 shots (O), 5 shots (□), 15 shots (◊), and 40 shots (x) at 157 nm, ~ 1.0 mJ/ cm^2 per shot (A and B); 0 shots (O), 5 shots (□), 15 shots (◊), 30 shots (x), 60 shots (+) at 193 nm, ~ 0.3 mJ/ cm^2 per shot (C and D); 0 shots (O), 3 shots (□), 6 shots (◊), 30 shots (x) at 248 nm, ~ 8.0

mJ/ cm^2 per shot (E and F); 1.11 x 10^{-2} M (PAG1), 1.16 x 10^{-2} M (PAG2), and 2.60 x 10^{-3} C6.

At 193 nm, after an overall exposure to 18.0 mJ/ cm^2, PAG2 forms more acid than PAG1 (figure 3-4 C and D), favored also by its higher absorbance at 193 nm (figure 3-3). Absorbance spectra recorded following exposure to an overall dose of 240.0 mJ/ cm^2 at 248 nm show very good acid formation ability for PAG1 (figure 3-4 E). The very low efficiency of PAG2 at 248 nm (fig 3-4 F) is due to its low absorbance at this wavelength (fig 3-3). Due to the carbonyl chromophore, PAG1 shows a peak at approximately 250 nm. The ratio of absorbances characteristic to C6 and $C6H^+$ before irradiation and after exposure (A_{520}/ A_{450}) to the three wavelengths are shown in table 3-1. The absorbance centered at ~ 520 nm is proportional to the formation of protonated Coumarin 6, thus being a measure of acid formation following exposure. Formation of the peak at ~ 520 nm coincides with disappearance of the peak at 450 nm, characteristic to neutral C6. A ratio of the absorbance of protonated C6 *vs.* neutral C6 gives a good measure of how much acid was formed during exposure of the polymer film. These data prove that both PAGs work well at 157 nm, PAG1 at 248 nm and PAG2 at 193 nm. This procedure offers qualitative information and is useful in assigning acid formation abilities at different wavelengths. It also shows quantitative differences between the two PAGs at different exposure wavelengths, table 3-1. The protocol is useful in assigning the abilities to form acid at different wavelengths using absorption spectroscopy and the acid sensor Coumarin 6. While at 157 nm the two PAGs show similar acid formation abilities, at 193 nm and 248 nm the differences are one order of magnitude bigger, showing clearly which PAG is suitable for that particular exposure wavelength. Similar results were obtained by monitoring the fluorescence of the protonated Coumarin 6. The trade-off between absorbance and transparency of the PAG at the exposure wavelength is best observed for the two PAGs at 193 and 248 nm. PAG1 shows an excellent acid formation ability at 248 nm, a wavelength at which it has a peak in absorbance. At the same % loading, PAG2 forms more acid

than PAG1 when exposure wavelength was 193 nm. Its absorbance at 193 nm is more than two times higher than that of PAG2.

The excess acid present in the polymer films could lead to double protonated Coumarin 6, with an absorption centered around 365 nm, as it was observed during experiments done with C6 in 2-heptnone solution, to which hydrochloric acid (HCl) was added in excess. The double protonation occurs at the second N atom from the amino moiety, and it disturbs the push – pull mechanism of the fluorescence (chapter 2, section 2.2.1). Small aliquots of HCL (38 %) were added to 10.0 mL of C6 2.0 x 10^{-5} M in 2-heptanone, and the absorption was monitored. The absorbance shifts first to the red, with a maximum at ~ 510 nm, characteristic to $C6H^+$, then as more HCl was added a new peak with a maximum at 365 nm appeared (data not shown here for space considerents). As it can be seen from figure 3-4, it is not the case in the present experiments, no peak at 365 nm was formed, so it is right to assume that the only two forms of C6 present in the film are neutral and protonated C6.

A_{520}/ A_{445}	**157 nm** **40 mJ/ cm²**	**193 nm** **18 mJ/ cm²**	**248 nm** **45 mJ/ cm²**
PAG1	5.50	0.15	3.90
PAG2	10.60	3.90	0.30

Table 3-1. Ratio of absorbances of monoprotonated C6 (A_{520}) and neutral Coumarin 6 (A_{445}) in FP films (~ 400 nm thick) containing PAG1 and PAG2; the films were exposed to various doses of laser radiation totaling 40.0 mJ/ cm² at 157 nm, 18.0 mJ/ cm² at 193 nm, and 45.0 mJ/ cm² at 248 nm. The PAG loading represented 2.0 % relative to the polymer's weight.

The ratio A_{520}/ A_{445} may be used to get some quantitative evaluation of the amount of acid formed as a function of incident energy. This ratio should be used for the same exposure wavelength, since the incident doses were different at the three exposure wavelengths.

3.4 A protocol for acid quantification and comparison of acid formation in polymer films using fluorescence spectroscopy. Comparing PAGs at 157 and 193 nm.

The ability of five photoacid generators to form acid upon exposure was studied and compared at 157 and 193 nm using fluorescence spectroscopy. The structures of the PAGs are shown in chart 3-3. To check for the behavior of different structures and for the influence of the anion on photoacid generation, two sets of PAGs were selected: two iodonium salts : *di*-(4-*tert*-butyl-phenyl) iodonium perfluorooctane sulfonate (DTBPI-PFOS, MW = 892)) and *di*-(4-*tert*-butyl-phenyl) iodonium orthocamphor sulfonate (DTBPI-OCS, MW = 619)), and two heterocyclic sulfonium salts : *tert*-butyl-phenyl pentamethylsulfonium triflate (TBPPMS-OTf, MW = 384) and *tert*-butyl-phenyl pentamethylsulfonium perfluorobutane sulfonate (TBPPMS-PFBS, MW = 534).

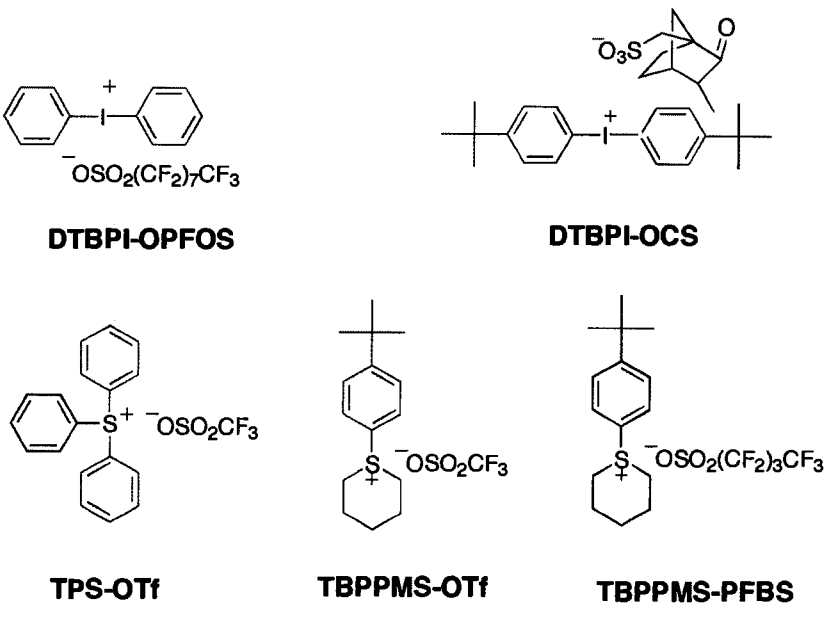

Chart 3-3. Structure of the five photoacid generators used to develop the protocol at 157 and 193 nm: two iodonium salts (DTBPI-OCS and DTBPI-PFOS), and three sulfonium

salts, from which two were heterocyclic sulfonium salts (TBPI-OTf and TBPI-PFBS), and TPS-OTf.

Triphenylsulfonium triflate (TPS-OTf, MW = 412) was selected as a standard, since it has previously been reported to work very well at both 193 and 248 nm. [37, 38]

The absorption spectra of the five PAGs selected for this study are shown in figure 3-5. The absorption spectra were recorded using thin films obtained by spin coating, at 3000 rpm for 20 s, solutions containing 20.0 weight % wt FP, 80.0 % weight 2-heptanone and photoacid generators 3.0 % from polymer's weight. Their molar concentrations in the stock solutions were: TBPPMS-OTf 1.42 x 10^{-2} M, TBPPMS-PFBS 1.02 x 10^{-2} M, DTBPI-OCS 9.00 x 10^{-3} M, DTBPI-PFOS 6.10 x 10^{-3} M, TPS-OTf 1.33 x 10^{-2} M. For each PAG the baseline was the thin polymer film without PAG, coated on the quartz disc. The thickness of these films was ~ 400 nm, as measured with the Luzchem thin film analyzer TFA-11. After spin coating the films were baked at 90 °C for 60 s inside an oven. The films were brought to room temperature (RT) prior to recording the absorption.

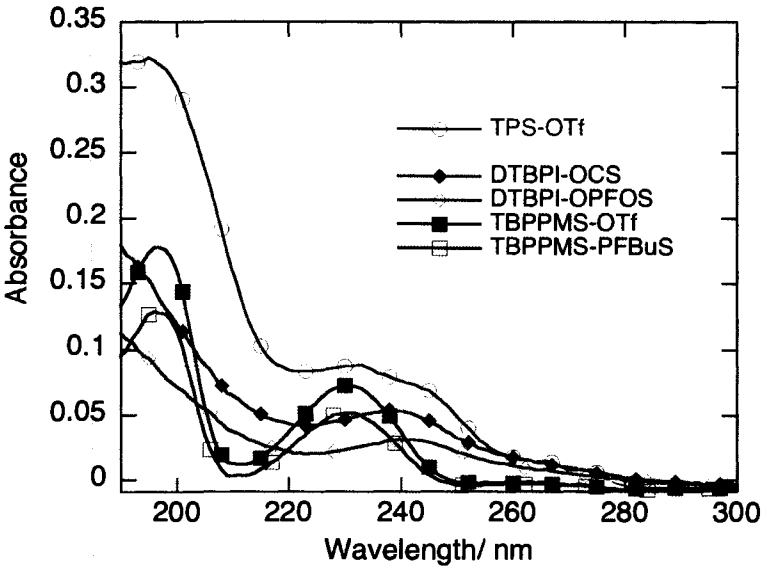

Figure 3-5. Absorption spectra of the five selected photoacid generators in polymer films. The baseline was the FP film without PAG, with a thickness of ~ 400 nm. The PAG's loading represented 3.0 % relative to the polymer's weight (TBPPMS-OTf 1.42 x 10^{-2} M,

TBPPMS-PFBS 1.02 x 10^{-2} M, DTBPI-OCS 9.00 x 10^{-3} M, DTBPI-PFOS 6.10 x 10^{-3} M, TPS-OTf 1.33 x 10^{-2} M).

Quantitative data was obtained by doing *in-film* titrations. The solutions containing PAGs were prepared according to the following procedure: first, 12 g of stock solution containing 20 wt % FP (2.4 g), 80 wt % 2-heptanone (9.6 g) were prepared. To this solution there were added C6 (0.5 wt % based on polymer weight – 12 mg) and PAG (3.0 wt % based on FP weight – 72 mg). This was further divided into six vials, each containing 2.0 g of solution. The base 2-piperidin-1-yl-ethanol (2-PE), diluted with 2-heptanone, was added to the vials containing 2.0 g of photoresist solution, in various 2-PE : PAG mole ratios. For the solutions containing DTBPI-OCS the 2PE : DTBPI-OCS mole ratios were 0.0, 0.1, 0.21, 0.32, 0.43, and 0.54, while for DTBPI-PFOS the molar ratios 2PE : DTBPI-PFOS were 0.0, 0.14, 0.28, 0.42, 0.56 and 0.70. The solutions contained acid sensor Coumarin 6 in a concentration of 2.6 x 10^{-3} M, DTBPI-OCS 9.0 x 10^{-3} M, and DTBPI-PFOS 6.1 x 10^{-3} M. All the films were obtained on one inch quartz discs following spin coating at 3000 rpm for 20 s. After spin coating, the films were baked at 95 °C for 60 s to eliminate the solvent, then rapidly cooled to room temperature on a metal surface and exposed to laser radiation. After exposure, the films were baked again at 95 °C in order to speed up the protonation of Coumarin 6 cooled to room temperature and then fluorescence spectrum was recorded (λ_{ex} = 510 nm).[5] The spectra obtained are shown in figures 3-6 – 3-8. The molar ratios were DTBPI-OCS : C6 = 3.5 : 1 and DTBPI-PFOS : C6 = 2.3 : 1. For this study we exposed all the films to the same incident dose at 157 and 193 nm, 3.2 mJ/ cm^2.

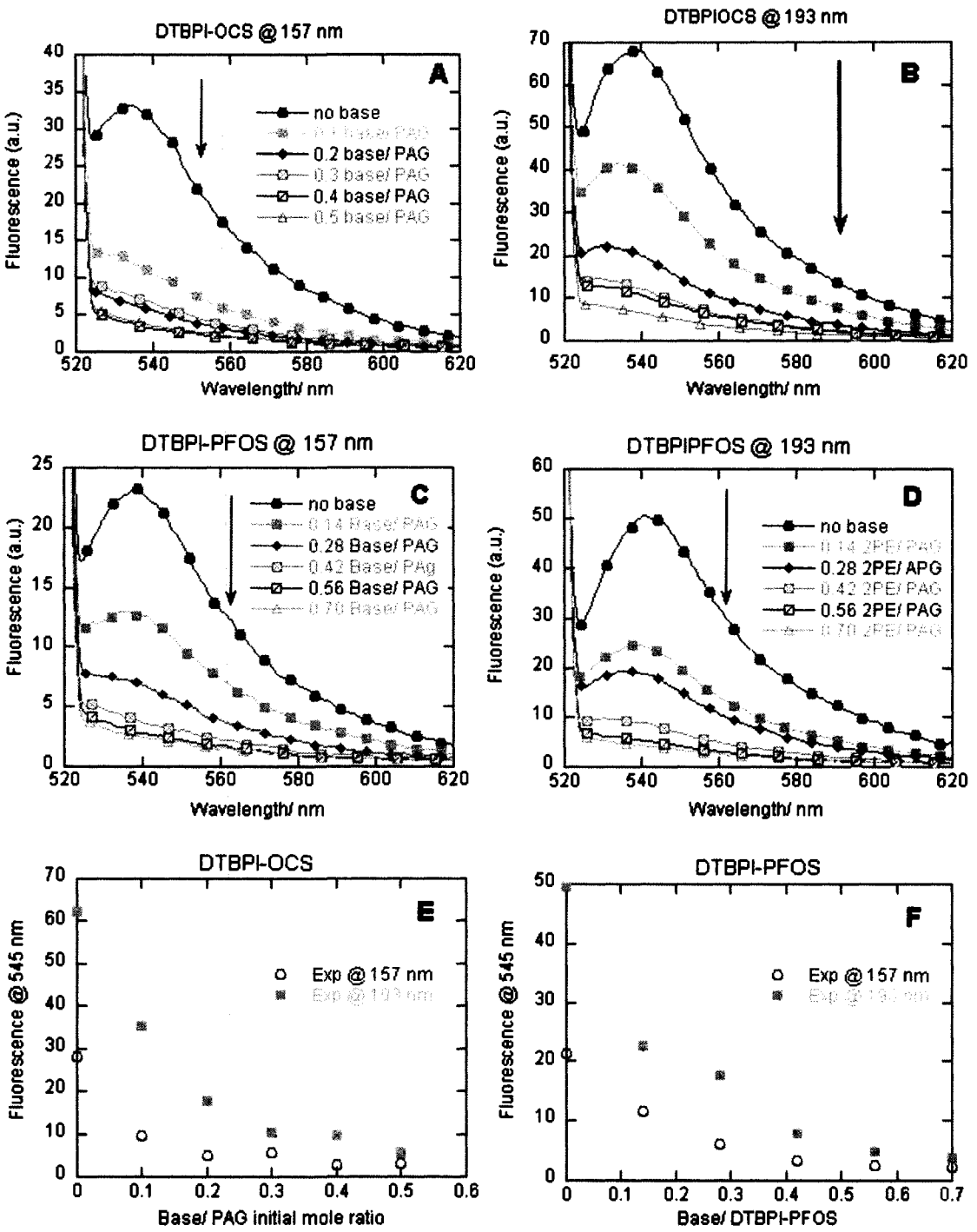

Figure 3-6. Fluorescence spectrum (λ_{ex} = 510 nm) of $C6H^+$ in a film containing DTBPIOCS, recorded following exposure to 3.2 mJ/ cm^2 at 157 nm (A), and 193 nm (B), and DTBPI-PFOS exposed to 157 nm (C) and 193 nm (D), averaged over two sets of experiments; fluorescence traces were recorded with films containing from top to bottom:

0.0, 0.1, 0.21, 0.32, 0.43, 0.54 2PE/ DTBPIOCS and 0.0, 0.14, 0.28, 0.42, 0.56, 0.70 2PE/ DTBPI-PFOS mole ratio. The values of fluorescence intensity at 545 nm for $C6H^+$ are shown as a function of base/ PAG mole ratio for films containing DTBPIOCS (E) and DTBPI-PFOS (F) exposed to radiation at 157 nm (O) and 193 nm (■).

The influence of the chemical structure of the PAG and the influence of the counterion on acid formation abilities of the PAGs at 157 and 193 nm were monitored using C6 as fluorescent acid sensor, figures 3-6 – 3-8.

The acid formation abilities of DTBPI-PFOS and DTBPI-OCS at 157 and 193 nm are shown in figure 3-6. As the amount of base 2-PE added increases, the fluorescence of protonated C6 decreases, until eventually no peak characteristic to $C6H^+$ appears in the emission spectrum. For a qualitative classification, it would be enough to irradiate the polymer films containing PAG and C6, and no 2-PE. Adding 2-PE clearly shows when the number of moles of acid produced equals the number of moles of base present in the film. Thus, one can easily have a measure of how much acid was produced during irradiation. It is clear that DTBPI-OCS and DTBPI-PFOS perform better when exposed to 193 nm compared to 157 nm. At 193 and 157 nm, however, DTBPI-OCS forms more acid than DTBPI-PFOS when exposed to the same incident dose. The difference may be due to a few factors. In terms of moles, the ratio DTBPI-OCS : DTBPI-PFOS = 1.5 : 1, thus one could argue that since there are more moles of DTBPI-OCS, it is normal to obtain more acid during photolysis. For the same % loading, the absorbance of DTBPI-OCS is also higher at 193 nm, from figure 3-5 one can see that the absorbance of DTBPI-OCS is 0.16 as opposed to 0.10 for DTBPI-PFOS. A higher absorbance means that more photons are absorbed, leading to photolysis of more PAG molecules and consequently to the formation of more acid.

Exposure of TBPPMS-OTf (1.42×10^{-2} M) and TBPPMS-PFBS (1.02×10^{-2} M), the two heterocyclic sulfonium PAGs selected for this study, to radiation at 193 and 157 nm shows that for the same % loading, 3 wt % PAG based on the

polymer's weight, both PAGs form more acid at 193 nm compared to 157 nm, figure 3-7. At the same time, the two sulfonium salts form more acid at 193 nm compared to the iodonium salts. The molar ratios PAG : C6 were TBPPMS-OTf : C6 = 5.4 : 1 and TBPPMS-PFBS : C6 ~ 4 : 1.

An informative comparison could be made between DTBPI-OCS (MW = 610) and TBPPMS-PFBS (MW = 562). For the same % loading there are approximately the same numbers of moles of PAGs in the polymer films (TBPPMS-PFBS : DTBPI-OCS = 1.1 : 1). Thus, one can compare their efficiencies not only when the same % loading is employed, but also when approximately the same number of moles is present in the films. At 193 nm the absorbance of DTBPI-OCS is 0.16, while the absorbance of TBPPMS-PFBS is 0.11. At 193 nm the phenyl ring is the chromophore, thus DTBPI-OCS, as expected, shows a higher absorbance, since it has two phenyl rings per molecule, compared to only one found in the structure of TBPPMS-PFBS. However, from figure 3-9 one can notice that the amount of acid formed at 157 nm is approximately the same for the two PAGs, while at 193 nm TBPPMS-PFBS forms more acid than DTBPI-OCS for the same incident dose. One factor that may influence the efficiency of these PAGs is the counterion. The acid migrates throughout the film in tandem with its counterion, bulky anions diffusing slower through the film. At the same time, the interactions between FP matrix and the counterion may play a significant role.

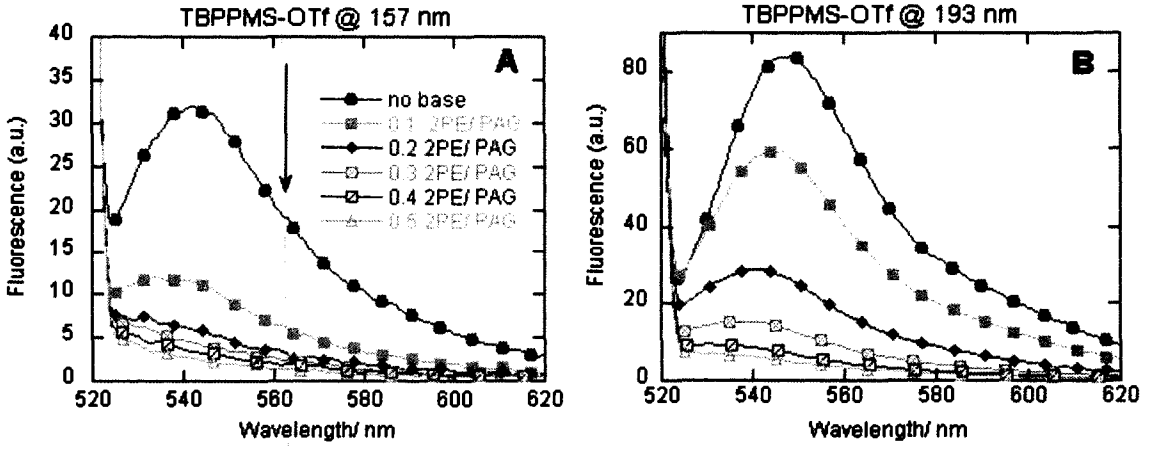

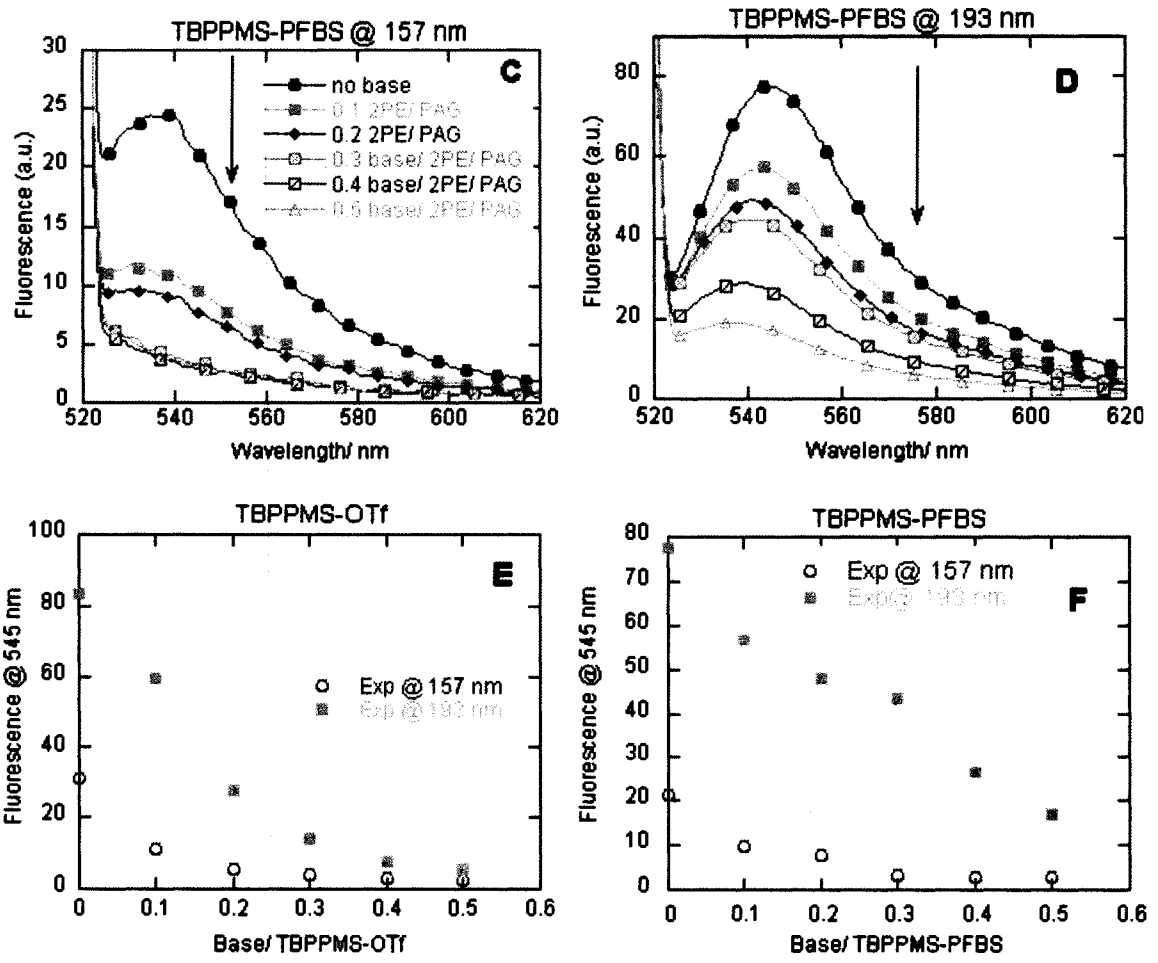

Figure 3-7. Fluorescence spectra (λ_{ex} = 510 nm) of C6H$^+$ in films containing TBPPMS-OTf exposed to 157 nm (A) and 193 nm (B), and TBP PMS-PFBS exposed to 157 nm (C) and 193 nm (D). The films were exposed to 3.2 mJ/ cm^2. Fluorescence spectra were recorded with films containing from top to bottom: 0.0, 0.1, 0.2, 0.3, 0.4, 0.5 2PE/ PAG mole ratio. The values of fluorescence intensity at 545 nm for C6H$^+$ are shown as a function of base/ PAG mole ratio for films containing TBPPMS-OTf (E) and TBPPMS-PFBS (F) exposed to radiation at 157 nm (O) and 193 nm (■).

One of the most studied PAGs is a triphenyl sulfonium salt bearing different anions (triflate, antimonite, ortho-camphorsulfonate, etc). [1] Fluorescence spectra of C6H$^+$ in FP films containing TPS-OTf and exposed to 157 and 193 nm are shown in figure 3-8. The films were obtained by spin coating a solution containing 80 wt % 2-

heptanone, 20 wt % FP, 3 wt % TPS-OTf based on polymer's weight (1.33×10^{-2} M) and 0.5 wt % C6 from polymer's weight (2.60×10^{-3} M) at 3000 rpm for 20 s. The thermal treatment (PAB and PEB) was done at 95 °C for 60 s inside an oven, followed by cooling to RT on a metallic surface. The incident dose for the films exposed to radiation at 157 nm was 3.2 mJ/ cm^2 (0.8 mJ/ cm^2/ shot) at a frequency of 1 shot/ s. For the films exposed to 193 nm, the total incident dose was 3.44 mJ/ cm^2 (0.43 mJ/ cm^2/ shot). All the spectra shown in figure 3-8 were averaged over three series of measurements. The average was done in KaleidaGraph by adding the values of fluorescence intensity (a.u.) of $C6H^+$ (λ_{ex} = 510 nm) at each wavelength in the emission interval, then dividing by 3. The data was obtained with three films spin coated using the same solution, exposed to the same incident dose, baked at the same temperature and for the same period of time. The values of fluorescence intensity and the shapes of the peaks for each film were reproducible and very close. Plots of fluorescence intensity at 545 nm as a function of the base/ PAG mole ratio are shown in figure 3-8 C for exposure at 193 and 157 nm.

Assuming that the molecules are evenly distributed in the polymer film and that all the solvent evaporated during PAB, the distance between two neighbor TPS-OTf molecules in a FP film (~ 400 nm thick), is ~ 2.6 nm for the films containing 3.0 % wt TPS-OTf based on the FP weight, and ~ 3.0 nm for the films containing 2.0 % wt TPS-OTf based on FP weight (the experimentally calculated density of the polymer is 1.3 g/ mL). The distance between two neighbor C6 molecules is ~ 4.5 nm for the same FP film containing 0.5 % wt C6 based on FP weight.

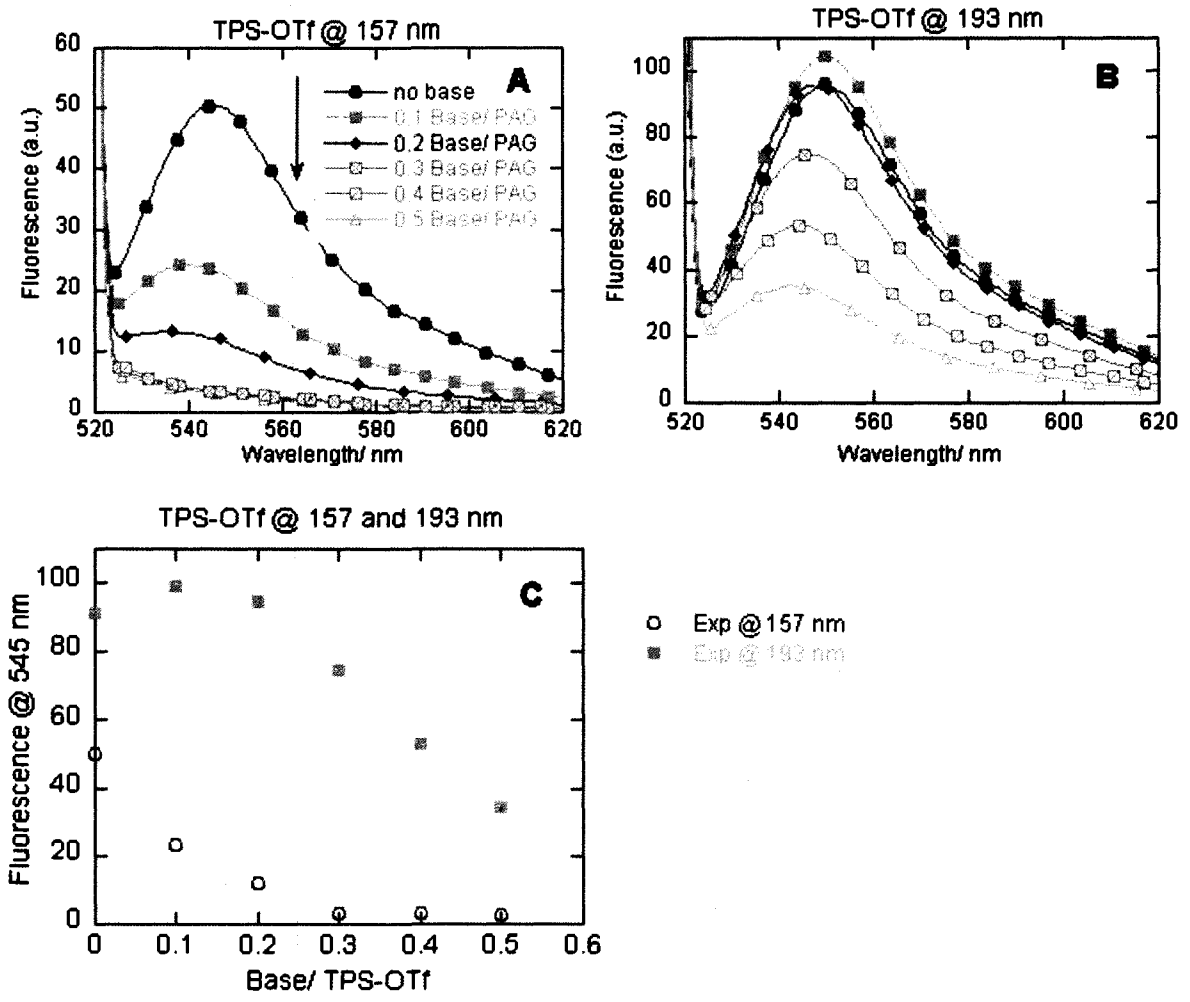

Figure 3-8. Fluorescence of $C6H^+$ (λ_{ex} = 510 nm) in FP films containing TPS-OTf, exposed to 3.2 mJ/ cm^2 at 157 nm (A), and 193 nm (B). The values of fluorescence intensity at 545 nm for $C6H^+$ are shown as a function of base/ PAG mole ratio for films containing TPS-OTf (C) exposed to radiation at 157 nm (O) and 193 nm (■). The spectra were averaged over three experiments. The concentrations of C6 (0.5 % relative to the FP weight) and TPS-OTf (3.0 % wt relative to the FP weight) in the spin coated solution were 2.6×10^{-3} M and 1.33×10^{-2} M respectively.

Following the pattern observed in the cases of iodonium and heterocyclic sulfonium PAGs, TPS-OTf forms more acid when exposed to 193 nm compared to 157 nm. This again may be due to the higher absorbance exhibited by the PAG

and its photoproducts at 157 nm compared to 193, acting like a screen for PAG molecules that are towards the bottom of the film. TPS-OTf contains three phenyl rings compared to two rings in the case of iodonium salts and one for the sulfonium heterocyclic compounds. Another contributing factor may be the absorbance of the polymer itself or of any water traces present in the film, which exhibit a higher absorbance at 157 nm compared to 193 nm. [26, 39] Thus, only PAG molecules that are close to the surface absorb photons, leading to photolysis and formation of acid. The incident number of photons at 157 nm is smaller compared to 193 nm, thus there are less photons available to be absorbed. The energy at 157 nm is 182 kcal/ mol, while at 193 nm is 148.3 kcal/ mole, which translates into 1.2 times more photons at 193 nm compared to 157 nm for the same incident energy.

Exposure of FP films containing TPS-OTf at 193 nm gives a unique curve of intensity of fluorescence at 545 nm plotted against base/ PAG molar ratio, figure 3-8 C. Contrary to results obtained with the other four PAGs, the first point corresponding to fluorescence maximum recorded when no base was added in the film, is lower than the second and the third points recorded for base/ PAG = 0.1 and 0.2 mole ratio respectively. This may be explained by taking into consideration that C6 can be double protonated. The number of moles of acid formed during exposure exceeds the number of moles of C6, leading to double protonation at the second N from the amine group. The mole ratio in the spin coated solution was TPS-OTf : C6 ~ 5 : 1. The absorbance of double protonated C6 is centered at ~ 365 nm (as noticed during experiments performed in solution with C6 2.0 x 10^{-5} M in 2-heptanone to which HCl in excess was added). Thus, when exciting at 510 nm the double protonated species does not absorb, and consequently the intensity of emission is low. As base is added to the film, some of the acid reacts with 2-PE, leading to less double protonated C6 and more of the monoprotonated species $C6H^+$, the point corresponding to base/ PAG = 0.1. The value of fluorescence

intensity at base/ PAG = 0.5 is not close to zero because even at that ratio there is more acid formed than the 2-PE added, and the excess acid protonates C6.

The intensities of fluorescence at 545 nm as a function of base/ PAG molar ratio for all the PAGs are shown in figure 3-9. From these plots it is clear that TPS-OTf gives the best results in FP films exposed to laser radiation at 157 and 193 nm. Although the two heterocyclic sulfonium salts form less acid than TPS-OTf, they may show an overall better result if one compares their absorbance at 193 nm, figure 3-5. With only one phenyl ring in their structure, TBPPMS-OTf absorbs ~ 3 times less than TPS-OTf, while TBPPMS-PFBS absorbs ~ 2.2 times less than TPS-OTf. While one needs more photons to produce acid in the case of TBPPMS salts (lower sensitivity compared to films containing TPS-OTf), one gains in terms of transparency.

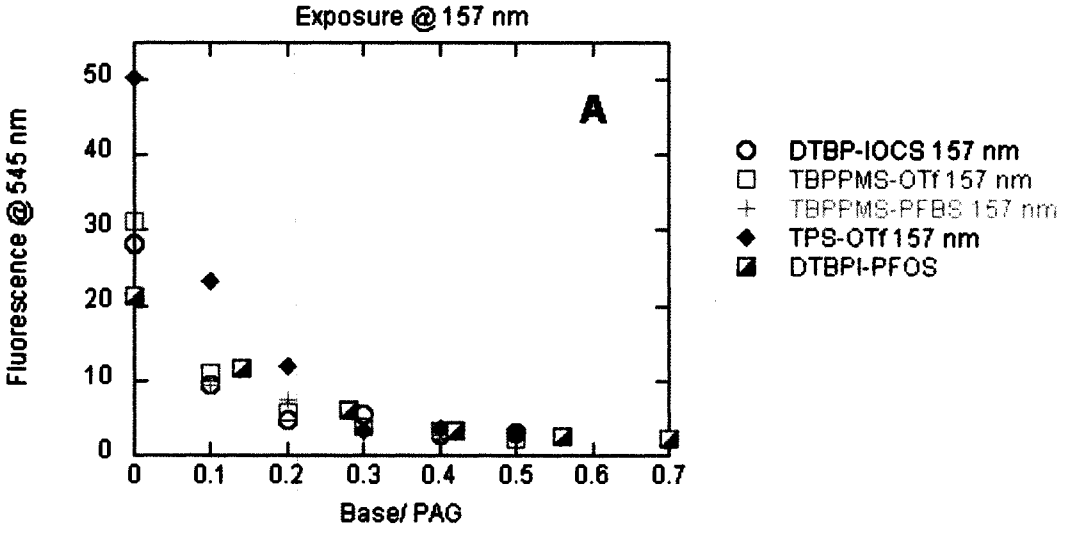

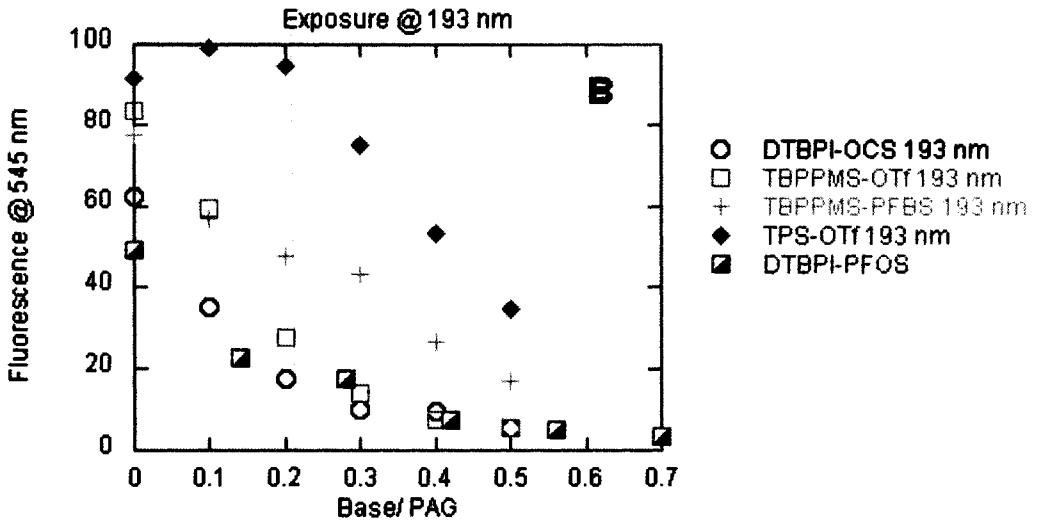

Figure 3-9. The intensity of fluorescence of monoprotonated C6 in FP films at 545 nm as a function of the amount of base added to the stock solution; exposure to 3.2 mJ/ cm^2 at 157 nm (A) and 193 nm (B) laser radiation. The excitation wavelength was 510 nm, C6 and PAGs loadings represented 0.5 % and 3.0 % based on FP weight.

The data in figure 3-9 was averaged over two sets of experiments for the diaryl iodonium compounds and for TBPPMS-PFBS, and over three sets of experiments for TPS-OTf and TBPPMS-OTf.

The incident dose on the films is relatively small, 3.2 mJ/ cm^2, 0.8 mJ/ cm^2/ shot, delivered in four shots at a frequency of 1 shot/ s, allowing the film to cool between shots. Some of the incident photons are absorbed by the polymer matrix, the excess energy being released as heat through vibrational relaxation. Some photons absorbed by the PAG do not lead to formation of acid, after all the quantum yield of acid generation is lower than 1.0. [37, 38] The PAG molecules that absorbed photons and did not photolyse, will release their excess energy as heat. While these PAGs are thermally stable during the thermal treatment at 95 °C inside an oven, they may not be as stable when the polymer matrix is heated by vibrational relaxation of the polymer and PAGs molecules, when the temperature can be very high. Thus it is important to allow enough time for the polymer matrix to cool, using a low frequency of shots. It is essential for the acid to be photogenerated and not

thermally generated. By heating the polymer matrix, one of the possible side reactions would be thermal production of acid in the immediate vicinity of the exposed areas, increasing the line edge roughness (LER). [40, 41] Heating, even at micrometer scale, may also lead to thermal degradation of the polymer, unwanted reactions which may alter its solubility in the developing solvent. The relatively small incident dose was chosen to allow formation of primary photoproducts only, avoiding formation of secondary photoproducts. At higher incident doses at 157 nm photodarkening may occur, reducing the number of photons that will reach the PAG molecules towards the bottom of the film. [27]

By plotting the fluorescence intensity at 545 nm (the peak in emission characteristic to $C6H^+$) as a function of base/ PAG mole ratio, it is possible to determine the number of moles of acid formed for a specific incident dose, figure 3-10. This protocol would give more quantitative information if it would be possible to work with smaller incident doses and with more base/ PAG mole ratio, allowing for more points in the plot. However, the lasers available in the laboratory did not allow small energy doses per shot. As the energy/ shot was decreased (by adjusting the voltage or by changing the composition of the gas mixture), the laser power became unstable and the energy/ power started to fluctuate. However, from figure 3-9 one can notice that it is possible to obtain quantitative information about the PAG's performance. It means that for 3.2 mJ/ cm^2 at 157 nm there were photolysed ~ 25 % of the moles of PAG present in the exposed areas (~ 2.0 cm^2). Knowing the thickness of the film and the exposed area, one can calculate the exposed volume. Measurements of the film thickness before and after PAB did not show a significant difference in film thickness (the difference in film thickness was within the error range, $\pm$ 15 nm). Thus, when calculating the volume of the exposed film, the thickness was considered to be the same for the baked and non-baked film, namely 400 nm. For an exposed area of 2.0 cm^2, the volume of the exposed film is 8.0 x 10^{-5} cm^3 (mL). The density of the spin coated solution was 0.9 mg/ cm^3, and 1.0 g of solution contained 0.97 x 10^{-5} moles of TPS-OTf. In the exposed volume there were 1.06 x 10^{-9}moles of PAG. From figure 3-10 the onset corresponds to a base/

PAG mole ratio of 0.25, which means that the number of moles of acid formed during exposure to 3.2 mJ/ cm^2 at 157 nm represents 25 % of the initial number of moles of PAG from the exposed volume, namely 2.7 x 10^{-10} moles.

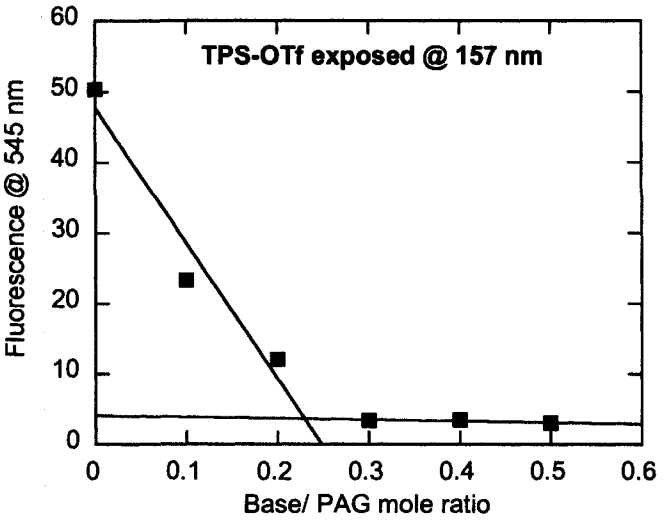

Figure 3-10. Fluorescence intensity of $C6H^+$ at 545 nm (λ_{ex} = 510 nm) as a function of base/ TPS-OTf mole ratio for an incident dose of 3.2 mJ/ cm^2 at 157 nm. The onset in the graph gives the moles of acid formed in the exposed area for an incident dose of 3.2 mJ/ cm^2

3.5 Case study for two photoacid generators: PAG2 and TPS-OTf

Two photoacid generators, TPS-OTf and PAG2 were selected to assess their acid formation abilities at 193 nm. *In-situ* acid-base titrations were used to detect the amount of acid formed and to distinguish between the two PAGs. Fluorescence and excitation spectra were recorded using C6 as acid sensor. Fluorescence microscopy was used to map acid formation and to record latent images in thin polymer films.

3.5.1 Use of fluorescence and excitation spectroscopy to detect and quantify acid formation in FP films exposed to radiation at 193 nm

In the previous section, *in-situ* acid-base titrations were done by varying the base/ PAG molar ratio for a constant incident dose. A similar approach is presented in this section, where the acid formation abilities of PAG2 and TPS-OTf at 193 nm are shown using a similar procedure. The difference is that this time the molar ratio of base/ PAG is constant, while the incident dose is varied. PAG 2 and TPS-OTf were selected for this study.

PAG2 was selected because it showed better acid formation abilities than PAG1 at 193 nm, while TPS-OTf was selected as a standard. The films were obtained by spin coating a solution containing 20 wt % FP, 80 wt % 2-heptanone, 2 wt % PAG based on the dry polymer weight (PAG2 1.16 x 10^{-2} M, and TPS-OTf 8.85 x 10^{-3} M in the stock solutions), and 0.5 wt % C6 based on the polymer weight (2.6 x 10^{-3} M). The films were baked after coating at 90 °C for 60 s, and cooled to room temperature prior to exposure to laser radiation at 193 nm, 0.46 mJ/ cm^2/ shot. The same film was exposed to increasing number of shots, and after each exposure it was baked inside the oven at 90 °C for 60 s. For all the spectra the excitation and emission slits inside the fluorimeter were the same, and the excitation wavelength was 510 nm. The results for PAG2 are shown in figure 3-11 for two films: one without 2-PE (A) added in the spin coated solution, and the other containing 2-PE in a 0.2 molar ratio (B) with respect to the PAG.

As the incident energy dose increases, so does the emission of $C6H^+$, showing that more acid is formed. A plot showing the maximum of emission at 550 nm as a function of the incident dose expressed in mJ/ cm^2 is shown in figure 3-13 for the films with and without added base.

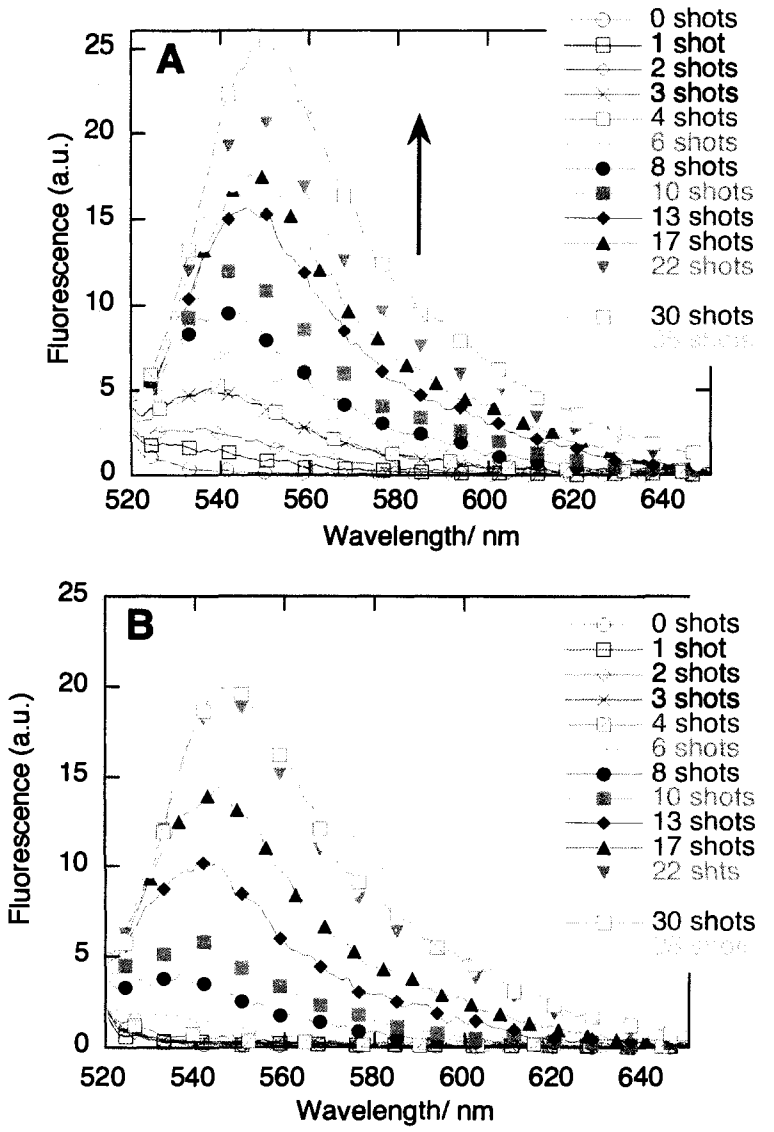

Figure 3-11. Fluorescence of $C6H^+$ (λ_{ex} = 510 nm) in FP films containing PAG2 and 2-PE in 0.0 (A) and 0.2 (B) base/ PAG2 molar ratio. The films were exposed to 193 nm, 0.46 mJ/ cm^2/ shot. PAG2 was 1.16 x 10^{-2} M, and C6 2.6 x 10^{-3} M in the spin coated solution.

Solutions containing similar concentrations of polymer (20 wt %), solvent 2-heptanone (80 wt %), photoacid generator (TPS-OTf 2.0 wt % based on FP weight, or 8.85 x 10^{-3} M), C6 (0.5 wt % based on FP weight or 2.6 x 10^{-3} M), and 2-PE (0.0 and 0.2 molar ratios relative to the TPS-OTf content) were prepared. The films containing 2-PE/ TPS-OTf = 0.0 and 0.2 molar ratios were obtained by spin coating a few drops of the stock solution at 3000 rpm for 20 s, followed by PEB inside the

oven at 90 °C for 60 s, and exposure to laser radiation at 193 nm to ~ 0.24 mJ/ cm^2/ shot. Following exposure, emission and excitation spectra of $C6H^+$ were recorded, figure 3-12, showing the versatility of this technique based on fluorescent acid sensors embedded in the film. For both films without base (figure 3-12 A and B) and with base (figure 3-12 C), the fluorescence and excitation spectra were in agreement. The excitation spectra were recorded by monitoring the emission at 550 nm, figure 3-12 B. They show a decrease of the peak at ~ 460 nm, characteristic to absorption of neutral C6, while the intensity of the peak centered at ~ 520 nm increases with the total incident dose. This is normal, since the neutral C6 is protonated by the acid produced by TPS-OTf during exposure. Similar to the emission spectra, a plateau is reached after approximately 20 shots. Excitation spectra were in agreement with the fluorescence spectra recorded for the film containing 2-PE/ TPS-OTf = 0.2 molar ratio, although they are not shown here for space considerations.

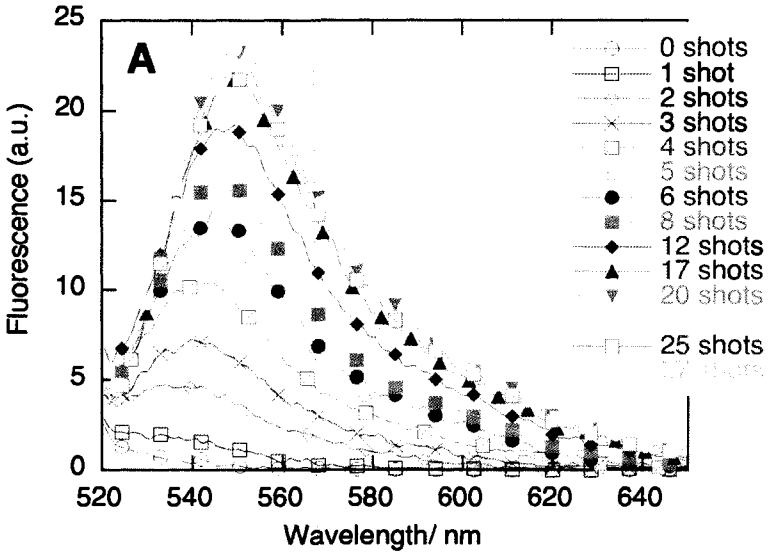

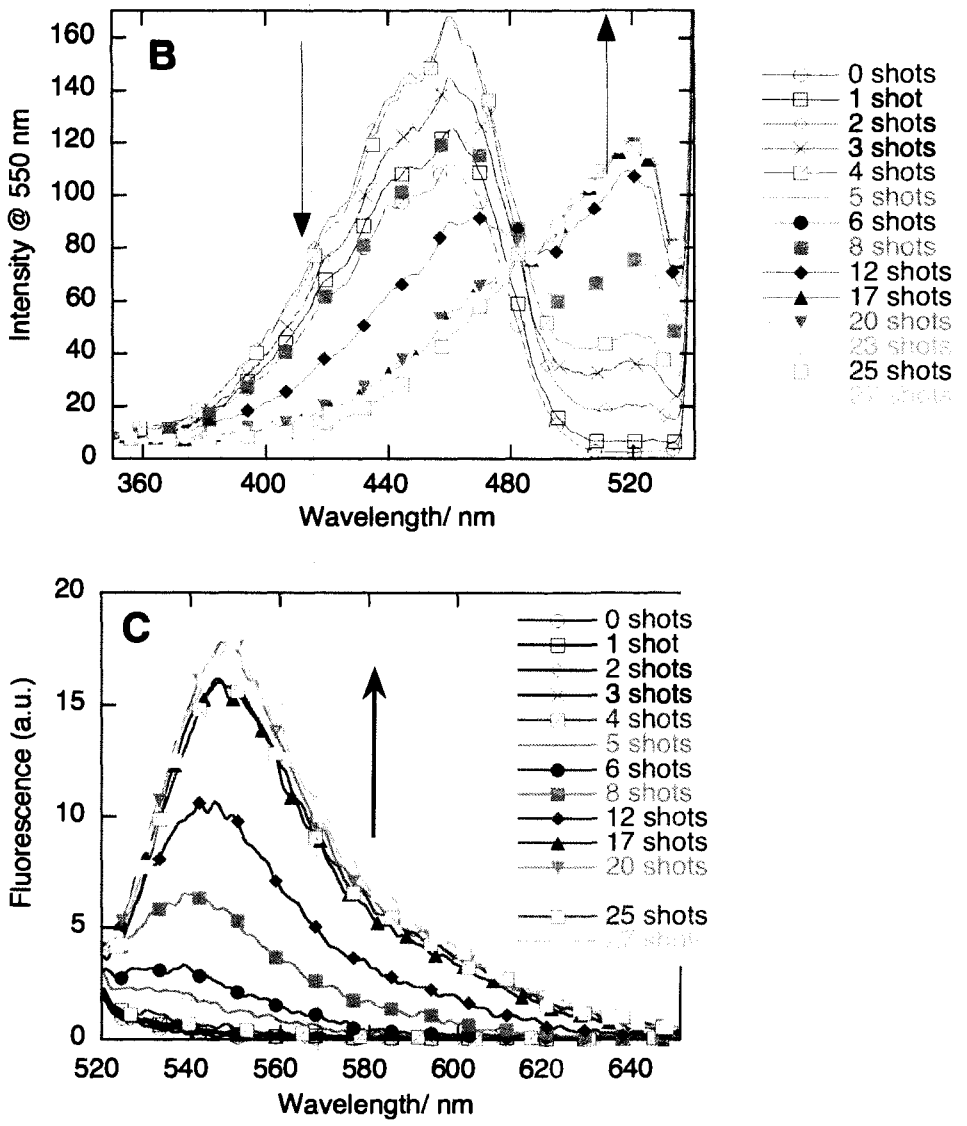

Figure 3-12. Fluorescence of $C6H^+$ (A and C), λ_{ex} = 510 nm, and excitation spectra monitored at 550 nm (B) of FP films containing TPS-OTf 2.0 wt % based on FP weight. The films were obtained by spin coating at 3000 rpm for 20 s, PAB and PEB at 90 °C for 60 s. Exposure was done at 193 nm, 0.24 mJ/ cm^2 at a frequency of 1 shot/ s. The 2-PE/ TPS-OTf molar ratio was 0.0 (A, B) and 0.2 (C). The concentration of TPS-OTf in the spin coated solution was 8.85 x 10^{-3} M.

In order to have a better image of the performance of the PAGs, the intensity of fluorescence at 550 nm was plotted as a function of the incident dose for both salts in the same graph, figure 3-13.

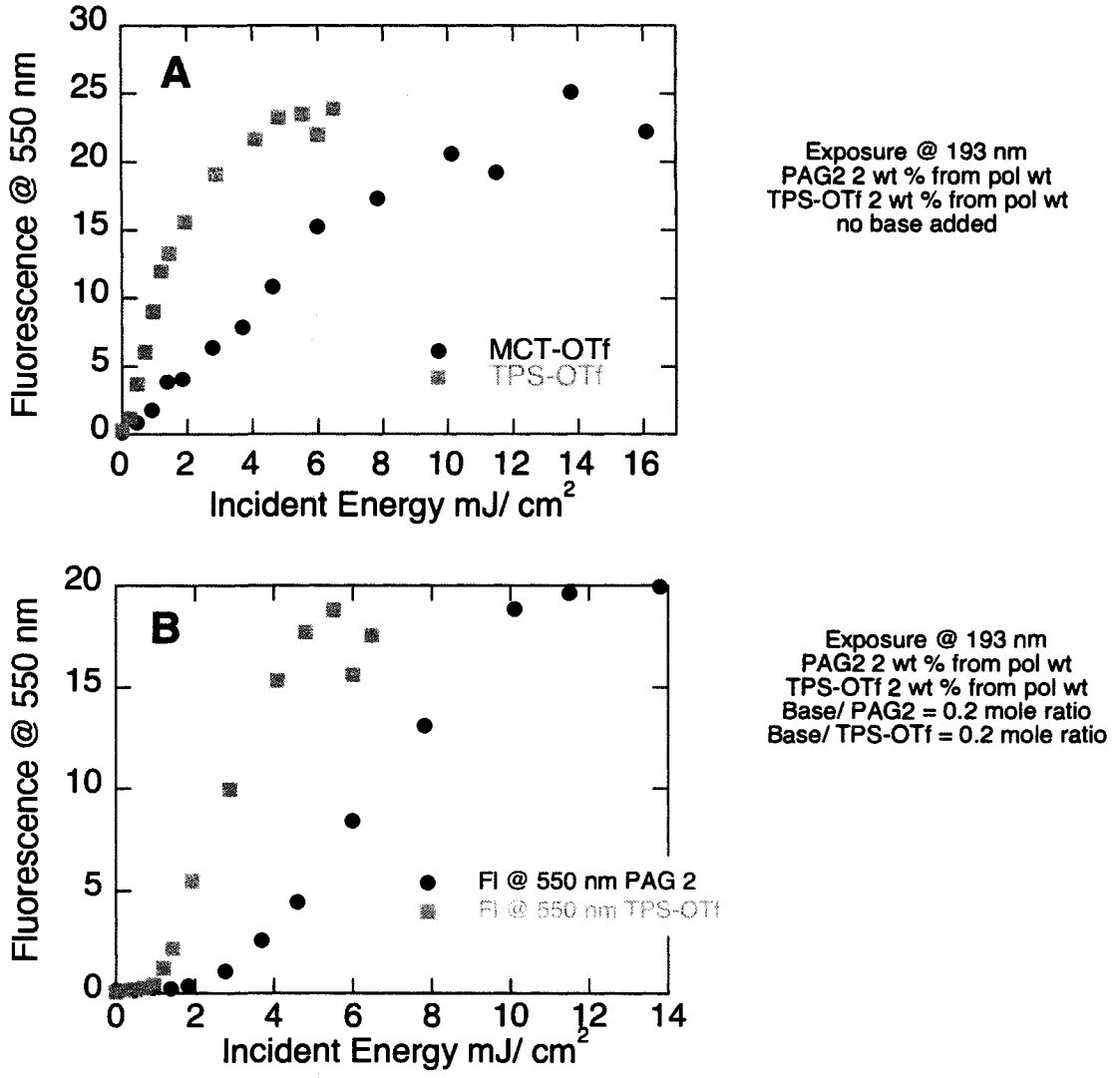

Figure 3-13. Fluorescence intensity of C6H$^+$ (λ_{ex} = 510 nm) at 550 nm as a function of incident energy dose for FP films exposed to 193 nm, containing TPS-OTf and PAG2 (2.0 % relative to the FP weight), and 2-PE/ PAG 0.0 (A) and 0.2 (B) molar ratio. The films containing PAG2 were exposed to 0.46 mJ/ cm^2/ shot, while those containing TPS-OTf were exposed to 0.24 mJ/ cm^2/ shot. The concentrations of the two PAGs in the stock solutions were 1.16 x 10^{-3} M for PAG2 and 8.85 x 10^{-3} M for TPS-OTf, and C6 2.6 x 10^{-3} M.

Although the plateau reached in fluorescence intensity is approximately the same, TPS-OTf forms acid faster than PAG2. For the films without 2-PE, the value of fluorescence in the plateau region is of ~ 25 a.u., figure 3-13 A. The film

containing TPS-OTf reaches this value after ~ 5.0 mJ/ cm^2, while the film containing PAG2 reaches this value after ~ 14.0 mJ/ cm^2. It is clear that PAG2 needs ~ 2.8 times more photons to form the same amount of acid as TPS-OTf. The value of the plateau is reached when all the C6 was protonated, since in this case C6 is the limiting reagent. The molar ratio in the stock solutions (solutions that are spin coated) are TPS-OTf : C6 = 3.4 : 1 and PAG2 : C6 = 4.4 : 1.

When 2-PE is added in the solution to be spin coated, such that the molar ratio PAG : 2-PE = 1 : 0.2, the value of the emission intensity characteristic to C6 in the plateau region is ~ 20 a.u. for both PAGs, figure 3-13 B. This value in the plateau region is ~ 20 % lower than in the case of results obtained without base, figure 3-12 A. At the same time, at lower incident doses, there is a lag in fluorescence build up, caused by the fact that the *in-situ* formed acid reacted with 2-PE first, then when all 2-PE was consumed, the excess acid started to protonate C6. The onset in figure 3-13 B gives the dose at which the number of moles of acid formed starts to exceed the number of moles of base. For TPS-OTf this value is ~ 1.0 mJ/ cm^2, while for PAG2 it is ~ 2.4 mJ/ cm^2. Thus PAG2 needs ~ 2.4 times more photons to protonate all the 2-PE present in the film, a value close to the result from figure 3-13 A, where PAG2 needs ~ 2.8 times more photons than TPS-OTf in order to form the same amount of acid.

The protocol developed here, based on *in-situ* acid base titrations, has proven a valuable tool in characterizing and assessing PAGs' abilities to form acid, and even more, to quantify the amount of acid formed as a function of the incident dose.

3.5.2 Use of fluorescence imaging to detect acid formation in thin films exposed to laser radiation at 157 nm

Comparison of the abilities of PAG2 and TPS-OTf to form acid at 157 nm was done using fluorescence microscopy, figure 3-14.

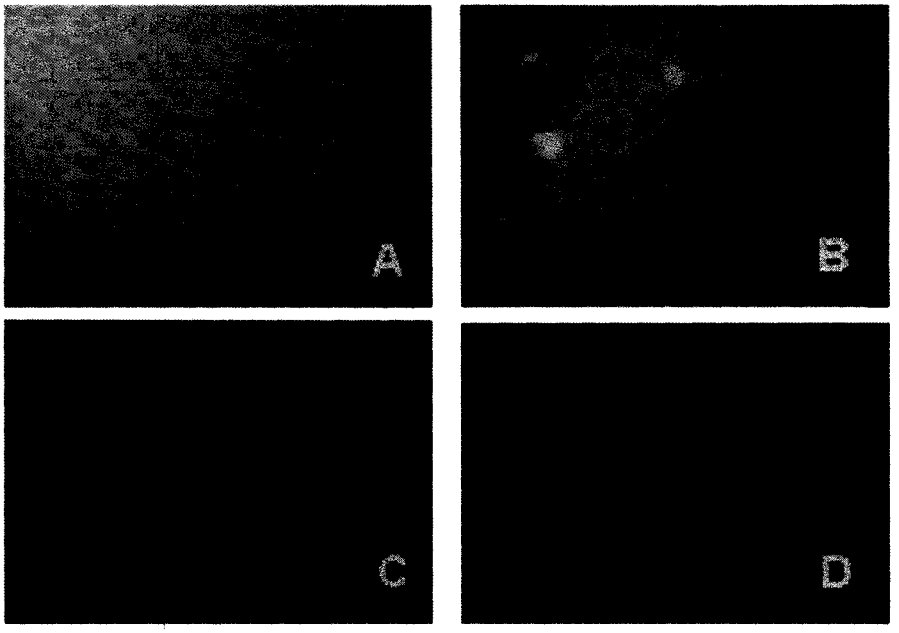

Figure 3-14. Fluorescence images of neutral Coumarin 6 (A and B) and protonated Coumarin 6 (C and D) in thin FP films containing 0.5 wt % C6, 2.0 wt % PAG2 (A, C) and 2.0 wt % TPS-OTf (B, D) based on polymer weight, exposed to 1 shot at 157 nm, 2.5 mJ/ cm^2/ shot.

The films were obtained from a solution containing 80 wt % 2-heptanone, 20 wt % fluorinated polymer (FP), and 0.5 % C6 and 2.0 % PAG relative to the polymer's weight. The solution was spin coated on top of one inch (2.54 cm) quartz discs at 3000 rpm for 20 s, followed by PAB at 90 °C inside the oven. The films were cooled to RT prior to exposure. After exposure the films were baked at 90 °C for 60 s, and cooled to RT prior to recording the fluorescence images. Copper grids

with hexagonal holes were placed on top of the films, then exposed to laser radiation at 157 nm inside a nitrogen box. The incident dose was 2.5 mJ/ cm^2/ shot, the same dose for the films used to record images from figure 3-1. Similar images were obtained with various incident doses, however, they are not shown here for space considerations.

From figure 3-14 one can notice that both positive ($C6H^+$) and negative (C6) images of Coumarin 6 were recorded. From the positive images (C, D) it is noticeable that the film containing TPS-OTf shows a more intense red in the exposed regions, confirming that TPS-OTf is a more effective photoacid generator than PAG2. The fact that both positive and negative fluorescence images were recorded is a proof that the two PAGs form acid upon photolysis with light at 157 nm. These results are encouraging and show that PAG2 is a viable choice for CA photoresists at 157 and 193 nm.

3.6 Measuring absorbance of PAGs at 157 nm

Absorbance is the key parameter in DUV and VUV photolithography. Knowing the actual value of absorbance at the exposure wavelength helps adjusting the resist formulation, concentrations of chemical compounds used or thickness of the film. It is a common practice in the microlithography industry to express the absorbance of a film at the exposure wavelength in μm^{-1}. The absorbance at 157 nm is measured with a vacuum ellipsometer, using a technique called variable angle spectroscopic ellipsometry. [42] Unfortunately this equipment was not available in our department during the time this thesis was completed. Thus, there was a need to develop another method that would help determine the approximate absorbance of the photoresist, PAG or polymer at 157 nm.

The experimental set up used to measure absorbance at 157 nm is described in figure 3-15. This set up gives the value of absorbance at 157 nm for that particular film thickness, not an absorption spectrum.

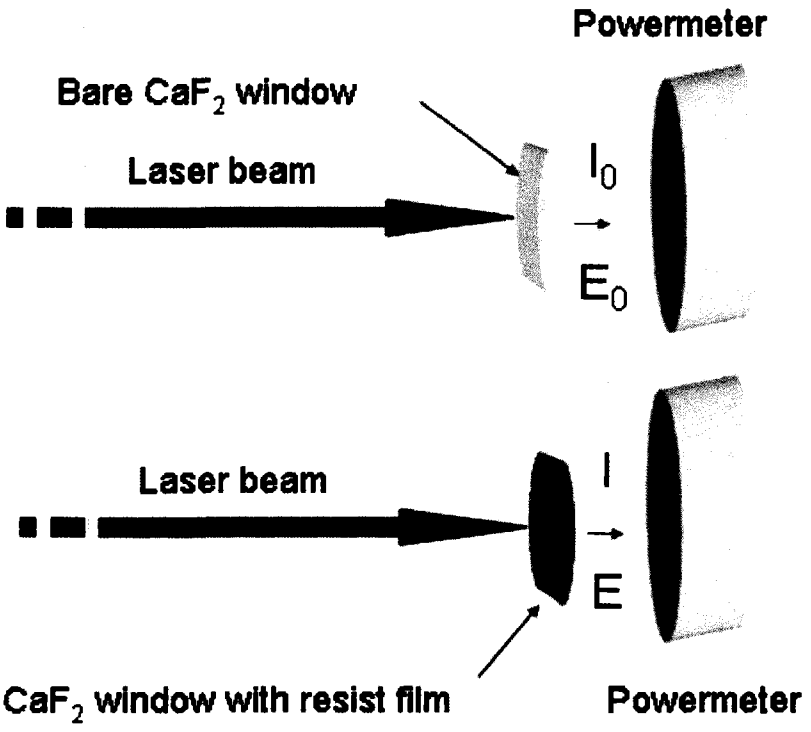

Figure 3-15. Experimental set up for determination of absorbance at 157 nm using the laser as a light source.

The principle of this method is based on the definition of absorbance, the Lambert-Beer law, equation 3-1.

$$A = \log_{10} \frac{I_0}{I} = \varepsilon c l \qquad \text{eq. 3-1}$$

where ε is the absorption coefficient at a certain wavelength (it is a constant), l is the length of the light path (unit is cm), c is the concentration expressed in $mol \times L^{-1}$, I_0 is the intensity of the incident light, I is the intensity of the transmitted light.

The films are spin coated on top of CaF_2 windows, a substrate that has a very low absorbance at 157 nm, thus allowing light to penetrate and reach the powermeter. The difference between the incident energy and the energy measured

by the powermeter behind the bare CaF2 window is considered to be E_0, while the difference in energy between the incident beam and the energy measured behind the CaF_2 window with a film coated on top is considered to be E. The difference between incident energy on the film and the transmitted energy gives the energy (photons) absorbed by the film. The energy of the laser beam is the sum of energies of each photon at 157 nm, thus it depends on the intensity of the laser beam. Measurements done with the powermeter after spin coating polymer films on top of the substrate clearly show a decrease in the energy of the beam reaching the photodetector, compared to the energy transmitted by the bare CaF_2 window. The difference is given by the number of photons absorbed by the polymer film. By dividing this energy with the energy of a photon, it is possible to calculate the number of photons absorbed. This number could later be used to calculate the quantum yield of acid generation at 157 nm.

The energy of a photon is given by the formula:

$$E = h\nu = h\frac{c}{\lambda} \qquad \text{eq. 3-2}$$

where E – energy of a photon, h – Planck's constant (6.626×10^{-34} J s), c – speed of light in air (2.998×10^{8} m s^{-1}), λ – the wavelength of radiation in m.

Experiments using the CaF_2 window with a thin polymer film on top (E_0) and with a polymer film containing the PAG (E) were done and the absorbance of the PAG was calculated, but the errors were too big. The difference in energy of the light reaching the photodetector for the polymer film without PAG and with PAG was caused by the absorbance of the PAG. Using the equation 3-1 and replacing I_0 by E_0 and I by E, the value of absorbance was calculated, for a given thickness and concentration of the film. Using this methodology, it is possible to determine the extinction coefficient of different PAGs at 157 nm.

Although the method is easily applicable, it has its limitations. First of all, one has to make sure that the energy of the beam incident on the surface of the film with and without PAGs is the same. E_0 and E are the values of energy that is transmitted in the absence and the presence of the PAG, and in order to use these values it is necessary to have the same number of photons incident on the film in both cases. This was impossible to achieve, since, unlike in the case of 248 and 193 nm lasers, the 157 nm laser used showed fluctuations in energy from one laser shot to the other. The reported values for 157 nm are averages registered over a considerable number of shots. The GSI-Lumonics laser was designed for high energy output, tens or hundreds of mJ/ cm^2/ shot, while for this experiment it was used to obtain values of energy of ~ 2.5 mJ/ cm^2/ shot.

Another aspect is related to the photochemistry of the PAG during measurements. All the measurements should be done with only one incident shot, since during the first shot, some of the PAG starts to photolyse. Thus, for the second shot the absorbance recorded does not reflect the absorbance of the initial number of moles of PAG, since some of it was photolysed during the first shot. Even more, some of the photoproducts may absorb. Thus it is crucial to be able to absorb the energy transmitted when only one incident shot is used.

Assuming that this condition may be achieved, the next thing to consider is how many of the incident photons are scattered by the PAG present in the film and how many are absorbed.

The difference in the transmitted energy between the polymer film containing the PAG and the one without the PAG is very small, after all the thickness of the film (light path) is a few hundreds of nanometers. One needs very sensitive and precise measurements of the energy of the transmitted light.

The method proposed here to measure the absorbance at 157 nm is applicable once the limitations and sources of error are eliminated. The result obtained here may help to calculate the quantum yield of acid generation at 157 nm. The quantum yield, (Φ), is given by the ratio *moles of acid produced/ moles of photons absorbed*. With the methods presented in this chapter one can calculate

the moles of photons absorbed by the PAG and the moles of acid produced, obtaining in the end the quantum yield of acid generation at 157 nm.

As a proof that the method described above gives plausible results, it was used to calculate the quantum yield at 193 nm. The selected PAGs for this study were TPS-PFBS and TBPPMS-OTf. The quantum yields obtained were 0.39 for TPS-PFBS and 0.15 for TBPPMS-OTf, values that are reasonable and in the range previously reported for PAGs.[1, 33, 34]

3.7 Experimental

3.7.1 Materials

Coumarin 6 (98%), 2-heptanone (99%), and 2-piperidin-1-yl-ethanol (2PE) (99%) were purchased from Aldrich and used as received. The five photoacid generators from chart 3-3 (DTBPI-OCS, DTBPI-PFOS, TBPPMS-OTf, TBPPMS-PFBS, and TPS-OTf) and the fluorinated polymer (FP) were a kind gift from Rohm and Haas Electronic Materials, and they were used as received. The two photoacid generators from chart 3-2 (PAG1 and PAG2) were synthesized in our laboratory by Dr. Carlos Sanrame, purified and characterized by ^{1}H and ^{13}C NMR, and GC/ MS (article in preparations).

3.7.2 Equipment

The exposures were done at 157, 193 and 248 nm using GSI Lumonics excimer lasers with F_2, ArF and KrF respectively as gas mixtures (fwhm 12-15 ns). The energy of the laser beam was varied either by varying the voltage of the laser cavity or by using different concentrations of fluorine gas. The energy of the laser beam was measured with a JD2000 joulemeter radiometer and a Coherent J45LP-MB photon detector. For the experiments involving fluorescence imaging, copper masks with hexagonal holes were placed on top of the films. The centers of the hexagons were 60 μm (micrometers) apart.

Absorption spectra were recorded using a Cary 50 Bio UV-Visible spectrophotometer. Fluorescence spectra were recorded using a front-face set up in a LS-50 Perkin Elmer luminescence spectrometer. The excitation wavelengths were 510 nm for the detection of protonated Coumarin 6, $C6H^{+}$, and 450 nm for the neutral form, C6.

For the set of experiments involving the photoresists XP 1215Aa, figure 3-2, the exposure at 157 nm was done under a nitrogen atmosphere using an MSX-250 excimer laser from MPB Technologies connected to the sample compartment through a sealed pipe. The incident dose was ~ 2.3 mJ/ cm^2/ shot and the repetition rate was 1-3 Hz. The fluorescence images were recorded with a Zeiss Universal microscope, having a 50-watt mercury arc lamp as a light source. The optical excitation filters used were 485 $\pm$ 20 nm band pass and reflected by a 510 nm long pass dichroic beam splitter for the negative images. The positive images were recorded with an excitation filter at 546 $\pm$ 12 nm band pass, with a 580 nm long pass dichroic beam splitter and emission monitored with a 590 nm long pass filter. The microscope had a 4X objective and 0.4 numerical aperture, with a finite tube length of 170 mm. The images were recorded with a Sony digital camera. The filters used for recording fluorescence latent images were rather a limitation of the available equipment in the laboratory.

Wherever the exposure wavelength used in experiment was 254 nm, the source was a Hg lamp in an Exposure Unit from Hybrid Technology Group, California. The power output of the lamp was 39.7 W/ m^2 or 3.97 mW/ cm^2, as measured with the Luzchem Research spectroradiometer.

The fluorescence images recorded with PAG2 and TPS-OTf in FP films were obtained using a Leica DMSL fluorescence microscope with a 20x objective, and a 50 W Hg lamp as a light source. Filter cubes E4 (excitation: centered at 436 nm, emission: long pass 470 nm) and M2 (excitation: centered at 546 nm, emission: long pass 590 nm) from Leica were used to monitor the fluorescence of C6 and protonated C6 respectively. The fluorescence images were acquired using the software Leica IM50 version 4.0 release 117 from Leica Microsystems Imaging Solutions Ltd.

All the exposure at 157 nm were done under a N_2 atmosphere in a sealed chamber connected to the laser with a metal pipe.

3.7.3 Experimental techniques

All the films were obtained by spin coating the solutions on top of either quartz discs (1.0 inch diameter or 2.54 cm) or CaF_2 windows from Aldrich. The coating speed was either 2000 or 3000 rpm (it is specified in the text for each particular experiment) for duration of 20 s. Following spin coating, the films were baked inside an oven at 95 – 100 °C for 60 s, then cooled to RT on a metallic surface prior to exposure, absorbance or fluorescence measurements.

For the measurements of absorbance at 157 nm using the laser, the photodetector connected to the power meter was kept at the same distance from the CaF_2 window and in the same position during all the measurements. The box in which exposure was done was purged with nitrogen for the same time interval before each exposure. To ensure that there was a higher pressure inside the box, the nitrogen flow was reduced but not completely shut down during the exposure.

The fluorescence was measured with the Perkin Elmer fluorimeter using a holder especially designed for films, in a front face set up. However, the angle was not 45°, thus avoiding any reflection of the incident beam and capturing only the light emitted by the sample.

The base 2-pyperidine ethanol (2PE) was added to separate vials containing known volumes of the solutions before spin coating. The base was diluted in the same solvent, 2-heptanone, obtaining a stock solution, then added with a μL (microliter) syringe so that the right base/ PAG mole ratio would be obtained.

The thickness of the films was measured before adding Coumarin 6 to the stock solution. This was necessary because the absorbance of the dye would diminish the reflectance signal in the TFA.

The values of energy for different lasers were averaged over many series of ten shots using the same frequency (shots/ s) that would be used for the actual exposure of the samples.

3.8 References

(1) Ito, H., "Chemical Amplification Resists for Microlithography", *Adv. Polym. Sci.* **2005**, *172,* 37-245.

(2) Wallraf, G. M.; Hinsberg, W. D., "Lithographic techniques for the formation of nanoscopic features", *Chem. Rev.* **1999**, *99,* 1801-1021.

(3) Moore, G. E., "Cramming more components onto integrated circuits", *Electronics* **1965**, *38,*

(4) Ito, H.; Wilson, C. G.; Fréchet, J. M. J., "Résines pour UV lointain mettant en oeuvre un méchanisme d'amplification chimique. Sensitive deep UV resist incorporating chemical amplification", *Symp. VLSI Technol.* **1982**, *260,* 262.

(5) Frenette, M.; Ivan, M. G.; Scaiano, J. C., "Use of fluorescent probes to determine catalytic chain length in chemically amplified resists", *Can. J. Chem.* **2005**, *83,* 869-874.

(6) Mc Kean, U. S. D.; MacDonald, S. A., "Acid Photogeneration from Sulfonium Salts in Solid Polymer Matrices", *J. Polym. Sci. A: Polym. Chem.* **1989**, *27,* 3927.

(7) Crivello, J. V., "The Discovery and Development of Onium Salts Cationic Photoinitiators", *J. Pol. Sci. A: Pol. Chem.* **1999**, *37,* 4241-4254.

(8) Crivello, J. V.; Lee, J. L., "Photosensitized Cationic Polymerization Using Dialkylphenacylsulfonium and Dialkyl(4-hydroxyphenyl) Sulfonium Salt Photoinitiators", *Macromolecules* **1981**, *14,* 1141-1147.

(9) Ito, H., "Chemical amplification resists: History and development within IBM", *IBM J. Res. Develop.* **2000**, *44,* 119-130.

(10) Reichmanis, E.; Houlihan, F. M.; Nalamasu, O.; Neenan, T. X., "Chemical Amplification Mechanism for Microlithography", *Chem. Mater.* **1991**, *3,* 394-407.

(11) Dektar, J. L.; Hacker, N. P., "Photochemistry of Diaryliodonium Salts", *J. Org. Chem.* **1990**, *55,* 639-647.

(12) Dektar, J. L.; Hacker, N. P., "Photochemistry of Triarylsulfonium Salts", *J. Am. Chem. Soc.* **1990**, *112,* 6004-6015.

(13) Dektar, J. L.; Hacker, N. P., "Triphenylsulfonium Salt Photochemistry. New Evidence for Triplet Excited State Reactions", *J. Org. Chem.* **1988**, *53,* 1833-1835.

(14) Knapczyk, J. W.; McEwen, W. E., "Photolysis of Triarylsulfonium Salts in Alcohol", *J. Org. Chem.* **1970**, *35,* 2539-2543.

(15) Tagawa, S.; Nagahara, S.; Iwamoto, T.; Wakita, M.; Kozawa, T.; Yamamoto, Y.; Werst, D.; Trifunac, A. D., "Radiation and Photochemistry of Onium Sal Acid Generators in Chemically Amplified Resists", *Proc. SPIE* **2000**, *3999,* 204-213.

(16) Pohlers, G.; Scaiano, J. C.; Sinta, R., "Determination of Photoacid generation Efficiencies", *Chem. Mater.* **1997**, *9,* 3222.

(17) Salvagione, H. J.; Miras, M. C.; Barbero, C., "Photolithographic Patterning of a Conductive Polymer Using a Polymeric Photoacid Generator and a Traceless Removable Group", *Macromol. Rapid Commun.* **2006**, *27,* 26-30.

(18) Corrent, S.; Hahn, P.; Pohlers, G.; Connolly, T.; Scaiano, J. C.; Fornes, V.; Garcia, H., "Intrazeolite Photochemistry. 22. Acid-Base Properties of Coumarin 6. Characterization in Solution, the Solid State, and Incorporated into Supramolecular Systems", *J. Phys. Chem. B* **1998**, *102,* 5850-5858.

(19) Pohlers, G.; Suzuki, Y.; Chan, N.; Cameron, J., "Transparency vs. Efficiency in 193 nm Photoacid Generator Design", *Proc. SPIE* **2002**, *4690,* 178-190.

(20) Bloomstein, T. M.; Rotschild, M.; Kunz, R. R.; Goodman, R. B.; Palmaci, S. T., "Critical issues in 157 nm lithography", *J. Vac. Sci. Technol. B* **1998**, *16,* 3154.

(21) Dentinger, P. M.; Lu, B. L.; Taylor, J. W.; Bukofsky, S. J.; Feke, G. D.; Hessman, D.; Grober, R. D., "On-wafer photoacid determination and imaging technique for chemically amplified photoresists", *J. Vac. Sci. Technol. B* **1998**, *16,* 3767-3772.

(22) Liberman, V.; Bloomstein, T. M.; Rotschild, M.; Sedlacek, J. H.; Uttaro, R. S.; Bates, A. K.; Peski, V. C.; Orvek, K. J., "Materials issues for optical components and photomasks in 157 nm lithography", *J. Vac. Sci. Technol. B* **1999**, *17,* 3273.

(23) Scaiano, J. C.; Laferriere, M.; Ivan, M. G.; Taylor, G. N., " A Protocol for the Verification of Acid Generation in 157 nm Lithography", *Macromolecules* **2003**, *36,* 6692.

(24) Leigh, W. L.; Cook, B. H. O., "Stereospecific (Conrotatory) Photochemical Ring Opening of Alkylcyclobutenes in the Gas Phase and in Solution. Ring Opening from the Rydberg Excited State or by Hot Groung State Reaction", *J. Org. Chem.* **1999**, *64,* 5256.

(25) Kim, J. B.; Kwon, Y. G.; Choi, J. H.; Jung, M. H., "Acid Diffusion and evaporation in chemically amplified resists", *Proc. SPIE* **1999**, *3678,* 536-543.

(26) Farmanara, P.; Steinkellner, O.; Wick, M. T.; Whittmann, M.; Korn, G.; Stert, V., "Ultrafast internal conversion and photodissociation of molecules excited by femtosecond 155 nm laser pulses", *J. Chem. Phys.* **1999**, *111,* 6264-6270.

(27) Lee, K.; Jockusch, S.; Turro, N. J.; French, R. H.; Wheland, R. C.; Lemon, M. F.; Braun, A. M.; Widerschpan, T.; Dixon, D. A.; Li, J.; Ivan, M.; Zimmerman, P., "157 nm Pellicles (Thin Films) for Photolithography: Mechanistic Investigations on the VUV and UV-C Photolysis of Fluorocarbons", *J. Am. Chem. Soc.* **2005**, *127,* 8320.

(28) Yatsuhashi, T.; Nakashima, N., "VUV Laser Chemistry - Formation of Hot Molecules and Their Reactions in the Gas Phase", *Bull. Chem. Soc. Jpn.* **2001**, *74,* 579-593.

(29) Costela, A.; Garcia-Moreno, I.; Florido, F.; Figuera, J. M.; Sastre, R.; Hooker, S. M.; Cashmore, J. S.; Webb, C. E., "Laser ablation of polymeric materials at 157 nm", *J. Appl. Phys.* **1995**, *77,* 2343-2350.

(30) Fedynyshyn, T. H.; Kunz, R. R.; Sinta, R. F.; Goodman, R. B.; Doran, S. P., "Polymer photochemistry at advanced optical wavelengths", *J. Vac. Sci. Technol. B* **2000**, *18,* 3332.

(31) Irie, S.; Hagiwara, T.; Fuji, K.; Itakura, Y.; Kawasa, Y.; Egawa, K.; Uchino, I.; Sumitani, A.; Itani, T., "Evaluation of outgassing from a fluorinated resist for 157 nm lithography", *J. Vac. Sci. Tech. B* **2004**, *22,* 3513-3517.

(32) Garza, C. M.; Bierschenk, T., "Degradation Mechanism and Materials for 157 nm Pellicles", *Optical Microlithography XVII, Proc. SPIE* **2004**, *5377,* 527-536.

(33) Feke, G. D.; Grober, R. D.; Pohlers, G.; Moore, K.; Cameron, J. F., "On wafer spectrofluorometric method for determination of relative quantum yields of photoacid generation in chemically amplified resists", *Anal. Chem.* **2001**, *73,* 3472-3480.

(34) Feke, G. D.; Hessman, D.; Grober, R. D., "On-wafer spectrofluorometric evaluation of the response of photoacid generator compounds in chemically amplified photoresists", *J. Vac. Sci. Technol. B* **2000**, *18,* 136-139.

(35) Dagani, R., *Chem. Eng. News* **2003**, *81,* 44.

(36) Ivan, M. G.; Laferriere, M.; Sanrame, C. N.; Scaiano, J. C., "On the Question of Acid Generation upon 157-nm Laser Exposure of Fluorinated Polymers", *Chem. Mater.* **2006**, *18,* 2635-2641.

(37) Ray, C.; Mason, M.; Grober, R. D.; Pohlers, G.; Staford, C.; Cameron, J. F., "Quantum yield of Photoacid Generation in 193-nm Chemically Amplified Resists by Fluorescence Imaging Spectroscopy", *Chem. Mater.* **2004**, *16,* 5726-5730.

(38) Tsiartas, P. C.; Schmid, G. M.; Johnson, H. F.; Stewart, M. D.; Willson, C. G., "Quantifying acid generation efficiency for photoresist applications", *J. Vac. Sci. Tech. B* **2005**, *23,* 224-228.

(39) Getoff, N.; Schenk, G. O., "Primary Products of Liquid Water Photolysis at 1236, 1470 and 1849 Å", *Photochem. Photobiol.* **1968**, *8,* 167.

(40) Pawloski, A. P.; Nealy, P. F.; Nealy, C., "Micromolar Concentrations of base quenchers impact the apparent efficiency of photoacid generation in chemically amplified resists", *J. Vac. Sci. Technol. B* **2002**, *20,* 2162-2168.

(41) Pawloski, A. P.; Nealy, P. F., "The Multifunctional Role of Base Quenchers in Chemically Amplified Photoresists", *Chem. Mater.* **2002**, *14,* 4192.

(42) Wagner, T.; Hilfiker, J. N.; Tiwald, T. E.; Bungay, C. L.; Zollner, S., "Materials Characterization in the Vacuum Ultraviolet with Variable Angle Spectroscopic Ellipsometry", *Phys. Stat. Sol (a)* **2001**, *188,* 1553-1562.

Determination of the Catalytic Chain Length in Chemically Amplified Resists

4. Determination of the Catalytic Chain Length in Chemically Amplified Resists

4.1 Introduction

In microlithography, and in particular in photolithography, chemically amplified (CA) photoresists based on the catalytic effect of small amounts of acid, formed throughout the polymer film during exposure to light of various wavelengths, are the core of the advancement towards smaller and faster computer processors. [1-3] The concept of CA resists was introduced at the beginning of 1980's by Ito, Fréchet, and Wilson. [4] The need for a breakthrough in microlithography was caused by the inherent limitations of diazoquinone/ novolac resists which required several photons for one useful product, thus limiting the sensitivity of the photoresist. [5] Chemical amplification was initially thought to work on three directions: for negative imaging through crosslinking, positive imaging through depolymerization, and positive/ negative imaging through cleavage of pendant groups, which would induce a change in polarity/ solubility. From the three possible directions, deprotection through cleavage of pendant groups was implemented and further developed at industrial scale. The first resist which used the concept of chemical amplification was a two-component resist, consisting of poly(4-*tert*-butoxycarbonyloxystyrene) (PBOCST) and an acid generator. [1, 6] The acid produced *in situ* catalyzes the deprotection of pendant *tert*-butoxycarbonyl (*t*-Boc) group, resulting poly(4-hydroxystyrene) (PHOST), CO_2 and a tertiary carbocation which rearranges to give isobutene and a proton, scheme 1. [1, 3, 6-8] The chemical amplification comes from the fact that one proton can catalyze many deprotection reactions and be recovered after each deprotection step.

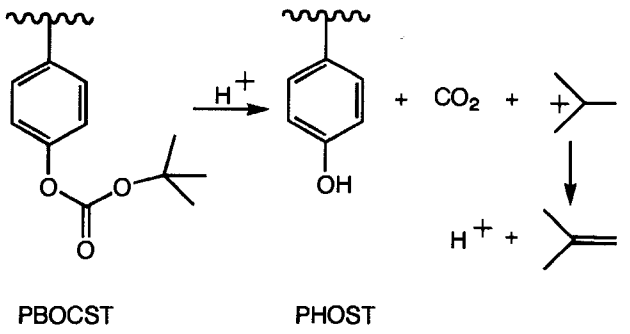

Scheme 4-1. Catalytic cycle for a poly(4-*tert*-butoxycarbonyloxystyrene) (PBOCST) chemically amplified resist designed for photolithography at 248 nm. The proton, previously obtained through a photolysis reaction of a PAG, catalyzes deprotection of a pendant esteric group, leading to formation of (4-hydroxystyrene) (PHOST), CO_2 and a tertiary carbocation. The tertiary carbocation rearranges to isobutene, and the proton is recovered, thus completing the catalytic cycle.

The catalytic chain length (CCL) is given by the number of groups deprotected by one proton. Values previously reported are in the range 100 – 1000.[9] The values of CCL reported depend on the system studied and on the diffusion of H^+ throughout the polymer film.[9-12] The acid is obtained during a photolysis process from a precursor called photoacid generator (PAG) (see chapter 3 for more details on PAGs). For decades the industrial and academic research have focused on developing new polymers and PAGs suitable for shorter wavelengths. Polystyrene bearing various pendant groups (esters, ethers) capable of being deprotected by acidolysis was used in two component CA resists for photolithography at 248 nm. A few structures of these polymers are shown as examples in chart 1. Polymers containing phenolic rings are too absorptive at 193 nm, the wavelength used in industry after the 248 nm era. New acrylic polymers were developed, but the solubility switch, *t*-Boc group, remained the same. Further, for 157 nm photolithography, the development of new polymers was necessary since the absorbance of the acrylic resists used at 193 nm was too high. [13, 14]

Copolymers of norbornene derivatives with fluorinated monomers and acrylic groups bearing the solubility switch, as well as polysilsesquioxanes, were studied, with promising results. [1, 15] Although the exposure wavelength has decreased, the resists currently employed by industry still make use of the CA concept. At the same time with the research involving new polymers, new PAGs were designed, synthesized and tested. PAGs are organic salts with either an organic or inorganic counterion, which upon absorption of a photon can decompose releasing Brönsted acid and other photoproducts.

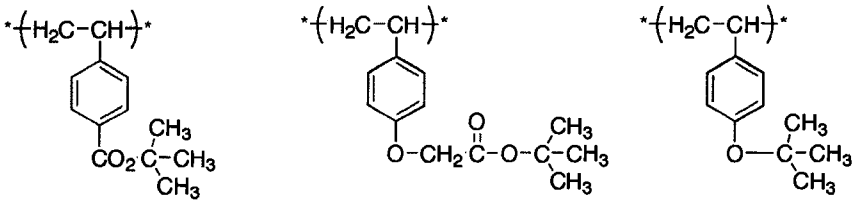

Chart 4-1. Structures of polystyrene bearing ether and ester acid-cleavable pendant groups, employed for 248 nm CA photolithography.

Previous reports in literature used IR spectroscopy as a tool to monitor the disappearance of the signal at ~ 1750 cm^{-1} characteristic to the carbonyl group. [9, 12] The goal of the project described in this chapter is to develop a new method to determine the CCL in thin polymer films, mimicking the conditions encountered in industry during the fabrication process. The detection and quantification of acid formed was done in polymer films exposed to radiation. Previous reports showed the advantage of determining the acid formed *in situ* rather than doing titrations after the film had been developed.[16-18] The techniques developed for this project were based on fluorescent sensors capable of revealing the amount of acid formed in the film,[19, 20] and the number of *t*-Boc groups deprotected.[21, 22] The project was a collaboration with M. Frenette, a graduate student in our group. For detection and quantification of acid, the fluorescent sensor used was Coumarin 6 (C6), a molecule already reported as an excellent acid sensor, since it drastically changes its

absorption and emission properties upon protonation.[20] A known amount of base, 2-piperidine-1-yl-ethanol (2PE) was added to the film.[23-25] The in situ formed acid reacted first with 2PE, a stronger base than C6, scheme 4-2 reaction 3. When the acid formed exceeded the amount of 2PE, C6 started to get protonated, indicating clearly the end point at which the complete protonation of 2PE occurred. The deprotection yield was measured using a fluorescent sensor, 7-hydroxy-4-methylcoumarin (C4), to which a *t*-Boc group was attached, yielding the nonfluorescent 7-(tert-butoxycarbonyloxy)-4-methylcoumarin (C4*t*-Boc). Upon deprotection of the non-fluorescent C4*t*-Boc (reaction 2, scheme 2), the resulting C4 shows a strong fluorescence centered at ~ 380 nm when excited at 320 nm, where its maximum absorbance is centered. [21] C4*t*-Boc was used with a double role: it functioned as a prefluorescent sensor and it mimicked the *t*-Boc polymer. The reactions involving the two sensors are shown in scheme 4-2. The ratio between the number of *t*-Boc deprotected groups and the number of H^+ gave the CCL. [22]

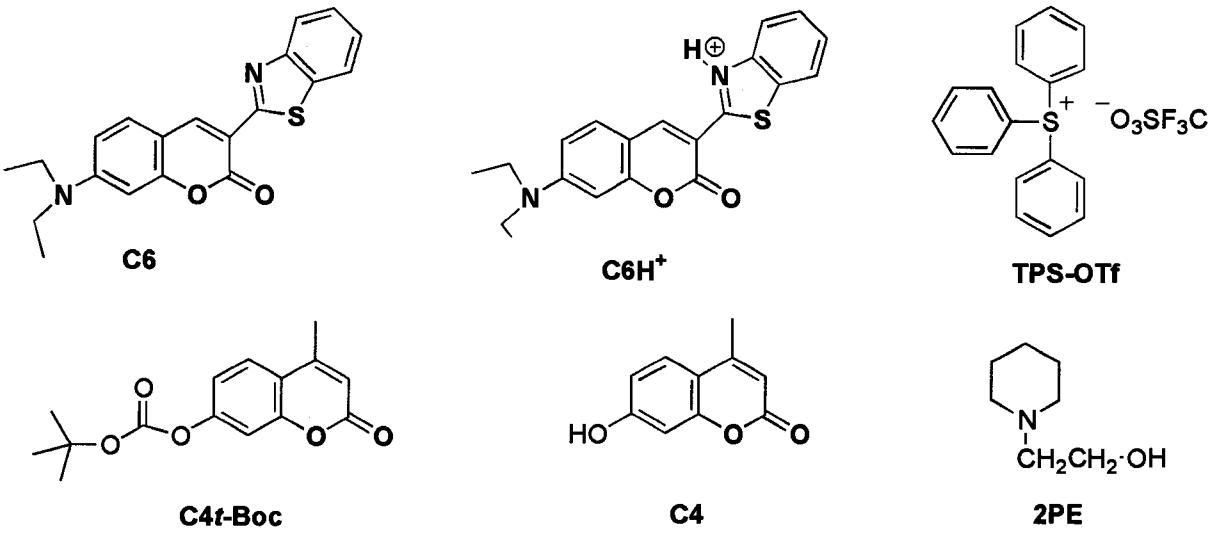

Chart 4-2. Structures of chemical compounds used throughout this chapter: C6 – Coumarin 6 (λ_{abs} max ~ 445 nm, λ_{fl} max ~ 500 nm), C6H$^+$ - protonated Coumarin 6 ((λ_{abs} max ~ 520 nm, λ_{fl} max ~ 550 nm), C4*t*-Boc – 7-hydroxy-4-methyl-coumarine ((λ_{abs} max ~ 320 nm, non-fluorescent), C4 – 7 hydroxycoumarine ((λ_{abs} max ~ 320 nm, λ_{fl} max ~ 385 nm), TPS-OTf – triphenyl sulfonium triflate, 2PE – 2-piperidine-1-yl-ethanol.

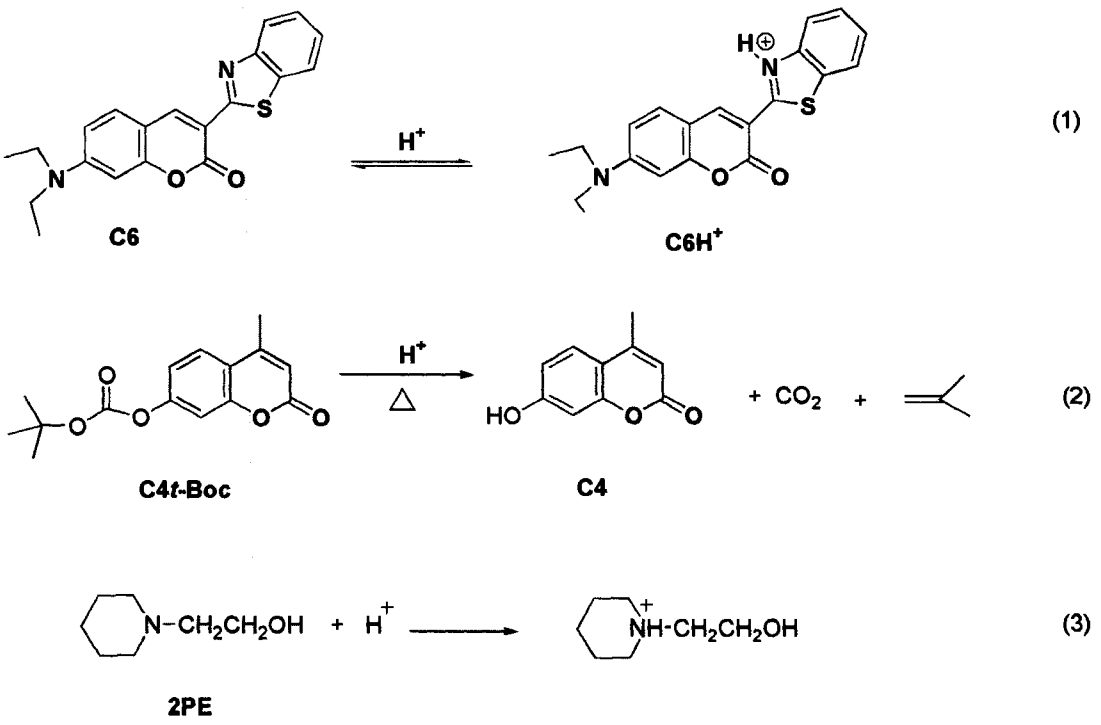

Scheme 4-2. Protonation of C6, reaction (1), deprotection of C4*t*-Boc, reaction (2), and reaction between added base 2-piperidine-1-yl-ethanol (2PE) and H^+, reaction 3.

4.2 Results

The project is comprised of two parts: determination of the amount of acid formed in polymer films and the number of *t*-Boc groups deprotected. The emphasis in this chapter will be on the quantitative detection of acid formed during irradiation, however, work done by M. Frenette on *t*-Boc deprotection will be introduced as well since it completes the second half of the project.

4.2.1 Matching absorbance

The experiments were done in thin films obtained by spin coating a solution containing the polymer, a PAG, acid sensor C6 and a base used for titrations, 2PE. Poly(methyl methacrylate) (PMMA), 15.0 weight %, was dissolved in solvent 2-heptanone, 85 % weight. The same stock polymer solution was used for the quantification of H^+ and *t*-Boc groups deprotected. The PAG triphenylsulfonium triflate (TPS-OTf) was added to the polymer solution and represented 3.0 % of the dry PMMA weight or 9.30×10^{-3} M), the indicator C6 was 0.5 % of the dry polymer weight (1.82×10^{-3} M), C4*t*-Boc 10 % from polymer weight (4.62×10^{-2} M), and 2PE was added such that the molar ratio 2PE : initial number of moles of TPS-OTf varied between 0.0 to 0.5. All throughout this chapter the amounts of C6, C4*t*-Boc, TPS-OTf will be expressed as % wt, however, they represent % wt relative to the mass of the dry polymer used to prepare the initial PMMA and 2-heptanone solution (15 : 85 wt %). Adding small amounts of base (amines or ionic hydroxide salts) into resists has been previously shown to lengthen the shelf life time, and to improve the contrast by neutralizing the acid diffusing into the unexposed areas.[23-26]

The solution containing PMMA, TPS-OTf, C6, and 2PE was filtered through a 0.45 μm Teflon filter before spin coating on 1 inch (2.54 cm) quartz disks at 3000

rotations per minute (rpm) for 20 s. Following spin coating, the residual solvent was removed by baking the disk on a metal surface in an oven at 90 °C for 60 s. After post-application baking (PAB), the discs were immediately cooled to room temperature (RT) on a metallic surface. The thickness of the obtained films was 854 ± 14 nm, as measured by interferometry with a Thin Film Analyser from Luzchem. Following PAB and cooling to RT, the films were irradiated for up to 100 s in an exposure unit equipped with a 249 (± 5) nm filter. The power of the lamp with the filter was 0.82 W/ m^2, figure 4.1 C, while the power of the lamp without the filter was 39.7 W/ m^2, figure 4.1 B. For the films used in quantification of *t*-Boc group deprotection, C4*t*-Boc (10 % from dry PMMA weight) was added instead of C6. After exposure, all the films were subjected to a post-exposure bake (PEB) which ensured that protonation or deprotection occurred. Changes in emission of C6 and C4*t*-Boc were monitored using a front-face set up in a Perkin Elmer fluorimeter (*vide infra*).

An important aspect for the two types of films used (for acid quantification and for *t*-Boc quantification) was the amount of light that was available for the PAG to absorb. In both experiments the same number of photons at 249 (± 5) nm had to be available for the PAG to absorb, thus ensuring comparable conditions. In the films used for acid quantification there was one component which was not present in the films for *t*-Boc quantification: C6. Absorption spectra of films used throughout the experiments are shown in figure 4-1 A, averaged over three films. The spectrum of the radiation emitted by the exposure unit, incident on the film surface, is very narrow, with a maximum at 249 nm. From figure 4-1 A, the fraction of light absorbed by each component was calculated to be: TPS-OTf 44.1 %, C4*t*-Boc 44.3 %, and C6 7.7 %, respectively, the difference up to 100 % being the contribution of the polymer matrix. The difference in absorbance for the samples used for acid and *t*-Boc quantification is insignificant at 249 nm.

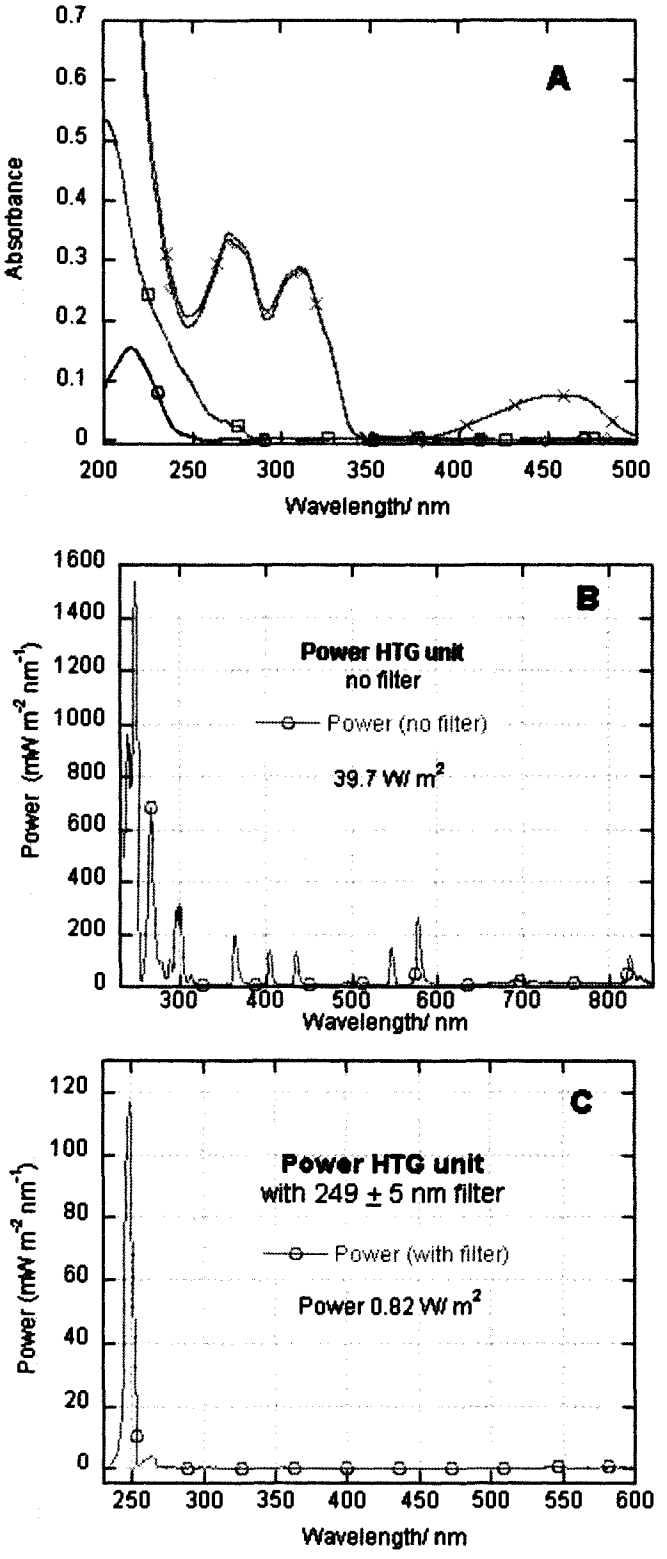

Figure 4-1. UV-vis absorption spectra of PMMA films containing various additives (A). Legend: TPS-OTf = 3 wt.-%, C4*t*-Boc = 10 wt.-% and C6 = 0.5 wt.-% based on the dry

PMMA weight; (o) - PMMA; (□) - PMMA + TPS-OTf; (◊) - PMMA + TPS-OTf + C4*t*-Boc; (x) - PMMA + TPS-OTf + C4*t*-Boc + C6; power spectrum of the incident radiation without the filter (B) and with the band bass filter centered at 249 (± 5) nm (C). The concentrations of the additives in the spin coated solutions were as follows: TPS-OTf 9.3 x 10^{-3} M, C6 1.82 x 10^{-3} M, and C4*t*-Boc 4.62 x 10^{-2} M.

4.2.2 In film titrations

The protocol for *in polymer* titrations relies on the addition of small amounts of base 2PE, keeping the concentration of TPS-OTf constant. Being a stronger base than C6, 2PE will be protonated first, and only when the concentration of the acid formed is higher than that of 2PE, C6 will be protonated. [22-26] Different films, corresponding to different molar ratios 2PE : TPS-OTf (0.0, 0.05, 0.08, 0.12, 0.15, 0.18, 0.2, 0.3, 0.4, 0.5), were exposed to radiation at 249 nm for the same time interval. Following exposure, the films were baked at 90 °C for 60 s to speed up the diffusion of the proton, then cooled to RT on a metallic surface before the fluorescence spectra were recorded. The emission of protonated C6 ($C6H^+$) was monitored by exciting at 510 nm, a wavelength at which neutral C6 does not absorb. The molar ratio TPS-OTf : C6 = 5 : 1 in the spin coated solution. As the amount of base 2PE increased, the emission of protonated C6 decreased, until it eventually reached a plateau, figure 4-2 A and C. The spectra in figure 4-2 were recorded after 20 s (A) and 10 s (C) exposure. A plot of maximum of fluorescence at 550 nm as a function of base : PAG mole ratio gives the plot from figure 4-2 B (for 20 s) and 4-2 D (for 10 s).

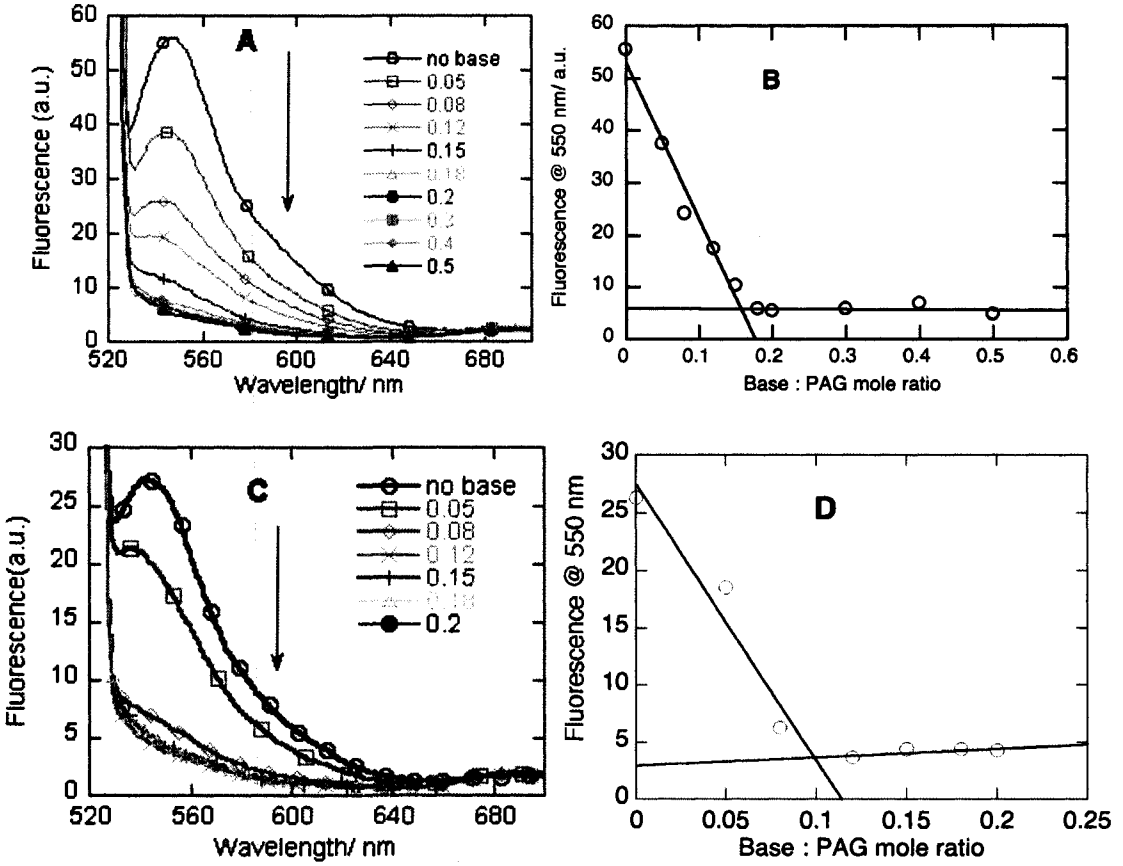

Fig. 4-2. Fluorescence spectra (λ_{exc} = 510 nm) of $C6H^+$ in PMMA films containing TPS-OTf and 2PE, after 20 seconds (A) and 10 s (C) of exposure to 249 nm inside the exposure unit. Fluorescence intensity was measured at 550 nm as a function of base to PAG mole ratio, i.e., 2-PE-to-TPS-OTf for the spectra recorded after 20 s (B) and 10 s (D). The initial stock solution contained 85 % wt 2-heptanone (solvent), 15 wt % PMMA, TPS-OTf 3.0 % based on PMMA weight (9.3 x 10^{-3} M), C6 0.5 % (1.82 x 10^{-3} M) based on PMMA weight. This solution was divided in ten vials to which was added 2PE in various molar concentrations relative to the TPS-OTf concentration (see legend inserted in the graph area), which were later spin coated.

The onset of fluorescence, figure 2 B and D, shows the ratio of base : PAG where the amount of base added into the film starts to exceed the amount of acid formed during 20 s and 10 s respectively of exposure at 249 nm. By varying the

exposure time it is possible to obtain a plot that shows the formation of acid as a function of exposure time for a certain composition of the film, figure 4-3. To obtain such a curve the composition must be the same for all the films and the number of photons available for the PAG to absorb to be the same. The absorbance of 2PE at 249 nm is negligible. This curve is characteristic for a given PAG, a given wavelength and light intensity, and for a particular fraction of the incident light being absorbed by the PAG.

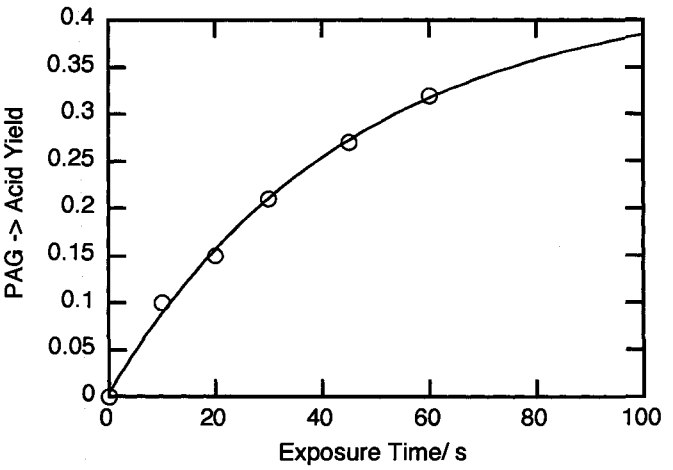

Figure 4-3. Yields of formation of H^+ from TPS-OTf (3 wt % loading relative to the polymer) in a PMMA film (854 nm thick) exposed to radiation at 249 nm inside a HTG unit, as a function of exposure time.

4.2.3 Quantification of t-Boc deprotection

From the curve in figure 4-3, one may obtain information regarding the amount of acid formed for a certain exposure time. Using the same type of curve, but this time for the system containing C4*t*-Boc, it is easy to obtain data regarding

the yield of deprotection. The solution used for deprotection studies contained PMMA, TPS-OTf, and C4*t*-Boc. The strong base 2PE and C6 were not added to the solution since they react with the acid before C4*t*-Boc (*vide infra*). Typical fluorescence spectra of C4 (λ_{ex} = 320 nm) are shown in figure 4-4 A, where films of PMMA containing TPS-OTf and C4*t*-Boc were exposed to 249 nm for increasing time intervals (0, 10, 20, 30, and 45 s), followed by PEB at 95 °C for 60 s. The fluorescence of C4, centered at ~ 385 nm increases as the exposure time increases. This is a consequence of the increasing amount of acid as a function of the exposure time, which deprotects a higher number of *t*-Boc groups. As the exposure time increases even more, a plateau is eventually reached, due to the complete deprotection of C4*t*-Boc present in the film. Deprotection occurs during PEB and it is very slow at room temperature. For the deprotection studies the PEB was done at 90 °C for 60 s on a hot plate inside an oven and on a hot plate in the open air in the laboratory, mimicking the exact conditions from industry where baking is done in the open air. In other words, in the latter case the plate is at 90 °C but the air on top is not, while in the oven both the plate and the air are at 90 °C. The difference is noticeable from the plots in figure 4-4 B. For the same exposure time, fluorescence (yield of deprotection) is higher for the disks baked inside the oven and the plateau is reached faster compared to the films baked on the hot plate in the laboratory.

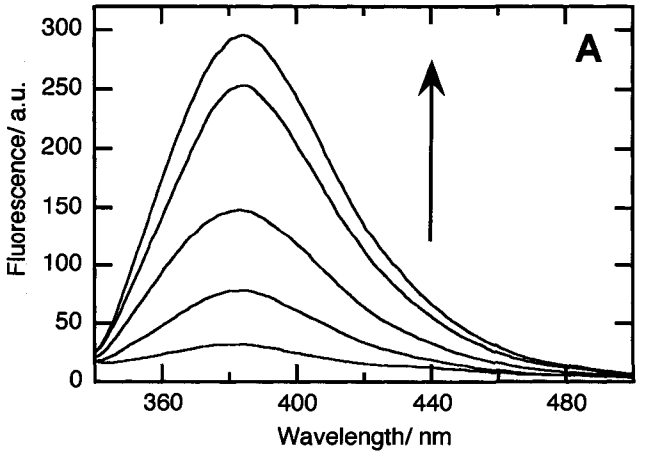

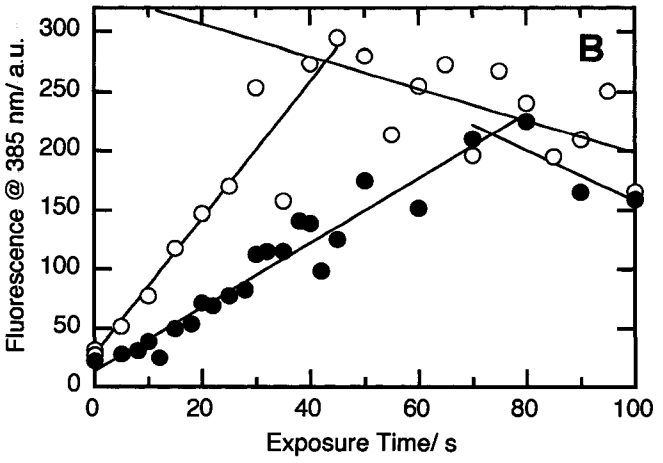

Figure 4-4. Increase in fluorescence (λ_{ex} = 320 nm) of C4 formed by H^+ catalyzed deprotection of C4*t*-Boc, as a function of exposure time (from bottom up 0, 10, 20, 30, and 45 s) for PMMA films coated on top of 1 inch quartz discs, containing TPS-OTf (3.0 % wt based on PMMA weight) (9.3 x 10^{-3} M) and C4*t*-Boc (10.0 % wt based on PMMA weight, 4.62 x 10^{-2} M) exposed at 249 nm (A); fluorescence intensity at 385 nm as a function of exposure time for disks baked at 90 °C for 60 s inside an oven (O) and on a hot plate (●) (B)

After reaching the maximum, fluorescence intensity decreases slowly, rather than staying constant, figure 4-4 B. This may be caused by the acid present in the film which influences negatively the emission of C4 which is a dye sensitive to its environment. [27, 28] Another cause may be the aggregation of newly formed C4, which may result in formation of small clusters, less fluorescent than the dispersed molecules.

4.2.4 Calculations of the Catalytic Chain Length

The correlation between results obtained with films containing C6 and C4*t*-Boc for the same exposure time gives the catalytic chain length (CCL). The values

reported previously for CCL are higher than what was found using the method proposed here, table 1, some reports even mention 1000 *t*-Boc cleavages per proton. [9] The CCL values that are reported in table 4-1 are smaller than other reports simply because the concentration of C4*t*-Boc is low, in other words there are less *t*-Boc groups available for the protons to deprotect than in the case of a *t*-Boc protected polymer. The data from the last line (values in italics) was obtained by heating the disc on a hot plate at 90 °C, and not in the oven as it is the case for the three lines above it. The exposure time shown in table 4-1 are the times necessary to reach the near-plateau region.

PEB time (s)	Exposure time (s)	Catalytic Chain Length (CCL)
30	50	17
60	43	19
90	33	22
60	*74*	*14*

Table 4-1. Catalytic chain length for different exposure times and PEB conditions. The results are for PMMA films (~ 850 nm thick) which contained 3.0 wt % TPS-OTf based on PMMA weight and 10.0 wt % C4*t*-Boc based on PMMA weight as well. The films were exposed to radiation from an Hg lamp, with radiation passing through a band pass filter centered at 249 (± 5) nm; see output spectrum and power in figure 4-1 C.

Due to the limited number of *t*-Boc groups present in the PMMA film, the catalytic chain length depends on the concentration of acid in the present system. The concentration of C4*t*-Boc is limited by its solubility in the solutions used for spin coating. A plot of CCL as a function of the acid concentration is shown in figure 4-5.

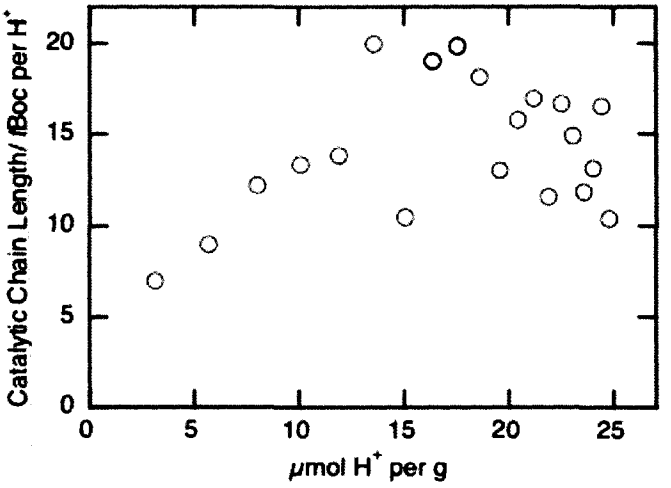

Figure 4-5. Catalytic chain length (number of *t*-Boc groups deprotected by one proton) as a function of number of micromoles of acid present in one gram of PMMA film. The PMMA films (854 nm thick) contained 3 wt % TPS-OTf and 10.0 wt % C4*t*-Boc based on PMMA weight, and were exposed to radiation at 249 nm for different time intervals.

4.2.5 Acid diffusion in PMMA films

The protocol presented (*vide supra*) so far is the result of numerous experimental observations and changes during the time it took to complete this project. Acid diffusion throughout the PMMA film does not occur easily at room temperature, figure 4-7. PEB is a key step that allows the proton to diffuse throughout the PMMA film, thus allowing protonation of C6 before the fluorescence spectra were recorded. PMMA films containing 3.0 wt % TPS-OTf based on PMMA weight, 0.5 wt % C6 based on PMMA weight and various 2PE/ TPS-OTf mole ratios were exposed to radiation at 249 nm for 45 s, figure 4-6 A. Although one would expect a decrease in the fluorescence of $C6H^+$ as more 2PE is present in the film, for the films not baked after exposure but left at room temperature the points representing the maximum of fluorescence of $C6H^+$ are scattered without a clear trend, figure 4-6 B. Similar results were obtained for different periods of exposure (10, 20, 30, 45, 60, 75 s) at 249 nm.

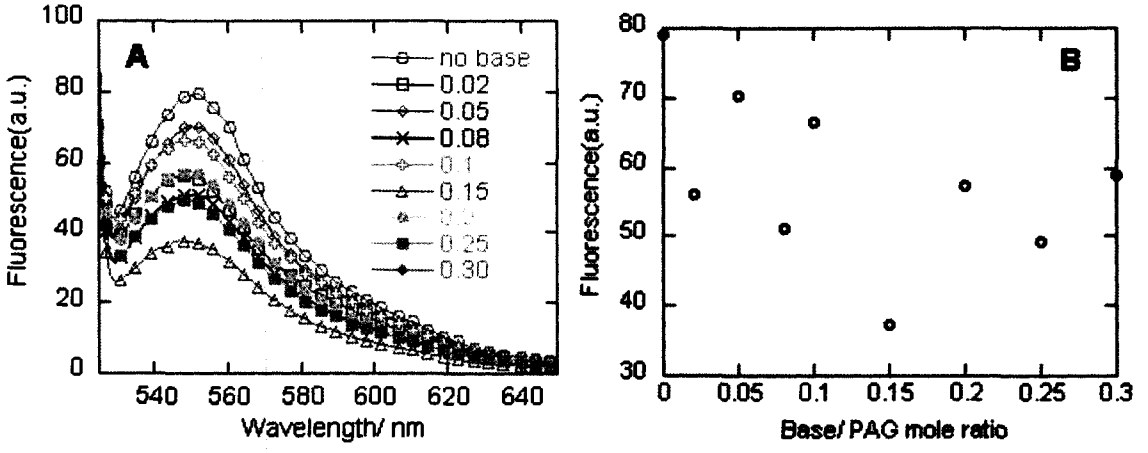

Figure 4-6. Fluorescence of C6H$^+$ (λ_{ex} = 510 nm) in PMMA films containing TPS-OTf as PAG and 2PE as base in increasing amounts (see legend in figure A), exposed to radiation at 249 nm for 45 s (A); fluorescence intensity (arbitrary units) at maximum emission (550 nm) from the spectra in figure 4-6 A as a function of base/ PAG mole ratio. The spectra were recorded shortly after exposure without PEB, with the films at RT.

In order to check for the time H$^+$ needs to diffuse throughout the film, the fluorescence of C6H$^+$ was monitored as function of time, for a PMMA film exposed to radiation at 249 nm. The solution, spin coated at 3000 rpm for 20 s, contained 15 % weight PMMA, 85 wt % 2-heptanone, 10 wt % C4*t*-Boc based on polymer weight, 3 % TPS-OTf based on polymer weight, base 2PE/ TPS-OTf = 0.2 molar ratio, and 0.5 % C6 based on polymer weight. PAB was performed at 90 °C for 60 s inside an oven, the excitation wavelength was 510 nm. The spectra were recorded at different time intervals, and the maximum intensity at 550 nm was plotted as a function of time, figure 4-7. The first value of fluorescence, at time zero, was recorded immediately after exposure.

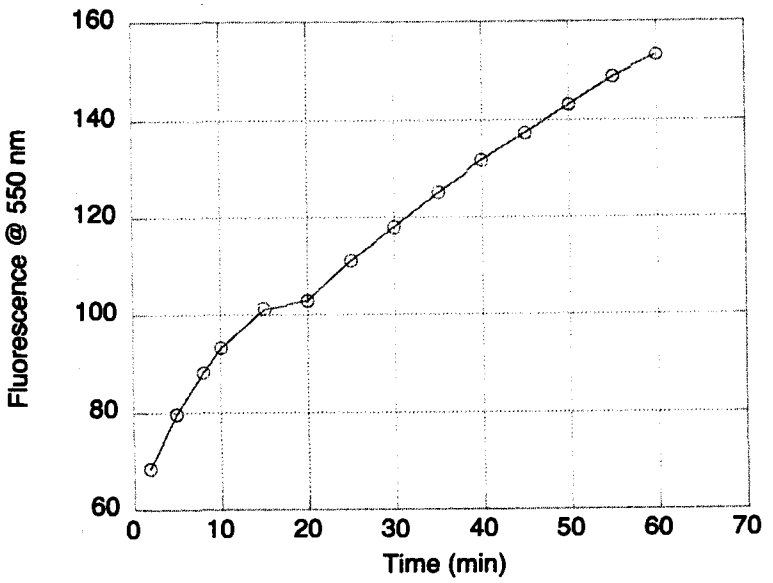

Figure 4-7. Fluorescence intensity of protonated C6 ($C6H^+$)(a.u.) at 550 nm as a function of time, after exposure of a PMMA film containing 2PE/ TPS-OTf = 0.2 mole ratio, C6 , and C4*t*-Boc to radiation at 249 nm for 60 s. After exposure the film was kept at room temperature inside the fluorimeter, λ_{ex} = 510 nm.

In the formulations used to determine the yield of *t*-Boc deprotection, there is no C6 and no 2PE, and consequently all the acid formed will react with C4*t*-Boc. The solutions used to quantify the amount of H^+ produced during exposure contained C6 (0.5 % based on PMMA weight), 2PE, and C4*t*-Boc (10.0 % based on PMMA weight), thus it was possible that the excess acid remained after protonation of 2PE could react either with C6 or C4*t*-Boc. C4*t*-Boc was added so that the absorbance at the exposure wavelength in both types of experiments was the same. Thus it is important to establish whether or not H^+ reacts first with C6 or with C4*t*-Boc. Control experiments with PMMA films containing C6 and C4*t*-Boc show that C6 is protonated first, and that no increase in fluorescence characteristic to C4 occurs, figure 4-8. The fluorescence characteristic to C4 (λ_{ex} = 320 nm) has a maximum centered at ~ 380 nm (see chapter 2 for more details on C4). From figure 4-8 one can notice that the fluorescence in the region characteristic to C4 is almost zero and remains constant for all base/ PAG mole ratio.

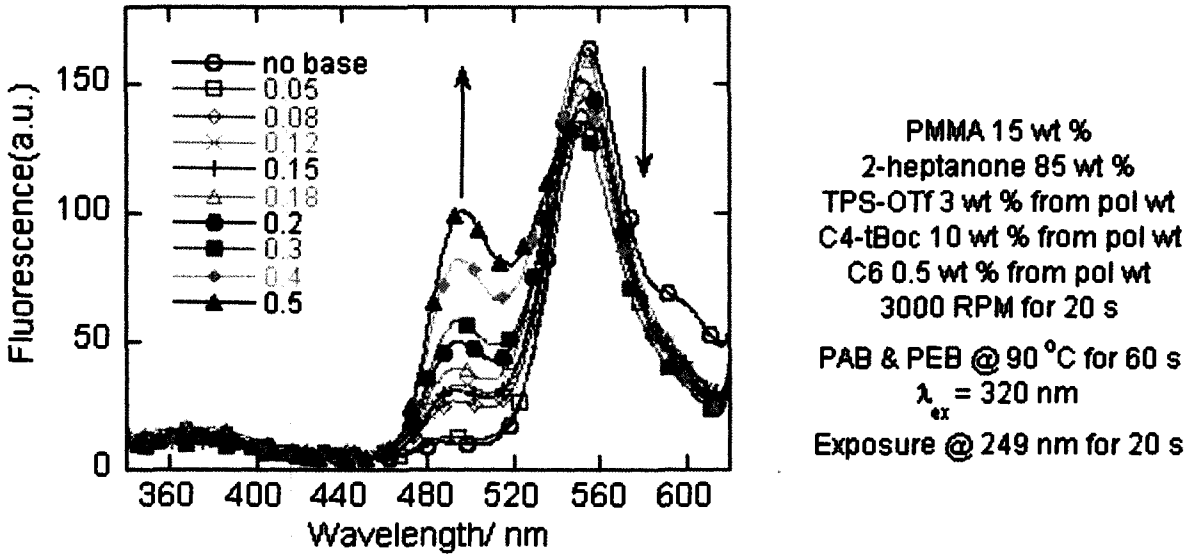

Figure 4-8. Fluorescence spectra (λ_{ex} = 320 nm) of PMMA films containing TPS-OTf 3 wt %, C4*t*-Boc 10 wt %, C6 0.5 wt %, obtained by spin coating at 3000 rpm for 20 s, PAB at 90 °C for 60 s, exposed to radiation at 249 nm for 20 s, PEB at 90 °C for 60 s. The mole ratio 2PE/ TPS-OTf was 0.0, 0.05, 0.08, 0.12, 0.15, 0.20, 0.30, 0.40, 0.50 (see the legend inserted).

4.2.6 Control experiments

An important aspect is related to the thermal stability of TPS-OTf and C4*t*-Boc. Thermally produced H^+ could deprotect C4*t*-Boc or protonate C6 in the same way that the photoproduced H^+ would do. At the same time, C4*t*-Boc could be thermally unstable, leading to *t*-Boc deprotection during baking. PMMA films without 2PE and with 2PE/ TPS-OTf = 0.18 mole ratio were baked for 60 and 120 s without being exposed to radiation. Fluorescence of C4 was monitored by exciting at 320 nm, but no change in emission characteristic to C4, centered at ~ 380 nm,

was noticed, figure 4-9 A. The same films used to record spectra from figure 4-9 A were used to check for emission of $C6H^+$. The fluorescence spectrum of $C6H^+$ did not show any increase, and no peak characteristic to fluorescence of $C6H^+$ (maximum at ~ 550 nm) was noticed, proving that no acid was formed during the thermal treatment of the films, figure 4-9 B.

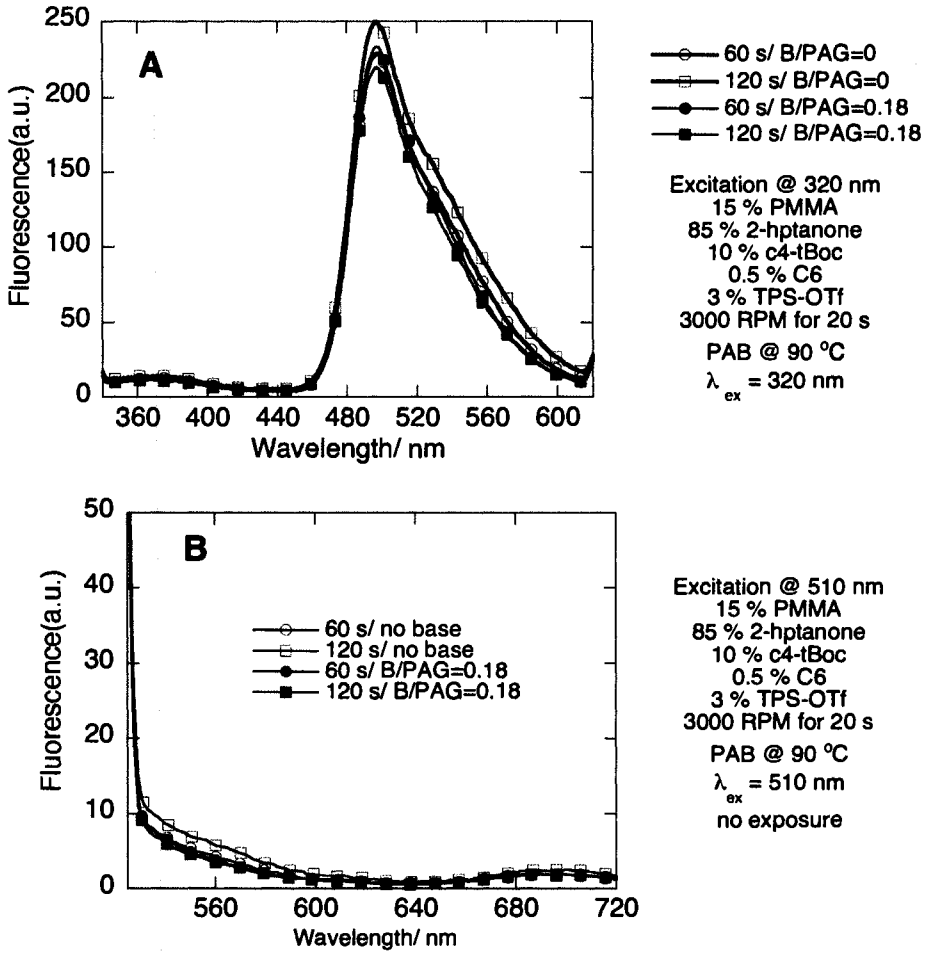

Figure 4-9. (A) Fluorescence spectra (λ_{ex} = 320 nm) of PMMA films containing C4*t*-Boc 10 wt %, C6 0.5 wt %, and TPS-OTf 3 wt % based on polymer weight. The films were not exposed to radiation, only baked inside an oven at 90 °C for 1 or 2 minutes. Legend: bake 60 s, 2PE/ TPS-OTf = 0.0 mole ratio (O); bake 120 s, 2PE/ TPS-OTf = 0.0 mole ratio (□); bake 60 s, 2PE/ TPS-OTf = 0.18 mole ratio (●); bake 120 s, 2PE/ TPS-OTf = 0.18 mole ratio (■). (B) Emission spectra of the same films analyzed in figure 9 A, with an excitation wavelength λ_{ex} = 510 nm

A study of protonation of C6 as a function of temperature shows how the acid diffusion in PMMA films is influenced by the temperature of the environment. It is also necessary to show that the experimental protocol followed throughout this project was correct, and that during the 60 s baking at 90 °C all the acid formed protonated C6. Results with PMMA films containing TPS-OTf 3 wt % based on PMMA weight, and C6 0.5 wt % based on polymer weight are shown in figure 4-10. The films were baked, after spin coating, at 90 °C for 60 s, then cooled to RT and exposed for 10 s at 249 nm inside the exposure unit. The fluorescence of $C6H^+$ was recorded immediately after exposure (λ_{ex} = 510 nm) without PEB, this point corresponding to time = 0 s in figure 4-10. Other films were baked for 10, 20, 30, 40, 50, 60, and 70 s respectively after exposure.

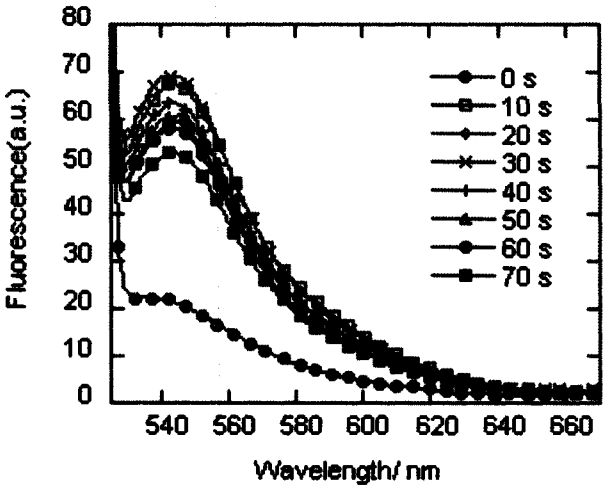

A

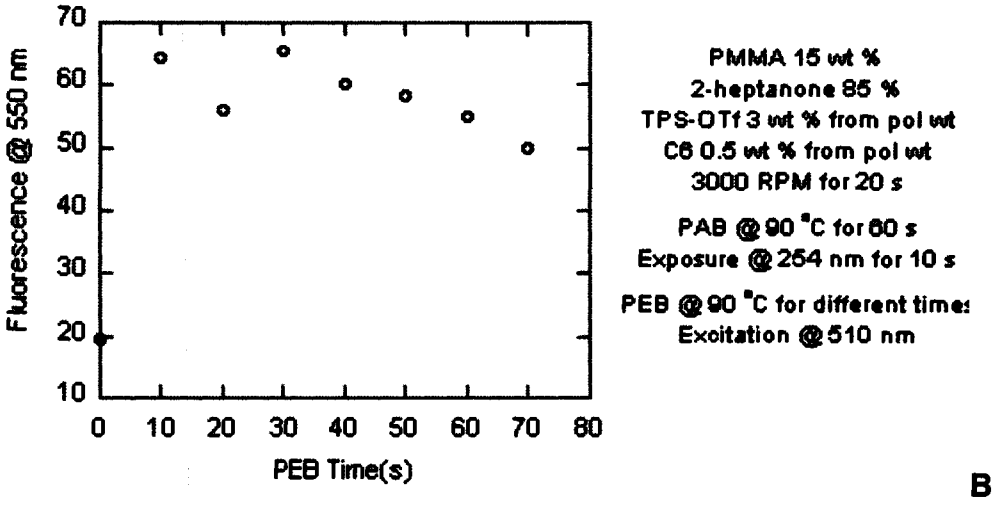

Figure 4-10. (A) Fluorescence spectra (λ_{ex} = 510 nm) of $C6H^+$ as a function of post exposure baking (PEB) time in PMMA films containing TPS-OTf 3 wt %, and C6 0.5 wt % based on polymer, exposed to 249 nm for 10 s, followed by PEB at 90 °C for different time intervals (see legend inside figure 4-10 A); (B) fluorescence maximum at 550 nm for $C6H^+$ as a function of PEB time.

4.3 Discussion

Diffusion of the proton throughout the polymer film and the readily available *t*-Boc groups are the most important factors that influence the CCL. Previous studies showed that acid diffusion depends on polymer matrix, duration and temperature of PAB and PEB. [10-12, 29-32] Previously reported values of CCL were obtained by monitoring the disappearance of the carbonyl signal at 1760 cm^{-1} as deprotection reaction occurred, while the signal of the new –OH group increases at ~3500 cm^{-1}. [9] McKean at al. reported a catalytic chain length in the range 800 – 1100, with a diffusion range of 50 Å for a CCL averaging 1000. [9]

The method proposed in this chapter uses fluorescence spectroscopy as a tool for determining the CCL. There are two important parameters to be determined: the amount of acid produced, and the number of *t*-Boc groups deprotected. The number of moles of acid formed during irradiation are determined by an *in polymer* titration using a base, 2PE, and as acid sensor C6. 2PE has previously been reported as a strong base used for *in situ* titrations in resist films. [23-25, 29] Thus 2PE was selected as titrating base since it has been shown to react in equimolar concentrations with the acid. [23]

It is considered that the acid obtained through photolysis of TPS-OTf completely protonated the base present in the film only when the decrease in fluorescence of $C6H^+$ reached a plateau, figure 4-2. As the concentration of 2PE increases, the amount of acid which could protonate C6 decreases, until eventually all the acid produced protonates 2PE. Thus only the neutral form of C6 is present in the film.

The number of *t*-Boc groups deprotected per proton in our system is smaller than previously reported values. This is due to the limited number of *t*-Boc groups available in our PMMA films, only 3.3 % of the sample weight, while in polymers used in industry the value can be as high as 45 % of the total sample weight. The diffusion of the acid through the PMMA matrix plays a key role as well. [4, 5, 10, 29, 30, 32, 33]

The diffusion range of the proton throughout the PMMA film can be calculated, assuming a spherical diffusion and a density of the film of 1.15 g/ mL. The calculated diffusion range in the present system is 27 Å for a CCL of 19 (PAB and PEB at 90 °C for 60 s inside an oven), the same order of magnitude as the value of 50 Å previously reported. [7-10, 22] More values for CCL are reported in table 4-1 for different PEB and exposure times. The distance between two neighbor C4*t*-Boc molecules is ~ 1.6 nm, calculated assuming even distribution throughout the PMMA film (~ 854 nm thick), 10.0 % wt loading of C4*t*-Boc based on PMMA weight, and that all the solvent (2-heptanone) evaporated during PAB. The calculated distance between two neighbor TPS-OTf molecules in the PMMA film (~ 854 nm thick) is ~ 2.7 nm, assuming 1.15 g /mL density of PMMA, even distribution of the PAG molecules in the film (in the center of a cube), and complete evaporation of the solvent during PAB. When calculating the distance, the C4*t*-Boc and TPS-OTf molecules are assumed to be in the centers of two neighboring cubes.

Post exposure baking (PEB) is a key step which determines the diffusion length and in the end the value of CCL. [4, 7] Diffusion of the proton occurs very slowly at RT. In figure 4-6 the results with films containing different amounts of 2PE show a random value of fluorescence intensity at 550 nm. One would expect a trend in fluorescence intensity as the amount of base increases, but this was not the case. Further attempts to allow for all the acid formed to protonate C6 are shown in figure 4-7, where the exposed film was left inside the fluorimeter for one hour at RT. The fluorescence intensity at 550 nm kept increasing even after 60 minutes, proving that the diffusion of the proton in PMMA is a very slow process at RT. This prompted a change in the experimental protocol in that after exposure the film was baked for 60 s at 90 °C inside the oven. The results were drastically different, allowing for a fast diffusion of H^+ throughout the polymer film. As it can be seen from figure 4-10, for a film exposed at 249 nm for 10 s it was enough to bake for 10 s to reach the plateau in terms of protonation of C6. Longer PEB did not result in an increase of fluorescence intensity at 550 nm.

It is very important to prove that, in the PMMA films used to monitor acid formation, the proton was not simultaneously involved in *t*-Boc deprotection, since this introduces errors in the titration reaction, the amount of acid detected being lower than the real one. Films containing C4*t*-Boc, C6 and base 2PE : TPS-OTf in different ratios (0.0, 0.05, 0.08, 0.12, 0.15, 0.18, 0.2, 0.3, 0.4, 0.5), exposed to 249 nm for the same period of time, show no change in intensity of emission characteristic to C4 when excited at 320 nm, figure 4-8. The emission of C4 is almost zero and it does not change, proving that deprotection of C4*t*-Boc does not compete with protonation of 2PE or C6. Although the excitation wavelength was 320 nm, one can notice emission characteristic to C6 or $C6H^+$. This is due to the tale in absorption of both species at 320 nm. The trend in emission of neutral and protonated coumarin 6 follows the expected path: when no base was added, only emission from $C6H^+$ was noticed (maximum at ~ 550 nm); as the amount of base increases, emission of $C6H^+$ decreases, while that of C6 increases.

It is clear that the acid formed is due to photolysis of TPS-OTf and not to thermal degradation during PAB, figure 4-9. There was no emission characteristic to C4 when the excitation wavelength was 320 nm, and the only peak present is characteristic to neutral C6. Excitation at 510 nm does not lead to any increase in fluorescence of $C6H^+$, as it can be noticed from figure 4-9 B.

By plotting the CCL at different acid concentrations, one obtains a graph similar to that in figure 4-5. CCL increases until a plateau is reached, followed by a decrease. The decrease in CCL is normal, considering that the number of moles of acid increases, while that of *t*-Boc remains constant. Thus the number of *t*-Boc groups available per proton decreases, leading to a decrease in CCL above 15 μmol H^+/ g resist. The lower CCL at concentrations of H^+ below 15 μmol H^+/ g resist is counterintuitive, since there are more *t*-Boc groups available per mole of acid. The explanation proposed is that some of the acid is involved in reactions with air-born base contaminants, common in chemistry laboratories. Some of the acid is used in a sacrificial manner to react with the air-born bases, thus having less acid available for C4*t*-Boc deprotection. To counterbalance the effect of air born

contaminants, the spin coating, PAB, exposure, and PEB are done in the so called clean rooms. In these clean rooms the air is filtered through special filtration systems that remove the base contaminants and other solid impurities. The air in a clean room in lithography industry is ~ 10,000 times cleaner than in a surgery room in ordinary hospitals. Base contaminants react with the acid close to the surface of the film, inducing T-shaped defects in the developed images.

The results presented within this chapter show that a novel method to measure the CCL was developed. C6 and C4*t*-Boc worked excellent as fluorescent sensors, selective monitoring of the two probes being possible due to their different absorption and emission properties.

While the CCL values reported here are quite different from those reported previously, this reflects the "abundance" of *t*-Boc groups available for deprotection in our films. The lower values of CCL reported here are limited by the low concentration of *t*-Boc groups present in these films compared to the *t*-Boc protected polymers. In terms of diffusion length, the value we obtained is about half of the previously reported values.

4.4 Experimental

Coumarin 6 (98%), 2-heptanone (99%), and 2-piperidin-1-yl-ethanol (2PE) (99%) were purchased from Aldrich and used as received. 7-*tert*-butoxycarbonyloxy-4-methylcoumarin (C4*t*-Boc) was prepared in house as previously described, from 7-hydroxicoumarin (C4) and di-*tert*-butyl-dicarbonate. [21] Poly(methyl methacrylate) (PMMA) (M_w ~ 1.0 x 10^6, polydispersity ~ 1.1) was purchased from Polysciences Inc. Triphenyl sulfonium triflate (TPS-OTf) was a kind gift from Rohm and Haas Electronic Materials, and it was used as received.

All the films were obtained by spin coating the respective solutions on 1 inch (2.54 cm) quartz discs at 3000 rpm for 20 s, followed by post application baking (PAB) on a metallic surface inside an oven at 90 °C for 60 s. After PAB the films were cooled to RT on a metallic surface. The thickness of the films was measured using a Thin Film Analyser TFA-11CT from Luzchem Research, and it was found to be 854 ± 14 nm. Exposure was done in a Hybrid Technology Group exposure tool, model 64-10X, using a 249 (± 5 nm) filter. The power output of the lamp throughout these experiments was 0.82 W/ m^2, and it was obtained by placing a bandpass filter in front of the lamp, figure 4-1 C. The power spectrum of the lamp, without the filter, is shown in figure 4-1 B, with an output of 39.7 W/ m^2. The power of the lamp was measured with a Luzchem Research Spectroradiometer. Fluorescence spectra were recorded using a front-face set up in a LS-50 Perkin Elmer luminescence spectrometer. The excitation wavelengths were 510 nm for the detection of protonated Coumarin 6, $C6H^+$, and 320 nm for detection of 7-hydroxycoumarin (C4). The experimental methods for detection of H^+ and *t*-Boc deprotection are described in the Results section of this chapter.

4.5 References

(1) Ito, H., "Chemical Amplification Resists for Microlithography", *Adv. Polym. Sci.* **2005**, *172,* 37-245.

(2) Ito, H.; Wilson, C. G., "Chemical Amplification in the Design of Dry Developing Resist Materials", *Pol. Eng. Sci.* **1983**, *23,* 1012-1018.

(3) Reichmanis, E.; Houlihan, F. M.; Nalamasu, O.; Neenan, T. X., "Chemical Amplification Mechanism for Microlithography", *Chem. Mater.* **1991**, *3,* 394-407.

(4) Ito, H.; Wilson, C. G.; Frechet, J. M. J., "Résines pour UV lointain mettant en oeuvre un méchanisme d'amplification chimique. Sensitive deep UV resist incorporating chemical amplification", *Symp. VLSI Technol.* **1982**, *260,* 262.

(5) Ito, H., "Chemical amplification resists: History and development within IBM", *IBM J. Res. Develop.* **2000**, *44,* 119-130.

(6) *Introduction to Microlithography.* ACS Professional Reference Book, ed. Thompson, L. F., Willson, C. G., and Bowden, M. J. 1994, Washington, DC: American Chemical Society.

(7) Schlegel, L.; Ueno, T.; Shiraishi, H.; Hayashi, N.; Iwayanagi, T., "Acid Formation and Deprotection Reaction by Novel Sulfonates in a Chemically Amplification Positive Resist", *Chem. Mater.* **1990**, *2,* 299-305.

(8) Ichikawa, R.; Hata, M.; Okimoto, N.; Setsuko, O. H.; Tsuda, M., "Acid-Catalyzed Deprotection Mechanism of *tert*-Butyloxycarbonyloxy Polymers in Chemically Amplified Resists", *J. Pol. Sci. A: Pol. Chem.* **1998**, *36,* 1035-1042.

(9) Mc Kean, U. S. D.; MacDonald, S. A., "Acid Photogeneration from Sulfonium Salts in Solid Polymer Matrices", *J. Polym. Sci. A: Polym. Chem.* **1989**, *27,* 3927.

(10) Itani, T.; Yoshino, H.; Hashimoto, S.; Yamana, M.; Samoto, N.; Kasama, K., "A study of acid diffusion in chemically amplified deep ultraviolet resist", *J. Vac. Sci. Technol. B* **1996**, *14,* 4226-4228.

(11) Fryer, D. S.; Bollepali, S.; Pablo, J. J.; Nealy, P. F., "Study of acid diffusion in resist near the glass transition temperature", *J. Vac. Sci. Technol. B* **1999**, *17,* 3351-3355.

(12) Schlegel, L.; Ueno, T.; Hayashi, N.; Iwayanagi, T., "Determination of Acid Diffusion in Chemical Amplification Positive Deep-UV Resists", *Jpn. J. Appl. Phys.* **1991**, *30,* 3132-3137.

(13) Kunz, R. R.; Bloomstein, T. M.; Hardy, D. E.; Goodman, R. B.; Downs, D. K.; Curtin, J. E., "Outlook for 157 nm resist design", *J. Vac. Sci. Technol. B* **1999**, *17,* 3267-3272.

(14) Toriumi, M.; Satou, I.; Itani, T., "Vacuum ultraviolet spectra of fluorocompounds for 157 nm lithography", *J. Vac. Sci. Technol. B* **2000**, *18,* 3328-3331.

(15) Tegou, E.; Bellas, V.; Gogolides, E.; Argitis, P.; Eon, D.; Cartry, G.; Cardinaud, C., "Polyhedral Oligomeric Silsesquioxane (POSS) Based Resists: Material Design Challenges and Lithographic Evaluation at 157 nm", *Chem. Mater.* **2004**, *16,* 2567-2577.

(16) Feke, G. D.; Hessman, D.; Grober, R. D., "On-wafer spectrofluorometric evaluation of the response of photoacid generator compounds in chemically amplified photoresists", *J. Vac. Sci. Technol. B* **2000**, *18,* 136-139.

(17) Dentinger, P. M.; Lu, B. L.; Taylor, J. W.; Bukofsky, S. J.; Feke, G. D.; Hessman, D.; Grober, R. D., "On-wafer photoacid determination and imaging technique for chemically amplified photoresists", *J. Vac. Sci. Technol. B* **1998**, *16,* 3767-3772.

(18) Houle, F. A.; Hinsberg, W. D.; Sanchez, M. I., "Acid-base titrations in a positive tone chemically amplified photoresist and their effect on imaging", *J. Vac. Sci. Technol. B* **2004**, *22,* 747-757.

(19) Pohlers, G.; Scaiano, J. C.; Sinta, R., "Determination of Photoacid generation Efficiencies", *Chem. Mater.* **1997**, *9,* 3222.

(20) Scaiano, J. C.; Laferriere, M.; Ivan, M. G.; Taylor, G. N., "A Protocol for the Verification of Acid Generation in 157 nm Lithography", *Macromolecules* **2003**, *36,* 6692.

(21) Frenette, M.; Coenjarts, C.; Scaiano, J. C., "Mapping Acid-Catalyzed Deprotection in Thin Polymer Films: Fluorescence Imaging Using Prefluorescent 7-Hydroxycoumarin Probes", *Macromol. Rapid Commun.* **2004**, *25,* 1628.

(22) Frenette, M.; Ivan, M. G.; Scaiano, J. C., "Use of fluorescent probes to determine catalytic chain length in chemically amplified resists", *Can. J. Chem.* **2005**, *83,* 869-874.

(23) Pawloski, A. P.; Nealy, P. F.; Nealy, C., "Micromolar Concentrations of base quenchers impact the apparent efficiency of photoacid generation in chemically amplified resists", *J. Vac. Sci. Technol. B* **2002**, *20,* 2162-2168.

(24) Pawloski, A. P.; Nealy, P. F., "The Multifunctional Role of Base Quenchers in Chemically Amplified Photoresists", *Chem. Mater.* **2002**, *14,* 4192.

(25) Pawloski, A. P.; Nealy, C.; Nealy, P. F., "A Standard Addition Technique to Quantify Photoacid Generation in Chemically Amplified Photoresist", *Chem. Mater.* **2001**, *13,* 4154-4162.

(26) Houle, F. A.; Hinsberg, W. D.; Morrison, M.; Sanchez, M. I.; Wallraff, G.; Larson, C.; Hoffnagle, J., "Determination of coupled acid catalysis-diffusion processes in a positive-tone chemically amplified photoresist", *J. Vac. Sci. Technol. B* **2000**, *18,* 1874-1885.

(27) Schulman, S. G.; Rosenberg, L. S., "Tautomerization Kinetics of 7-Hydroxy-4-methylcoumarin in the Lowest Excited Singlet State", *J. Phys. Chem.* **1979**, *83,* 447.

(28) Abdel-Mottaleb, M. S. A.; El-Sayed, B. A.; Abo-Aly, M. M.; El-Kady, M. Y., "Fluorescence Properties and Excited State Interactions of 7-hydroxy-4-methylcoumarin Laser Dye", *J. Photochem. Photobiol. A: Chem.* **1989**, *46,* 379-390.

(29) Schlegel, L.; Ueno, T.; Hayashi, N.; Iwayanagi, T., "Determination of acid diffusion in chemical amplification positive deep ultraviolet resists", *J. Vac. Sci. Technol. B* **1991**, *9,* 278-289.

(30) Yoshimura, T.; Nakayama, Y.; Okazaki, S., "Acid-diffusion effect on nanofabrication in chemical amplification resist", *J. Vac. Sci. Technol. B* **1992**, *10,* 2615-2619.

(31) Jessop, J. L. P.; Goldie, S. N.; Scranton, A. B.; Blanchard, G. J.; Rangarajan, B.; Capodieci, L.; Subramanian, R.; Templeton, G. J., "Characterizing Acid Mobility in Chemically Amplified Resists via Spectroscopic Methods", *Proc. SPIE* **1999**, *3678,* 914-921.

(32) Kim, J. B.; Kwon, Y. G.; Choi, J. H.; Jung, M. H., "Acid Diffusion and evaporation in chemically amplified resists", *Proc. SPIE* **1999**, *3678,* 536-543.

(33) Lu, B. L.; Taylor, J. W.; Cerrina, F.; Soo, C. P.; Bourdillon, A., "Study of acid diffusion in a positive tone chemically amplified resist using an on-wafer imaging technique", *J. Vac. Sci. Technol. B* **1999**, *17,* 3345-3350.

Polymer Photochemistry at Advanced UV Wavelengths

5. Polymer Photochemistry at Advanced UV Wavelengths

5.1 Introduction

Lithography has developed tremendously over the last two decades, the semiconductor industry advancing at an incredible pace. The seemingly never ending need for faster processors and smaller size computers has pushed the resolution limit towards nanometer regime, nowadays computers having processors with 65 nm spatial resolution obtained with 193 nm lithography, moving towards 45 nm node within the next two years.[1,2] The availability of microlithographic tools, excimer lasers with wavelengths at 308, 246, 193, and 157 nm and the development of optical and imaging systems helped to decrease the size of the lines and spaces (resolution) according to the well known formula:

$$R = k_1 \lambda / NA \qquad \text{Eq. (5.1)}$$

where R = resolution, λ – exposure wavelength, NA – numerical aperture, and k_1 – constant in the range 0.4 –1.0.[3,4] From this formula it is clear that a decrease in resolution can be achieved by increasing the NA, by lowering k_1 and the exposure wavelength (λ). The best approach is to work all the parameters, and as a consequence microelectronics industry shifted towards using lasers at lower wavelength, processors, DRAM memories and NAND flash memories being currently manufactured with exposure at 193 nm. Striving to follow Moore's law,[5] the industry has looked into new solutions, new materials and exposure tools. The technique used today in positive resists is chemical amplification (CA), developed by Ito and Frèchet at the beginning of 1980's and described as well in the first and

Polymer Photochemistry at Advanced Wavelengths

5. Polymer Photochemistry at Advanced Wavelengths

5.1 Introduction

Lithography has developed tremendously over the last two decades, the semiconductor industry advancing at an incredible pace. The seemingly never ending need for faster processors and smaller size computers has pushed the resolution limit towards nanometer regime, nowadays computers having processors with 65 nm spatial resolution obtained with 193 nm lithography, moving towards 45 nm node within the next two years.[1,2] The availability of microlithographic tools, excimer lasers with wavelengths at 308, 246, 193, and 157 nm and the development of optical and imaging systems helped to decrease the size of the lines and spaces (resolution) according to the well known formula:

$$R = k_1 \lambda / NA \qquad \text{Eq. (5.1)}$$

where R = resolution, λ – exposure wavelength, NA – numerical aperture, and k_1 – constant in the range 0.4 –1.0.[3,4] From this formula it is clear that a decrease in resolution can be achieved by increasing the NA, by lowering k_1 and the exposure wavelength (λ). The best approach is to work all the parameters, and as a consequence microelectronics industry shifted towards using lasers at lower wavelength, processors, DRAM memories and NAND flash memories being currently manufactured with exposure at 193 nm. Striving to follow Moore's law,[5] the industry has looked into new solutions, new materials and exposure tools. The technique used today in positive resists is chemical amplification (CA), developed by Ito and Frèchet at the beginning of 1980's and described as well in the first and

fourth chapters.[6] CA was quickly adopted by industry and made its way to mass production.[7] 157 nm was thought as the next logical step after 193 nm, but problems with transparency of materials, pellicles, polymers, and masks as well as birefringence[8] in CaF_2 have influenced the industry, who decided to shift focus away from photolithography with 157 nm laser towards immersion, double patterning, and double exposure at 193 nm.[9] If in 1999 predictions saw 157 nm as the wavelength used by industry in 2005 with an expected resolution of 100 nm,[3] at the time this thesis is written, 2006, the current technology used is 193 nm photolithography and a resolution of 65 nm. The next milestone, 45 nm resolution, will most likely enter the production lines in less than two years. However, research at 157 nm continued, and resist formulations, polymers and photoacid generators developed for this wavelength were used at 193 nm with excellent results.

State of the art photoresists that are currently employed in the lithographic industry are based on the concept of chemical amplification (CA). As the wavelength gets smaller, the absorbance of the materials increases and the photochemistry of the polymer cannot be ignored. A key condition, among many others, for a polymer to be used in a resist at 157 or 193 nm, is to have a low absorbance. Phenolic resists used for photolithography at 248 nm absorb too much at 193 nm, so a new generation of acrylic *t*-Boc polymers were developed.[3] Even these polymers were too absorbant at 157 nm, so new solutions had to be found. One solution to the high absorbance problem was the use of silicon-containing polymers, namely polysiloxanes and polysilsesquioxanes as components of photoresists.[10,11] Upon exposure to radiation at 157 nm, photocrosslinking occurs (see chapter 6), making these polymers suitable only for negative photoresists, while the microelectronics industry uses mainly positive photoresists. Although Si-O bond is transparent compared to C-H bonds, a better choice is the use of compounds containing C-F bonds. Substitution of H with F represents a solution, the absorbance of fluorinated polymers at 157 nm being close to the optimal values required in photolithography.[12,13] Copolymers synthesized from monomers

responsible for the required properties (transparency, good adhesion, solubility switch, etch resistance) were the compromise solution. In the present study the polymer used is a fluorinated copolymer (FP) from DuPont, whose structure is shown in chart 5-1. A characteristic of these polymers is the presence of norbornene, tetrafluoroethylene and the hexafluorinated alcohol groups. The *t*-Boc ester group is the same solubility switch used in previous generations of polymers. For control experiments other polymers, whose structures are shown in chart 5-1, have been used.

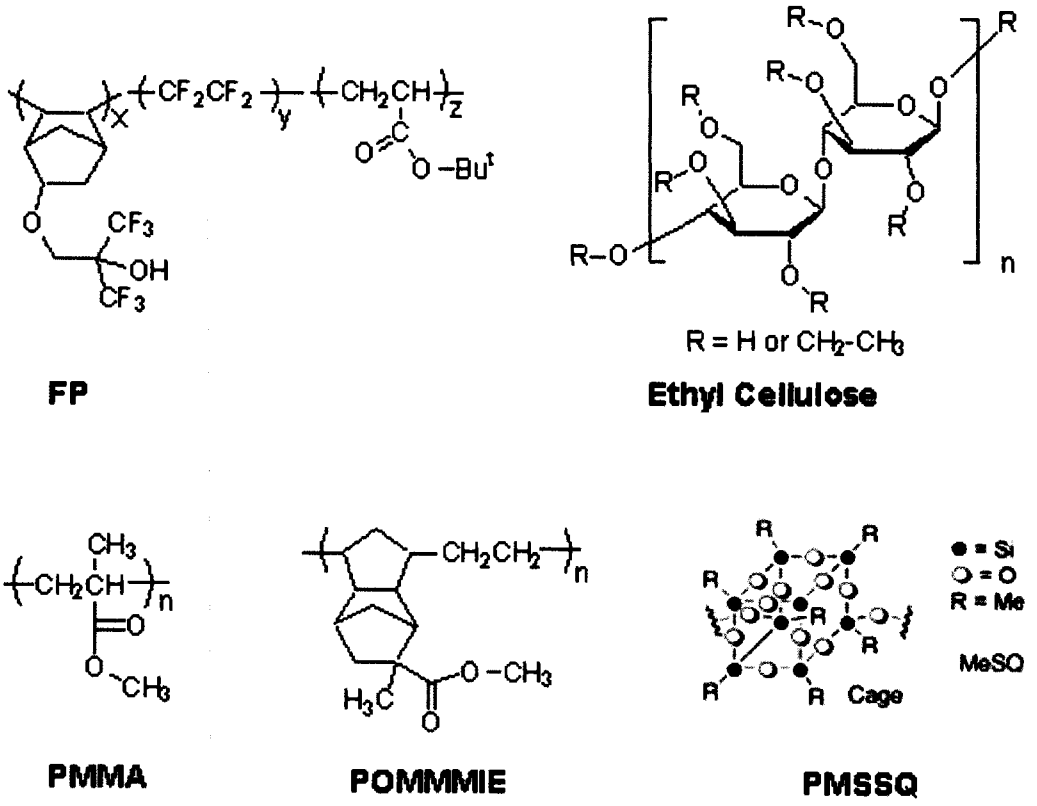

Chart 5-1. Structures of polymers used in the present study: FP, ethyl cellulose (EC), poly(methyl methacrylate) (PMMA), POMMIE, and PMSSQ.

Exposure of polymers to laser radiation at advanced optical wavelengths leads to photochemical and photothermal changes in the polymer structure,

degradation, ablation, and acid formation.[14] Depending on the type of polymer and the exposure wavelength, outgassing, films loss, crosslinking or chain scission may occur.[14-16] Ablation is another phenomenon that occurs when polymer films are exposed to laser radiation, and in particular to 157 nm.[17] Photons at 157 nm have a high energy, 7.9 eV or 182 kcal/ mole of photons, enough to break almost any chemical bond and lead to formation of "hot" intermediates.[18] The quest for materials capable to withstand long term exposure has been triggered by the need for pellicles used in photolithography at 157 nm. Fluorinated polymers undergo photodarkening and photodegradation when exposed to high incident doses at 157 nm.[19] Volatile photoproducts obtained during irradiation and outgassing of fluorinated polymers at 157 nm tend to deposit on optics and create opaque films which absorb photons. There is one photoproduct which is of particular concern. Previous reports on fluorinated polymers exposed to 157 nm advance the idea that hydrofluoric acid (HF) is formed during irradiation.[19] HF is a very corrosive acid, and is of great concern for industry since it reacts easily with glass from optical parts. In the present study HF formation in FP exposed to laser radiation at 157 nm was detected using a fluorescent sensor capable of detecting F^-.

5.2 *Results*

To study the chemical and topological changes that occurred in polymer films exposed to laser radiation, a series of techniques have been employed: UV-VIS and FTIR absorbance, fluorescence spectroscopy and microscopy, laser flash photolysis, NMR, EPR, and atomic force microscopy (AFM).

Experiments involving EPR showed strong signals characteristic to peroxyl radicals, but they could not be assigned to a particular radical due to the broad shape. However, the signal did increase with exposure dose. Attempts to deaerate the films were not successful in completely removing the oxygen. However, signals characteristic to carbon centered radicals were recorded with a Jeol EPR instrument.

^{1}H and ^{19}F NMR experiments did not show significant differences between the exposed and unexposed samples. *D6*-acetone was used as solvent. An important observation was that the exposed samples were not easily soluble after irradiation, compared to the unexposed samples, which were readily soluble. This was a proof that photocrosslinking occurred during irradiation.

5.2.1 Absorption Spectroscopy in Polymer Films

Films of FP were exposed to increasing doses of radiation at 157 nm. The films were obtained by spin coating a solution containing 60.0 % weight 2-heptanone as solvent and 40 % weight dry polymer. The higher loading of polymer was chosen because of the low initial absorbance of the film, thus allowing for a better signal to noise ratio. Two spin coating speeds were employed: 1000 rotations per minute (rpm) and 2000 rpm for 20 s, followed by PAB at 90 °C on a hot metallic plate inside an oven for 2 minutes. The longer baking time was determined

by the higher loading of polymer, allowing for the solvent to evaporate. Using the thin film analyzer (TFA), the thickness was measured and averaged over three experiments for both spin coating speeds. Films spin coated at 1000 rpm had a thickness of 2770 nm, while those obtained with 2000 rpm were 2050 nm thick. The films obtained at 2000 rpm were used for further experiments, due to their smaller thickness.

In figure 5-1 there is a plot showing increase in absorbance of a FP film exposed to laser radiation at 157 nm, 2 shots/ s, with an energy of 1.1 – 1.2 mJ/ cm^2/ shot. The polymer solution contained 40 % weight polymer, 60 % weight 2-heptanone. The film was obtained by spin coating the above solution at 2000 rpm for 20 s, followed by baking for 2 minutes at 90 °C inside an oven, then rapidly cooled to room temperature (RT) on a metallic surface before measuring absorbance. The clean quartz disc was used as baseline. The thickness of the film before exposure was 2050 nm, after 3500 shots the measured thickness was 1950 nm.

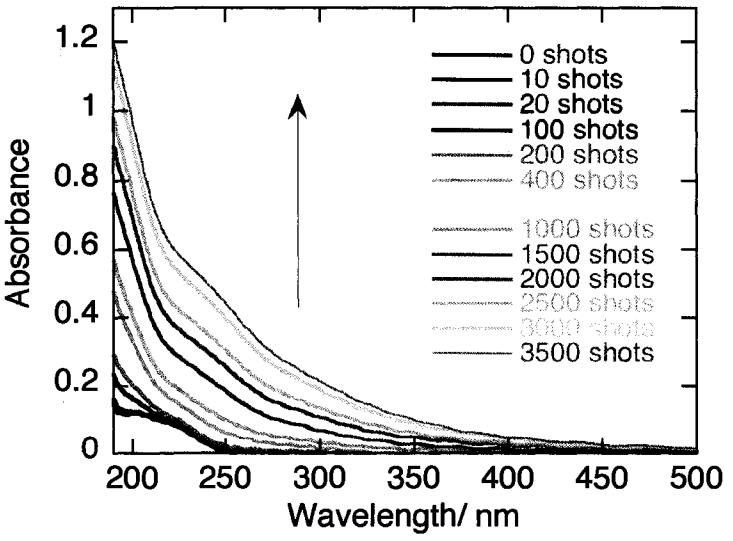

Figure 5-1. Absorption spectra of a FP film (2047 nm initial thickness) exposed to 157 nm, 2 shots/ s, 1.1 – 1.2 mJ/ cm^2/ shot, up to a total of 3500 shots.

As the incident dose increased, the film became yellow and turned brown towards 3000 shots, and although the thickness decreased, the absorbance increased.

Control experiments were done, using non-fluorinated polymers which absorb more at 157 nm compared to FP. A polymer bearing esteric pendant groups, poly[[octahydro-5-(methoxycarbonyl)-5-methyl-4,7 methano-1H-indeno-1,3—diyl]-1,2-ethanediyl] (POMMMIE), was used for exposure at 157 nm. Experiments with PMMA films gave the same result: the films change from transparent to brown in color after a few thousands of mJ/ cm^2.

Films of POMMMIE were obtained by spin coating a solution containing 15 % weight polymer and 85 % weight 2-heptanone as solvent at 3000 rpm for 20 s, followed by PAB at 90 °C for one minute. After cooled down to RT, the film was exposed to increasing doses of radiation at 157 nm, 1.5 mJ/ cm^2/ shot, and absorbance was measured after each exposure, figure 5-2. The thickness of the film was 1100 nm after the first 100 shots, and 1000 nm after 10000 shots. After 15,000 shots the film was brown in color

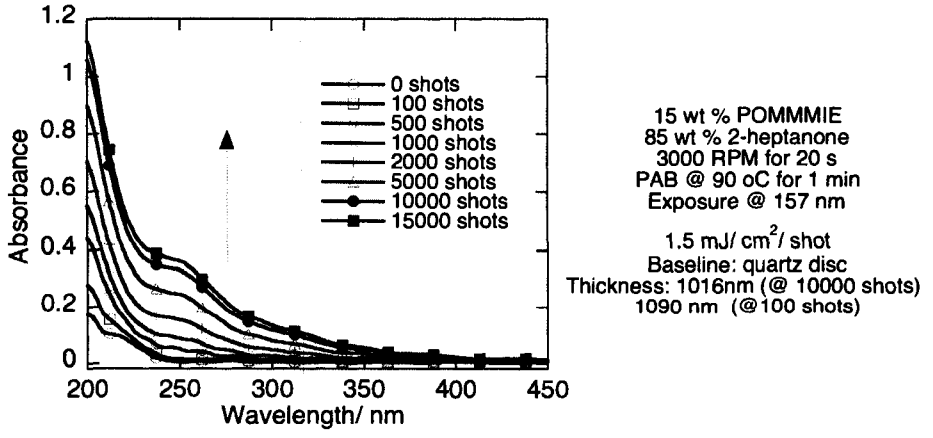

Figure 5-2. Absorbance of a POMMMIE film obtained by spin coating a solution containing 15 weight % dry polymer and 85 weight % 2-heptanone at 3000 rpm, followed by

PAB at 90 °C for 1 minute. The film was exposed to increasing doses of radiation at 157 nm, 1.5 mJ/ cm^2/ shot, up to 15 000 shots.

5.2.2 Use of Fluorescence Spectroscopy and Microscopy

Absorption spectroscopy shows that the films change color upon irradiation, become brown and absorb more as the incident dose increases, but it is not enough to get an insight into the photoproducts obtained during interaction of the highly energetic photons from 157 nm and the polymer film. Since previous reports mentioned HF as a possible product[16],[19] we decided to use fluorescence sensors capable to detect acid and in particular HF, as tools to investigate the photochemistry of the polymer.

Coumarin 6 is an excellent fluorescent sensor for acid. [20] Its maximum in absorption and emission change upon protonation, making it easy to monitor acid using optical spectroscopy techniques, figure 5-3. Depending on the amount of acid present in the film, Coumarin 6 can be mono- or di-protonated, see chapter 2 for the chemical reaction. The absorbance and fluorescence plots from figure 5-3 were obtained with the same PMMA film, containing 3 % triphenylsulfonium triflate (TPS-OTf) and 0.5 % Coumarin 6 based on polymer weight. Before TPS-OTf and C6 were added, dry PMMA represented 15 weight % and 2-heptanone 85 weight % from the stock solution. The solution was spin coated at 3000 rpm for 20 s, then the film baked at 90 °C for 1 minute to ensure removal of the solvent. Flood exposure was done at 254 nm in the HTG Exposure Unit (39.7 W/ m^2, see figure 4-1 B for power spectrum), followed by PEB at 90 °C for 1 minute, allowing for the photochemically formed acid to diffuse and protonate the Coumarin 6. For the fluorescence spectra, the excitation wavelengths were 450 nm for the neutral form, and 510 nm for the protonated form. The molar absorption coefficient for neutral C6 is 5.4 x 10^4 L mol^{-1} cm^{-1}.[21]

Previous experiments with Coumarin 6 in films containing PAGs showed the ability of this dye to function as an acid sensor.[20,22] In the presence of PAGs, only a

small dose of incident light is necessary to obtain absorbance and emission characteristic to the protonated form of C6.[23]

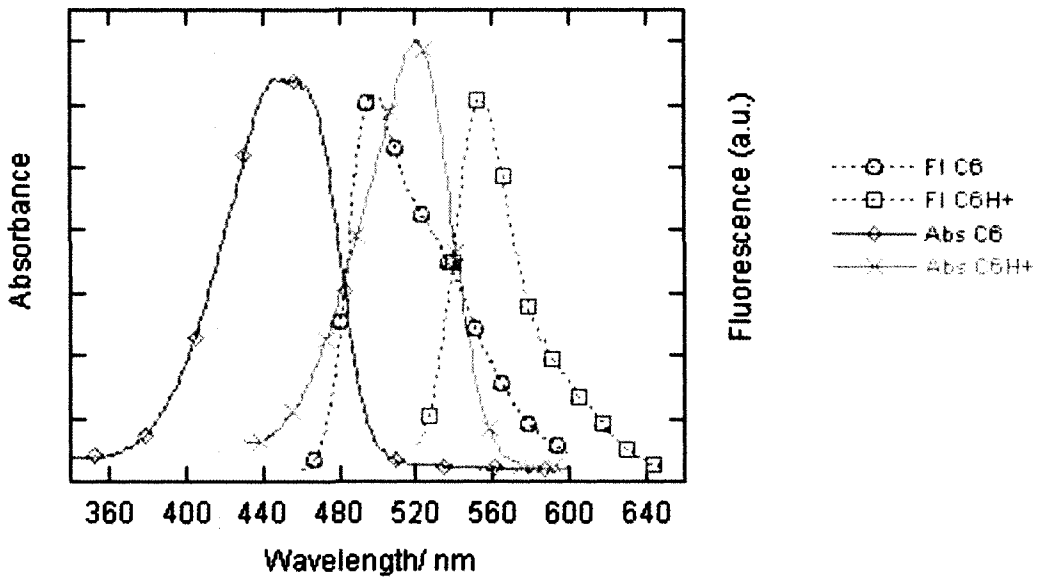

Figure 5-3. Absorbance of neutral (◊), protonated (x), and fluorescence of neutral (O), and protonated (□) Coumarin 6 in a PMMA film (~ 850 nm thick) containing TPS-OTf (3.0 % based on PMMA weight) and C6 (0.5 % based on PMMA weight), and exposed to continuous wavelength at 254 nm. Excitation wavelengths for fluorescence spectra were 450 nm for the neutral form of C6 (before exposure) and 510 nm for the protonated form of C6 (after exposure).

To test the formation of acid upon exposure, in the present experiments no PAG was added to the polymer solutions spin coated and exposed to laser radiation at 157 nm, only polymers and Coumarin 6 (0.5 wt % based on polymer). Coumarin 6 has been used before for imaging purposes.[23,24] Two other polymers were used in this study as control experiments: ethyl cellulose (EC) and poly(methylsilsesquioxane) (PMSSQ), figure 5-4. Due to the small amount of protonated Coumarin 6 ($C6H^+$) present in the films, the emission characteristic to this species recorded in the fluorimeter was too low. The technique used to monitor

acid formation was fluorescence microscopy, which proved to be more sensitive than fluorescence spectroscopy. The software and the digital camera attached to the fluorescence microscope allow the user to distinguish even very low emission in the exposed areas, in contrast to the unexposed ones, making this imaging technique suitable for this type of films. Polymer films were obtained by spin coating solutions containing polymer and 2-heptanone so that their thickness after 1 minute PAB was 400 nm for EC, 485 nm for PMSSQ, and 350 nm for FP. Exposure at 157 nm was done through a copper mask with hexagonal holes, 60 micrometers center-to-center, figure 5-4.

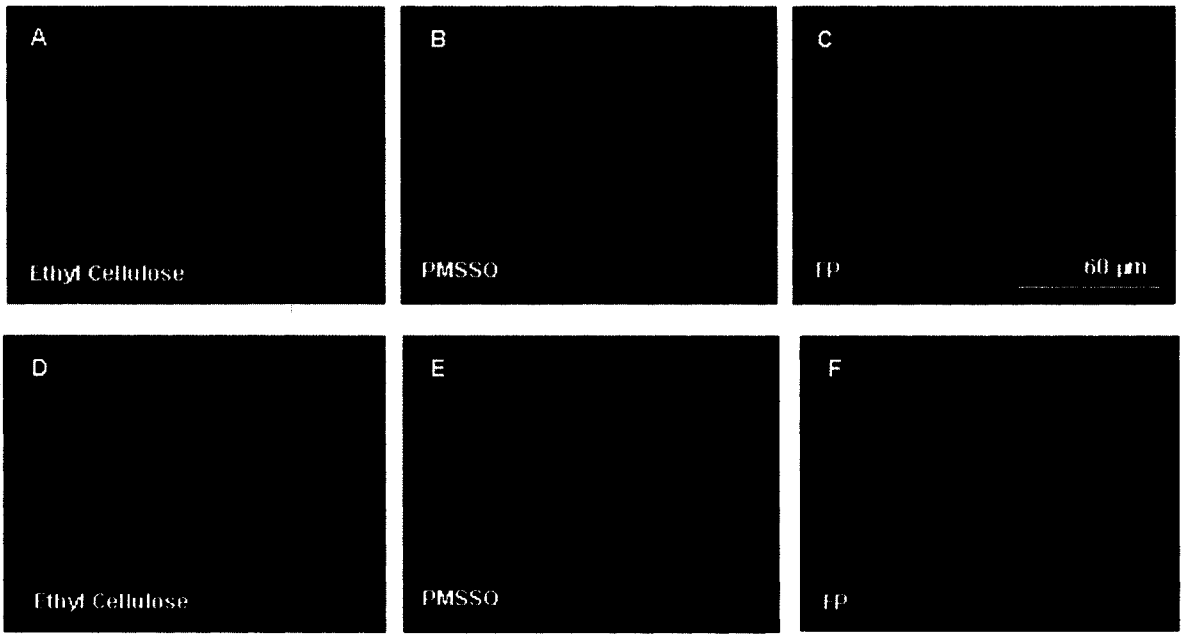

Figure 5-4. Fluorescence images of polymer films (ethyl cellulose – A, D, PMSSQ – B, E, FP – C, F) containing Coumarin 6 (0.5 weight % based on polymer weight), and exposed to laser radiation at 157 nm, 1.4 mJ/ cm^2/ shot, 30 shots (total incident dose 42 mJ/ cm^2). The images show emission from neutral Coumarin 6 (A, B, C) recorded with the E4 filter, and from protonated Coumarin 6 (D, E, F) obtained with M2 filter. The distance between the centers of two consecutive hexagons was 60 µm.

Fluorescent images were recorded with E4 optical filter (maximum ~ 437 nm) for images showing neutral C6, and M2 optical filter (maximum centered at ~ 548 nm) for protonated $C6H^+$. The spectra of the light incident on the film surface in the fluorescence microscope, with M2 and E4 optical filters are shown in figure 5-5. Although C6 and $C6H^+$ do not have maxima of absorbance coinciding with the maximum of the incident light, they still show a good overlap of their absorbance with the spectrum of the incident radiation.

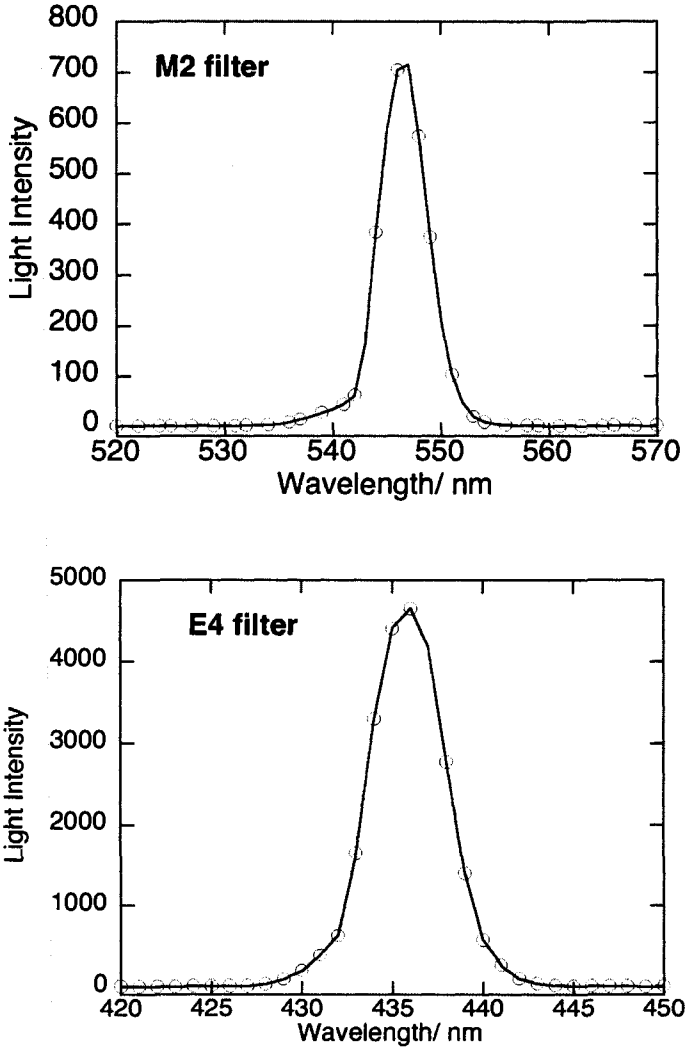

Figure 5-5. Spectra of light incident on the film surface, when using microscope filters M2 and E4. The intensity of light with the E4 filter was ~ 6.5 times higher than in the case of M2 filter.

Further control experiments with PMMA, FP, and PMSSQ films containing C6 were done exposing at 157 nm for 200 shots, 2.5 – 2.6 mJ/ cm^2/ shot. It is important to remember that no photoacid generators were added to these films. For resist formulations containing PAGs, chapter 3, the minimum dose required to obtain a strong emission from the protonated C6 was ~ 1.0 - 2.0 mJ/ cm^2, whereas in the case of FP films without PAG the minimum dose to see a weak emission characteristic to C6 was ~ 10.0 mJ/ cm^2 at 157 nm. In the experiments done without PAG, the acid originates from the polymer.

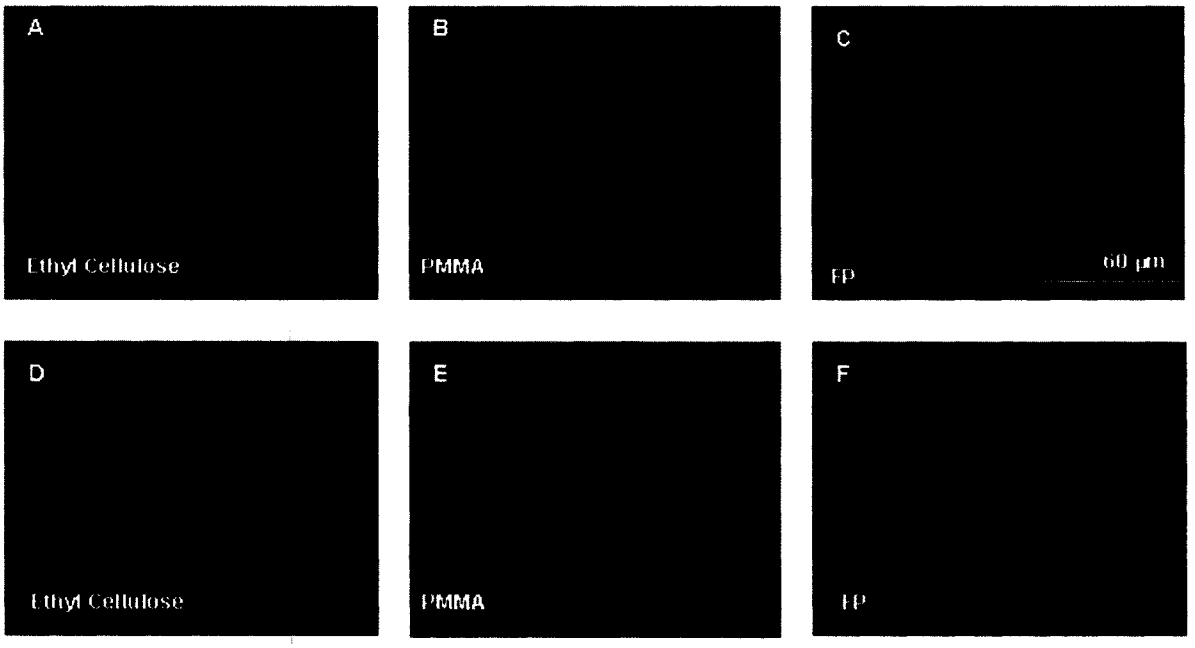

Figure 5-6. Fluorescence images of EC (A, D), PMMA (B, E), and FP (C, F) films containing Coumarin 6 (0.5 %based on polymer weight), exposed, through a copper mask with hexagonal holes, to 200 shots of laser radiation, 2.5 – 2.6 mJ/ cm^2/ shot, at 157 nm. The images were recorded using E4 (A, B, C) and M2 (D, E, F) optical filters. The green fluorescence corresponds to neutral C6, while the red emission corresponds to the protonated form $C6H^+$. The dark regions correspond to the unexposed areas masked by the copper grid, which was removed when the images were recorded. The center-to-center distance between two consecutive hexagons was 60 µm.

5.2.3 Detection of fluoride using fluorescence techniques

Previous reports mention formation of HF in films of fluorinated polymers exposed to laser radiation at 157 nm, however, a straightforward detection of HF is rather difficult, partly because of the small amount formed during irradiation.[19] Employing fluorescence microscopy and imaging techniques, one could easily detect the presence of HF in the irradiated areas of the FP film by using a fluorescence sensor for HF. While C6 is an excellent sensor for acid, it is not a specific sensor for HF. FP films containing C6 and spin coated on top of 1 inch quartz discs were left for ~ 10 minutes in atmospheres of various acid vapors, hanged inside beakers containing hydrochloric acid (HCl), hydrofluoric acid (HF), and acetic acid, and emission characteristic to the monoprotonated C6 was recorded. A sensor sensitive to the presence of HF is desirable, and a derivative of Coumarin 4, already presented in chapter 2, has been synthesized in the group, and successfully tested in FP films within this project. [25]

A dye from the coumarines family, 7-hydroxy-4-methylcoumarin (Coumarin 4, C4) was reacted with triisopropylsilyl chloride (TIPSCl) and imidazole in dimethylformamide (DMF), giving 4-methyl-7-(tri-isopropylsilanyloxy)-coumarin (C4TIPS), scheme 1 (A). The crude product was purified by column chromatography with silica gel, using a mixture of hexane : dichloromethane as eluent. [25]

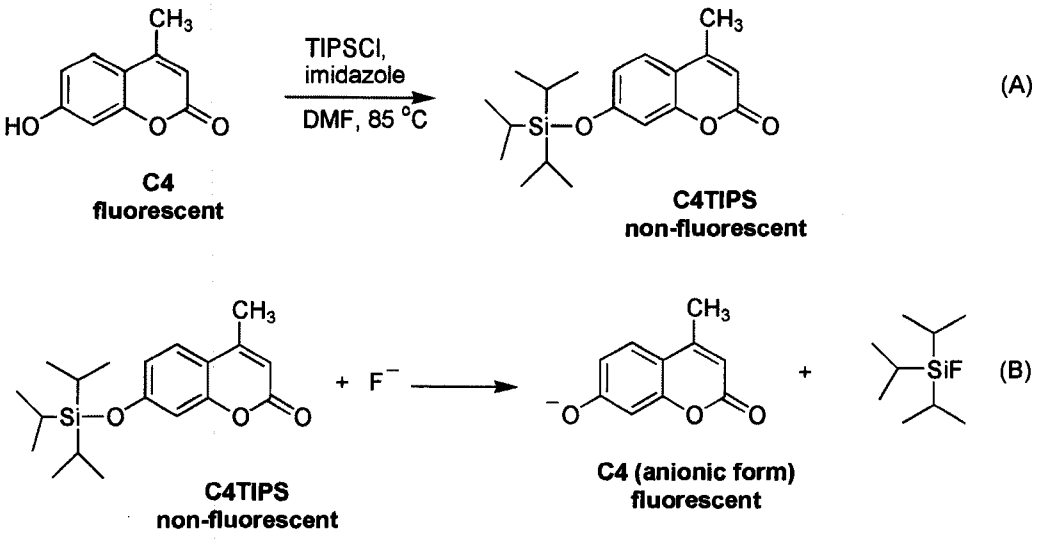

Scheme 5-1. Synthesis of HF fluorescent sensor C4TIPS from C4 and TIPSCl (A), and release of protective group triisopropylsilanyl upon reaction of C4TIPS with F^-, and recovery of fluorescencent C4 in anionic form (B).

The principle of HF detection is based on the recovery of fluorescence of C4TIPS upon deprotection, scheme 1 (B). C4 is a strong fluorescent dye which upon protection of 7-hydroxy group with TIPSCl becomes nonfluorescent. The ability of C4TIPS to restore its fluorescence upon deprotection has been the key to monitor HF formation in thin FP films exposed to 157 nm. Emission spectra of a C4 and C4TIPS are shown in figure 5-7. C4 and C4TIPS were dissolved in acetonitrile, the final solutions having the same concentration, 5.0×10^{-5} M. The spectra were recorded in a 10 x 10 mm quartz cell, and the excitation wavelength was 340 nm.

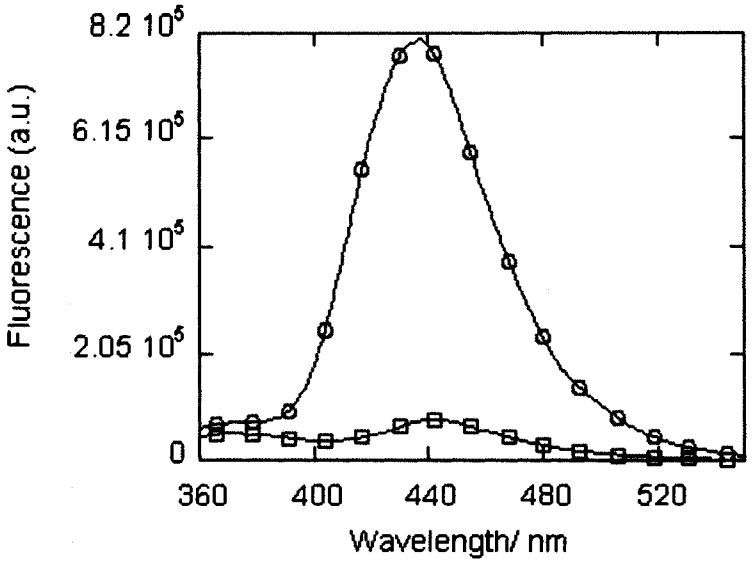

Figure 5-7. Emission of Coumarin 4 (O) and C4TIPS (□) 5.0 x 10^{-5} M in acetonitrile, in a 1.0 cm x 1.0 cm rectangular quartz cuvette. For both spectra the excitation wavelength was 340 nm.

Although fluorescence spectroscopy works very well in solution at 5 x 10^{-5} M concentration, in FP polymer films the amount of HF produced is much lower, and consequently the deprotection of C4TIPS does not occur on a large scale, making it hard to monitor the emission of the *in situ* formed C4. To overcome this difficulty, fluorescence microscopy was the technique chosen to investigate the deprotection of C4TIPS by HF.

Films of PMMA containing C4TIPS and C4, and FP films containing C4TIPS, were exposed to laser radiation at 157 nm through a copper mask having hexagonal holes with 60 micrometers center to center. PMMA films were obtained by spin coating a stock solution containing 11 weight % PMMA, 89 weight % 2-heptanone, and 5.0 % C4TIPS or C4 based on dry PMMA weight (C4TIPS and C4 were added to the stock solution of 2-heptanone (89 % weight) and PMMA (11 % weight)). FP films were obtained by spin coating a solution containing polymer 18 weight %, 2-heptanone 82 weight %, and C4TIPS 5 weight % based on polymer

weight. The quartz discs were spin coated at 2000 rpm for 20 s, followed by PAB on a metallic surface at 90 °C inside an oven for one minute. Attempts to obtain films of FP containing C4 were unsuccessful because C4 did not dissolve in the solution used for spin coating at 5.0 % loading based on FP weight.

As control experiments, films of PMMA containing C4 and C4TIPS were obtained by spin coating a solution at 2000 rpm for 20 s. Exposure was done at 157 nm for 50 and 100 shots, 1.9 mJ/ cm^2/ shot, 2 shots/ s. The films were exposed through the copper mask, and images recorded in the fluorescence microscope using the XF02-2 optical filter from Omega Optical with a maximum at 367 nm (see figure 6-10 for the spectrum of the filter), figure 5-8. The mask was removed from the surface of the films during recording of fluorescence images, so the dark areas represent the absence of emission from the unexposed areas.

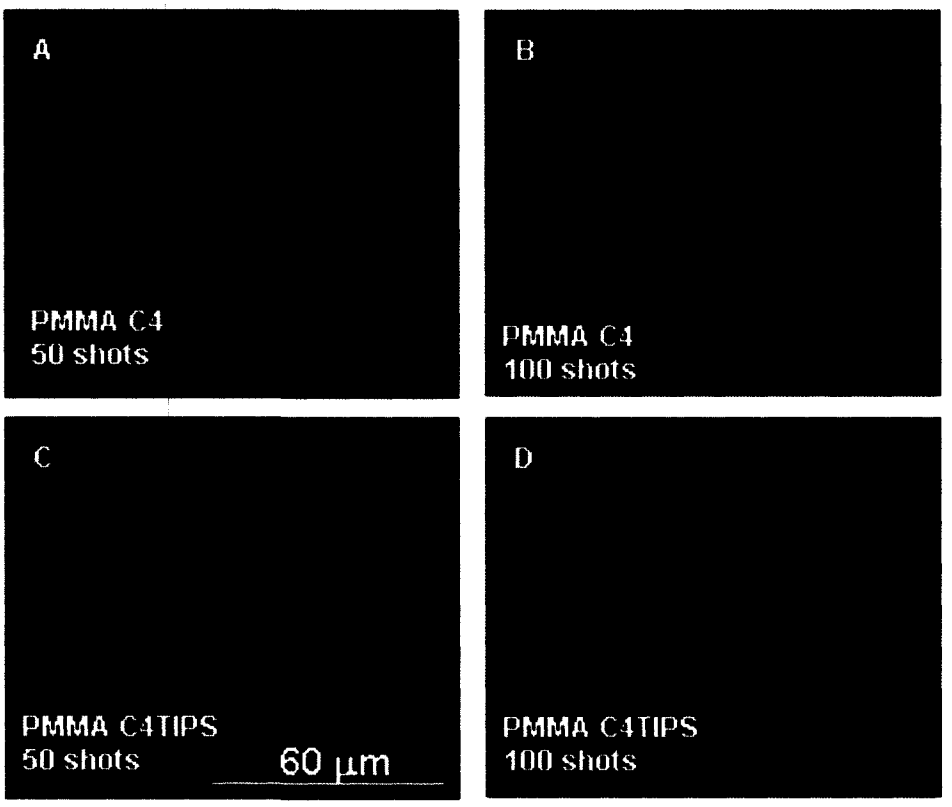

Figure 5-8. Fluorescence images of PMMA films containing C4 (A, B) and C4TIPS (C, D), and exposed to 95 mJ/ cm^2 (A, C), and 190 mJ/ cm^2 (B, D) at 157 nm. The distance

between the centers of two consecutive hexagons was 60 μm, the excitation optical filter used was XF02-2 with a maximum excitation wavelength at 367 nm. The incident energy was 1.9 mJ/ cm^2/ shot, delivered at a frequency of 2 shots/ s.

As expected, the PMMA films containing C4 (figure 5-8 A and B) are more fluorescent than those containing C4TIPS (fig. 5-8 C and D). The next exposure was done to increasing doses of radiation (20, 50 and 100 shots, 1.9 mJ/ cm^2/ shot) at 157 nm using FP films containing C4TIPS, figure 5-9. For the sake of comparison and for a better contrast, images obtained with PMMA films and shown in figure 5-8 C and D are shown below images obtained with FP films, figure 5-9 D and E.

All these images are recorded after the copper mask was removed from the top of the films.

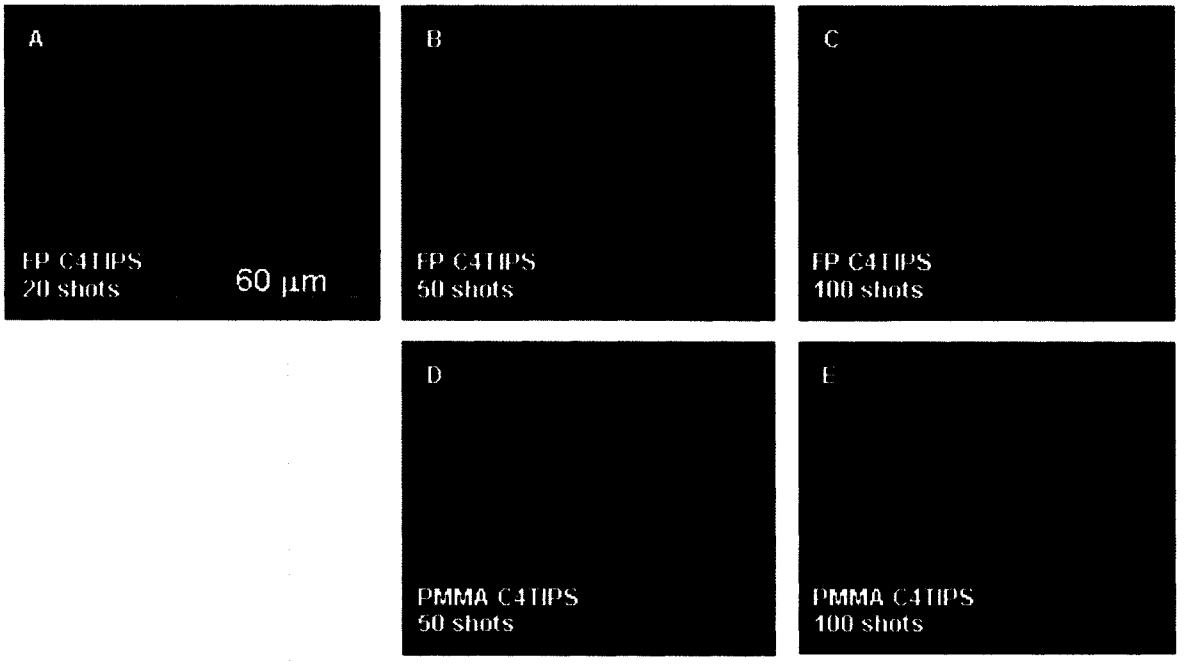

Figure 5-9. Fluorescence images of FP films exposed at 157 nm to 38.0 mJ/ cm^2 (A), 95 mJ/ cm^2 (B), and 190 mJ/ cm^2 (C), and PMMA films exposed to 95.0 mJ/ cm^2 (D) and 190 mJ/ cm^2 (E). Images were obtained using the XF02-2 optical filter, with

an excitation maximum at 367 nm. The incident energy was 1.9 mJ/ cm^2/ shot, delivered with a frequency of 2 shots/ s.

Due to the high energy of the photons, a possible process caused by radiation at 157 nm is electron ejection. Marie Laferrière, a PhD student from the group, monitored the absorption of the solvated photoejected electron by laser flash photolysis (LFP) at 600 – 700 nm.[25] The electron was obtained by photoejection from 1, 4 –dimethoxybenzene (1,4-DMB) in methanol by laser radiation at 266 nm under N_2 and N_2O atmospheres. The resulting radical cation was identified by its absorption at ~ 430 nm. Using varying concentrations of hexafluoro-2-propanol, one could easily determine the rate constant for the scavenging of the solvated electron by monitoring the decay of the signal characteristic to the solvated electron. The determined rate constant for electron scavenging by HFP, a moiety that is found also in FP, chart 5-1, is 3.6 x 10^{10} M^{-1} s^{-1}. Another experiment involving benzyl acetate as electron scavenger gave a rate constant of only 2.9 x 10^8 M^{-1} s^{-1}.

5.2.4 AFM Experiments

Exposure of polymer films to laser radiation causes ablation, a phenomenon already reported in the literature for different wavelengths and materials. (ref) Films exposed at 157 nm through the copper mask were analyzed by AFM to determine the impact of radiation on the surface of the film. Films of EC (ethyl cellulose) and PMMA containing C6, and FP films with and without C6 were examined, figures 5-10 and 5-11. The polymer films had a thickness of approximately 400 nm and were obtained on a glass disc with a diameter of 1.8 cm from VWR Scientific, Inc., suitable for the AFM sample holder. The thickness was adjusted by varying the content of the polymer in the solution or the speed of spin coating. The PMMA solution contained 11 wt % dry polymer and 89 wt % 2-heptanone, and 0.5 wt % C6 from polymer wt; it was spin coated at 3000 rpm for 20 s, followed by PAB at 90 °C inside the oven for one minute, and the thickness of the obtained film was 392 nm. The EC films were obtained by Marie Laferriére by spin coating, on a glass disc at 1000 rpm for 20 s, a solution containing 1 wt % EC dissolved in chloroform. The thickness obtained for the EC films was ~ 400 nm. FP films were obtained by spin coating on a glass disc, at 3000 rpm for 20 s, a solution containing 18 wt % FP dissolved in 2-heptanone. The films with C6 contained 0.5 wt % C6 from polymer weight. The thickness of the FP film without C6 was 350 nm. The thickness of the FP film containing C6 was 366 nm. All solutions were filtered through a 0.45 μm Teflon filter before spin coating.

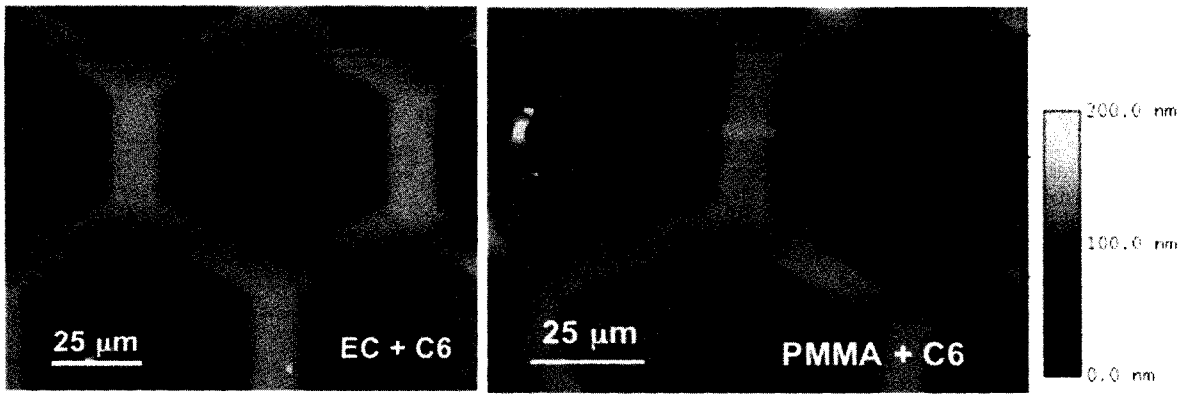

Figure 5-10. AFM images of an EC + C6 film exposed through a copper mask to 200 shots at 157 nm, 2.5 mJ/ cm^2/ shot (A); AFM images of a PMMA film containing C6, exposed to 200 shots through the hexagonal copper mask, 2.5 mJ/ cm^2/ shot (B).

The film loss in the exposed areas, expressed as the difference between the unexposed regions and the center of the hexagon, was different for each polymer: for EC films containing C6 the depth of ablation was 30 nm, for PMMA films containing C6 the depth was 20 nm, for FP with C6 the depth was 25 nm, while for FP films without C6 the depth was 15 nm.

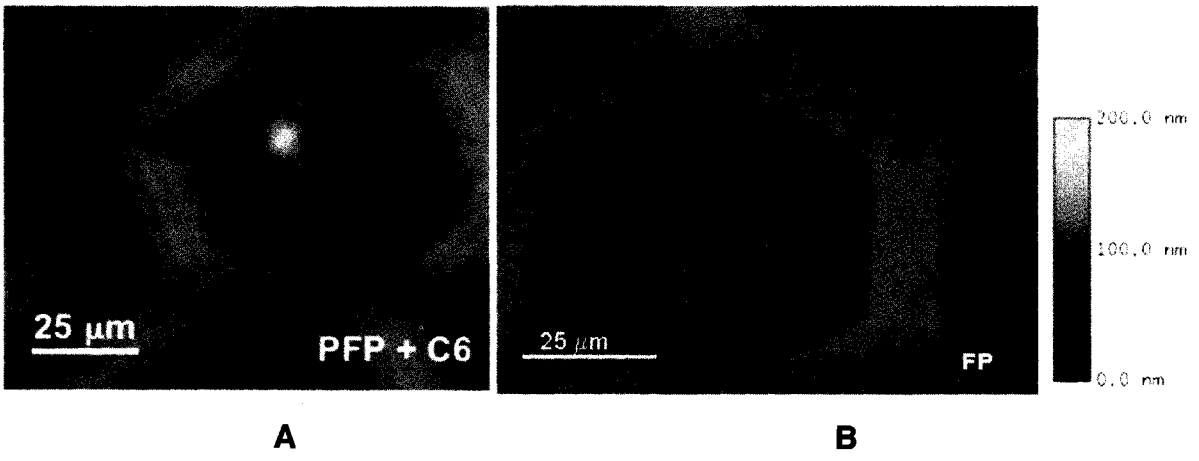

Figure 5-11. AFM image of a FP film exposed to laser radiation at 157 nm, 200 shots, 2.5 mJ/ cm^2/ shot, with C6 (A) and without C6 (B). The average depth was 15-20 nm for the

film without C6, 25 nm for the film with C6.

Laser induced periodic structure (LIPS) are clearly observed in figure 5-11 A when a FP film containing C6 was exposed. The origin of these structures will be analyzed in the discussion part of this chapter.

Another series of experiments was carried out with films of polymethylsilsesquioxane (PMSSQ) dissolved in 2-heptanone. The solution contained PMSSQ 25 % weight and 2-heptanone 75 weight %. The films were obtained by spin coating on the same substrate as in the previous examples at 3500 rpm for 20 s, followed by PAB at 90 °C for 60 s. After PAB the film was cooled to RT before exposure at 157 nm through the copper mask, giving a thickness of ~ 485 nm. For an incident dose of 460 mJ/ cm^2, the film loss was 17 nm for the PMSSQ film.

5.3 Discussion

In photolithography the polymer matrix has been traditionally seen as an inert medium from the photochemical point of view, due to its transparency at the exposure wavelengths. From novolac (I-line), to polyhydroxystyrene (248 nm), to polyacrylates (193 nm) based photoresists, in the chemically amplified resists the polymer is modified by the acid produced during the photolysis of the PAG. The pendant ester *t*-Boc group, which acts as a solubility switch, is deprotected, and the exposed regions become soluble in the developing solvent. The developer is a base, usually tetramethylammonium hydroxide or tetrabutylammonium hydroxide. At 157 nm one of the most critical issues is the transparency of the polymer, since at this wavelength almost all chemicals absorb. Thus, one cannot avoid absorption of photons by the polymer matrix and consequently photochemical or photothermal reactions. As a consequence, the photoresists are less efficient because there are less photons available to be absorbed by the PAG, and, even more, there may appear unwanted photochemical reactions involving the polymer: chain scission or photocrosslinking.[14] Photocrosslinking is the opposite effect of what is expected in the exposed regions of positive photoresists, since through crosslinking polymers become less soluble in the developing solution.

The goal of this research was to study the physical and chemical transformations that occur in the FP films exposed to laser radiation at 157 nm, and in particular to detect formation of acid (HF). Among the possible photochemical reactions involving polymers used in photoresists, there are Norrish type I, Norrish type II, ester elimination, and main chain scission. [14] Outgassing is another side effect in photolithography at 157 nm, small molecules and fragments of polymer or PAG being ejected from the surface of the film. [15,16,26-29] To study the outgassing products, the exposure is usually coupled with gas chromatography and mass spectrometry (GC-MS) as detection techniques. A copolymer with the structure similar to FP (the norbornene monomer did not have the hexafluoroisopropyl unit

attached, and the ratio of the monomers in the backbone was different) used in the present study was irradiated at 157 nm, and the outgassing products detected with GC-MS and reported by others. [29] The main products detected by GC-MS were isobutene and acetone.

The bonds most likely to break by the direct irradiation for the FP polymer used in this study are shown in chart 5-2. Norrish type I reactions occur when the C – C bond between the carbonyl and the polymer chain is broken, giving rise to a carbon radical center localized on the polymer chain. This can further recombine with another carbon center radical from a polymer chain, leading to crosslinking. It has been previously reported that polymethacrylates favor Norrish type I, while polyacrylates favor Norrish type II photochemical reactions.[14] Although the unexposed polymer readily dissolves in *d6*-acetone when samples were prepared for NMR, dissolving the polymer after exposure to 157 nm was a challenging task, the polymer becoming hardly soluble. This was a valuable observation, suggesting that in the polymer film crosslinking occurred during exposure. Due to the small amounts of polymer used throughout the experiments and the decreased solubility after exposure, there was not enough sample to run a GPC experiment which could have shown the increased molecular weight of the polymer after exposure. However, photolysis leads to formation of radicals which were detected using EPR spectroscopy.

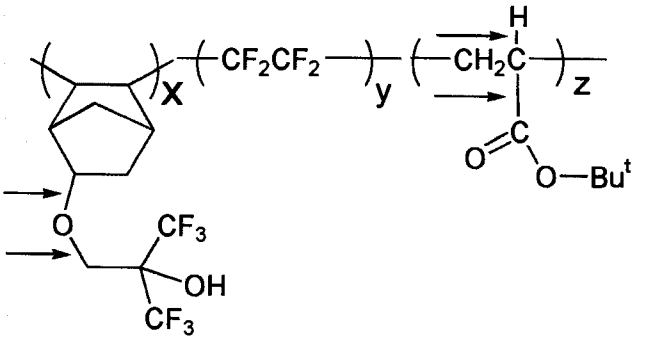

Chart 5-2. Possible bond breaking in the FP polymer exposed to 157 nm (Norrish type I, Norrish type II, main chain scission, C-O and C-H bond breaking).

From the optical spectroscopy measurements, one can notice an increase in the overall absorbance of FP as the incident radiation dose at 157 nm increases. This is often referred to as yellowing or photodarkening, and has been reported before for fluorinated and non-fluorinated compounds alike. [19,30] It is assumed that the photodarkening is caused by formation of double bonds through elimination of HF from the $-CH_2-CF_2-$ sequence in the polymer and from the hexafluoroisopropyl group, scheme 5-2. [30] We have already reported detection of HF using a fluorescence sensor and fluorescence microscopy, thus the explanation advanced by Garza *et. al* appears reasonable. [25]

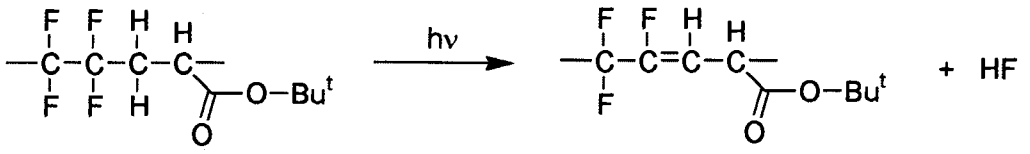

Scheme 5-2. Dehydrofluorination involving the tetrafluorinated and the solubility switch moieties of the FP following exposure to 157 nm, formation of alkene, and elimination of HF.

Photodarkening is related to the content of H, the lower the H content the higher the incident dose required for photodarkening. [19,30] From figures 5-1 and 5-2 one can notice that the absorption spectra have similar shapes. Plotting value of absorbance at 220 nm as a function of the incident dose shows that the increase in absorbance is linear at small exposure doses, and it slows down as the incident dose increases, figure 5-12 A (FP) and B (POMMMIE).

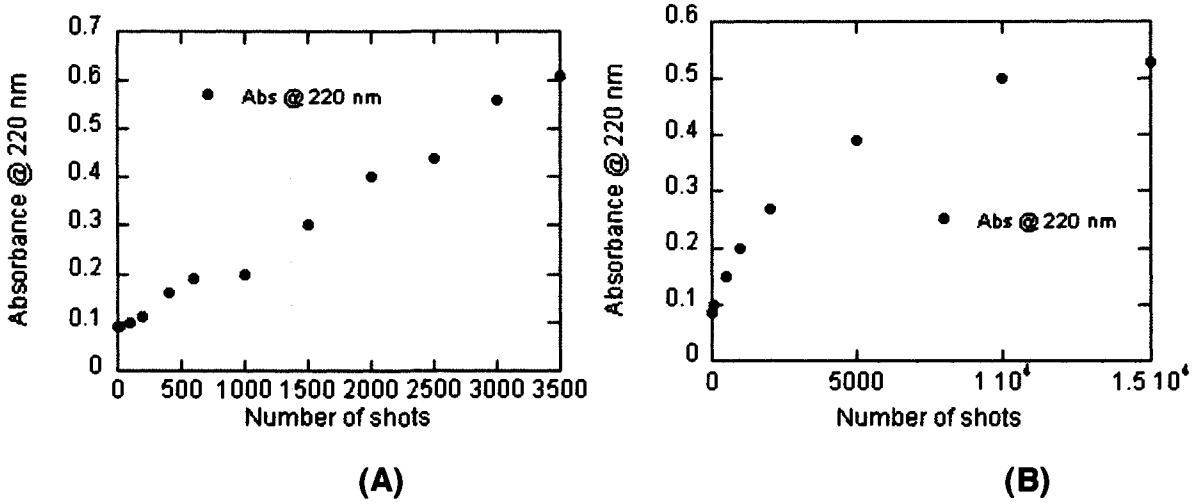

Figure 5-12. Absorbance of a FP film (2050 nm thick) exposed to laser radiation at 157 nm, 1.1 – 1.2 mJ/ cm^2/ shot, 2 shots/ s (A) and a POMMMIE film (~1100 nm thick) exposed to laser radiation at 157 nm, 1.5 mJ/ cm^2/ shot (B).

The absorbance increase for FP film, shown in figure 5-12 (A), as a function of incident dose is linear, however, more exposure leads to a deviation from linearity and eventually a plateau is reached just like in the case of POMMMIE film from figure 5-12 (B).

Exposure of FP films containing C6 to 157 nm shows unequivocally formation of acid, although no PAG was present in the film. Previous experiments, done with photoresist films containing C6 and PAG, showed formation of acid at very low incident doses, 1-2 mJ/ cm^2.[23] For the present study the smallest incident dose necessary to obtain a fluorescence image in FP films without PAG was 10 mJ/ cm^2. Coumarin 6 is an excellent fluorescent acid sensor, and it has already been discussed in chapter 2. It works excellent as acid sensor when a PAG is present in the irradiated film and the technique used for detection is fluorescence spectroscopy. However, when no PAG is present in the film, the amount of acid generated is much smaller and the *in situ* formed protonated Coumarin 6 ($C6H^+$) is in a concentration too small to be detected by fluorescence spectroscopy. To

overcome this disadvantage, a more sensitive technique, namely fluorescence microscopy, was used to monitor acid formation in polymer films exposed to laser radiation at 157 nm. By exposing the polymer films through a copper mask with hexagonal holes, one has the advantage of observing the contrast between the exposed and unexposed regions of the film in the same image. From figures 5-4 and 5-6 it is easy to distinguish the two forms of C6: neutral (emission in green) and protonated (emission in red). Three other polymers were used as control for experiments involving C6 and fluorescence microscopy: EC, PMSSQ, and PMMA. Using the software DigitalColor Meter v. 3.2 from Apple Computer Inc., it was possible to obtain quantitative data about the amount of red and green from the exposed and unexposed regions of the films. This software application magnifies the pixel at which the mouse arrow is pointing, and then quantifies the contribution of the three basic colors (red, green, and blue) to the color of that particular area. It is important to detect the protonated form of C6 rather than to observe a decrease in the emission of neutral C6 in the exposed areas compared to the unexposed ones. It is clear from figures 5-4 and 5-6 (A, B, and C) that the intensity of emission of C6 in the exposed areas is smaller compared to the unexposed ones. A simple decrease in emission of C6 in the exposed areas could be caused, besides protonation and consequently shifting of emission to longer wavelengths, by simply destroying C6 during irradiation at 157 nm. Another reason for lower emission of C6 in green in the exposed areas could be the film loss due to ablation, thus the amount of C6 which emits is lower. Thus it is important to have a positive evidence that in the exposed regions the lower emission from C6 is due mainly to protonation of C6. This is shown in figure 5-4 D E, and F, where emission in red, characteristic to $C6H^+$ is recorded. The contributions of red, green, and blue in the exposed and unexposed areas of figure 5-4 D, E, and F are measured with the software DigitalColor Meter v. 3.2 from Apple Computer Inc., and reported in table 5-1.

Table 5-1. Contributions of red, green, and blue in the fluorescence images presented in figure 5-4 D, E, and F with EC, PMSSQ, and FP films containing C6 (0.5 wt % based on polymer weight), and exposed to 42 mJ/ cm^2 at 157 nm

Color/Pol	EC		PMSSQ		PFP	
	Exp	Unexp	Exp	Unexp	Exp	Unexp
Red	15700	1300	6700	0	11600	0
Green	1550	0	0	0	1000	0
Blue	0	0	0	0	500	0

Pol = polymer, EC = ethyl cellulose, PMSSQ = polymethylsilsesquioxane, FP = fluorinated polymer, Exp = exposed areas (center of the hexagonal hole), Unexp = unexposed areas (line of the mask) The values of red, green, and blue were red as actual values from 16-bit images using the RGB color scale.

In the above table the most important value is the contribution from red, since this is the region of the optical spectrum where $C6H^+$ emits. PMSSQ shows the weakest emission characteristic to $C6H^+$, although it has the highest thickness. PMSSQ has the lowest absorbance at 157 nm (no C-H, O-H, C-O bonds) and is expected to suffer the least damage upon interaction with radiation. FP is a polymer especially designed for photolithography at 157 nm, so it has a lower absorbance compared to EC. FP film is 50 nm thinner compared to EC film. Thus it is not surprising that EC films shows a higher emission in red in the exposed regions compared to FP.

While C6 is an excellent choice to detect acid formation in polymers, one needs a sensor that is specific for fluoride. A fluorescent sensor, C4TIPS, designed and synthesized by Dr. Carlos Sanrame in the group, scheme 1, was used to detect formation of HF in polymer films.[25] 7-hydroxy-4-methylcoumarin is highly fluorescent when excited at 340 nm, figure 5-7. Upon protecting the hydroxy group

with triisopropylsilyl chloride, scheme 5-1 (A), the resulting C4TIPS is practically non fluorescent, figure 5-7. This sensor works as a switch, fluorescence being restored after reaction with fluoride or other halides, scheme 5-1 (B). It is obvious that in these films the only halide present is fluoride. The emission spectra of the two molecules in acetonitrile are shown in figure 5-7.

Exposure of FP films, and as control experiments PMMA, to laser radiation at 157 nm through the copper mask, showed formation of latent images, figure 5-8 and 5-9. To prove that C4TIPS is a sensor specific for HF, PMMA films containing C4 and C4TIPS were exposed to 50.0 and 100.0 mJ/ cm^2 at 157 nm. The images recorded with PMMA films containing C4TIPS show almost no emission characteristic of deprotected C4TIPS in the exposed regions, unlike the films containing C4. The contribution of blue to the final image is reported in table 5-2. The ratio of blue between the exposed and unexposed regions shows an increase in the exposed regions compared to the unexposed ones. Surprisingly, there is an increase in blue in the exposed areas for PMMA films containing C4. This can be explained by the physico-chemical changes in the polymer matrix that triggered the enhance in emission of C4. A cause could be that by irradiating the film, aggregates of C4 were dispersed and this increased the overall fluorescence. The ratio of I_{exp}/ I_{unexp} for PMMA films containing C4 shows a decrease for 100 shots compared to 50 laser shots. We already reported that too much acid present in the environment may suppress the fluorescence due to protonation of –OH group from the 7 position.[22,31] Schulman and Rosenberg also reported that fluorescence of 7-hydroxy-4-methyl coumarin is pH dependent.[31] From figure 5-6 E one can notice that PMMA films containing C6 show abundant acid formation when exposed to laser radiation at 157 nm, and this may explain why intensity of blue in the exposed regions of PMMA film containing C4 decreased from 50 to 100 shots. The same explanation may account for the increase in blue in PMMA films containing C4TIPS, the *in situ* formed acid catalyzing the deprotection of the triisopropylsilyl group. Unlike in the case of C4, the acid will not suppress fluorescence by protonation of

the –OH group, but it will help increasing it by deprotection, and this is seen from table 5-2 where data shows an increase in fluorescence from 50 to 100 laser shots. An increase in fluorescence in the exposed regions of PMMA films containing C4TIPS cannot be explained in the same manner as for C4, since fluorescence of C4TIPS does not increase by simply destroying the aggregates. It is also possible that photolysis of C4TIPS may have a contribution to the increase in fluorescence in the exposed regions.

Table 5-2. Contribution of blue in the exposed and unexposed regions for PMMA films containing C4 and C4TIPS (5.0 wt % based on PMMA weight) exposed to laser radiation at 157 nm, figure 5-8. The incident energy was 1.9 mJ/ cm^2/ shot, delivered with a frequency of 2 shots/ s.

PMMA Blue	C4		C4TIPS	
	50 shots 95 mJ/ cm^2	**100 shots 190 mJ/ cm^2**	**50 shots 95 mJ/ cm^2**	**100 shots 190 mJ/ cm^2**
Exposed	22400	23100	8500	10800
Unexposed	7200	11900	4400	4400
Exp/ Unexp	3.1	1.95	1.94	2.47

In the case of FP films containing C4TIPS and exposed to radiation at 157 nm, the data from table 5-3 clearly shows an increase in blue with the incident dose. As expected, the increase is higher compared to PMMA films containing C4TIPS, figure 5-9. The ratio I_{exp}/ I_{unexp} from table 5-3 more than doubles from 20 to 50 shots, while from 50 to 100 laser shots it increases by 1.2 times, showing that at higher doses a plateau is reached. This is explained by the fact that C4TIPS is deprotected by the *in situ* formed HF. Since the amount of HF is a function of the

incident light dose, the intensity of fluorescence also depends on the incident dose for FP films. These control experiments with PMMA clearly show that C4TIPS works as an HF sensor.

Table 5-3. Contribution of blue in the exposed and unexposed regions of FP films containing C4TIPS (5.0 % wt based on dry FP weight) and exposed to laser radiation at 157 nm, 38.0 mJ/ cm^2, 95 mJ/ cm^2, and 190 mJ/ cm^2 respectively. The energy was 1.9 mJ/ cm^2/ shot, delivered with a frequency of 2 shots/ s.

PFP Blue	C4TIPS		
	20 shots 38 mJ/ cm^2	**50 shots 95 mJ/ cm^2**	**100 shots 190 mJ/ cm^2**
Exposed	11800	31400	51100
Unexposed	8000	9500	12600
I_{Exp}/ I_{Unexp}	1.48	3.30	4.06

Since the rate constant for electron scavenging is two orders of magnitude higher for hexafluoro-2-propanol (HFP) compared to the ester unit, it is expected that the HFP traps the electron ejected from the nonfluorinated moieties of the molecule, releasing fluoride. The $-CF_2-CF_2-$ unit from the main chain is also expected to trap the ejected electrons and release fluoride. In the non-fluorinated moieties of the polymer, following photoejection, a proton is eliminated, which together with the fluoride anion leads to a non-concerted formation of HF.[25]

AFM experiments show film loss and formation of LIPS upon exposure at 157 nm. Ablation and LIPS observed in the AFM images, figures 5-10 and 5-11, have been reported previously by others too. [17, 32-34] The nature of the processes induced by photons from the laser radiation has been a controversial one. Some scientists suggest photochemical reactions, while other propose that photothermal reactions are responsible for the etching and ablative damage of polymers exposed to laser

radiation of different wavelengths. [35,36] From the AFM images one can notice a larger film loss for FP films containing C6 compared to films of pure polymer. This is expected since C6 has a much higher absorbance at 157 nm compared to FP and it acts as a dopant for photoablation of the polymer.

5.4 Experimental

Polymers FP and PMSSQ were a gift from Rohm & Haas Electronic Materials (Marlborough, Massachusetts) and used as received. 3-(2-Benzothiazolyl)-7-(diethylamino) coumarin (Coumarin 6) 98 %, 7-hydroxy-4-methylcoumarin (Coumarin 4) 97 %, 2-heptanone 99 %, and ethyl cellulose (EC) 48 % ethoxyl content, 100 cP, were purchased from Aldrich and used as received. PMMA, MW ~ 1 x 10^6, M_w/M_n = 1.10 was purchased from Polysciences Inc., and used as received. C4TIPS was obtained by reacting C4 with triisopropylchloride (TIPSCl, 97 %) and imidazole (99%) in *N, N*-dimethylformamide (DMF). DMF, imidazole and TIPSCl were also purchased from Aldrich. The acetonitrile (Omnisolv) used to record fluorescence of C4 and C4TIPS was from EM Sciences.

The polymer films were obtained by spin coating the solutions of polymers using a spin coater from Specialty Coating Systems, Inc. The thickness of the films was measured with a thin film analyzer TFA-11 from Luzchem Research.

Exposure of the films to laser radiation was done using a GSI-Lumonics fluorine excimer laser (12-15 ns fwhm). The composition of the gas mixture was F_2 0.09 %, the rest up to 100 % being He. The Pressure of the gas mixture was 2950 mbar. The area of the beam was ~ 2 cm^2 and the energy was measured with a Molectron JD2000 joulemeter radiometer and a Coherent J45LP-MB photon detector. For exposure the films were placed in a chamber under nitrogen atmosphere. The hexagonal patterns were obtained by placing a copper mask with hexagonal holes on top of the films, which was removed prior to recording the fluorescence images with the fluorescence microscope. The distance between the centers of two consecutive hexagons was 60 μm.

The fluorescence of C4 and C4TIPS solutions was recorded with a PTI spectrofluorimeter from Photon Technology International, using a 1 cm x 1 cm quartz cuvette. The emission of C6 and $C6H^+$ in films was recorded using a Perkin

Elmer LS 50 luminescence spectrometer. Fluorescence images were recorded using a Leica DMLS fluorescence microscope with a 20 x objective. The lamp used was a 50 W Hg lamp and the camera was a Leica DFC300 FX. The software used was Leica IM50 version 4.0 release 117 from Leica Microsystems Imaging Solutions Ltd. The filter cubes used to monitor emission from C6 and $C6H^+$ were E4 (excitation centered at ~ 436 nm, emission long pass 470 nm) and M2 (excitation centered at 546 nm, emission long pass 590 nm) from Leica. Emission of C4 was monitored using the XF02-2 filter cube (excitation centered at ~ 330 nm, emission long pass 470 nm) from Omega Opticals.

Atomic Force Microscopy (AFM) experiments were carried out with a Multimode Nanoscope III atomic force microscope (Digital Instruments, Santa Barbara, CA) at National Research Council facilities on Sussex Road in Ottawa. Silicon nitride tips (spring constant 60 mN/ m) were used for the measurements.

For laser flash photolysis experiments performed by M. Laferrière, the radiation source was either a 266 nm –the fourth harmonic of a Nd:YAG laser (Surelite), or a 308 nm from a Lumonics Excimer-500 laser with pulse duration around 7 – 10 ns; a similar system was described in an earlier publication.[37]

Readings of red, green, and blue from the fluorescence images were done with the application DigitalColor Meter version 3.2 from Apple Computer Inc. reading the RGB as actual value, 16-bit image. This application displays the color value (arbitrary units) of any pixel from the computer screen. It quantifies the contribution of the three basic colors (red, green, and blue) to that pixel.

5.5 References

(1) Ronse, K.; Bisschop, P. D.; Goethals, A. M.; Hermans, J.; Jonckhreere, R.; Light, S.; Okoroanyanwu, U.; Watso, R.; McAfferty, D.; Ivaldi, J.; Oneil, T.; Sewell, H. "Status and critical challenges for 157-nm lithography", *Microelectronic Eng.* **2004**, *73-74*, 5-10.

(2) Itani, T.; Toshifumi, S.; Wakamiya, W. "Total solution in 157 nm lithography for below 65 nm node semiconductor devices", *Microelectronic Eng.* **2004**, *73-74*, 11-15.

(3) Wallraff, G. M.; Hinsberg, W. D. "Lithographic Imaging Techniques for the Formation of Nanoscopic Features", *Chem. Rev.* **1999**, *99*, 1801-1821.

(4) Ivan, M. "Optical Projection Lithography - Enabling Nanolithography", *L'Actualite Chimique Canadienne Canadian Chemical News* **2005**, *57*, 16.

(5) Moore, G. E. "Cramming more components onto integrated circuits", *Electronics* **1965**, *38*.

(6) Ito, H.; Wilson, C. G.; Frechet, J. M. J. "Résines pour UV lointain mettant en oeuvre un mé chanisme d'amplification chimique. Sensitive deep UV resist incorporating chemical amplification", *VLSI Technol.* **1982**, *260*, 262.

(7) Ito, H. "Chemical amplification resists: History and development within IBM", *IBM J. Res. Develop.* **2000**, *44*, 119-130.

(8) Burnett, J.; Levine, Z. H.; Shirley, E. L. "Intrinsic birefringence in calcium fluoride and barium fluoride", *Phys. Rev. B* **2001**, *64*, 241102-241101 - 241102-241104.

(9) Lin, B. J. "The 157-nm Good/ Bad News from Intel", *J. Microlith. Microfab. Microsyst.* **2003**, *2*, 165-166.

(10) Bellas, V.; Tegou, E.; Raptis, I.; Gogolides, E.; Argitis, P.; Iatrou, H.; Hadjichristidis, N.; Sarantopoulou, E.; Cefalas, A. C. "Evaluation of siloxane and polyhedral silsesquioxane copolymers for 157 nm lithography", *J. Vac. Sci. Tech. B* **2002**, *20*, 2902-2908.

(11) Tegou, E.; Bellas, V.; Gogolides, E.; Argitis, P.; Eon, D.; Cartry, G.; Cardinaud, C. "Polyhedral Oligomeric Silsesquioxane (POSS) Based Resists: Materials Design Challenges and Lithographic Evaluation at 157 nm", *Chem. Mater.* **2004**, *16*, 2567-2577.

(12) Rotschild, M.; Bloomstein, T. M.; Fedynyshyn, T. H.; Liberman, V.; Mowers, W.; Sinta, R.; Switkes, M.; Grenville, A.; Orvek, K. "Fluorine - An enabler in advanced photolithography", *J. Fluorine Chem.* **2003**, *122*, 3-10.

(13) Toriumi, M.; Ishikawa, T.; Kodani, T.; Hkoh, M.; Moryia, T.; Yamashita, T.; Araki, T.; Aoyama, H.; Yamazaki, T.; Furukawa, T.; Itani, T. "Fluoropolymers for 157 nm single-layer resists", *J. Vac. Sci. Tech. B* **2004**, *22*, 27-30.

(14) Fedynyshyn, T. H.; Kunz, R. R.; Sinta, R. F.; Goodman, R. B.; Doran, S. P. "Polymer photochemistry at advanced optical wavelengths", *J. Vac. Sci. Technol. B* **2004**, *18*, 3332.

(15) Shirai, M.; Shinozuka, T.; Tsunooka, M.; Itani, T. "Vacuum Ultraviolet (VUV)-Light-Induced Outgassing from Resist Polymers: A Study Using in Stiu Quartz Crystal Microbalance (QCM) Technique", *Jpn. J. Appl. Phys.* **2003**, *42*, 3900-39004.

(16) Vasilets, V. N.; Hirata, I.; Iwata, H.; Ikada, Y. "Photolysis of a Fluorinated Polymer Films by Vacuum Ultraviolet Radiation", *J. Pol. Sci. A: Pol. Chem.* **1998**, *36*, 2215-2222.

(17) Costela, A.; Garcia-Moreno, I.; Florido, F.; Figuera, J. M.; Sastre, R.; Hooker, S. M.; Cashmore, J. S.; Webb, C. E. "Laser ablation of polymeric materials at 157 nm", *J. Appl. Phys.* **1995**, *77*, 2343-2350.

(18) Yatsuhashi, T.; Nakashima, N. "VUV Laser Chemistry - Formation of Hot Molecules and Their Reactions in the Gas Phase", *Bull. Chem. Soc. Jpn.* **2001**, *74*, 579-593.

(19) Lee, K.; Jockusch, S.; Turro, N. J.; French, R. H.; Wheland, R. C.; Lemon, M. F.; Braun, A. M.; Widerschpan, T.; Dixon, D. A.; Li, J.; Ivan, M.; Zimmerman, P. "157 nm Pellicles (Thin Films) for Photolithography: Mechanistic

Investigations on the VUV and UV-C Photolysis of Fluorocarbons", *J. Am. Chem. Soc.* **2005**, *127*, 8320.

(20) Coenjarts, C.; Cameron, J. F.; Pohlers, G.; Scaiano, J. C.; Zampini, A. "An *in situ* Method for Measuring Acid Loss from Polymer Films", *J. Appl. Polym. Sci.* **2000**, *78*, 1897.

(21) Reynolds, G. A.; Drexhage, K. H. "New Coumarin Dyes with Rigidized Structure for Flashlamp-pumped Lasers", *Opt. Comm.* **1975**, *13*, 222.

(22) Frenette, M.; Ivan, M. G.; Scaiano, J. C. "Use of fluorescent probes to determine catalytic chain length in chemically amplified resists", *Can. J. Chem.* **2005**, *83*, 869-874.

(23) Scaiano, J. C.; Laferriere, M.; Ivan, M. G.; Taylor, G. N. "A Protocol for the Verification of Acid Generation in 157 nm Photolithography", *Macromol.* **2003**, *36*, 6692-6694.

(24) Ray, K.; Mason, M. D.; Grober, R. D.; Pohlers, G.; Staford, C.; Cameron, J. F. "Quantum Yield of Photoacid Generation in 193 nm Chemically Amplified Resists by Fluorescence Imaging Spectroscopy", *Chem. Mater.* **2004**, *16*, 5726-5730.

(25) Ivan, M. G.; Laferriere, M.; Sanrame, C. N.; Scaiano, J. C. "On the Question of Acid Generation upon 157-nm Laser Exposure of Fluorinated Polymers", *Chem. Mater.* **2006**, *18*, 2635-2641.

(26) Dentinger, P. "Outgassing of photoresists materials at extreme ultraviolet wavelengths", *J. Vac. Sci. Technol. B* **2000**, *18*, 3364-3370.

(27) Irie, S.; Fuji, K.; Itakura, Y.; Kawasa, Y.; Egawa, K.; Uchino, I.; Sumitani, A.; Itani, T. "Evaluation of outgassing from a fluorinated resist for 157 nm lithography", *Adv. Res. Technol. Process., Proceed. SPIE* **2004**, *5376*, 226-237.

(28) Matsui, Y.; Umeda, S.; Matsui, S.; Seki, S.; Tagawa, S.; Ishikawa, S.; Itani, T. "Dependence of outgassing characters and total amount of outgassed species at 157 nm exposure on the structures of resist base polymer", *Adv. Res. Technol. Process., Proceed. SPIE* **2003**, *5039*, 121-128.

(29) Irie, S.; Hagiwara, T.; Fuji, K.; Itakura, Y.; Kawasa, Y.; Egawa, K.; Uchino, I.; Sumitani, A.; Itani, T. "Evaluation of outgassing from a fluorinated polymer for 157 nm lithography", *J. Vac. Sci. Tech. B* **2004**, *22*, 3513-3517.

(30) Garza, C. M.; Bierschenk, T. "Degradation mechanism and materials for 157 nm pellicles", *Optical Microlithography XVII, Proc. SPIE* **2004**, *5377*, 527-536.

(31) Schulman, S. G.; Rosenberg, L. S. "Tautomerization Kinetics of 7-Hydroxy-4-methylcoumarin in the Lowest Excited Singlet State", *J. Phys. Chem.* **1979**, *83*, 447.

(32) Lippert, T.; Dickinson, J. T. "Chemical and Spectroscopic Aspects of Polymer Ablation: Special Features and Novel Directions", *Chem. Rev.* **2003**, *103*, 453.

(33) Lu, X.; Lu, Q.; Zhu, Z. K.; Yin, J.; Wang, Z. G. "Laser-induced periodic surface structures on polyimide doped with lecithin", *Mater. Lett.* **2003**, *57*, 3636.

(34) Csete, M.; Marti, O.; Bor, Z. "Laser-induced periodic surface structures on different polycarbonate films", *Appl. Phys. A: Mater. Sci. Proc.* **1998**, *73*, 521.

(35) Brannon, J. H.; Lankard, J. R.; Baise, A. I.; Burns, F.; Kaufman, J. "Excimer laser etching of polyimide", *J. Appl. Phys.* **1985**, *58*, 2036-2042.

(36) Srinivasan, R.; Braren, B.; Dreyfus, R. W. "Ultraviolet laser ablation of polyimide films", *J. Appl. Phys.* **1987**, *61*, 372-376.

(37) Scaiano, J. C. "Solvent Effects in the Photochemistry of Xanthone", *J. Am. Chem. Soc.* **1980**, *102*, 7747.

Photoinduced Assembly of Pyrene in Films

6. Photoinduced Assembly of Pyrene in Polymer Films

6.1 Introduction

Pyrene, benzophenone, and ruthenium trisbipyridyl are probably three of the most studied molecules in photochemistry. An interesting property of polyaromatic condensed hydrocarbons, and in particular of pyrene, is their ability of forming dimers in excited state, called excimers. In solution, at concentration of ~ 3.0 mM or higher, pyrene can form excimers upon irradiation with light of a suitable wavelength. The ideal distance between the excited pyrene – donor (D) and the ground state molecule – acceptor (A) that allows the two molecules to form an excimer is 3.5 Å, scheme 1.[1] The emission of pyrene monomer and excimer has been studied in liquid solutions and in crystals, as well as in polymer films. Excited singlet pyrene can decay through radiative and radiationless processes, intersystem cross to triplet state, or form excimers.[1,2]

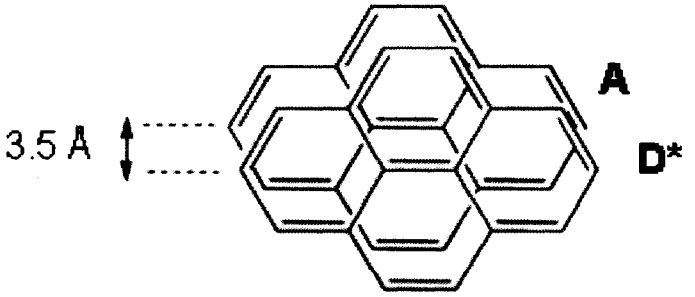

Scheme 6-1. Pyrene excimer structure: A – acceptor, pyrene molecule in ground state, D* - donor, excited pyrene molecule

The binding energy in an excimer is 9.4 kcal mol^{-1}, while the repulsion energy of the two monomers in ground state is 7.65 kcal mol^{-1}.[1] Thus the two pyrene molecules are in the sandwiched like arrangement only in excited state, once the energy was released as light or heat, they fall apart. The reported fluorescence lifetime of the monomer is ~ 400 ns, while the excimer lifetime is ~ 50 ns.[3]

Depending on the concentration of pyrene in films, emission from the monomer, excimer or aggregates has been observed.[4-11] Due to its sensitivity to the surrounding medium, pyrene has been used as fluorescent probe in different environments such as thin polymer films[5,6,10-14], Langmuir-Blodget films[15-17], clays[18,19], zeolites[20] and micelles[21,22]. Recently, pyrene nanostructures in the shape of nanorods have been synthesized in micellar environment (sodium dodecyl sulphate - SDS) and their optical properties studied.[23]

Pyrene has been used as fluorescent probe to monitor kinetics, phase transitions, mobility, and polarity in polymers, either as a physical mixture[14,24-26] or chemically attached to polymer chains[13]. Most studies on pyrene emission in polymers have been concerned with the influence of pyrene concentration on emission. At lower loadings emission from the monomer is observed, while at high loadings a structureless emission spectrum shifted to red, characteristic to the excimer or aggregates is recorded.[4,7,8,11] In thin films aggregation occurs differently at the interface between the films and substrate, compared to aggregation in film.[7]

Laser induced ablation of polymers, and in particular of poly(methyl methacrylate) (PMMA), has been extensively studied at different wavelengths, especially in UV region.[27,28] Applications of PMMA laser induced ablation in lithography have been previously reported, especially at 248 nm and at 308 nm using dopants.[29-32] Laser induced ablation is comprised by two processes: absorption of photons and release of the photon's energy through photochemical or photophysical processes. The result is a change in structure and morphology of the polymer. The most important condition for a polymer to be ablated is to absorb at

that wavelength. Polymers that do not absorb at the irradiation wavelength are doped with compounds that absorb and that ideally do not decompose during irradiation. Condensed polyaromatic hydrocarbons were extensively used as dopants for photoinduced ablation of polymer films.[29,30,33,34]

The work done in this chapter is concerned with photo-induced formation of pyrene excimers or pyrene aggregates in polymer films containing pyrene, and exposed to laser radiation at 157 nm, 248 nm, and 308 nm. Previous reports on laser ablation of polymer films doped with pyrene were concerned with the transformations and chemical processes that occur in the polymer or on the surface, with the depth of ablation as a function of incident dose, frequency of shots or wavelength of the radiation used.[27,31,33] Fluorescence spectroscopy, absorbance and fluorescence microscopy were the techniques used in the present study to monitor the behavior of pyrene rather than that of the polymer. Furthermore, polymer changes may be inferred from the observations on pyrene behavior.

Fluorescence microscopy was largely used to discriminate between the exposed and unexposed regions of a polymer film containing pyrene due to its higher sensitivity compared to absorbance spectroscopy. Some of the fluorescence images show formation of laser induced periodic structures (LIPS), already discussed in chapter 5 and reported by others before.[35-37]

The results obtained show excimer formation or aggregation of pyrene in the exposed regions. There are differences between polymers and different wavelengths used as it can be seen from the results part of this chapter. The origins of these differences and the results are interpreted and explained further in the discussion section.

6.2 Results

6.2.1 Spectroscopic data in solution

Although most of the work from this chapter involves experiments done in thin polymer films, the emission properties of pyrene in solution will be presented first. Emission spectra of pyrene in solutions using 2-heptanone as solvent and containing a fluorinated terpolymer, FP (XP0921 is the commercial name of the fluorinated polymer) (20 weight %) were recorded, exciting at 345 nm, figure 6.1.

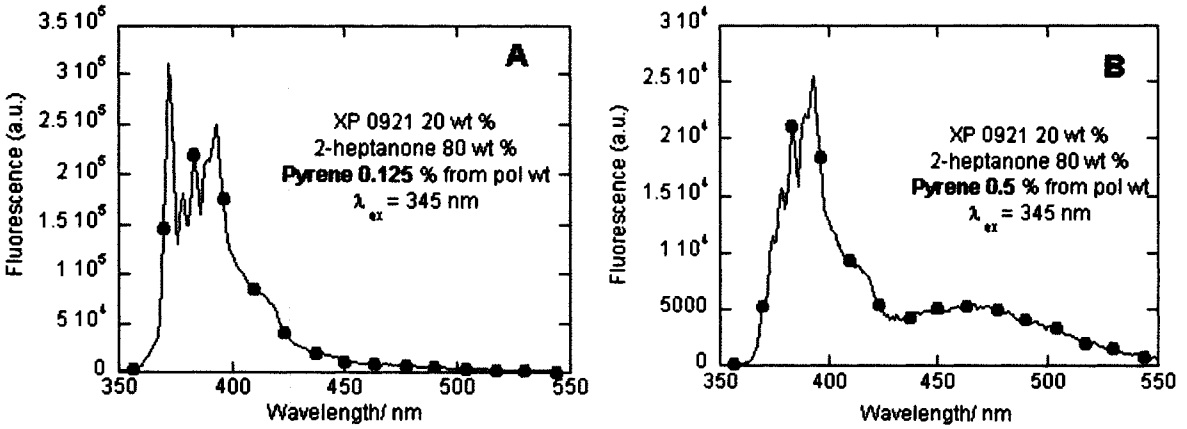

Figure 6.1 Fluorescence spectra (λ_{ex} = 345 nm) of two solutions containing 2-heptanone (80 % weight) as solvent, FP (20 % weight), pyrene 0.125 % wt (A) and 0.5 % wt (B) based on polymer weight. The actual molar concentrations of pyrene in the two solutions were 1.13 x 10^{-3} M (A), and 4.50 x 10^{-3} M (B) respectively. The spectra were recorded with a rectangular, 1.0 cm x 1.0 cm quartz cell.

The ratio of vibronic bands in the emission spectrum of the monomer is sensitive to the polarity of the environment and to the concentration of pyrene in

solution.[4,21] The highest intensity of the pyrene monomer emission in the solutions containing 2-heptanone as solvent (80 weight %) and FP (20 weight %) was obtained with an excitation wavelength of 345 nm. The solutions used in these measurements were the same used later for experiments in thin polymer films obtained by spin coating. The amount of pyrene added to the solution is expressed as percentage based on the dry polymer weight, this being the usual way the lithography industry expresses concentrations and amounts of different reactants present in the photoresist solution. The measured density of a solution containing 80 weight % 2-heptanone, 20 weight % dry PFP and 0.5 weight % pyrene from the dry polymer weight is 0.910 g/ mL, measured at room temperature and averaged over six measurements. Thus, the molar concentration of pyrene in the above solution used to record the emission spectrum in figure 6.1 (B) was 4.50×10^{-3} M (0.5 % pyrene based on FP weight), while in the solution used to record the fluorescence spectrum in figure 6.1 (A) pyrene was 1.13×10^{-3} M (0.125 % based on FP weight). The density of 2-heptanone is 0.815 g/ mL, which means that the density of FP is 1.3 g/ mL.

It is interesting to notice the changes in emission intensity in the two plots. Although in figure 6.1 (A) the concentration of pyrene is four times lower compared to the case in figure 6.1 (B), the intensity of bands III and IV from the monomer fluorescence is ten times higher. Emission characteristic to the excimer, centered at ~ 470 nm is noticeable in figure 6.1 (B). However, the intensity of emission at 470 nm is 1.54 times higher in figure 6.1 (A) compared to 6.1 (B), even though the concentration of pyrene is four times lower and the emission peak characteristic to the excimer is not defined, being covered by the stronger emission of the monomer.. The decrease in emission of both the monomer and the excimer may be the effect of an "inner filter effect", where light emitted by excited pyrene molecules is absorbed by those in ground state. This is probably why the (0,0) band in the emission in figure 6-1 B does not appear in the spectrum recorded. The

experiments were done using a rectangular quartz cuvette with 1.0 cm optical path. The thin polymer films obtained by spin coating the above mentioned solution have a thickness between 400 – 950 nm, approximately five orders of magnitude smaller than the optical path in the quartz cuvette. Thus it is reasonable to assume that the "inner filter effect" will not affect the emission in thin polymer films.

6.2.2 Results in polymer films

For the polymer films we used three different polymers: poly(methyl methacrylate) (PMMA), a fluorinated terpolymer (FP) especially designed by DuPont for photolithography at 157 nm, and polymethylsilsesquioxane (PMSSQ). The structures of the polymers are shown in figure 6.2.

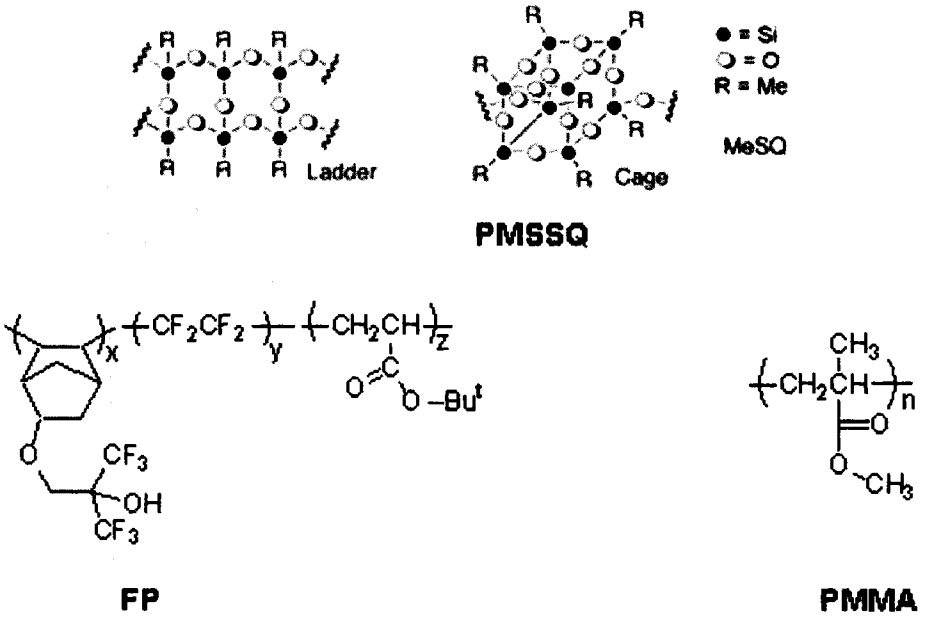

Figure 6-2 Structures of polymers used in this study: polymethylsilsesquioxane (PMSSQ), fluorinated terpolymer (FP), and poly(methyl methacrylate) (PMMA)

The choice of polymers was determined by their different glass transition temperatures (Tg). The decreasing order of Tg in bulk is: Tg PFP > Tg PMMA > Tg PMSSQ. However, upon addition of dopants (small molecules) the Tg of the polymers decreases; the Tg decreases also when the polymer is spin coated in thin

films, so in the case of the pyrene-containing thin polymer films these two factors add, leading to a lower Tg than in bulk.[38] However, we were not able to measure the Tg of the polymer films. For the FP in bulk, the Thermogravimetric Analysis (TGA) and the Differential Scanning Calorimetry (DSC) analysis reveal a Tg of 216 °C, figure 6-3. The sample analyzed weighed 12.76 mg, the heating rate was 20 °C/ minute (from room temperature to 1000 °C), with an air flow of 100.0 mL/ minute. The Tg for PMMA is 104 – 105 °C in bulk, but it differs in thin films and brushes,[38] while that of PMSSQ is situated below room temperature, as observed during the experiments. The stock PMSSQ was stored inside a fridge (4 °C) before the solutions were prepared. When left for a longer period at room temperature (RT), PMSSQ pellets become liquid with a relatively low viscosity.

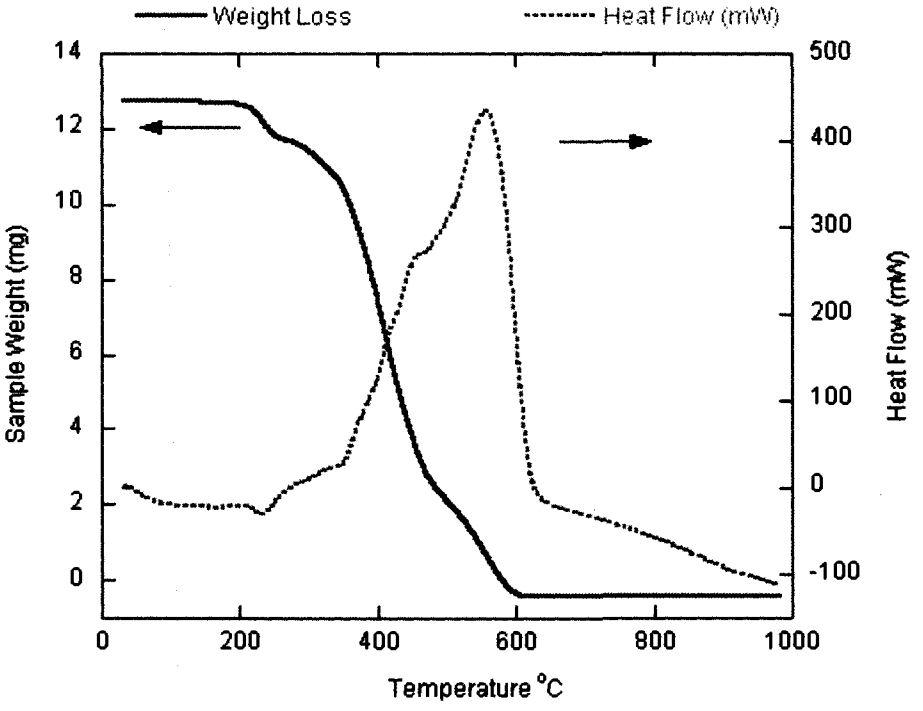

Figure 6-3. Thermogravimetric analysis (TGA – continuous line), and differential scanning calorimetry (DSC - dashed line) curves for a probe of 12.76 mg FP, obtained under air flow (100.0 mL/ min), with a heating rate of 20 °C/ minute. The left y axis represents the weight loss of the sample as a function of temperature, while the right y axis represents the

amount of energy (heat), expressed in mW, delivered to the sample, so that it would have the temperature shown on the x axis (exo up).

The absorption spectra of thin polymer films of PMMA, FP, and PMSSQ are shown in figure 6-4. The thickness of the films were 930 nm for PMMA, 441 nm for FP, and 476 nm for PMSSQ.

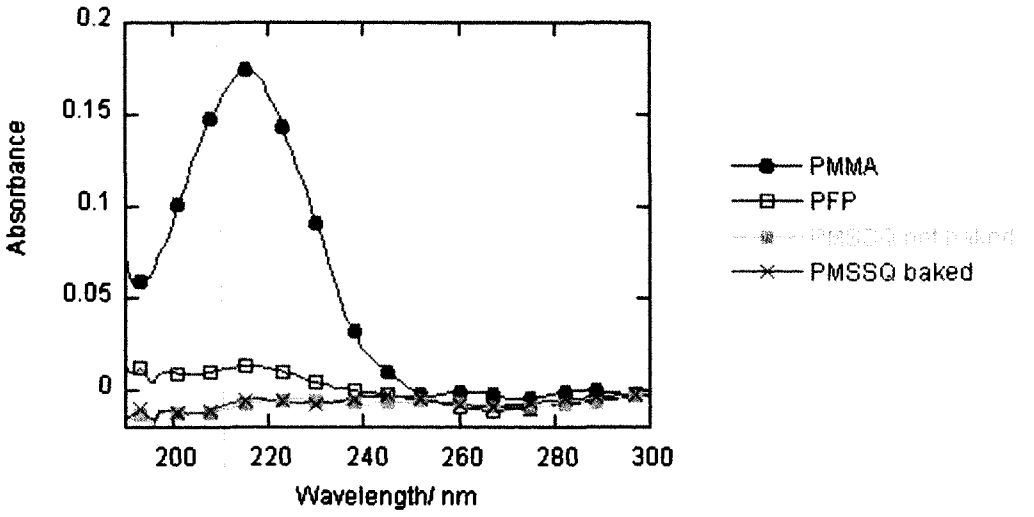

Figure 6-4. Absorbance of thin polymer films of PMMA (●), FP (□), PMSSQ (x) and PMSSQ not baked after coating (■). The thickness of the films spin coated on top of one inch quartz discs were: 930 nm for PMMA, 441 nm for FP, and 476 nm for PMSSQ. The baseline was the bare quartz disc.

6.2.3 Spectroscopy and microscopy in high Tg polymers

Films of PMMA containing 0.33 weight % pyrene based on the dry polymer, and of FP containing 0.5 weight % pyrene based on the dry polymer weight were

exposed to laser radiation at 157, 248, and 308 nm. Films were also exposed to continuous wavelength (CW) radiation from the HTG exposure unit at 254 nm.

The density of a solution containing 85 wt % 2-heptanone and 15 wt % PMMA is 0.85 g/ mL, as measured with the analytical balance for volumes of 1.0 mL of solution at RT. Thus, the concentration of pyrene in a solution containing 15 wt % PMMA, 85 wt % 2-heptanone and 0.33 wt % pyrene based on PMMA weight is 2.1×10^{-3} M. Based on the density of the solvent 2-heptanone (0.815 g/ mL), the density of the final solution and the % weight, the calculated density of the PMMA is 1.05 g/ mL. The absorbance and emission spectra of pyrene in PMMA films, obtained by spin-coating a few drops of solution on top of a one-inch quartz disc, are shown in figure 6.5. The disc was spin coated at 2000 rpm (rotations per minute) for 20 s, then baked inside an oven on a hot plate at 96 °C for 60 s, followed by fast cooling to room temperature on a metallic surface. The fluorescence spectrum was recorded at room temperature using an excitation wavelength of 330 nm.

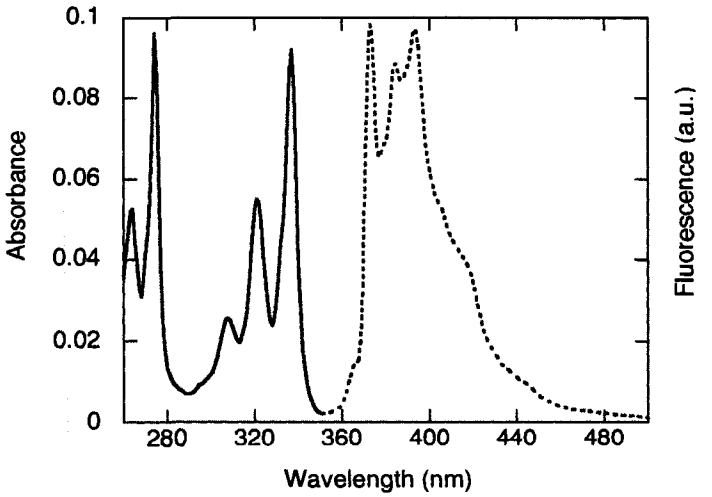

Figure 6-5. Absorption (continuous line) and fluorescence (dashed line) of a PMMA film (~ 930 nm thick) containing 0.33 weight % pyrene based on polymer weight; the excitation

wavelength was 330 nm. The concentration of pyrene in the stock solution that was spin coated is 2.1 x 10^{-3} M.

Absorption and fluorescence were recorded before and after exposure to 157 nm laser radiation. Solutions containing 0.125 weight % pyrene from dry FP weight were spin coated and absorbance and emission spectra were recorded before and after exposure to different energy doses of radiation at 157 nm (figure 6.6). The incident radiation was delivered with a pulsed laser (12 – 15 ns pulse duration) at a repetition rate of 3 shots/ s, with an incident energy of 1.7 – 1.8 mJ/ cm^2/ shot. From the absorption spectra (figure 6-6 A) one can notice absorbance peaks centered on 270 and 330 nm. Fluorescence spectra were recorded using these two wavelengths for excitation (figure 6-6 C and D). Since in both cases emission showed a maximum around 393 nm, an excitation spectrum (figure 6-6 B) was recorded too, in an attempt to determine which one was the suitable wavelength for excitation. Whereas in the case of fluorescence recorded in solution the highest intensity of fluorescence characteristic to the monomer was obtained by exciting at 345 nm, in polymer films the highest intensity was obtained by exciting at 270 nm and 330 nm. Excitation at 270 nm in solution was not possible due to the high absorbance of the solution at that wavelength. Attempts to measure the absorbance of pyrene in the solutions used for fluorescence were unsuccessful, the absorbance in 1 cm optical path cells being too high.

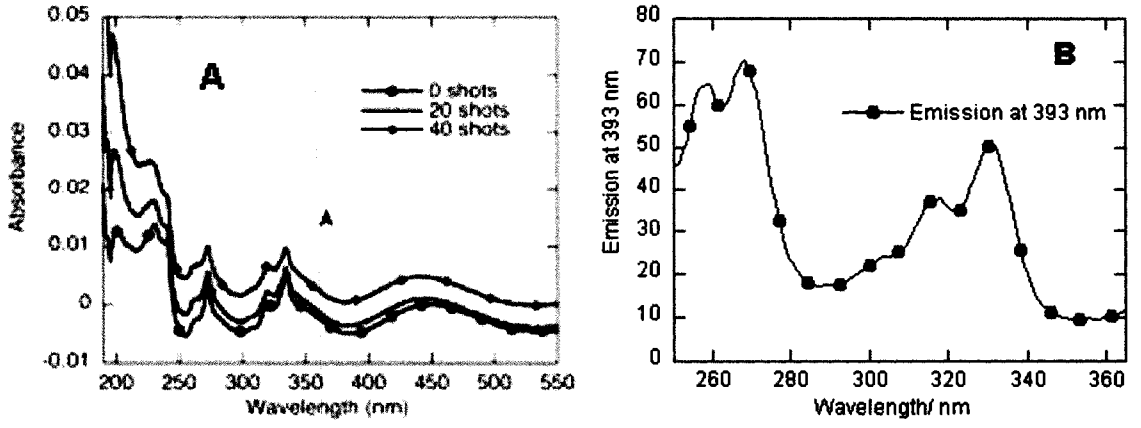

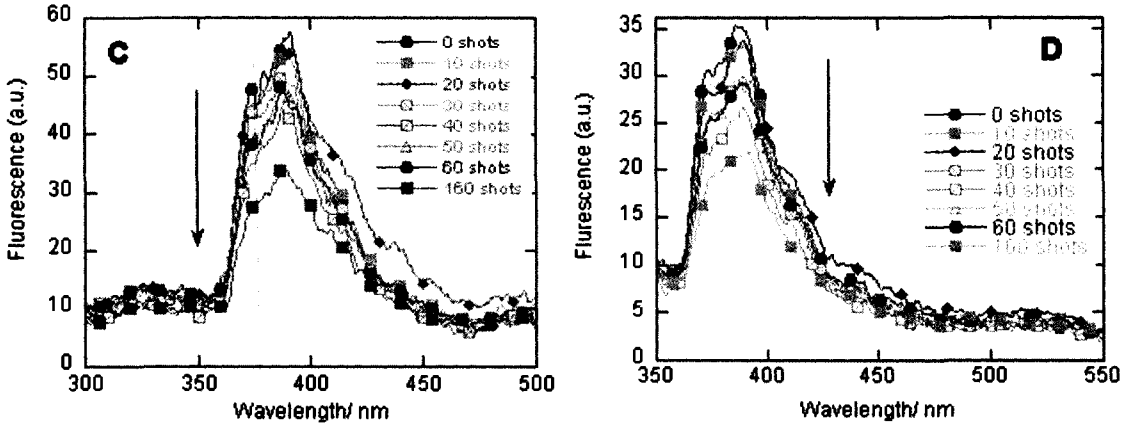

Figure 6-6. Absorption (A), excitation (B), fluorescence, λ_{exc}= 270 nm (C) and fluorescence λ_{exc}= 330 nm (D) spectra of pyrene (0.125 weight % based on FP weight) in FP films. The incident energy was 1.7 – 1.8 mJ/ cm^2/ shot, frequency 3 shots/ s.

Due to the low absorbance of the films, the loading of pyrene was increased to 0.5 weight % in order to get a better signal-to-noise ratio in absorbance and fluorescence spectra. Using the same procedure reported above, FP films containing 0.5 weight % pyrene based on FP weight were prepared and exposed to radiation at 157 nm, followed by monitoring of absorbance and fluorescence changes. The spectra recorded are shown in figure 6-7.

6.2.4 Effect of rate of energy delivery

Influence of the way the energy was delivered (number of shots/ s) was studied by exposing different films to the same number of shots, 200, but at different repetition rates: 1, 2, 5, 8, 10, 12, 15, and 20 shots/ s. The energy incident to the film surface was 2.4 – 2.5 mJ/ cm^2/ shot. For exemplification, two plots, showing fluorescence before and after exposure, will be shown. In the first case, the

repetition rate was 5 shots/ s and in the second example the frequency was 20 shots/ s, figure 6-7 A and B.

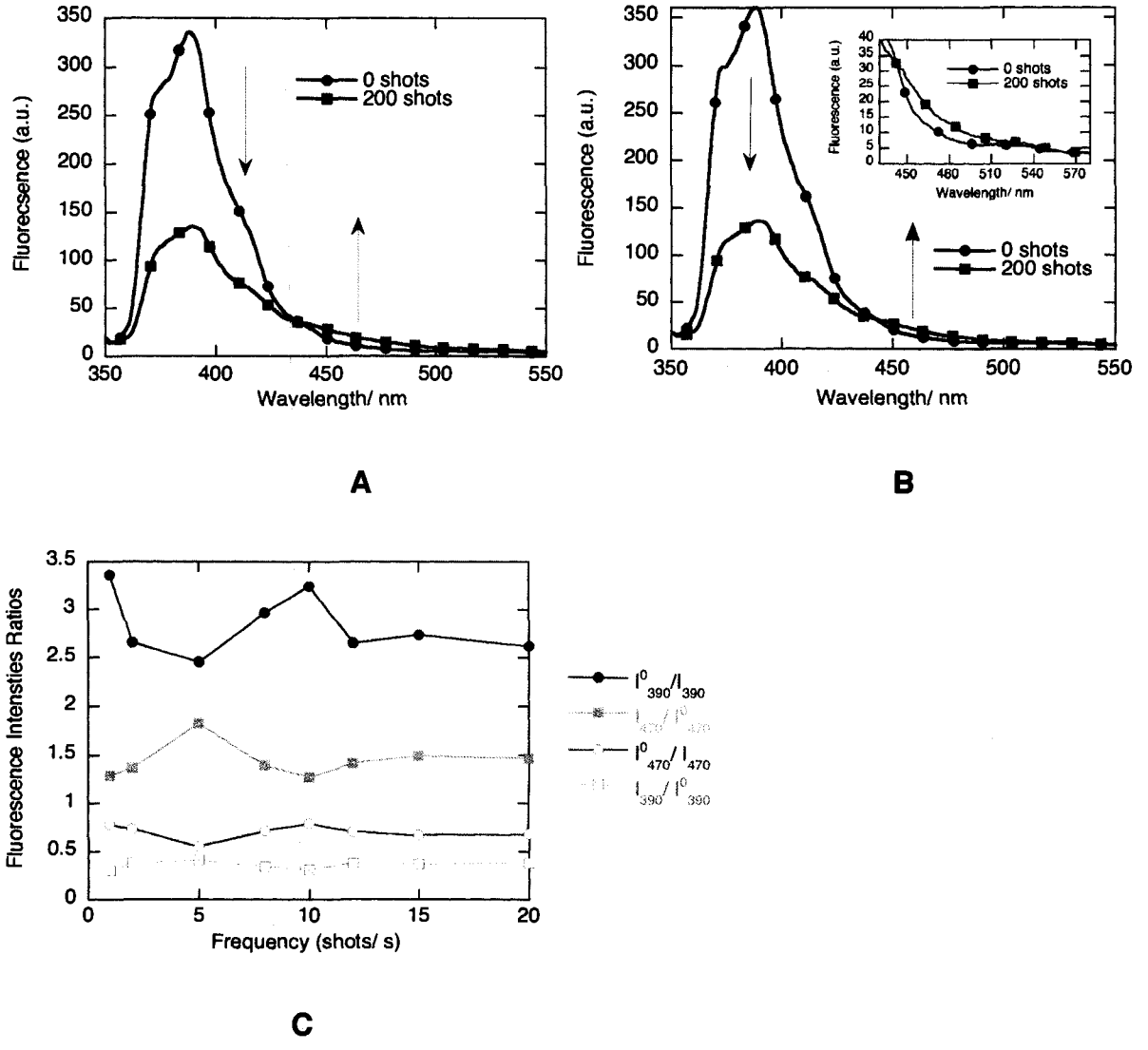

Figure 6-7. Fluorescence intensity of pyrene (0.5 wt % based on FP weight) in FP films (~440 nm thick) after exposure to 200 shots (480 – 500 mJ/ cm^2) at 157 nm, as a function of the frequency of shots; 5 shots/ s (A); 20 shots/ s with the inset showing the region characteristic to excimer emission (B); ratios of fluorescence intensities I^0_{390}/ I_{390}, I^0_{470}/ I_{470}, I_{390}/ I^0_{390}, and I_{470}/ I^0_{470} (C). The wavelengths selected in graph C represent the maximum emission of the monomer (390 nm) and of the excimer (470 nm) before (I_0) and after (I) exposure to laser radiation.

The fluorescence intensity of the monomer at 390 nm decreases approximately 3 times, while the intensity at 470 nm, characteristic to the excimer, increases 1.5 times compared to the unexposed film. Excessive exposure leads to complete quenching of the monomer's fluorescence, figure 6-8. The films were prepared by spin coating on 1-inch quartz discs at 2000 rpm, for 20 s, a solution containing 2-heptanone (80 weight %), FP (20 weight %) and pyrene (0.5 % based on polymer weight). After spin coating, the film was dried in an oven at 90 °C for 60 s. The exposure was done at 157 nm, with a frequency of 15 shots/ s, the energy being 1.7 – 1.8 mJ/ cm^2/ shot. After 400 shots (680 – 720 mJ/ cm^2) the fluorescence characteristic to pyrene excimer decreases as the incident energy dose increases further. This proves that there is a threshold value above which the excimer emission does not grow anymore. The intensity of the monomer emission, on the other hand, decreases faster at the beginning, the decrease being slower after 800 shots. The causes for this behavior will be discussed further in the chapter.

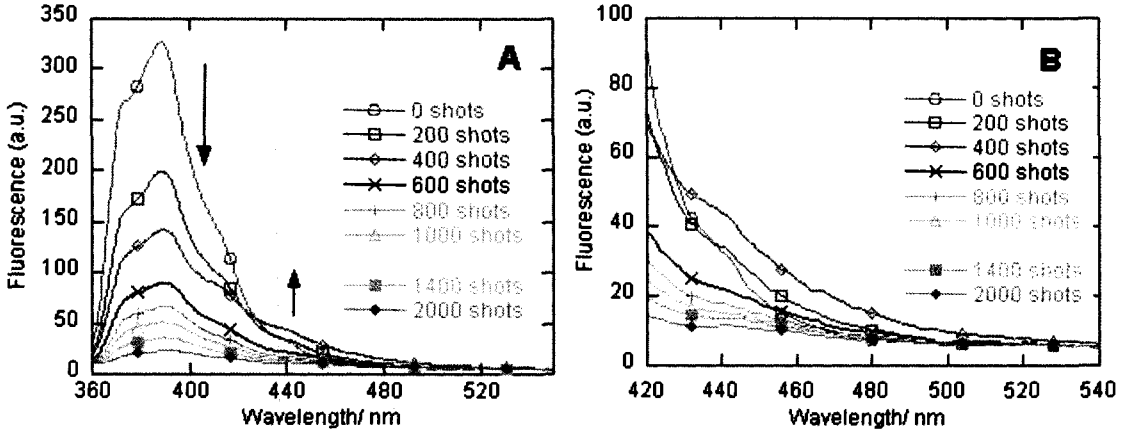

Figure 6-8. Fluorescence of a FP film (~ 440 nm thick) containing 0.5 weight % pyrene based on polymer's weight, exposed to laser radiation at 157 nm, 1.7 – 1.8 mJ/ cm^2/ shot, frequency 15 shots/ s (A); the expanded region between 420 and 540 nm (B), λ_{exc} = 330 nm.

6.2.5 *Fluorescence microscopy*

Although fluorescence spectroscopy is much more sensitive than absorbance, in the emission spectra presented in figures 6-6 to 6-8 the increase in intensity characteristic to pyrene excimers, although noticeable, is relatively small and sometimes hidden by the emission from the monomer. To gain more information and to better discriminate between the exposed and unexposed areas of the films, fluorescence microscopy was employed. Films were prepared as previously described, using solution of PMMA (with 0.33 weight % pyrene based on PMMA weight) and FP (with 0.5 weight % pyrene based on FP weight). Images were recorded with a Leica fluorescence microscope using the XF02-2 optical filter from Omega Opticals (maximum excitation wavelength at ~ 367 nm), figure 6-9. The hexagonal masks used during exposure were removed prior to recording the fluorescence images. The filter used allows excitation of both the monomer and the excimer (see spectra of incident light in figure 6-10).

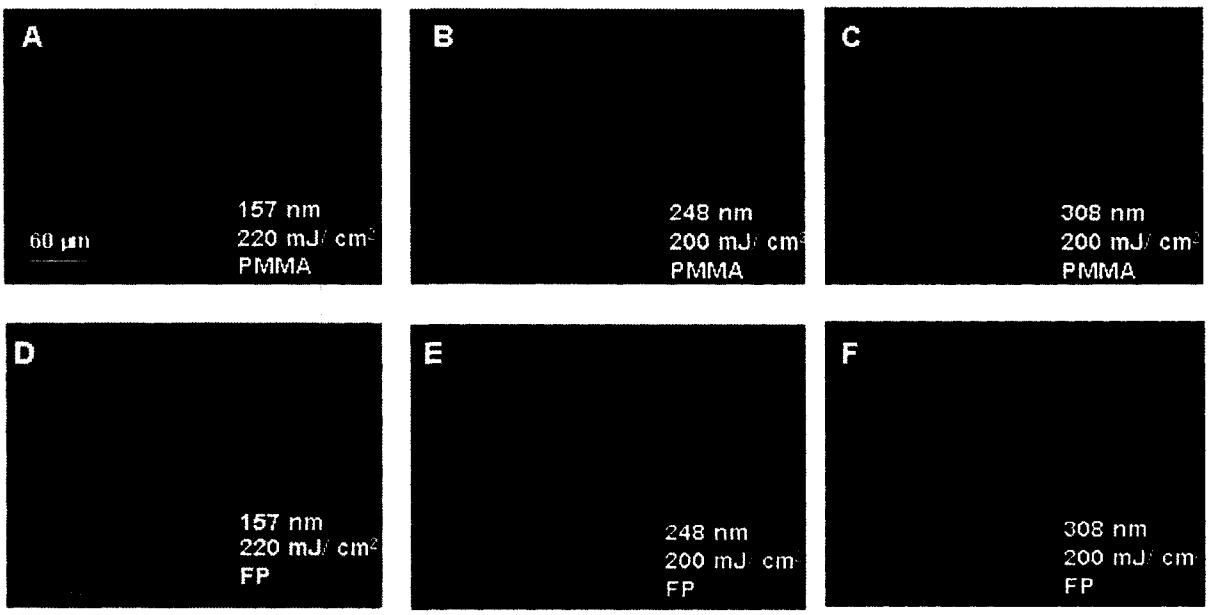

Figure 6-9. Fluorescence microscopy images of thin films of PMMA (A, B, C) and FP (D, E, F) containing pyrene (0.5 % based on FP weight, and 0.33 % based on PMMA weight)

and exposed to 220 mJ/ cm^2 laser radiation at 157 nm (A, D), 248 nm (B, E) and 308 nm (C, F), recorded with a 20x magnification objective. The energy / shot delivered was 4.32 mJ/ cm^2/ shot at 308 nm, 3 shots/ s (47 shots); 4.46 mJ/ cm^2/ shot at 248 nm, 3 shots/ s (45 shots); 1.1 mJ/ cm^2/ shot at 157 nm, 5 shots/ s, (200 shots).

To better translate into quantitative information the fluorescent images from figure 6-9, an application called DigitalColor Meter version 3.2 from Apple Computer Inc. was used to measure the contributions from red, green, and blue in the exposed and unexposed regions using RGB color standard. This application displays the color value (arbitrary units) of any chosen pixel from the screen. The emission of excimer is centered around 470 nm in the blue region of the visible spectrum, thus one would expect an increase in the contribution of blue after exposure. The values are reported in table 6-1.

Table 6-1. Contribution of red, green and blue (a.u.) in the fluorescence images (excitation filter XF02-2) recorded following exposure of PMMA and FP films containing pyrene (0.33 % and 0.5 % respectively, based on polymer weight), through a copper mask at 157 nm (220 mJ/ cm^2), 248 nm (200 mJ/ cm^2), and 308 nm (200 mJ/ cm^2), fig 6-9. The color composition was determined using the DigitalColor Meter v.3.2 from Apple Computer Inc.

Color	Exp/ Unexp	PMMA 157 nm	PMMA 248 nm	PMMA 308 nm	PFP 157 nm	PFP 248 nm	PFP 308 nm
red	exposed	8200	11800	9800	14650	9250	7200
	unexposed	7000	7000	8200	8200	5150	6200
green	exposed	15100	23400	17700	35200	16700	11600
	unexposed	11100	11800	12100	14400	8000	9000
blue	exposed	55000	65500	65500	65500	31400	23650
	unexposed	34700	40600	41400	29300	15700	16500

Three different wavelengths, 157, 248, and 308 nm, were used in order to characterize the influence of the radiation on the formation of excimers in these films. The fact that the intensities of blue for PMMA films exposed at 248 and 308 and for the FP exposed at 157 nm are identical and have the biggest value suggests that there is saturation.

Due to limited availability of optical filters for the microscope in the laboratory, the filter used was XF02-2 from Omega Optical with a maximum at 367 nm. The spectrum of the incident light that actually excited the sample in the fluorescence microscope, as measured with the SPR-1 Luzchem spectrophotometer, is presented in figure 6-10.

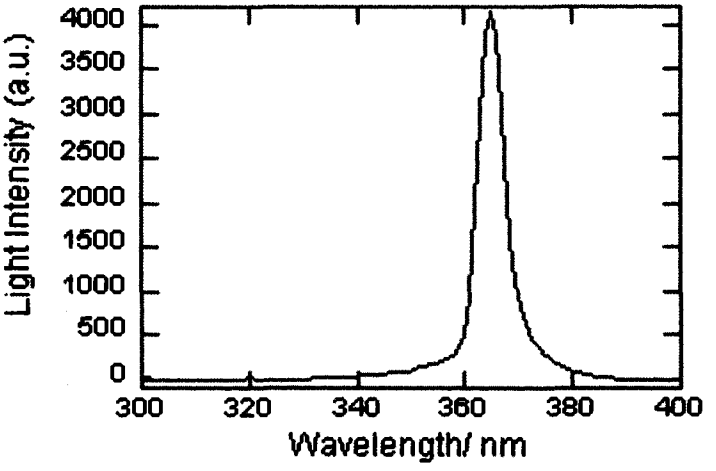

Figure 6-10. The optical spectrum of the excitation light, incident on the surface of the polymer films when using optical filter XF02-2 in the Leica optical microscope. This spectrum was recorded with the Luzchem Spectroradiometer SPR-1.

6.2.6 Influence of temperature on the fluorescence of pyrene in films of polymers with high Tg studied by fluorescence microscopy

It is interesting to investigate the influence of the temperature on the fluorescence images obtained with PMMA and FP films. Depending on their different Tg temperatures, the two polymer films show different behavior when baked. The films were obtained by spin coating solutions containing 2-heptanone as solvent, 15 % weight PMMA and 0.33 weight % pyrene based on PMMA weight, and 20 weight % FP and 0.5 weight % pyrene based on FP weight respectively. The thickness of the films, spin coated at 2000 rpm for 20 s was ~ 480 nm for FP and ~ 900 nm for PMMA. The exposure was done at 157 nm with a frequency of 5 shots/ s. The incident energy was delivered in 200 shots, 1.1 –1.2 mJ/ cm^2/ shot. After spin coating the films were baked at 98 °C for 60 s then cooled to room temperature on a metal surface, prior to exposure. The exposure was done using copper masks with hexagonal holes placed on top of the films, with 60 microns the distance between the centers of the holes. After exposure to 220 – 240 mJ/ cm^2, the latent images were recorded before baking (figure 6-11 A and D), then the films were baked for various periods of time: first for one minute, then for three minutes (four minutes overall), then for five minutes (nine minutes overall fig. 6-11 B and E) and lastly for six and five minutes (nineteen minutes total baking time fig. 6-11 C and F). After each baking period, the films were cooled to room temperature and fluorescent images were recorded. The differences between the images baked for short time intervals were not easily distinguishable for PMMA, that is why images selected for figure 6-11 show films after nine and nineteen minutes of baking.

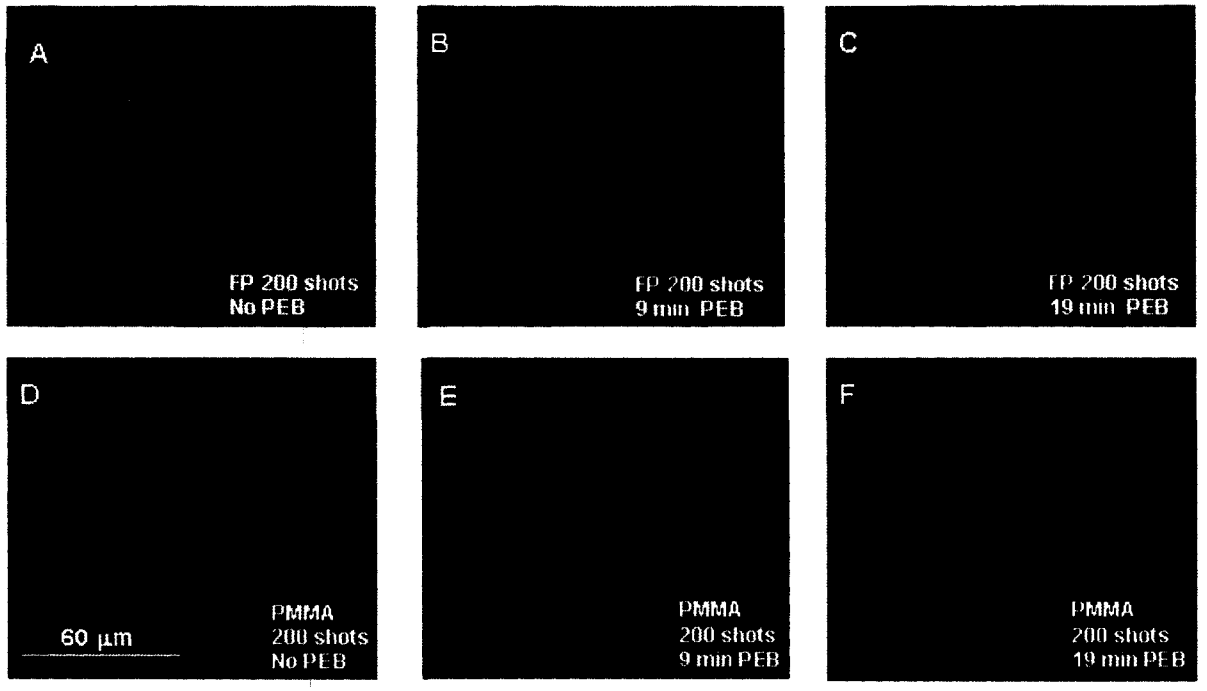

Figure 6-11. Fluorescence latent images of pyrene in FP (A-C) and PMMA (D-F) films (0.5 wt % pyrene based on FP weight, and 0.33 wt % pyrene based on PMMA weight) exposed to 200 shots of laser radiation at 157 nm, 5 shots/ s, 1.1 –1.2 mJ/ cm^2/ shot; no baking after exposure (A, D), 9 minutes baking (B, E), and 19 minutes baking (C, F) at 98 °C. XF02-2 optical filter from Omega Opticals was used to record the images, with a maximum at 367 nm.

The images presented in figure 6-11 reveal an interesting result. Images recorded with FP films do not show almost any change during baking, while those with PMMA films show dramatic change after nineteen minutes. The image is faded while the color also changes. In fact the color obtained with PMMA films, containing pyrene (0.33 % based on polymer weight) exposed to 157 nm, followed by nineteen minutes of baking, is the same as that of PMMA films containing pyrene but unexposed to laser radiation, figure 6-12. This proves that pyrene excimers followed during exposure to 157 nm are broken apart during baking so that the color that is seen is the emission from the monomer.

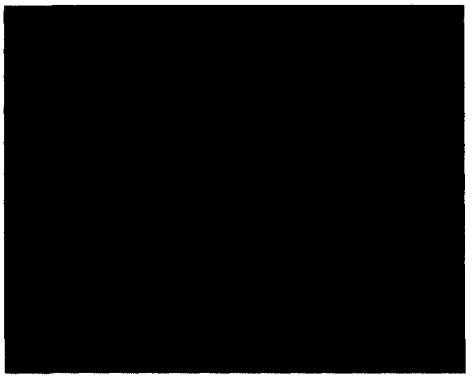

Figure 6-12. Fluorescence image of a PMMA film containing pyrene (0.33 wt % based on PMMA weight), recorded before exposure to laser radiation, using the XF02-2 filter, with a maximum at 367 nm.

Some of the fluorescent images recorded show features parallel to the unexposed regions, figure 6-13. There are alternating dark and blue lines, similar to those obtained with films containing Coumarin 6. We assign these line to the same phenomenon of laser induced periodic surface structures (LIPS) observed with FP films containing Coumarin 6 in chapter 5 and previously reported by others in literature.[35-37]

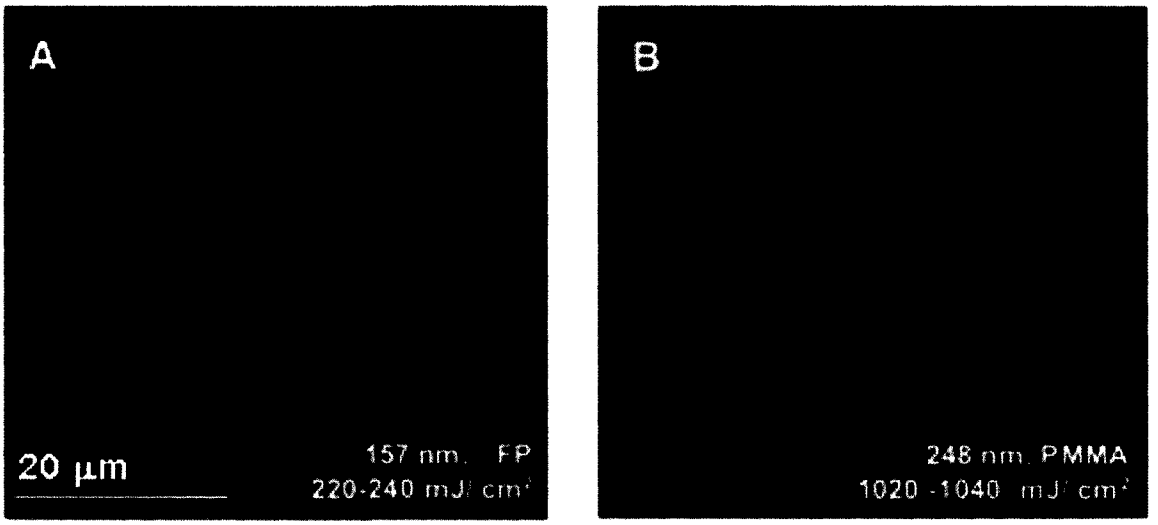

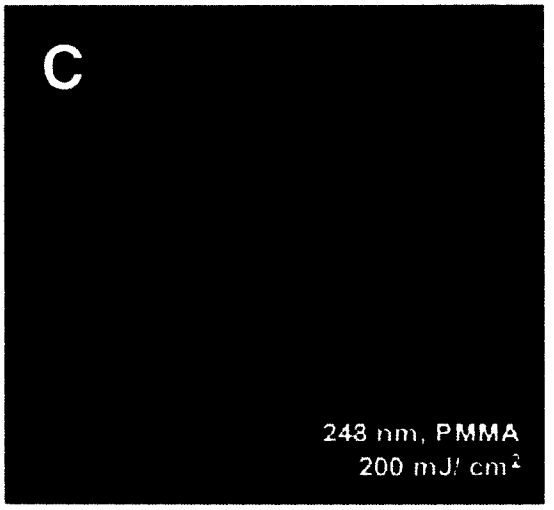

Figure 6-13. Fluorescence images, 100x magnification objective, showing laser induced periodic structures obtained with a FP film containing pyrene (0.5 wt % relative to FP), exposed to 200 shots of laser radiation at 157 nm, 5 shots/ s, 1.1 –1.2 mJ/ cm^2/ shot (A) and PMMA film containing pyrene (0.33 % based on PMMA weight) exposed to 248 nm, 200 shots, 1 shot/s, 5.1 – 5.1 mJ/ cm^2/ shot, 1020 mJ/ cm^2 total dose (B) and to 200 mJ/ cm^2 (C).

The images presented in figure 6-13 were recorded with 100x magnification objective, thus allowing a better imaging of LIPS.

Figure 6-14. Effect of sequential double imaging at 157 nm on PMMA films containing pyrene (0.33 wt % based on PMMA weight); 1.1 mJ/ cm^2/ shot, 5 shots/ s; 200 shots (A),

and 400 shots with the mask placed in a different position after the first 200 shots (B). The images were recorded with the 20x objective using the XF02-2 optical filter from Omega Opticals. The second exposure was done after image (A) was recorded, with the copper mask placed at a different position on top of the film.

The effect of double imaging is shown in figure 6-14, where a film of PMMA containing 0.33 weight % pyrene was exposed to radiation at 157 nm, 1.1 mJ/ cm^2/ shot, 5 shots/ s. The stock solution containing 15 wt % PMMA, 85 wt % 2-heptanone, and 0.33 wt % pyrene was spin coated on top of a quartz disc at 2000 rpm for 20 s, followed by baking inside an oven at 117 °C to ensure removal of the solvent. The film was cooled to room temperature before exposure through the copper mask with hexagonal holes to a first series of 200 shots. The same film from figure 6-14A was further exposed to another dose of 200 shots, so a total incident dose of 440 mJ/ cm^2 was incident to the film. For the second exposure the mask was placed on top of the film but in a different position than during the first exposure, allowing this time irradiation of some of the dark areas unexposed the first time. As it can be seen from figure 6-14 B, there are now three distinct regions: unexposed (3), exposed to 220 mJ/ cm^2 (1), and exposed to 440 mJ/ cm^2 (2). The unexposed regions after the first 200 shots can further be imaged. It is interesting to notice that the color in different 1 regions is similar. Color measurements for figure 6-14 are presented in table 6-4, followed by discussion.

6.2.7 Spectroscopy and Microscopy in low Tg polymer films

In order to study the influence of polymer Tg on imaging, films of polymethylsilsesquioxane were prepared according to the method described in the experimental part. The solutions to be spin coated contained 20 wt % PMSSQ, 80

wt % 2-heptanone and 0.5 wt % pyrene based on PMSSQ weight. The films were prepared by spin coating the stock solution on a one inch quartz disc at 2000 rpm for 20 s, followed by PAB. Films baked at 100 °C in the oven, after coating, were cooled to room temperature then exposed to radiation at 157 nm, 200 mJ/ cm^2, at a repetition rate of 5 shots/ s. The images recorded with the fluorescence microscope using the same setup as in previous experiments showed no hexagonal pattern characteristic to the copper mask, even more, the color of the film was black, figure 6-15A. Two phenomena could have caused this: either fluorescence of pyrene was quenched by PMSSQ or pyrene was removed (sublimed) from the polymer during PAB. Exposure of another film to 157 nm, without PAB, resulted in formation of latent images just like in previous experiments with PFP and PMMA. This intriguing observation prompted further investigations in an attempt to clarify the influence of temperature on imaging in PMSSQ.

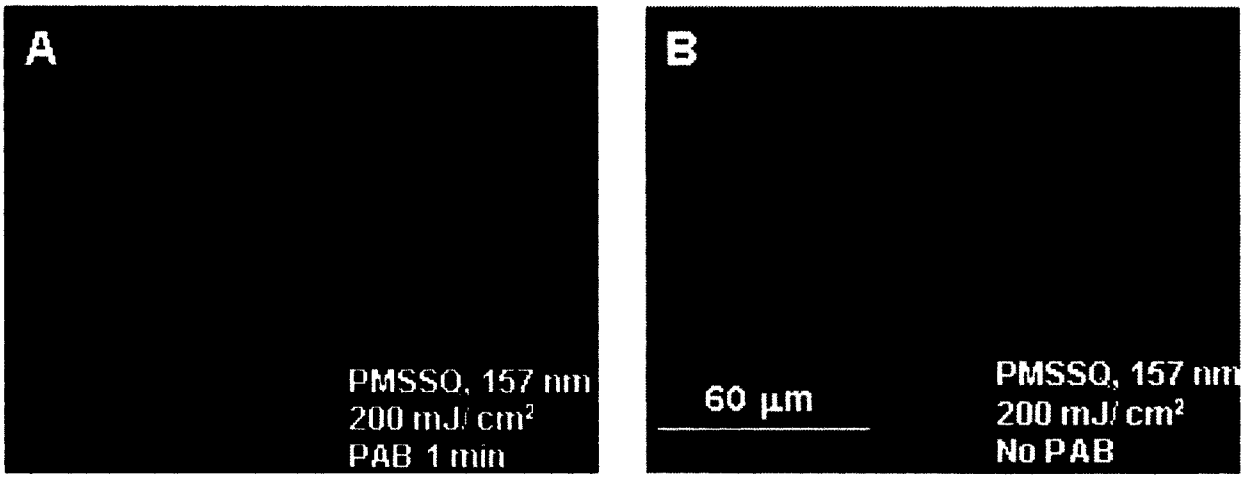

Figure 6-15. Fluorescent images of PMSSQ films containing pyrene (0.5 wt % based on PMSSQ weight), and exposed to 157 nm, 200 mJ/ cm^2, 5 shots/ s, baked (A) and non-baked (B) prior to exposure. The excitation filter in the fluorescence microscope was XF02-2 from Omega Opticals with a maximum at 367 nm.

6.2.7.1 *Spectroscopy in PMSSQ films containing pyrene*

Spectroscopic investigations of PMSSQ films containing pyrene showed interesting results. Absorption and fluorescence spectra recorded after spin coating without PAB showed the spectra characteristic to pyrene, while the spectrum of the same film, after baking at 98 °C for 60 s, showed no signal characteristic to pyrene, figure 6-16A.

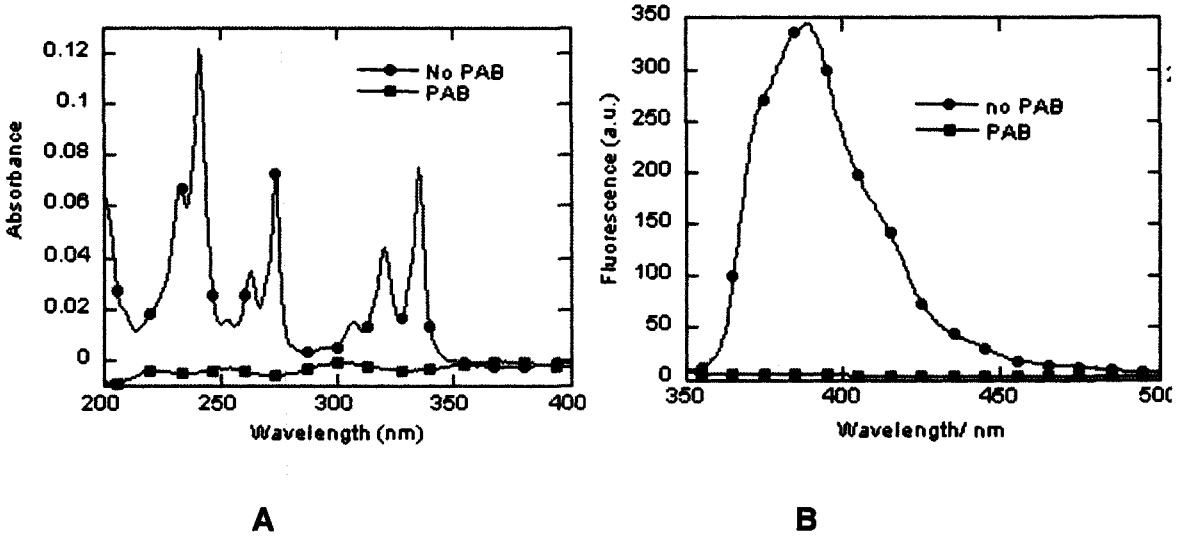

Figure 6-16 Absorbance (A) and fluorescence spectra (B) (λ_{ex} = 330 nm) of PMSSQ films containing pyrene (0.5 wt % based on PMSSQ weight), baked (■) and non baked (●) at 98 °C for 60 s after spin coating. The thickness of the films was ~ 463 nm.

The films of PMSSQ containing pyrene were obtained by using a stock solution containing 20 weight % polymer, 80 weight % 2-heptanone and 0.5 % pyrene from the dry polymer weight. The solution was spin coated on top of one inch quartz discs at 2000 rpm for 20 s, followed by PAB (where indicated) at 98 °C. The thickness, as measured with a Luzchem TFA was 463 nm. The excitation wavelength for the fluorescence experiment was 330 nm.

The results obtained with PMSSQ films containing pyrene showed that no pyrene was left in the film following PAB, unlike the case of high Tg polymers PMMA and FP, suggesting that pyrene sublimed during baking. To further verify that pyrene indeed sublimed, the next experiment was performed: PMSSQ films containing pyrene were baked with and without a one inch quartz disc on top. The role of the disc placed on top of the film was to stop pyrene from subliming during baking. The absorbance spectra obtained with the sandwiched and non-sandwiched PMSSQ films are shown in figure 6-17. The films were obtained following the same protocol as for the films analyzed in figure 6-16. The film sandwiched between two discs was baked for various times, 0, 2, 4 minutes, while the film without a disc on top was baked for 1 minute, enough for the pyrene to sublime. For the sandwiched films the baseline were the two quartz discs, while for the non-sandwiched films the baseline was one clean quartz disc.

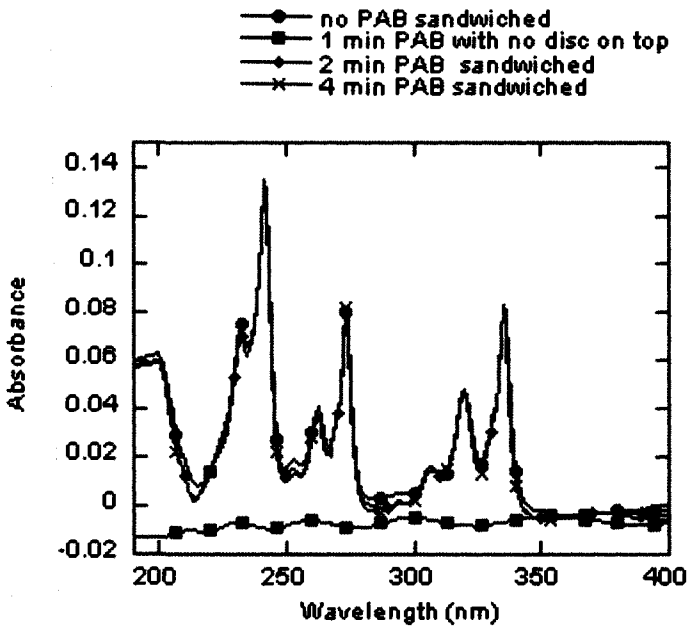

Figure 6-17. Absorbance spectra of pyrene in PMSSQ films non sandwiched (■) and sandwiched (●, ♦, x), with PAB at 98 °C for 1 min (■), 2 min (♦), 4 min (x) or no PAB (●).

6.2.7.2 The influence of temperature on PMSSQ films containing pyrene, studied by fluorescence microscopy

From the plot in figure 6-17 one can notice that the absorbance of pyrene in the sandwiched film baked for 2 or 4 minutes is the same as the one of the non-baked film, while a non-sandwiched film, baked for only one minute, shows no signal characteristic to pyrene. This proves that pyrene sublimes during baking of the unexposed films. This is a major difference between the PMSSQ films and PMMA and FP polymer films. However, as noticed in figure 6-18, baking after exposure does not lead to sublimation of pyrene. Further investigations into the influence of PAB and the length of PEB were done and the results are shown in figure 6-18.

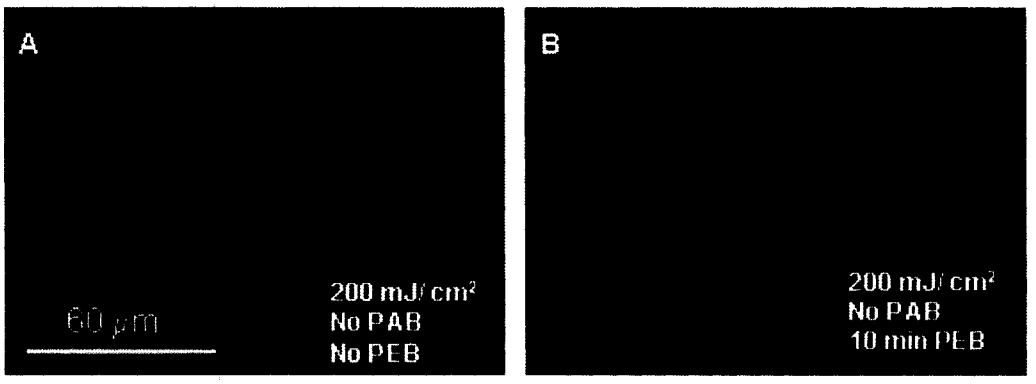

Figure 6-18. Fluorescence images of pyrene (0.5 wt % based on PMSSQ) in PMSSQ films exposed to laser radiation at 157 nm, 200 mJ/ cm^2, 5 shots/ s, no PAB and no PEB (A) and no PAB 10 min PEB at 100 °C (B). Magnification 20x, the excitation filter used in the fluorescence microscope was XF02-2 with a maximum at 367 nm.

PMSSQ films containing pyrene, exposed first and then baked, show hexagonal patterns transferred from the copper mask. PEB for 10 minutes, figure

6-18 B, does not remove the patterns, unlike in the case of PMMA films. This may be due to photocrosslinking of the PMSSQ film during the exposure step, or to chemical reactions involving pyrene molecules. In the event of photocrosslinking the pyrene molecules are trapped inside a network and cannot sublime during baking even for 10 minutes. This is an interesting finding, with important implications in photolithography using PMSSQ as photoresist polymer.

The effect of double imaging and of PEB time was studied in PMSSQ films containing pyrene, figure 6-19. The same film was exposed, baked and imaged in all A-D images. The film was exposed first to 200 mJ/ cm^2 without PAB, then baked for one minute, cooled to room temperature and then image 6-19 A was recorded. After recording the image, the copper mask was placed again on top of the film, in a different position, and the film was exposed to 200 mJ/ cm^2 for a second time, with a total of 400 mJ/ cm^2 delivered to the film. After exposure image 6-19 B was recorded, then the film was baked for another minute at 100 °C, cooled to room temperature and then image 6-19 C was recorded. The film was then baked for 30 minutes at 100 °C and image 6-19 D was recorded.

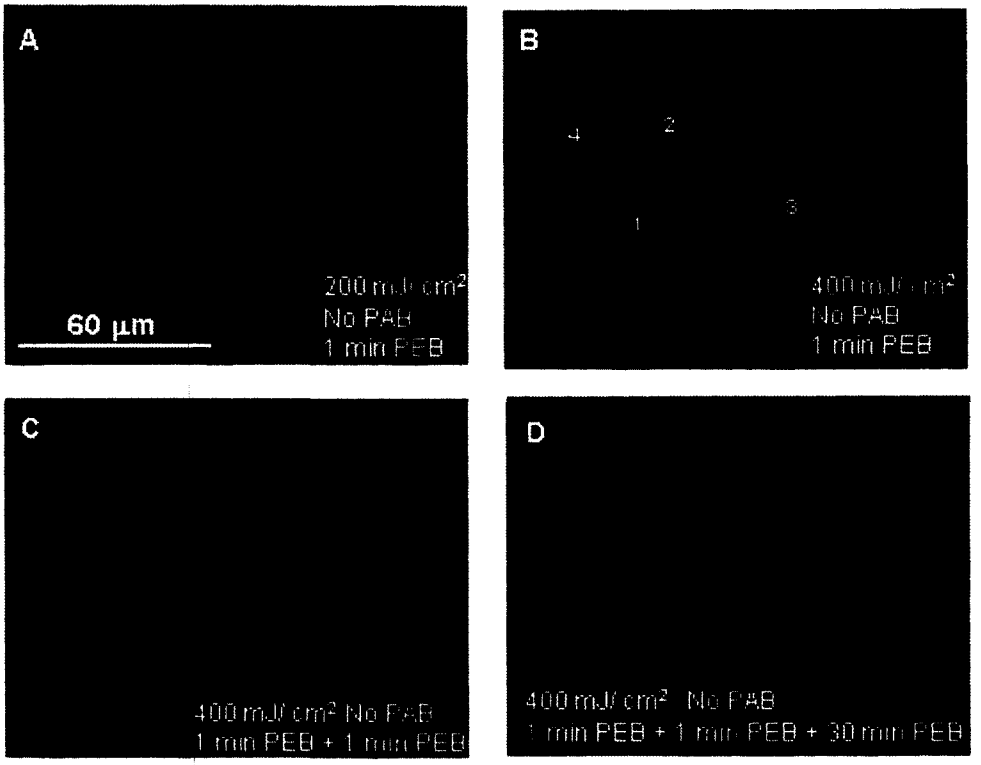

Figure 6-19. The effect of double exposure and of PEB on fluorescence images of pyrene (0.5 wt % based on PMSSQ loading) in PMSSQ exposed to 157 nm, 5 shots/s. The exposure conditions were: 200 mJ/ cm^2, no PAB, 1 min PEB (A), 400 mJ/ cm^2 1 min PEB (B), 400 mJ/ cm^2 no PAB 2 min PEB (C), 400 mJ/ cm^2 no PAB 32 min PEB (D). The film was ~ 460 nm thick, and the excitation filter in the fluorescence microscope was XF02-2 with a maximum at 367 nm.

PMSSQ films containing pyrene behave differently compared to PMMA and FP film when double imaged. As it can be seen from figure 6-19 B there appear the same three distinct regions: unexposed, exposed once and exposed twice. However, unlike in the case of PMMA and FP films, the regions unexposed during the first irradiation (the black regions in figure 6-19) cannot further lead to formation of pyrene excimers during the second exposure. Thus one can distinguish four regions in the image presented in figure 6-19 B: 1 – region non exposed (0 mJ/ cm^2), 2- region exposed first time, unexposed second time (200 mJ/ cm^2), 3- region

exposed two times (400 mJ/ cm2), and 4- region unexposed first time but exposed second time after 1 minute PEB (200 mJ/ cm^2).

6.2.8 Spectroscopy and microscopy in films under N_2 atmosphere

In order to determine how oxygen influences the emission of pyrene in polymer films, experiments under nitrogen atmosphere were performed. Absorption and fluorescence, and fluorescence microscopy images were recorded using PMMA films obtained by spin coating at 2000 rpm for 20 s a solution containing 85 wt % 2-heptanone, 15 wt % PMMA and pyrene 0.33 wt % based polymer weight. After coating the films were baked at 96 °C for 60 s, then cooled to RT and exposed to 200 shots of laser radiation at 157 nm, 1.7 – 1.9 mJ/ cm^2, 5 shots/ s. For the fluorescence spectra the excitation wavelength was 330 nm. The solutions were deaerated by bubbling N_2 for 15 minutes in a volume of solution of approximately 5.0 mL. Although the solutions were deaerated, during spin coating, baking, and recording of absorption spectra, the films were in open air. The absorbance and fluorescence spectra of deaerated and non-deaerated films are shown in figure 6-20.

Three solutions of PMMA, FP, and PMSSQ containing 0.33, 0.5, and 0.5 weight % respectively from the dry polymer weight were deaerated with N_2 for 15 minutes each, spin coated following the already mentioned procedure, then exposed through the copper masks to various energy doses at 157 nm, 1.5 -1.7 mJ/ cm^2/ shot, 5 shots/ s. PMSSQ films were not baked after spin coating, while PMMA and FP films were baked at 92 °C for 60 s. The fluorescence images were obtained having the whole set-up under N_2 atmosphere, the microscope being in a sealed plastic bag under nitrogen flow. The films were left overnight under nitrogen atmosphere on the microscope stage, and new images were recorded after twenty

four hours. Due to solvent evaporation during N_2 bubbling, the PMMA solution became too viscous and the quality of the films was poor. The images are shown in figure 6-21.

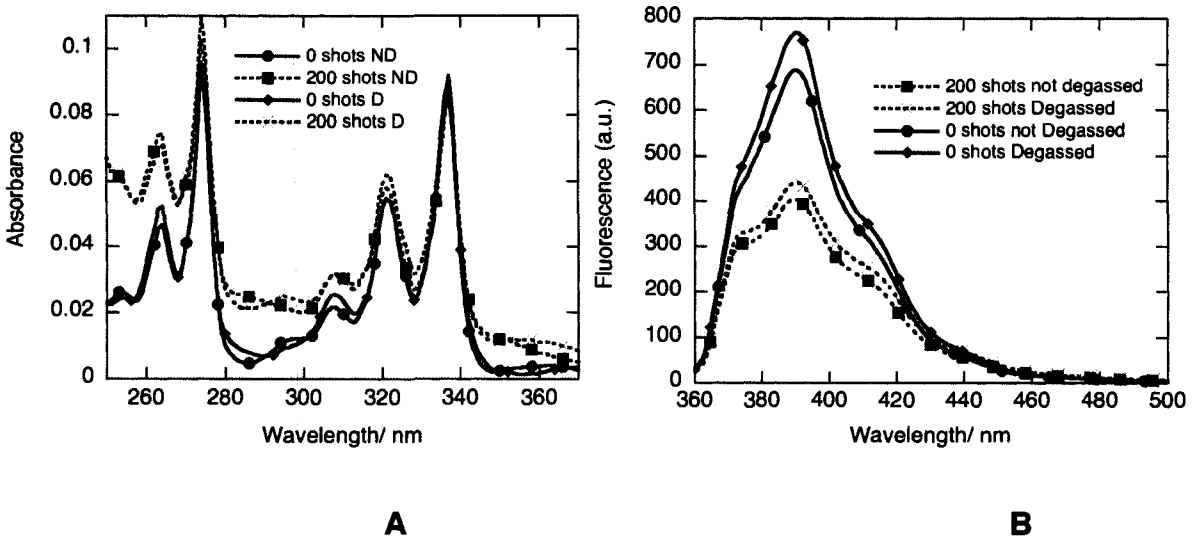

Figure 6-20. Absorbance (A) and fluorescence (B) spectra of PMMA films containing pyrene (0.33 wt % based on PMMA loading), exposed to 157 nm; ND – non deaerated, D – deaerated.

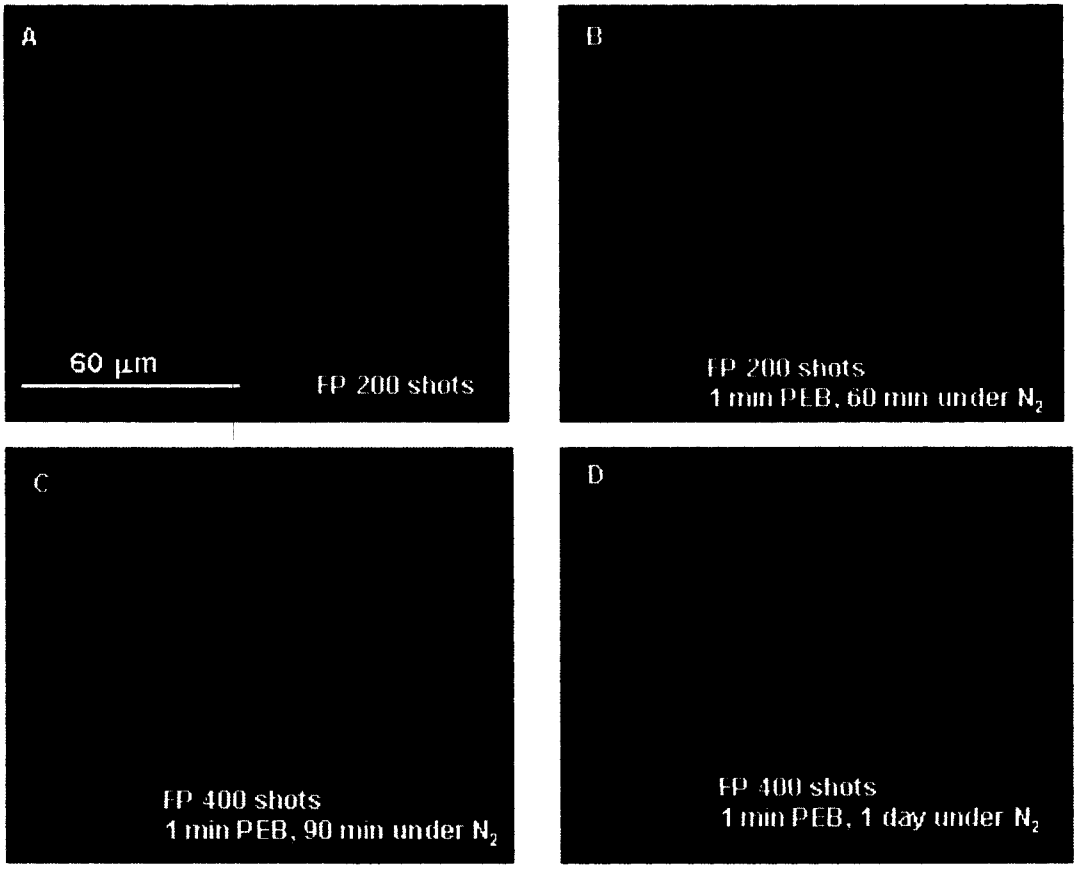

Figure 6-21. Fluorescence images of FP films containing pyrene (0.5 wt % based on FP), exposed to 157 nm, 1.5 -.7 mJ/ cm^2/ shot, 5 shots/ s. The solution was deaerated before coating and the films were under N_2 atmosphere during and after exposure. The excitation filter used in the fluorescence microscope had a maximum at 367 nm, and the film was ~ 480 nm thick.

The images in figures 6-21 and 6-22 were recorded according to the following experimental procedure: the polymer films prepared according to the experimental procedure were exposed first to 200 shots of laser radiation at 157 nm with a copper mask on top. The polymer solution containing pyrene (0.5 wt % based on polymer weight) was deaerated prior to coating, and the exposure was

done in a chamber under N_2 atmosphere. The film was placed then on the microscope stage under N_2 atmosphere. In between the recordings of the images the shutter was closed so that the sample was not under illumination from the microscope lamp.

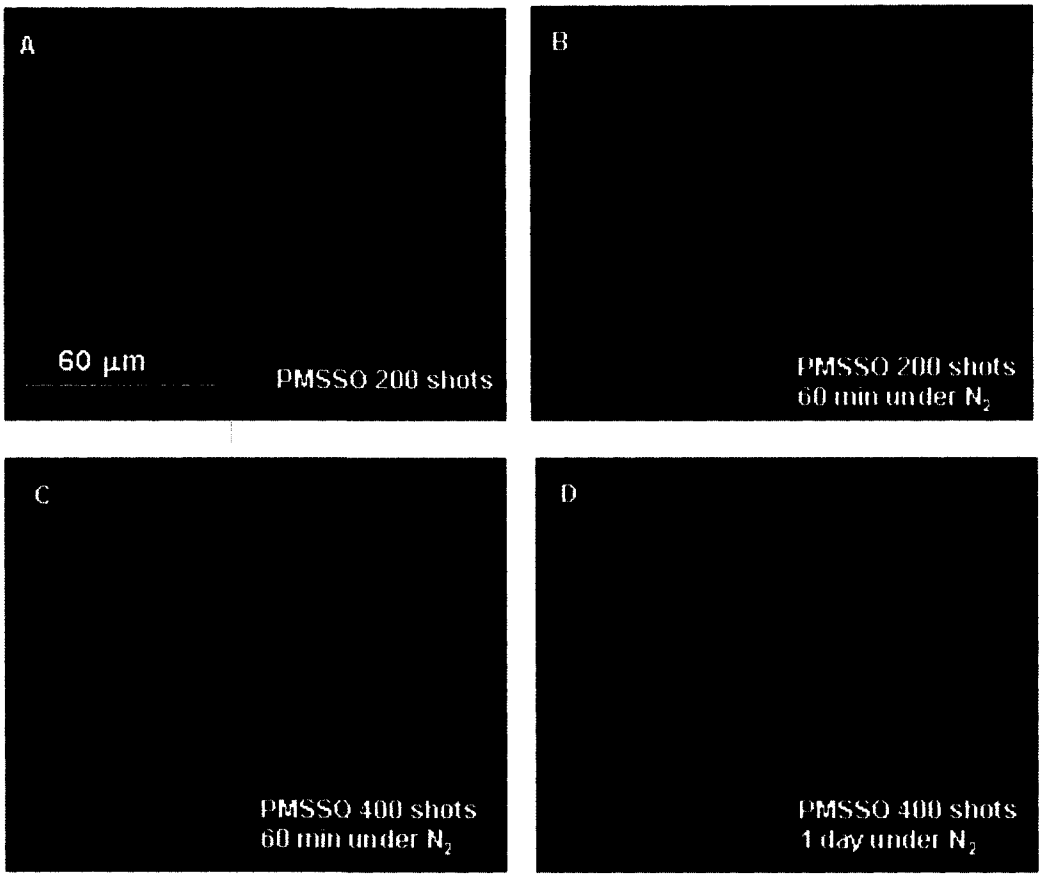

Figure 6-22. Fluorescence images of PMSSQ films containing pyrene (0.5 wt % based on polymer weight), exposed to 157 nm, 1.5 -1.7 mJ/ cm^2/ shot, 5 shots/ s. The solution was deaerated before coating and the films were under N_2 atmosphere during and after exposure. The thickness of the films was ~ 460 nm.

6.2.9 Continuous wave exposure

FP thin films containing pyrene (0.5 wt % based on polymer) were exposed to continuous wavelength radiation in a HTG exposure unit, and then analyzed using absorbance and fluorescence. The emission spectrum of the lamp is presented in figure 4-1B, chapter 4, the power of the lamp was 39.7 W/ m^2.

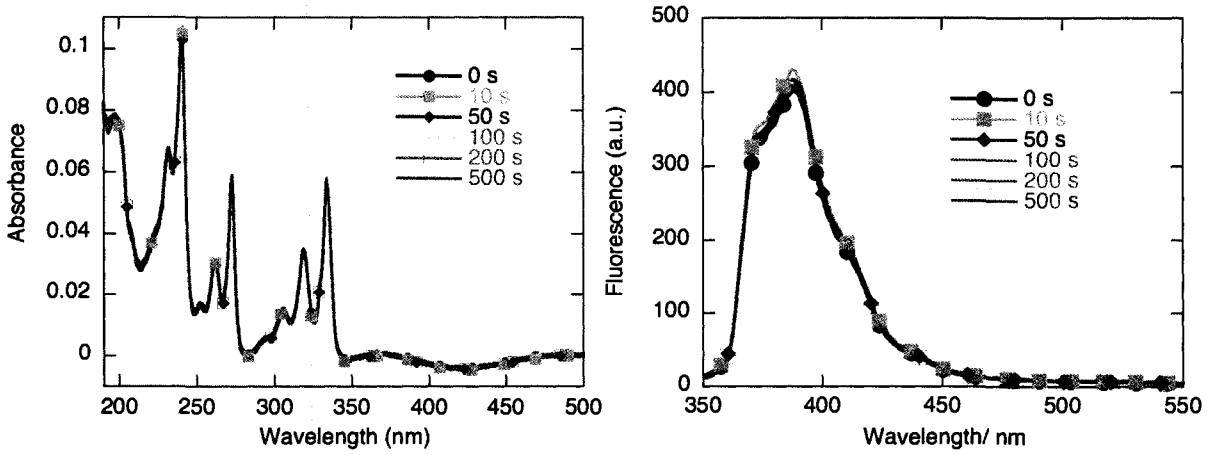

Figure 6-23. Absorbance (A) and fluorescence (λ_{ex} = 330 nm) (B) of a PMMA film containing pyrene (0.33 % based on PMMA weight), exposed to 254 nm CW radiation in an exposure unit for 0 s (●), 10 s (■), 50 s (◆), 100 s (x), 200 s (□), and 500 s (◊).

Exposure to continuous radiation from a Hg lamp does not induce any noticeable change in absorbance nor in fluorescence, even after 500 s of exposure, figure 6-23. This indicates that the changes are caused only by laser radiation and it depends on the properties of the laser beam.

6.3 Discussion

6.3.1 Discussion of results obtained with high Tg polymer films

Laser photoinduced processes in polymer films containing pyrene were studied using spectroscopy and fluorescence microscopy. All throughout these experiments pyrene plays a double role: it acts as sensitizer and as fluorescence probe at the same time. It absorbs incident photons and releases the excess energy either as light or as heat into the surrounding polymer matrix. The fact that the exposed films show a decrease in monomer fluorescence and an increase in the region around 470 nm (figures 6-7, 6-8) proves that pyrene forms excimers or aggregates during exposure. The experimental results obtained with fluorescence microscopy and the fact that the images are thermally erasable in some cases point out towards the same conclusion.

In interpreting the results obtained and presented in the experimental section of this chapter, no plausible explanation is ruled out. In fact, as seen from the references to literature, irradiated pyrene in polymer films and in solvents (liquids or matrixes) undergoes a complexity of photophysical and photochemical reactions which lead to formation of pyrene excimer transients in irradiated polymer films, photolysis of the solvent, and formation of covalent bonds between pyrene and the polymer or solvent matrix.[45-52] The fact that the excimer formation is connected to the ability of the molecules to diffuse through the polymer film, and is observed only at RT, supports the interpretation of experimental data presented in this chapter.

There are certain differences in terms of emission intensity among different polymer films. These differences are induced by polymer properties (Tg, polymer absorbance at the exposure wavelength, pyrene diffusion coefficient) and by the wavelength of the radiation. To be able to form excimers or aggregates, pyrene has

to diffuse throughout the polymer film during the laser pulse or shortly after, when the high temperature favors the liquid-like mobility of the molecules. The ability of pyrene to diffuse is related to the rigidity of the environment and it appears only in polymer films exposed to laser radiation. The Tg of the polymers in thin films containing pyrene is different than the Tg in bulk. There are two additive effects that lead to a decrease in the Tg of the films containing pyrene: the addition of the dopants and the fact that the polymer is a thin film.[38] Another contributory effect may be the chain scission, since the lower the M*w* of the polymer, the lower the Tg.

Besides decaying through emission, the pyrene molecules may be involved in photochemical reactions.[45-48] The films of PMMA containing pyrene (0.33 % based on polymer wt) exposed to continuous wave from a lamp do not show any change in their absorption or emission spectra even after 500 s of exposure, figure 6-23. This is in accordance with results previously reported by Thomas *et al.*, who noticed a change in absorption spectrum of pyrene covalently bonded to films of polyethylene, but that there was no bonding between pyrene and PMMA in γ-irradiated pyrene-containing PMMA films.[45] The fluorescence images show differences in the case of films of the same polymer but exposed to radiation of different wavelengths, figure 6-9. There are also differences in emission among PMMA and FP films exposed to radiation of the same wavelength.

An important parameter, when discussing the possibility of pyrene molecules to form excimers, is the distance that the molecules have to travel trough the polymer film in order to form an excimer. Based on the concentration of the pyrene, the calculated densities of the polymers (1.3 g/ mL for FP and 1.05 g/ mL for PMMA), assuming that all the solvent was removed from the film during baking and that the pyrene molecules are evenly distributed throughout the film, the calculated distance between two neighbor molecules are ~ 3.7 nm for the FP films (with 0.5 wt % pyrene based on polymer) and ~ 4.5 nm for the PMMA films (pyrene 0.33 % wt based on PMMA weight). The densities of the polymers were calculated by weighing volumes of 1.0 mL of the respective polymer solutions, and knowing the

density of 2-heptanone (0.815 g/ mL), and the % wt of the polymers and the solvent. This calculated distances between two pyrene molecules is valid only under the assumption that the molecules are evenly distributed throughout the film. However, the molecules may be more agglomerated towards the top surface of the film, towards the interface with the silica disc, or preferentially distributed around certain monomers or molecule segments, since the polymer molecules may have segments that form micro- or nano-crystalline regions during spin coating and solvent evaporation.

The increased contribution of blue, green and red in the exposed regions compared to the unexposed regions shows a shift of the emission towards longer wavelengths, as expected in the case of excimer formation. This increase is expressed as the ratio between the contribution of the basic colors blue red, and green between the exposed and unexposed regions, table 6-2. The excimer emits in the blue, with a maximum around 470 – 480 nm depending on the environment. Thus one expects an increase in blue and green in the exposed areas compared to the unexposed ones, and a less increase in red. This situation is suggested also by the data in table 6-2. The contribution of the three fundamental colors (red, green, and blue) to the final color of the images was analyzed with the software application DigitalColor Meter v. 3.0 from Apple Computer Inc.. This application may be used to determine the color value (arbitrary units) of any pixel on the screen.

Table 6-2. Ratio of the intensities of blue, red, and green colors (as determined with the DigitalColor Meter v.3.0 from Apple Computer Inc.) between the exposed and unexposed regions of PMMA and FP films containing pyrene 0.33 wt % relative to PMMA and 0.5 wt % relative to FP respectively. On top of the films there were placed copper masks with hexagonal holes, allowing selective irradiation of some areas. The films were exposed to laser radiation at 157 nm (220 mJ/ cm^2), 248 nm (200 mJ/ cm^2), and 308 nm (200 mJ/ cm^2), see figure 6-9.

Color	PMMA 157 nm	PMMA 248 nm	PMMA 308 nm	FP 157 nm	FP 248 nm	FP 308 nm
red	1.20	1.70	1.20	1.80	1.80	1.20
green	1.40	2.00	1.50	2.50	2.10	1.30
blue	1.60	1.60	1.60	2.20`	2.00	1.40

The mechanism proposed here for the formation of excimers in polymer films containing pyrene and exposed to laser radiation combines photochemical and photothermal effects of radiation. A first condition for these processes to occur is for the molecules to absorb the incident photons, causing them to go into their excited state. The excited molecules of pyrene and polymer release their energy either as light (fluorescence) or as heat through internal conversion. Thus a first condition is to absorb at the excitation wavelength. Pyrene in PMMA can absorb up to ten photons when exposed to laser pulses as long as 30 ns at 248 nm, and not be destroyed. [34] Fujiwara *et al.* studied PMMA ablation with pyrene as dopant and

determined that pyrene in a PMMA film exposed to one shot of laser radiation at 248 nm, 150 mJ/ cm^2, can absorb up to nine photons, form higher excited states (S_n, T_n, excited ions), and not be destroyed.[32,39] A similar experiment, with exposure at 308 nm of a PMMA film containing pyrene and done in a vacuum chamber coupled to a quadrupole mass spectrometer showed that pyrene was not destroyed during irradiation. [32] In the present work the exposure was done at much lower incident doses, thus it is correct to assume that pyrene was not destroyed and that decrease in fluorescence of the monomer (figure 6-7) was due to formation of excimers or aggregates, fluorescence quenching of the monomer, or simply to sublimation.

Excitation of pyrene with laser radiation at 248 nm leads to formation of higher excited states, since during a 30 ns laser pulse pyrene can absorb up to nine or ten photons when the incident energy is 150 mJ/ cm^2 or 200 mJ/ cm^2. [32] Pyrene in the first singlet excited state (S_1) can live 400 ns, more than ten times longer than the duration of the laser pulse which for the lasers used here is 12-15 ns full width at half maximum (FWHM). S_1 can absorb photons and go into higher excited states (S_n, T_n). These excited states are much shorter lived compared to S_1 or T_1 and they decay to the original transient state during the length of the laser pulse through internal conversion (IC) or vibrational relaxation (VR), releasing excess energy into the surroundings as heat. This process can occur many times during a laser pulse, causing the polymer matrix to be heated up around the pyrene molecules. The effect is a softening of the polymer matrix which approached a fluid environment, allowing excited and ground state pyrene molecules to diffuse more easily and to form encounters (excimers, dimers). The *in situ* formed excimers can release the energy either by emitting photons (fluorescence centered around 470 nm) or by decaying through IC. Upon cooling of the polymer matrix, some excimers are "frozen", the two pyrene molecules being trapped in the sandwich arrangement. Thus the two molecules, which in ground state are not associated in normal conditions due to energy considerations, are associated after cooling of the polymer

matrix. When excited in the fluorimeter or fluorescence microscope, the two pyrene molecules are already in a sandwich-like position, and emission from the excimer is recorded.

For PMMA films the biggest increase in blue and green contribution after exposure is obtained in films irradiated at 248 nm. PMMA absorption spectrum, figure 6-2, shows that there is a small absorbance at 248 nm. Thus both the polymer and pyrene absorb at this wavelength, compared to 308 nm where only pyrene absorbs, figure 6-5. At 157 nm both PMMA and pyrene have a high absorbance, probably too high for the photons to penetrate throughout a film that is 930 nm thick, causing images to be formed only near the top surface of the film. Part of the molecules present at the top may also sublime, thus a lower increase in blue and green is noticed compared to 248 nm. At 308 nm only pyrene absorbs a bit, figure 6-5, PMMA being transparent. Although light can penetrate throughout the film, the increase in blue and green after exposure is similar to the film exposed at 157 nm. The low absorbance at 308 compared to 157 nm is due to the overall lower absorbance of pyrene and PMMA at the exposure wavelength. Analyzing these images proves that there is an additive effect of the two absorbances: that of PMMA and that of pyrene. Following the same rationale one could explain the results obtained in FP films from table 6-2.

FP is a polymer especially designed for photolithography at 157 nm. One of the main conditions for a useful polymer in (CA) photolithography is to be transparent at the exposure wavelength. Although FP was especially designed for photolithography at 157 nm, it still shows some absorbance at this wavelength. In fact, one of the main reasons that determined the computer processors industry to shift its interest from 157 nm to 193 nm immersion lithography or beyond 157 nm (extreme ultraviolet, x-ray lithography, etc.) was the too high absorbance of materials at this wavelength. For the present work FP is an ideal environment: it absorbs at 157 nm, but not too much, allowing photons to penetrate throughout the polymer film and be absorbed by pyrene molecules. The results presented in table

6-2 for FP films follow the expected trend. The biggest increase is at 157 nm (polymer + pyrene absorbs), 248 nm (only pyrene absorbs), and finally 308 nm (only pyrene absorbs a bit).

A comparison between PMMA and FP films shows that at 157 and 248 nm in FP there are more excimers or aggregates formed compared to PMMA, while at 308 nm there are more excimers formed in PMMA. The comparison between two different polymers is not an easy one. Tg may influence the viscosity of the polymer, the higher the Tg, the more viscous the polymer. However, Tg is not the only parameter that could influence the intensity of the fluorescence. Polarity of the polymer matrix can determine a certain orientation or association of pyrene molecules. Fluorescence may be quenched in one film more than in the other through different mechanisms and it may be influenced by photoproducts obtained from polymer chain or pendant group scission. Orientation of the polymer chains and of pyrene molecules is important, and different orientations are achieved with different polymers exposed to laser radiation with or without dopants.[27,28]

The intensity of the emission for the monomer and for the excimer is independent from the rate of delivery, figure 6-7. When 200 shots were delivered at rates of 1, 2, 5, 8, 10, 12, 15, or 20 shots/ s, almost no difference between the emission of the monomer and the excimer was noticed. For example two plots of fluorescence for FP films containing pyrene and exposed to 157 nm at 5 shots/ s and 20 shots/ s are shown. Following irradiation, the intensity of monomer fluorescence decreases by approximately 3 times, while that for the excimer emission increases by 1.5 times. Excessive exposure leads to disappearance of the emission of the monomer and the decrease in emission of the excimer after an initial increase, figure 6-8. This decrease may have a multitude of causes. It is well known that excessive irradiation of polymer films with laser radiation at 157 nm leads to photodarkening or yellowing with absorbance increasing in the visible.[40] Thus photons emitted by the monomer and the excimer could be reabsorbed by the yellow film whose absorbance spans the emission spectrum of the two species.

Ablation may be another cause, the thickness of the film decreasing as the incident dose increases, (chapter 5, AFM images) less pyrene being available. At high incident doses sublimation may appear during the laser pulse due to the high temperature, especially in the case of pyrene molecules close to the film surface.

6.3.2 Influence of temperature upon emission of pyrene in FP and PMMA films

Experiments done with unexposed PMMA and FP films containing pyrene, and heated gradually show a decrease in monomer emission. The films were heated inside the fluorimeter on a special film holder that was connected to a thermostat which controlled the temperature. The films were allowed for ~ 5 minutes at the desired temperature to make sure they reached it. Going back from the highest temperature to room temperature was controlled with the thermostat as well, but it did not result in a recovery of fluorescence, suggesting that pyrene may have sublimed, figure 6-24.

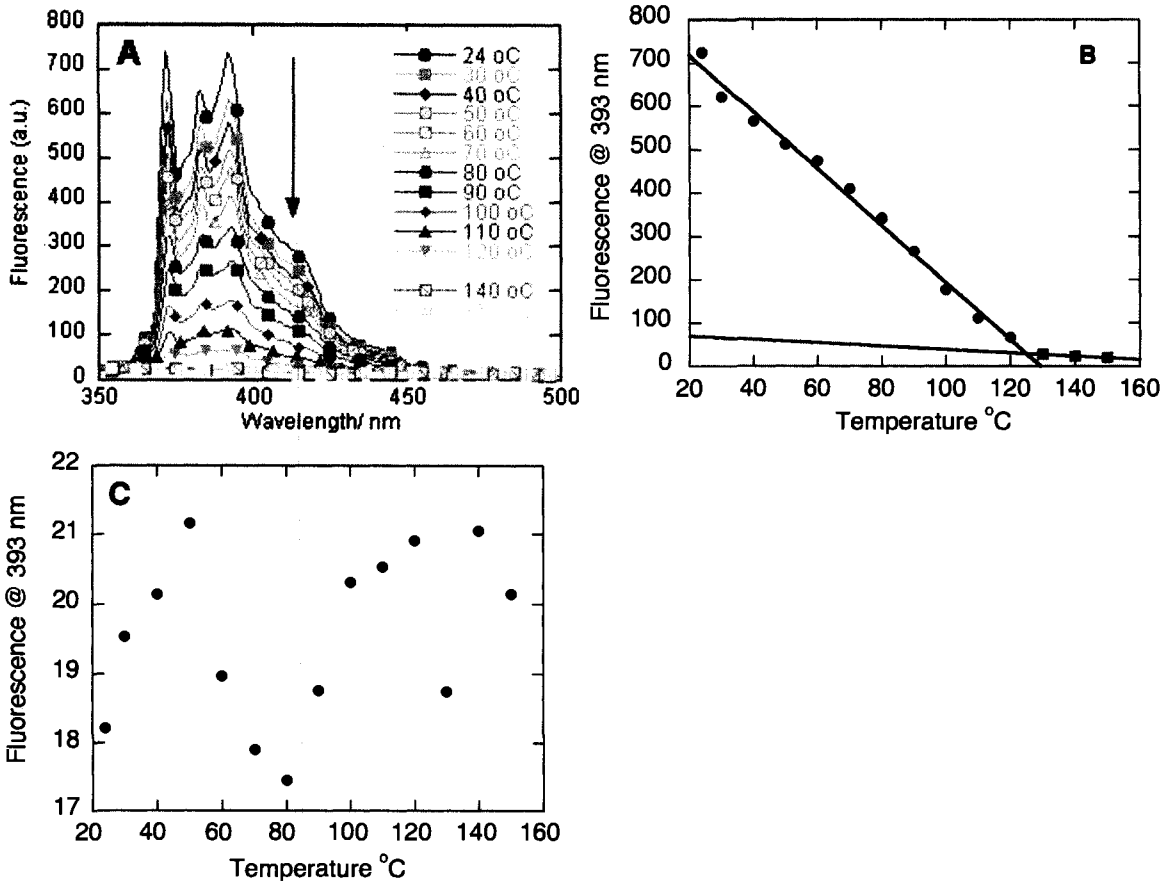

Figure 6-24. Fluorescence of FP films containing pyrene (0.5 wt % based on FP) as a function of temperature, λ_{ex} = 330 nm, (A); intensity of pyrene monomer emission at 393 nm as a function of temperature (B), and intensity of emission at 393 nm for the film cooled from 150 °C to room temperature (C).

The influence of the polymer's Tg is noticed when exposed films are baked at 90 – 100 °C in the oven, figure 6-11. The images obtained with FP films exposed to 200 mJ/ cm^2 at 157 nm were not altered even after 19 minutes of baking at 98 °C. Instead, images obtained with PMMA films containing pyrene, exposed to the same amount of incident light, and baked at 98 °C for 19 minutes were almost completely erased. The ratio of red, green, and blue from the exposed and unexposed regions, (I_{exp}/ I_{unexp}), were calculated after measuring the contribution of the three basic colors using the DigitalColor Meter from Apple Computer Inc., table 6-3.

Table 6-3. The ratios of red, green, and blue from the exposed and unexposed regions (I_{exp}/ I_{unexp}) of the FP and PMMA films containing pyrene (o.5 wt % based on FP, and 0.33 wt % based on PMMA), exposed to an incident dose of 200 mJ/ cm^2 at 157 nm, followed by baking (PEB) for 19 minutes at 98 °C. The values of each color were determined with the DigitalColor Meter v. 3.2 from Apple Computer Inc. The readings are based on the images from figure 6-11.

Color	FP		PMMA	
	0 min PEB	19 min PEB	0 min PEB	19 min PEB
red	1.84	1.67	1.17	1.07
green	2.55	2.40	1.31	1.17
blue	2.17	3.06	1.50	1.01

There is a contrasting difference between the two polymer films, due mainly to the value of their Tg. In the case of FP I_{exp}/ I_{unexp} decreases insignificantly for red and green, showing an increase for blue. This proves that the excimers were not destroyed during baking, the polymer matrix still acting like a rigid environment that did not allow separation of the two pyrene molecules. In the PMMA films the values of red, green, and blue in the exposed and unexposed regions reach almost the same value in the exposed and unexposed regions after 19 minutes of baking at 98 °C, since the ratio I_{exp}/ I_{unexp} is close to unity. Even without the digital color meter it is easy to notice that the exposed film baked for 19 minutes shows a color similar to that of an unexposed PMMA film containing pyrene, from figure 6-12. Since in the image recorded in figure 6-12 there are no excimers, the film being unexposed, one may conclude that the film from figure 6-11 F proves that the excimers, initially

formed after exposure, figure 6-11 D, were destroyed during baking. Bulk PMMA has a Tg of 104 – 105 °C, close to the baking temperature in the current experiments; doped thin PMMA films have a lower Tg than bulk PMMA, possibly lower than the PEB temperature. The polymer matrix lost its rigidity and became less viscous, allowing pyrene molecules from the trapped dimers formed during exposure to fall apart towards the thermodynamically preferred condition.

An intriguing property of polymer films exposed to laser radiation is their ability of forming LIPS (laser induced periodic surface structures). Using a 100x magnification objective, fluorescent images recorded with FP and PMMA films exposed to 220 – 240 mJ/ cm^2 at 157 nm and 200 mJ/ cm^2 at 248 nm show presence of LIPS, figure 6-13. Exposure of a PMMA film to 1.0 J/ cm^2 at 248 nm resulted in a more prominent LIPS, as revealed by the fluorescence image.

Table 6-4. Contributions of red, green, and blue in the exposed and unexposed areas from images obtained with a PMMA film containing pyrene (0.33 wt % based on PMMA weight) exposed to 200 and 400 shots at 157 nm, 1.1 mJ/cm^2/shot, images presented in figure 6-14. The film was ~ 900 nm thick, the colors were determined with DigitalColor Meter v 3.2 from Apple Computer Inc.

Colors	**A (200 shots)**		**B (400 shots)**		
	Exposed	**Unexposed**	**Region 1**	**Region 2**	**Region 3**
red	5400	3900	4100	5400	3600
green	9500	7200	8000	10300	7000
blue	39300	20000	39100	47500	25700

PMMA films containing pyrene, initially exposed to 220 mJ/ cm^2 at 157 nm can further be imaged with another dose of 220 mJ/ cm^2, figure 6-14 B. The values of red, green and blue in the exposed and unexposed regions in figure 6-14 A and in regions 1, 2, and 3 in figure 6-14 B are reported in table 6-4.

In figure 6-14 B there are three regions clearly delimitated: 1-single exposure, 2 – double exposure, and 3- no exposure. Region 3 in figure 6-14 B corresponds to the unexposed region in figure 6-14 A. While the value of green is close, blue is approximately 20 % more in region 3. This may be due to the fact that it is just a small area of unexposed film, surrounded by wide regions that emit in blue. It is hard to establish which region 1 (single exposure) was exposed first time or the second time, since all single-exposed regions have the same color. This proves that regions non-exposed first time can be imaged to the same extent as the areas exposed first. As expected, the value of blue in region 1 is very close to the value of blue in the exposed regions from 6-14 A, since both received the same incident dose. Region 2 shows the highest value for blue and green. However, the amount of blue comprising region 2 is only 1.2 times higher compared to region 1 or to the exposed region in figure 6-14 A. This shows that most of pyrene existed as dimers after the first 200 shots, and that only a small fraction was not associated when the next 200 shots were delivered to the film.

6.3.3 Studies of temperature effects on PMSSQ films containing pyrene

Since Tg is a determining parameter in the formation and evolution of images, a polymer with a very low Tg was selected for further investigations. Poly(methylsilsesquioxane), whose structure is shown in figure 6-3, has a Tg below room temperature (RT), and it is transparent at 248 and 308 nm, figure 6-4. Although absorbance at 157 nm was not determined, its absorbance must be low, since polysiloxanes and polyhedral silsesquioxanes were good candidates for lithography at 157 nm.[41] Imaging experiments with PMSSQ films containing pyrene were done following the same experimental procedure as in the case of PMMA and FP films. Irradiating a film at 157 nm with 200 mJ/ cm^2, after PAB, did not result in formation of hexagonal patterns, figure 6-15 A. The film irradiated without PAB showed clear and nice hexagonal patterns, with a stronger blue than in the case of FP and PMMA films, figure 6-15 B. This behavior prompted more investigations using spectroscopic techniques. Films without PAB showed clear absorption and fluorescence peaks characteristic to pyrene, figure 6-16. After baking 1 minute at 98 °C, the signals characteristic to pyrene disappeared. Experiments done with PMSSQ films containing pyrene and sandwiched between two quartz discs, figure 6-17, showed that pyrene signal is present in the absorption spectra even after 4 minutes of baking at 98 °C. The absorbance did not change even after four minutes, while for the non-sandwiched film the signal disappeared after only one minute. This suggests that pyrene sublimes from PMSSQ films during PAB, unlike in the case of PMMA and FP films.

Interestingly, images of PMSSQ films containing pyrene, exposed first to 200 mJ/ cm^2 at 157 nm, then baked at 100 °C even for 10 minutes, were not erased as in the case of PMMA films, but their intensity was slightly altered by the high temperature. While for unexposed PMSSQ films 1 minute of baking is enough to

allow all the pyrene to sublime, for exposed PMSSQ films 10 minutes of PEB is not enough to remove the pyrene from the exposed regions, figure 6-18 B. This means that pyrene is trapped inside the polymer matrix due to transformations that occur during exposure to radiation. The most probable transformation is photocrosslinking of the polymer chains induced by the high energy photons. Photocrosslinking may have created a network that trapped the pyrene molecules or the pyrene dimers, stopping them from sublimation. It is difficult to characterize the polymer after irradiation due mainly to the extremely small amount of samples available (films are ~ 470 nm thick with a one inch diameter). Further investigations using fluorescence microscopy as a tool were done with PMSSQ films double exposed to 157 nm, figure 6-19.

Another explanation for the retention of pyrene in the films exposed to laser radiation prior to any baking, is the possibility of photochemical reactions involving pyrene and the methyl CH_3- group from PMSSQ, as well as solvent molecules (the imaged PMSSQ films were not baked prior to exposure). This is even more strongly supported by the images which were not erased after 10 minutes of baking at ~ 100 °C, unlike in the case of PMMA in which the images were erased. Previous reports in literature show that polycyclic aromatic hydrocarbons may be chemically attached to the polymer chain following exposure to UV and γ radiation.[45-48] Thus pyrene may be covalently bound to the polymer network, stopping it from leaving the film during baking at ~ 100 °C. Crosslinking may also involve two neighbor hydroxyl group (HO-) which may lead to elimination of a water molecule and formation of a new -Si-O-Si- covalent bond. Elimination of water may be favored by the high temperatures which are probably reached during the laser pulse and immediately after. Thermal curing is one way by which PMSSQ films are obtained, at temperatures between 100 – 450 °C.[52]

There are more examples from the literature that deal with some of the possible routes that excited pyrene molecules in polymer films can follow to release their excess energy. Although pyrene is an aromatic polycyclic hydrocarbon

capable of absorbing up to ten photons at 248 nm forming higher excited states, then release the excess energy as heat or light,[34] there are previous reports in literature that show how pyrene is involved in photochemical reactions in polymer films exposed to radiation in the DUV and VUV, as well as gamma (γ) radiation.[45-47] Thomas et *al.* reported on covalently bound pyrene to polymer in polyethylene films irradiated with γ rays (10 kGy) at room temperature.[45] In their transient absorption spectra, they noticed signals characteristic to pyrene transients species at 420 nm ($^3Py^*$), 450 nm ($Py^{+\cdot}$), and 490 nm ($Py^{-\cdot}$). Their mechanism proposes that pyrene is attacked by polymer radicals, acting as a radical quencher. Irradiated polymer films without pyrene exhibited crosslinking, while those containing pyrene did not cross link.

In another literature report, Lamotte *et al.* described the photolysis of pyrene and perylene in cyclohexane solution exposed to UV radiation from a mercury lamp.[46] They observed the presence of ionic species, formed through photolysis of the solvent, a process that is possible through energy transfer from the pyrene molecule in a high triplet state to the solvent. These high triplet states may be formed via a two-photon mechanism. The first absorbed photon determines the S_0-S_1 transition of pyrene, followed by ISC to T_1. The longer lived pyrene triplet may absorb a second photon, being excited into higher triplet states (T_n). The same group had previously reported on solvent molecules covalently bound to pyrene in cyclohexane matrix at 77 K, exposed to radiation from an Hg lamp.

Weiss *et al.* reported on films of low density polyethylene (LDPE) doped with pyrene (2.4×10^{-2} M), then exposed to radiation from a 450-W Hg lamp under nitrogen, for one hour.[47] They demonstrated that the dopant molecules were covalently attached to the polyethylene chain. Their goal was to determine the preferred sites of the dopant in the LDPE films, discovering that pyrene is located near the less ordered regions, and not on the crystalline domains. This is an

important finding for the present work as well, since it is possible that pyrene may preferentially be located in certain micro- or nano-domains of the polymer films.

There are previous reports in literature that signal the formation of pyrene excimer transients in polymer films and particles during exposure to radiation. Szadkowska-Nicze *et al.* published a series of articles in which they noticed formation of pyrene excimers in γ-irradiated polyethylene films doped with pyrene.[49-51] After the radiolysis pulse they were able to record emission spectra with peaks at ~ 390 and 475 nm, characteristic to the fluorescence from the monomer and the excimer respectively (experiments done at 287 K). The lifetime of the excited monomer was found to be 410 ns for a concentration range $2.6 \times 10^{-3} - 1.24 \times 10^{-2}$ M. Their explanation is that the formation of the excimer is favored by the long lifetime of the excited monomer, and by the fact that the two molecules may be in close proximity, allowing an energy transfer from the excited molecule to the molecule in ground state, and formation of the excimer. They refer to results obtained by others, and consider that the liquid-like mobility of the molecules in amorphous regions of the polymer favors the diffusion of the pyrene molecules and thus formation of the excimer. They noticed this behavior only at room temperature; experiments performed at 200 K did not show any emission characteristic to the excimer. The lower temperature did not allow the diffusion of the pyrene molecules through the polyethylene film, and consequently the excimer did not form.

In the case of our experiments involving double exposure, PMSSQ films behave differently compared to PMMA films. While in the case of PMMA films after the second exposure one could distinguish three regions, in the case of PMSSQ films there are four regions easily distinguishable, figure 6-19 B: 1- unexposed region (0 mJ/ cm^2), 2 – region exposed first time, unexposed second time (200 mJ/ cm^2), 3 – region exposed two times (400 mJ/ cm^2), and 4- region unexposed first time, exposed second time (200 mJ/ cm^2). The PMMA films imaged second time were not baked after the first exposure, unlike the PMSSQ films. PMSSQ films were baked 1 minute after the first exposure, and this caused pyrene from the

unexposed regions to sublime. This shows better, on the same film, the difference between the exposed and unexposed regions of the PMSSQ films. To get quantitative data, the contribution of red, green and blue, in the exposed and unexposed regions from figure 6-19, were measured (a.u.) with the DigitalColor Meter v.3.2 from Apple Computer Inc., and the values are reported in table 6-5.

Table 6-5. The values of the colors red, green, and blue (a.u.) in the exposed, and unexposed regions from a PMSSQ film containing pyrene (0.5 wt % based on PMSSQ weight), and exposed through the copper mask to laser radiation at 157 nm, 200 mJ/ cm^2 and 400 mJ/ cm^2 respectively, figure 6-19 A and B. The thickness of the film is ~ 460 nm.

Colors	**A (200 mJ/ cm^2)**		**B (400 mJ/ cm^2)**			
	Exposed	**Unexposed**	**Region 1**	**Region 2**	**Region 3**	**Region 4**
red	3600	1300	1000	3600	3300	1000
green	15900	3100	4100	14100	13100	2800
blue	65000	9000	13400	59400	42900	9000

1 – region non exposed (0 mJ/ cm^2), 2- region exposed first time, unexposed second time (200 mJ/ cm^2), 3- region exposed two times (400 mJ/ cm2), and 4- region unexposed first time but exposed second time after 1 minute PEB (200 mJ/ cm^2).

The increase in the blue and green for PMSSQ films compared to PMMA and FP films is much higher. The increase in green and blue is associated with formation of excimers or aggregates which emit in the region centered at ~ 470 – 480 nm, which correspond to blue in the visible spectrum. While for PMMA and FP films the increase (I_{exp}/ I_{unexp}) in the regions exposed to the same dose of radiation at 157 nm, 200 mJ/ cm^2, is between 1.3 and 2.5, in the case of PMSSQ the increase (I_{exp}/ I_{unexp}) for green in the exposed region is 5.16, while for blue is 7.22. This can

also be noticed from the strong blue color (figure 6-18 A and 6-19 A) that appears in the fluorescent images recorded after exposure of PMSSQ films to radiation at 157 nm compared to the colors obtained with PMMA and FP films. This is partly related to the Tg below RT, allowing pyrene molecules to diffuse easier in PMSSQ films compared to PMMA and FP films. Previous reports in literature describe PMSSQ as a porous material[42], porosity favoring diffusion of pyrene molecules. Pyrene shows a high mobility and diffusion coefficient in a polymer similar to PMSSQ, poly(dimethylsiloxane), authors showing its ability to form excimers upon excitation with radiation at 337 nm.[43] Based on the results obtained in this work, one can conclude that pyrene diffuses easier in PMSSQ compared to PMMA and PFP, thus showing a higher diffusion coefficient. Region 3, double exposed, from figure 6-19 B shows less green and blue compared to region 2, as it can be seen from data presented in table 6-5. This is the opposite situation compared to PMMA films, where second exposure resulted in an approximately 20 % increase in blue, table 6-4 and figure 6-14 B. PEB for 32 minutes erased the difference between regions 2 and 3 and an overall decrease in blue and green in the exposed regions, figure 6-19 D. Quantitative data is reported in table 6-6.

Table 6-6. Values of red, green, and blue and their ratio (I_{exp}/ I_{unexp}) in the exposed and unexposed regions of the PMSSQ film containing pyrene (0.5 wt % based on PMSSQ) and exposed to 157 nm, 400 mJ/ cm^2/ shot, shown in figure 6-19 D.

Color	PMSSQ		
	Exposed	**Unexposed**	**I_{exp}/ I_{unexp}**
red	3900	1000	3.9
green	13100	2800	4.7
blue	47000	8700	5.4

The intensity of emission decreased after 32 minutes of PEB. The ratio I_{exp}/I_{unexp} decreased from 5.16 to 4.63 for green and from 7.22 to 5.38 for blue. However, it is still much higher compared to PMMA and FP films. This shows that PMSSQ retains pyrene much better than PMMA and FP due to photocrosslinking. Photocrosslinking may have as effect an increase in Tg. While PMSSQ shows crosslinking, PMMA and FP suffer most probably chain scission and pendant group scission as shown also in previous reports.[44] This finding is important in lithographic applications. In positive resists the exposed regions become soluble in developing solvents. Using PMSSQ at 157 nm is not the best option, photocrosslinking decreasing the solubility in the exposed regions, contrary to the expected effect.

To assess the influence of oxygen on emission and absorption of polymer films containing pyrene, experiments with deaerated solutions (nitrogen bubbled) were performed. PMMA films containing pyrene (0.33 wt % based on PMMA) obtained from a deaerated solution were spin coated and their absorbance measured and compared to that of films obtained from aerated solution, figure 6-20. Regarding absorbance and fluorescence, there is no difference between the two films before and after exposure to 200 shots at 157 nm. However, the films were under air when spectra were recorded for both absorbance and fluorescence. To overcome this inconvenient, fluorescence microscopy experiments were done, with the films under nitrogen atmosphere all the time, except spin coating and baking. The whole microscope set-up was under N_2 atmosphere. Double exposure experiments with FP films under N_2 show the same behavior as in open air. In figure 6-21 D the image shows that after one day at RT under N_2 atmosphere the image was preserved. PMSSQ films containing pyrene were also imaged under N_2 atmosphere, figure 6-22. Unlike FP films, the image in the case of PMSSQ films lost intensity after one day under N_2 at RT and only the non exposed regions (dark regions) were visible.

Continuous wave exposure did not produce any change in intensity of emission or in the absorption spectrum, figure 6-23, even after 500 s of exposure with a mercury lamp (see figure 4-1 C for the emission spectrum of the lamp). This shows that excimer formation is determined only by the laser radiation. The high density of photons per unit area is probably the key difference.

6.4 Experimental

6.4.1 Materials

Pyrene (Aldrich) was recrystalized from ethanol prior to using. Poly(methylsilsesquioxane) (PMSSQ) and the fluorinated polymer (FP) were a kind gift from Rohm and Haas Electronics Materials from Marlborough, MA, poly(methyl methacrylate) (PMMA) ($M_w \sim 1.0 \times 10^6$, polydispersity ~ 1.1) was purchased from Polysciences Inc.. The solvent 2-heptanone (Aldrich) was used as received.

6.4.2 Equipment and techniques

The thin films were obtained by spin coating solutions containing polymer and pyrene dissolved in 2-heptanone, on one inch (2.54 cm) diameter quartz discs at 2000 rpm (rotations per minute) for 20 s, using a spin coater from Specialty Coatings, Inc.. The solutions were filtrated through a 0.45 μm (micrometer) teflon filter prior to spin casting. The thickness of the polymer films was measured with a TFA-11 thin film analyzer from Luzchem Research, Ottawa, ON. The spin coated solutions contained: a) 80 % weight 2-heptanone, 20 % weight fluorinated polymer (FP) and pyrene 0.5 weight % based on the dry polymer weight, b) 15 % weight PMMA, 85 % weight 2-heptanone, and pyrene 0.33 % weight from dry PMMA weight, c) 80 weight % 2-heptanone, 20 weight % PMSSQ, and pyrene 0.5 weight % from PMSSQ weight. After coating the films were baked in an oven at 95 – 98 °C for one minute, allowing evaporation of the solvent.

Laser exposure was done using GSI-Lumonics Pulsemaster model 846 fluorine excimer lasers for 157 and 248 nm, and a Lumonics Excimer-500 laser

containing HCl for 308 nm. The gas mixture for 157 nm consisted of 0.09 % F_2 and the rest He up to 100 %, pressure 2950 mbar, while for 248 nm the mixture consisted of F_2 0.14 %, Kr 2.0 % and the balance gas was Ne for the difference up to 100 %, with a total pressure of 5000 mbar. Continuous wave exposure was done with a Hybrid Technology Group exposure unit using a mercury lamp and filter such that the light wavelength was centered at 248 nm (see figure 4-1 B for power and spectrum of the lamp). The energy of the incident laser beam was measured with a JD2000 joulemeter radiometer and a Coherent J45LP-MB photon detector. In order to obtain the patterns, copper masks with hexagonal holes were placed on top of the films. The centers of the hexagons were 60 μm (micrometers) apart. The mask had to have holes because laser radiation at 157 nm is absorbed by almost any material. The exposures at 157 nm were done under nitrogen atmosphere. For all the other wavelengths the exposure was done under air, in the laboratory atmosphere. Continuous wave exposure was done in a Hybrid Technology Group exposure tool, model 64-10X. Fluorescence spectra were recorded using a front-face set up in a LS-50 Perkin Elmer luminescence spectrometer.

The contribution of red, green, and blue in the images presented in this work was analyzed using the RGB standard and quantitatively measured with an application called DigitalColor Meter version 3.2 from Apple Computer Inc. This application determines and quantifies the fundamentals red, green, and blue colors that contribute to the final color of any pixel on the screen.

Fluorescence emission of the films was recorded using a Perkin-Elmer LS 50 fluorimeter in a front-face set-up and variable slits for emission and excitation. The temperature control for the experiments that required monitoring of fluorescence as a function of temperature was done by placing the disc on a hot surface whose temperature was controlled by a thermostat. The films were allowed to stay for five minutes at the temperature shown on the display of the apparatus in to ensure that they reached it. Solution emission was recorded with a Photon Technology

Instruments fluorimeter using 1 cm optical path quartz rectangular fluorescence cuvettes.

Fluorescence microscopy experiments were done using a Leica DMLS optical microscope with a 20 x magnifying objective for most of the experiments, except figure 6-13 where a 100x magnifying objective was employed. The power of the mercury lamp in the microscope was 50 W, and the images were recorded with a Leica DFC 300 FX camera. The software used to record images was IM50 version 4 release 117 from Leica. An XF-02 filter cube (excitation centered at 367 nm, emission long pass 470 nm) from Omega Optics was used to monitor fluorescence of pyrene excimers. The spectrum of this filter was recorded with a Luzchem SPR-1 spectroradiometer, and is displayed in figure 6-10.

The TGA and DSC of FP were recorded at the same time with a 2960 SDT V3.0F instrument, STD_MS method, with a heating rate of 20 °C/ min, between room temperature and 1000 °C, under an air flow of 100 mL/ min. The sample mass was 12.76 mg.

6.5 Conclusions

The experimental results presented in this chapter reveal an interesting behavior of pyrene in polymer films exposed to laser radiations of different wavelengths. Pyrene functions both as fluorescent probe and as dopant, inducing changes in the physico-chemical properties of the polymer films. As dopant pyrene helps in transferring energy from the incident photons to the polymer matrix, while as fluorescent probe it shows how diffusion and mobility of molecules in thin films exposed to laser radiation are affected. Diffusion of pyrene in films is favored by the softened polymer matrix. Heat released by pyrene molecules through vibrational relaxation (VR) and internal conversion (IC) is transferred to the polymer matrix, raising the temperature around the molecules of the dopant. This favors the encounter between a pyrene molecule in excited state and a molecule in ground state. The newly formed entity, the excimer, decays either through emission or IC. However, unlike the case of excimers in solution, in the polymer matrix the excimer is not destroyed, the molecules being forced by the surrounding matrix to stay together in the sandwich-like conformation even after relaxation to the ground state (GS). This is easily observed in the fluorescence spectra recorded with films exposed to laser radiation. The intensity of the monomer decreased, but the emission increased in the region around 470 - 480 nm, characteristic to excimer emission. Images recorded with the fluorescence microscope are even more suggestive, the strong blue in the exposed areas of films containing pyrene being a proof of excimer or aggregates formation.

The differences between polymers are emphasized by PMMA and PMSSQ films. While in PMMA the only changes regarding pyrene are formation of excimers, in the case of PMSSQ a combination of excimer formation and

photochemistry (photocrosslinking, pyrene bonding to the polymer) explain the experimental results obtained.

Formation of excimer is influenced by the properties of the polymer matrix. Polymers with different Tg were studied. The possibility of double imaging, the fact that some of the images resist even for days, while some are capable of withstanding high temperature without being erased could be exploited for application in information storage or in fabrication of security devices based on thin polymer films. Instead of having the hexagonal mask, one could have any text, writing or symbol such as a bar code, which is not visible with the naked eye but only under excitation with light of a suitable wavelength. Exploiting some of the results presented in this chapter may help to photochemically functionalize polymer films and nano- or micro-particles.

6.6 References

(1) Gilbert, A.; Baggot, J. *Essentials of Molecular Photochemistry* **1991**, *CRC Press*.

(2) Kropp, J. L.; Dawson, W. R.; Windsor, M. W. "Radiative and Radiationless Processes in Aromatic Molecules. Pyrene", *J. Phys. Chem.* **1969**, *73*, 1747-1752.

(3) Siu, H.; Duhamel, J. "Global Analysis of the Fluorescence Decays of a Pyrene-Labeled Polymer Using a Blob Model", *Macromolecules* **2004**, *37*, 9287-9289.

(4) Avis, P.; Porter, G. "Effect of Concentration on the Absorption and Fluorescence Spectra of Pyrene in a Solid Solution of Poly(methyl methacrylate)", *J. Chem. Soc., Faraday Trans. 2* **1974**, *70*, 1057-1065.

(5) Johnson, G. E. "Effect of Concentration on the Fluorescence Spectra and Lifetimes of Pyrene in Polystyrene Films", *Macromolecules* **1980**, *13*, 839 - 844; Nakashima, K., Winnik, M. A., Dai, K. H., Kramer, E. J., Washiyama, J. "Fluorescent Probe Studies on the Microstructure of Polystyrene-Poly(vinyl pyridine) Diblock Copolymer Film", *Macromolecules* **1992**, *25*, 6866-6870.

(6) Yanagimachi, M.; Toriumi, M.; Masuhara, H. "Selective Incorporation and Aggregation of Pyrene in a Segmented Poly(urethane urea) Film as revealed by Picosecond Total Internal Reflection Fluorescence Spectroscopy", *Chem. Mater.* **1991**, *3*, 413-418.

(7) Itaya, A.; Matsumoto, Y.; Iou, I.; Masuhara, H. "Aggregation of pyrene in poly(alkyl methacrylate) films revealed by time-resolved total internal reflection fluorescence spectroscopy", *Polymer* **1994**, *35*, 3920-3926.

(8) Siu, H.; Prazeres, T. J. V.; Duhamel, J.; Olesen, K.; Shay, G. "Characterization of Aggregates Made by Short Poly(ethylene oxide) Chains Labeled at One End with Pyrene", *Macromolecules* **2005**, *38*, 2865-2875.

(9) Nicze-Szadkowska, M.; Wolszczak, M.; Kroh, J.; Mayer, J. "Concentration Dependence of pyrene excimer formation in doped polyethylene", *J. Photochem. Photobiol. A: Chem.* **1993**, *75*, 125-129.

(10) Pujari, S. R.; Kambale, M. D.; Bhosale, P. N.; Rao, P. M. R.; Patil, S. R. "Optical properties of pyrene doped polymer thin films", *Mat. Res. Bull.* **2002**, *37*, 1641-1649.

(11) Anandan, C.; Bharathibai, J. B.; Rajam, K. S. "Study of the diffusion of pyrene in silicone polymer coatings by steady state fluorescence techniques: effect of pyrene concentration", *Eur. Pol. J.* **2004**, *40*, 1833-1840.

(12) Tseng, K. C.; Turro, N. J.; Durning, C. J. "Tracer diffusion in thin polystyrene films", *Polymer* **2000**, *41*, 4751-4755.

(13) Strukelj, M., Martinho, J. M. G., Winnik, M. A., Quirk, R. P. "Intermolecular Excimer formation for Pyrene-End-Capped Polystyrene: A Model for the Termination Process in Free-Radical Polymerization", *Macromolecules* **1991**, *24*, 2488-2492; Kim, D. S.; Torkelson, J. M. "Nanoscale Confinement and Temperature Effects on Associative Polymers in Thin Films: Fluorescence Study of a Telechelic, Pyrene-Labeled Poly(dimethylsiloxane)", *Macromolecules* **2002**, *35*, 5943-5952.

(14) Ellison, C. J.; Torkelson, J. M. "Sensing the Glass Transition Temperature in Thin and Ultrathin Polymer Films via Fluorescence Probes and Labels", *J. Pol. Sci.: Part B: Pol. Phys.* **2002**, *40*, 2745-2758.

(15) Sluch, M. I.; Vitukhnovsky, A. G.; Petty, M. C. "Pyrene Excimer Formation in Langmuir-Blodgett Films", *Thin Solid Films* **1996**, *284-285*, 622-626.

(16) Matsui, J.; Mitsuishi, M.; Miyashita, t. "A Study on Fluorescence Behavior at the Interface of Polymer Langmuir-Blodgett Films", *J. Phys. Chem. B* **2002**, *106*, 2468-2473.

(17) Dutta, A. K.; Misra, T. N. "A Spectroscopic Study of Nonamphiphilic Pyrene Assembled in Langmuir-Blodgett Films: Formation of Aggregates", *Langmuir* **1996**, *12*, 459-465.

(18) Cione, A. P. P.; Scaiano, J. C.; Neuman, M. G.; Gessner, F. "The excimer emission of aromatic hydrocarbons on clays", *J. Photochem. Photobiol. A: Chem.* **1998**, *118*, 205-209.

(19) Labbe, P.; Reverdy, G. "Adsorption Characteristics of Polycyclic Aromatic Compounds on Clay: Pyrene as a Photophysical Probe on Laponite", *Langmuir* **1988**, *4*, 419-425.

(20) Suib, S. L.; Kostapapas, A. "Intermolecular Pyrene Excimer-Formation in Zeolites. Decay Parameters and Ground-State Association", *J. Am. Chem. Soc.* **1984**, *106*, 7705-7710.

(21) Winnik, M. A., Bystryak, S. M., Siddiqui, J. "Interaction of Pyrene-Labeled Poly(ethylene imine) with Sodium Dodecyl Sulfate in Aqueous Solution", *Macromolecules* **1999**, *32*, 624-632; Kalyanasundaram, K.; Thomas, J. K. "Environmental Effects on Vibronic Band Intensities in Pyrene Monomer Fluorescence and Their Application in Studies of Micellar Systems", *J. Am. Chem. Soc.* **1977**, *99*, 2039-2044.

(22) Rharbi, Y., Chen, Liusheng, Winnik, M. "Exchange Mechanisms for Sodium Dodecyl Sulfate Micelles: High Salt Concentration", *J. Am. Chem. Soc.* **2004**, *126*, 6025-6024; Bohne, C.; Abuin, E. A.; Scaiano, J. C. "Triplet-Triplet Annihilation of Pyrene Derivatives as Mobility Probes in Sodium 1,4-Bis(2-ethylhexyl)sulfosuccinate/Water/Isooctane Reversed Micelles", *Langmuir* **1992**, *8*, 469-474.

(23) Zhang, X.; Zhang, X.; Shi, W.; Meng, X.; Lee, C.; Lee, S. "Morphology-Controllable Synthesis of Pyrene Nanostructures and its Morphology Dependence of Optical Properties", *J. Phys. Chem. B* **2005**, *109*, 18777-18780.

(24) Martins, T. D.; Yamaki, S. B.; Prado, E. A.; Atvars, T. D. Z. "Broadening of the fluorescence spectra of hydrocarbons in ethylene-vinyl acetate copolymers and the dynamics of the glass transition", *J. Photochem. Photobiol. A: Chem.* **2003**, *156*, 91-103.

(25) Mayer, J.; Szreder, T. "Excimer probing of phase transition in polypropylene", *J. Photochem. Photobiol. A: Chem.* **2000**, *134*, 71-75.

(26) Chu, D. Y.; Tohomas, J. K. "Photophysical Studies of Molecular Mobility in Polymer Films and Bulk Polymers. 3. Dynamic Excimer Formation of Pyrene in Bulk PDMS", *Macromolecules* **1990**, *23*, 2217-2222.

(27) Srinivasan, R.; Brare, B. "Ultraviolet Laser Ablation of Organic Polymers", *Chem. Rev.* **1989**, 1303 - 1316.

(28) Lippert, T. K.; Dickinson, J. T. "Chemical and Spectroscopical Aspects of Polymer Ablation: Special Features and Novel Directions", *Chem. Rev.* **2003**, *103*, 453-485.

(29) Lippert, T. K.; Webb, R. L.; Langford, S. C.; Dickinson, J. T. "Dopant induced ablation of poly(methyl methacrylate) at 308 nm", *J. Appl. Phys.* **1999**, *85*, 1838-1847.

(30) Hiroshi, M.; Hiraoka, H.; Domen, K. "Dopant-Induced Ablation of Poly(methyl methacrylate) by a 308-nm Excimer Laser", *Macromolecules* **1987**, *20*, 450-452.

(31) Webb, R. L.; Langford, S. C.; Dickinson, J. T.; Lippert, T. K. "Sensitization of PMMA to laser ablation at 308 nm", *Appl. Surf. Sci.* **1998**, *127-129*, 815-820.

(32) Fujiwara, H.; Fukumura, H.; Masuhara, h. "Laser Ablation of Pyrene-Doped Poly(methyl methacrylate) Film: Dynamics of Pyrene Transient Species by Spectroscopic Measurements", *J. Phys. Chem.* **1995**, *99*, 11844-11853.

(33) Webb, R. L.; Langford, S. C.; Dickinson, J. T.; Lippert, T. K. "Sensitization of PMMA to laser ablation at 308 nm", *Appl. Surf. Sci.* **1998**, *127-129*, 815-820.

(34) Fujiwara, H.; Hayashi, T.; Fukumura, H.; Masuhara, H. "Each dopant can absorb more than ten photons: Transient absorbance measurement at excitation laser wavelength in polymer ablation", *Appl. Phys. Lett.* **1994**, *64*, 2451-2453.

(35) Bolle, M.; Lazare, S.; Le Blanc, M.; Wilmes, A. "Submicron periodic structures produced on polymer surfaces with polarized excimer laser ultraviolet radiation", *Appl. Phys. Lett.* **1992**, *60*, 674-676.

(36) Niino, H.; Nakano, M.; Nagano, S.; Yabe, A.; Miki, T. "Periodic morphological modification developed on the surface of polyethersulfone by XeCl excimer laser photoablation", *Appl. Phys. Lett.* **1989**, *55*, 510-512.

(37) Dyer, P. E.; Farley, R. J. "Periodic surface structures in the excimer laser ablative etching of polymers", *Appl. Phys. Lett.* **1990**, *57*, 765-767.

(38) Yamamoto, S.; Tsujii, Y.; Fukuda, T. "Glass Transition Temperatures of High-Density Poly(methyl methacrylate) Brushes", *Macromolecules* **2002**, *35*, 6077-6079.

(39) Yatsuhashi, T.; Nakashima, N. "VUV Laser Chemistry - Formation of Hot Molecules and Their Reactions in the Gas Phase", *Bull. Chem. Soc. Jpn.* **2001**, *74*, 579-593.

(40) Lee, K.; Jockusch, S.; Turro, N. J.; French, R. H.; Wheland, R. C.; Lemon, M. F.; Braun, A. M.; Widerschpan, T.; Dixon, D. A.; Li, J.; Ivan, M.;

Zimmerman, P. "157 nm Pellicles (Thin Films) for Photolithography: Mechanistic Investigation of the VUV and UV-C Photolysis of Fluorocarbons", *J. Am. Chem. Soc.* **2005**, *127*, 8320-8327.

(41) Bellas, V.; Tegou, E.; Raptis, I.; Gogolides, E.; Argitis, P.; Iatrou, H.; Hadjichristidis, N.; Sarantopoulou, E.; Cefalas, A. C. "Evaluation of siloxane and polyhedral silsesquioxane copolymers for 157 nm lithography", *J. Vac. Sci. Technol. B* **2002**, *20*, 2902-2908.

(42) Burleigh, M.; Markowitz, M. A.; Spectors, M.; Gaber, B. P. "Porous Polysilsesquioxanes for Adsorption of Phenols", *Environ. Sci. Technol.* **2002**, *36*, 2515-2518.

(43) Chu, D. Y.; Thomas, J. K. "Photophysical Studies of Molecular Mobility in Polymer Films and Bulk Polymers. 3. Dynamic Excimer Formation of Pyrene in Bulk PDMS", *Macromolecules* **1990**, *23*, 2217-2222.

(44) Fedynyshyn, T. H.; Kunz, R. R.; Sinta, R. F.; Goodman, R. B.; Doran, S. P. "Polymer photochemistry at advanced optical wavelengths", *J. Vac. Sci. Technol. B* **2004**, *18*, 3332.

(45) Biscoglio, M.; Thomas, J. K. "Radiolysis of Polyethylene Films Containing Arenes: Bromopyrene Dissociation and Pyrene Binding in Polymer Films", *J. Phys. Chem B* **2000**, 104, 475 - 484.

(46) Lamotte, M.; Pereyre, J.; Joussot-Dubien, J.; Lapouyade, R. "The photolysis of Pyrene and Perylene in Cyclohexane Liquid Solution from Highly Excited Electronic States", *J. Photochem* **1987**, *38*, 177 – 188.

(47) Naciri, J.; Weiss, R. G. "New Methods for the Determination of Dopant Site Distributions and Dopant Rates of Diffusion in Polymer Films: Emission from Pyrenyl Groups Covalently Attached to Low-Density Polyethylene", *Macromolecules* **1989**, *22*, 3928 – 3936.

(48) Joussot-Dubien, J.; Lamotte, M.; Pereyre, J. "The indirect Two-Photon Photolysis of Polycyclic Aromatic Hydrocarbons and Benzene in Rigid Matrixes", J. Photochem. **1981**, *17*, 347 – 354.

(49) Szadkowska-Nicze, M.; Mayer, J.; Kroh, J. "Excimer formation in irradiated high density polyethylene doped with aromatics", *J. Photochem. Photobiol. A: Chem.* **1990**, *54*, 389 – 396.

(50) Szadkowska-Nicze, M; Wolszczak, M.; Kroh, J.; Mayer, J. "Concentration dependence of pyrene excimer formation in doped polyethylene" *J. Photochem. Photobiol. A: Chem* **1993**, *75*, 125 – 129.

(51) Szadkowska-Nicze, M.; Kroh, J; Mayer, J. "Excited State Formation in Pulse Irradiated Polyethylene Doped with Aromatics" *Radiat. Phys. Chem.* **1995**, *45(1)*, 87 – 91.

(52) Lazzeri, P.; Vanzetti, L.; Anderle, M.; Bersani, M.; Park, J. J.; Lin, Z.; Briber, R. M.; Rubloff, G. W.; Kim, H. C.; Miller, R. D. "Thin-film transformations and volatile products in the formation of nanoporous lok-k polymethylsilsesquioxane-based dielectric", *J. Vac. Sci. Technol. B.* **2005**, *23(3)*, 908 – 917.

Conclusions, Claims to Original Research, and Future Directions

7. Conclusions, Claims to Original Research, and Future Directions

7.1 Conclusions

The research done as a part of the PhD requirements at University of Ottawa, in the Department of Chemistry was focused on photochemical and photophysical processes that occur mainly in polymer films. The immediate application is in the microelectronics industry, but the results obtained here may be applied in other fields as well. The wavelengths of the light emitted by the irradiation sources used were 308, 254 (Hg lamp), 248, 193 and 157 nm. Experimental techniques and protocols that allow detection and quantification of the acid produced during exposure of polymer films containing PAGs were developed. The main challenge was to develop protocols that allow the researcher to work with very small amounts of material, in films that are only a few hundreds of nanometers thick.

The project at 157 nm was particularly challenging due to the high absorbance of almost all the organic compounds. The exposures were done under N_2 atmosphere at all times, in a box especially designed for this project. The experimental set up suffered a few changes during the years this research was carried, until an optimum design was acquired.

Many techniques were employed in order to gather information about the chemical and physical changes triggered by photons in the exposed materials. Absorption in UV-vis and fluorescence spectroscopy were extensively used, on daily basis. FTIR and excitation spectroscopy were also used. Fluorescencent sensors have been the most important way to monitor chemical species present in the films, but physical changes as well. A series of sensors were developed in

the lab, others were commercially available. Fluorescence microscopy was employed on a large scale since it is one of the best methods to observe changes in the polymer films exposed, showing a clear contrast between the exposed and unexposed areas in the same image. Atomic force microscopy revealed the physical transformation that occurred on the surface of the exposed films.

^{1}H, ^{13}C and ^{19}F NMR, gel permeation chromatography (GPC), high performance liquid chromatography (HPLC) coupled to MS, GC/MS, and EPR (electron paramagnetic resonance spectroscopy) were used for projects that were not presented here, but that also involved photochemistry.

7.2 Claims to Original Research

Fluorescent sensors were used in order to gain information about acid formation in thin films following photolysis of PAGs.

1. The fluorescent pH sensitive Coumarin 6 was used to quantify acid in polymer films exposed to 157 nm. While this dye had been previously been used at other wavelengths, it was shown here to work very well even when exposed to 157 nm, a very energetic radiation that may damage it.
2. A protocol that would allow detection of the catalytic chain length (CCL) was developed. This protocol is different than previously reported methods which employed monitoring of the carbonyl from the *t*-Boc group using FTIR spectroscopy. The method presented here is a new concept, and one of the few attempts made during the last few decades to measure the CCL. The precise quantification of acid by doing *in-film* acid-base

titration coupled with the use of Coumarin 6 as acid sensor, combined with the information about the number of *t*-Boc group deprotected, offered by C4*t*-Boc sensor, allowed calculations of CCL.

3. Hydrofluoric acid (HF) was detected to be formed in thin films of a fluorinated polymer exposed to 157 nm using the halide-sensitive sensor C4TIPS.
4. Other sensors for fluoride were characterized in solution, working very well even at small concentrations (BTTIPS and CNCTIPS).
5. New photoacid generators, benzofused sulfonium salts, more transparent and thus suitable for optical lithography in VUV region have been tested for the first time in conditions similar to those employed in industry.

The photochemical and photophysical changes of polymers exposed to laser radiation were studied.

1. It was found, using a fluorescent sensor that HF was formed in fluorinated polymers during exposure to radiation at 157 nm.
2. Pyrene was used to obtained information about polymers exposed to laser radiation. The results are very useful for photolithography using PMSSQ as polymer matrix. The formation of pyrene excimer and the fact that it remains in the sandwich-like arrangement after emission is a novel finding. The results obtained help to better understand the physical transformation that occur in the polymer film during exposure to energetic laser beams.
3. A method for measuring the absorbance using the laser as light source was designed and developed. It gave very good results at 193 nm, allowing calculation of quantum yields of acid generation. This method could work very well at 157 nm, provided that the laser beam is homogeneous and that the energy is very stable.

7.2.1 Collaborations

Some parts of projects presented in this thesis were realized in collaboration with other graduate students or post-doctoral researchers from the group. With Marie Laferrière I collaborated for detection of acid in polymer films containing photoacid generators, exposed to 157 nm, this being our first project involving exposure at this wavelength. The project on catalytic chain length was a collaboration with Mathieu Frenette, the result being a new method for calculation of this important parameter in CA photoresists. Photochemistry of polymers exposed to 157 nm was another example of collaboration with Marie Laferrière and Dr. Carlos Sanrame, who synthesized the fluorescent probes used to detect the formation HF in fluorinated polymer films.

Another project, not presented in this thesis, involved the study of photochemistry of monomeric materials exposed to laser radiation at 157 nm. Selected fluorinated monomers, that could be used to obtain fluorinated polymers for pellicles employed in photolithography in the VUV region, were exposed to 157 nm, and their photochemistry studied. This project was a collaboration with Kwangjoo Lee from the group of Prof. Nicholas J. Turro at Columbia University in New York.

The study of possible candidates for contrast enhancement materials used in optical lithography at 193 nm was a collaboration with Dr. Carlos Sanrame. The photochemistry of various acrylates exposed to 193 nm were studied in films using FTIR spectroscopy and in solution using GC/MS spectrometry, the paper being submitted for publication.

7.3 Future Directions

The field of microelectronics is a very dynamic one, with spectacular evolutions and cut edge science. Photochemistry has played a crucial role in the development of this field, and it is very likely to do so for many years to come. The topics covered in this thesis may further be developed and adapted to the evolutions in this field.

The detection and quantification of acid in thin films may be very useful in projects involving polymerization initiated by photo-induced formation of acid using PAGs as precursors. Since the PAG may play the role of the initiator, it is important to know how much initiator is produced. Immersion lithography at 193 nm which will be used for the coming years will still be based on CA resists.

CA amplified resists will son reach their limits in optical lithography applied for fabrication of CMOS, as the next projected radiation to be used is extreme ultraviolet (EUV) with a wavelength of only 13.4 nm. The projected size of the features to be obtained, 32, 22 nm and less, is too small and complications from acid diffusion will make it hard to obtain well defined walls and spaces. New, non-chemically amplified resists are tested. However, CA photoresists may be used in optical lithography for fabrication of MEMS (micro electromechanical systems), a field in which currently size feature is in the order of 3-5 μm, but is expected to reach the 1 μm size in the near future. In the fabrication of MEMS the current technology still employs diazonaphtoquinone/ novolac non CA resists. Thus, the findings regarding acid quantification may further be developed and employed in the case of these resists.

Photochemical and photophysical transformations of the polymers exposed to laser radiation may lead to new projects. Formation of pyrene excimers and the influence of the temperature may be studied further and the results exploited for creation of security features using thin polymer films. Using the right proper characterization tools one may look for formation of nanoaggregates of pyrene in thin films. The wavelength of the emitted light may depend on the size of the aggregates, which can be controlled by tuning the exposure wavelength, the molecular weight of the polymer, the concentration of pyrene, the solvent used for spin coating. Modified pyrene molecules can be used, or even chemically attached pyrene to the polymer backbone. Another possible application is photochemical modification of polymer micro- and nano-particles containing pyrene.

The results regarding the calculation of CCL using fluorescent probes can be applied into real *t*-Boc polymer systems, not just PMMA. By synthesizing a *t*-Boc protected polymer which upon deprotection may show fluorescence is a possible route. By doing calibration curves, it would then be possible to measure the extent of deprotection by looking at the intensity of fluorescence.

7.4 Publications

7.4.1 Articles in refereed journals

- **Marius G. Ivan**, Marie Laferrière, Carlos N. Sanrame, and J. C. Scaiano, „On the question of acid generation upon 157 nm laser exposure of fluorinated polymers", *Chemistry of Materials* 18, 2635 - 2641, **2006**.

- Kwangjoo Lee, Steffen Jockusch, Nicholas J. Turro, Roger H. French, Robert C. Wheland, M. F. Lemon, Andre M. Braun, Tatjana Widerschpan, David A. Dixon, Jun Li, **Marius Ivan**, Paul Zimmerman (2004) - *157 nm* „Pellicles for Photolithography: Mechanistic Investigation of the VUV and UV-C Photolysis of Fluorocarbons", *Journal of the American Chemical Society* **2005**, *127*, 8320-8327.

- M. Frenette, **M. G. Ivan**, and J. C. Scaiano: „Use of Fluorescent Probes to Determine Catalytic Chain Length in Chemically Amplified Resists", *Canadian Journal of Chemistry, 83*, 869-874, **2005**.

- Scaiano, J. C., Laferriere, M., **Ivan, Marius G.,** and Taylor, G. N. (2003) „A protocol for the verification of acid generation in 157 nm lithography" *Macromolecules* **2003**, *36*(18), 6692-6694.

- **Ivan, Marius G.**, Scaiano, J. C., „A New Approach for the Detection of Carbon-centered Radicals in Enzymatic Processes Using Prefluorescent Probes, *Photochemistry and Photobiology* **2003**, *78*(4), 416-419.

- Carlos N. Sanrame, Yujian You, Mike Talley, **Marius G. Ivan**, and J. C. Scaiano, „Direct Photobleaching of Acrylates in Polymethylsilsesquioxane Films by 193 nm Irradiation", submitted.

Note: three other manuscripts are in preparation. The topics covered in these three future papers are:

- photoacid generation of benzofused sulfonium PAGs at 157 and 193 nm
- detection of fluoride anions using fluorescent probes in solution and in thin polymer films
- effects of laser exposure on polymer films containing pyrene

7.4.2 Articles in non-refereed journals

- **Marius Ivan** – „Where Light and Matter Meet", *L'Actualite Chimique Canadienne Canadian Chemical News*, 58 (4) April, 20, **2006** (http://www.accn.ca/issues.html)

- **Marius Ivan** – „Optical Projection Lithography - Enabling nanolithography", *Canadian Chemical News*, October issue, 16, **2005.** For pdf file go to: http://www.accn.ca/accn2005/october2005/october2005toc.html